ABSTRACT

MODELING CONTAMINANT TRANSPORT AND FATE AND SUBSEQUENT IMPACTS ON ECOSYSTEMS

by
Ming Fan

Assessing risks associated with the release of metals into the environment and managing remedial activities requires simulation tools that depict speciation and risk with accurate mechanistic models and well-defined transport parameters. Such tools need to address the following processes: (1) aqueous speciation, (2) distribution mechanisms, (3) transport, and (4) ecological risk. The primary objective of this research is to develop a simulation tool that accounts for these processes. Speciation in the aqueous phase can be assessed with geochemical equilibrium models, such as MINEQL+. Furthermore, metal distribution can be addressed mechanistically. Studies with Pb sorption to amorphous aluminum (HAO), iron (HFO), and manganese (HMO) oxides, as well as oxide coatings, demonstrated that intraparticle diffusion is the rate-limiting mechanism in the sorption process, where best-fit surface diffusivities ranged from 10^{-18} to 10^{-15} cm^2 s^{-1}. Intraparticle surface diffusion was incorporated into the Groundwater Modeling System (GMS) to accurately simulate metal contaminant mobility where oxides are present. In the model development, the parabolic concentration layer approximation and the operator split technique were used to solve the microscopic diffusion equation coupled with macroscopic advection and dispersion. The resulting model was employed for simulating Sr^{90} mobility at the U.S. Department of Energy (DOE) Hanford Site. The Sr^{90} plume is observed to be migrating out of the 100-N area extending into other areas of the Hanford Site and beyond. Once bioavailability is understood, static or dynamic ecological risk

assessments can be conducted. Employing the ERA model, a static ecological risk assessment for exposure to depleted uranium (DU) at Aberdeen and Yuma Proving Grounds (APG and YPG) revealed that a reduction in plant root weight is considered likely to occur. For most terrestrial animals at YPG, the predicted DU dose is less than that which would result in a decrease in offspring. However, for the lesser long-nosed bat, reproductive effects are expected to occur through the reduction in size and weight of offspring. At APG, based on very limited data, it is predicted that uranium uptake will not likely affect survival of terrestrial animals and aquatic species. In model validation, sampling of pocket mice, kangaroo rat, white-throated woodrat, deer, and milfoil showed that body burden concentrations fall into the distributions simulated at both sites. This static risk assessment provides a solid background for applying the dynamic approach. Overall, this research contributes to a holistic approach in developing accurate mechanistic models for simulating metal contaminant mobility and bioavailability in subsurface environments.

MODELING CONTAMINANT TRANSPORT AND FATE AND SUBSEQUENT IMPACTS ON ECOSYSTEMS

by
Ming Fan

A Dissertation
Submitted to the Faculty of
New Jersey Institute of Technology
in Partial Fulfillment of the Requirements for the Degree of
Doctor of Philosophy in Environmental Engineering

Department of Civil and Environmental Engineering

August 2004

APPROVAL PAGE

MODELING CONTAMINANT TRANSPORT AND FATE AND SUBSEQUENT IMPACTS ON ECOSYSTEMS

Ming Fan

Dr. Lisa Axe, Dissertation Advisor — Date
Associate Professor of Civil and Environmental Engineering, NJIT

Dr. Sima Bagheri, Committee Member — Date
Professor of Civil and Environmental Engineering, NJIT

Dr. Hsin-Neng Hsieh, Committee Member — Date
Professor of Civil and Environmental Engineering, NJIT

Dr. Demetrius Papageorgiou, Committee Member — Date
Professor of Mathematical Sciences, NJIT

Dr. Trevor A. Tyson, Committee Member — Date
Professor of Physics, NJIT

Dr. Daniel Watts, Committee Member — Date
Director of the York Center for Environmental Engineering and Science, NJIT

BIOGRAPHICAL SKETCH

Author: Ming Fan

Degree: Doctor of Philosophy

Date: August 2004

Undergraduate and Graduate Education:

- Doctor of Philosophy in Environmental Engineering
  New Jersey Institute of Technology, Newark, NJ, USA, 2004
- Master of Science in Chemical Engineering
  New Jersey Institute of Technology, Newark, NJ, USA, 2004
- Master of Science in Environmental Engineering
  Nanjing University of Science and Technology, Nanjing, P.R. China, 1999
- Bachelor of Science in Environmental Engineering
  Nanjing University of Science and Technology, Nanjing, P.R. China, 1996

Major: Environmental Engineering

Publications:

Fan, M., Axe, L., Tyson, T.A. Modeling intraparticle surface diffusion and incorporating into a bulk transport code for groundwater modeling: case study for strontium (Sr) on the Hanford Site, Washington. *J. Contam. Hydrol.*, in review.

Fan, M., Boonfueng, T., Xu, Y., Axe, L., Tyson, T.A. Modeling Pb sorption to microporous amorphous oxides as discrete particles and coatings. *J. Colloid and Interface Sci.*, in press.

Fan, M., Thongsri, T., Axe, L., Tyson, T.A. Using a probabilistic approach in an ecological risk assessment simulation tool: test case depleted uranium (DU). *Chemosphere*, in review.

Wang, L., Fan, M., Sun, X., Huang, Z., 2000. Structure and thermal stability of supported titania membrane. *J. Functional Mater.*, 31 (3), 301-302, 305.

Wang, L., Liu, X., Yu, W., Sun, X., Fan, M., 2000. Treatment of polystyrene industrial wastewater by coagulation-biological contact oxidation process. *Chinese J. Environ. Eng.*, 18 (1), 24-26.

Wang, L., Fan, M., Sun, X., Zhou, X., 1997, Application of high-tension electronstatic deemulsification technology. *J. Nanjing Univ. Sci. Technol.*, 21(3): 249-252.

Presentations

Fan, M., Axe, L., Tyson, T.A. Incorporating intraparticle surface diffusion into a bulk transport code for groundwater modeling. The 228th American Chemical Society National Meeting, Philadelphia, PA, Aug. 22-26, 2004.

Fan, M., Thongsri, T., Axe, L., Tyson, T.A. A probabilistic risk assessment addressing metal mobility and bioavailability. The 20th Society of Environmental Toxicology and Chemistry Hudson-Delaware Chapter Annual Meeting, Sandy Hook, NJ, Apr. 22-23, 2004.

Fan, M., Axe, L., Tyson, T.A. A novel approach for ecological risk assessment combined with metal contaminant transport and fate models. The 24th Society of Environmental Toxicology and Chemistry Annual Meeting, Austin, TX, Nov. 9-13, 2003.

Fan, M., Xu, Y., Boonfueng, T., Yuan, W., Axe, L., Tyson, T.A. Intraparticle surface diffusion of lead in amorphous aluminum, iron, and manganese oxides. "Physicochemical Processes in Environmental Systems: A Symposium in Honor of Professor Walter J. Weber, Jr." at the 226th American Chemical Society National Meeting, New York, NY, Sept. 7-11, 2003.

Fan, M., Axe, L., Tyson, T.A. Modeling intraparticle diffusion of metal contaminants in amorphous oxide minerals. The 77th American Chemical Society Colloid and Surface Science Symposium, Atlanta, GA, Jun. 15-18, 2003.

Fan, M., Thongsri, T., Axe, L., Tyson, T.A. Metal contaminant mobility, bioavailability, and ecological risk assessment. The 23rd Society of Environmental Toxicology and Chemistry Annual Meeting, Salt Lake City, UT, Nov. 16-20, 2002.

Fan, M., Axe, L., Tyson, T.A. Ecological risk assessment for depleted uranium at U.S. Army Aberdeen Proving Ground and Yuma Proving Ground. The 34th Mid-Atlantic Industrial and Hazardous Waste Conference, New Brunswick, NJ, Sept. 20-21, 2002.

Dedicated to my beloved family

ACKNOWLEDGMENT

I would like to express my sincere gratitude to my dissertation advisor, Dr. Lisa Axe, who provided me with the opportunity to conduct research under her supervision. I am truly thankful for her guidance, encouragement, and full support through this research.

Special thanks to Dr. Trevor Tyson, who not only served as a committee member, but also met with me every Thursday to discuss my progress during the past four years. I will miss it.

I would like to extend my gratitude to Dr. Daniel Watts, who served as a committee member and also provided me invaluable resources and suggestions to make my research go forward. Acknowledgements are made to Dr. Sima Bagheri, Dr. Hsin-Neng Hsieh, and Dr. Demetrius Papageorgiou for serving as committee members, actively participating in my research, and thoughtful input. I would also like to thank Dr. Jim Dyer of DuPont Engineering Technology for his supervision and support during my internship at DuPont. My sincere thanks go to all my professors, laboratory staff, and secretaries in the Department of Civil and Environmental Engineering for constant guidance and help.

Last, but certainly not least, thanks should go to Tep, Helen, Ying, Tak, Aiqin, Sumeng, and Ben, for their great assistance and friendship throughout my studies here.

TABLE OF CONTENTS

TABLE OF CONTENTS
(Continued)

TABLE OF CONTENTS
(Continued)

TABLE OF CONTENTS
(Continued)

LIST OF TABLES

LIST OF FIGURES

LIST OF FIGURES
(Continued)

Figure **Page**

LIST OF FIGURES
(Continued)

Figure **Page**

CHAPTER 1

INTRODUCTION

Heavy metal contaminants released in the subsurface pose a threat to human health and the surrounding environment. Concerns about the detrimental effects have resulted in extensive research efforts to better understand the processes involved in the fate and transport of these contaminants in subsurface systems. Soils and aquifers are heterogeneous, subsurface systems composed of a large number of components including dissolved salts and metals, gases, minerals, natural and anthropogenic organics, microorganisms, animals, and plants. The subsurface is among the most complex systems studied by scientists and engineers today. Assessing risks associated with heavy metals to the surrounding environment and managing remedial activities requires simulation tools that depict speciation and risk with accurate mechanistic models and well-defined transport parameters. Such tools need to address the following processes: (1) aqueous speciation, (2) distribution mechanisms, (3) transport, and (4) ecological risk. The primary objective of this research is to develop a simulation tool that accounts for these processes.

Considering the fate and transport of metal contaminants in subsurface environments, a number of natural processes can be classified as transport and geochemical. Transport processes include aqueous-, nonaqueous- and gaseous-phase advection and dispersion, while geochemical processes include hydrolysis and complexation, precipitation-dissolution, oxidation-reduction, and sorption (Rubin, 1983; Axe and Anderson, 1998; Cheng and Yeh, 1998; Gauguly *et al.*, 1998; Herbert, 2001).

Among them, sorption is considered a significant process and is also the least well understood (Sposito, 1986; Mangold and Tsang, 1991). To predict the transport and fate of heavy metals in subsurface environments, a mechanistic understanding of sorption processes is needed. Such an understanding can improve the transferability of sorption measurements and the reliability of models used in interpreting past or in estimating future migration of contaminants.

One major factor that determines the amount of metals sorbed to soil and sediment is the quantity and composition of the sorption substrate. Because amorphous oxide minerals of aluminum, iron, and manganese have large surface areas, porous structures, and an abundance of binding sites, they can control the distribution of metal contaminants in many aquatic environments. These oxides occur as coatings on other mineral surfaces or as discrete particles and are pervalent in aquatic environments (Jenne and Zachara, 1987; Stumm and Morgan, 1996; Dong *et al.*, 2003).

Sorption can be defined as the accumulation of a substance or materials at an interface between the solid surface and bulk aqueous phase. Sorption is a general term that is used when the retention mechanism at a surface is unknown; adsorption, surface precipitation, diffusion, and polymerization are all examples of sorption. At equilibrium, there are three basic mathematical approaches to adsorption: distribution coefficient K_d (isotherm equations), mass action models, and surface complexation models (Sparks, 1995; Jenne, 1998; Herbert, 2001). However, equilibrium relationships comprise a set of limiting conditions for sorption processes, a set of conditions predicted on there being sufficient time for a system to achieve thermodynamic stability. In reality, the rates at which equilibrium is approached may significantly affect the process and the distribution

of metal contaminants among the phases of the system. In porous media, these rates are controlled either chemically or by molecular-level mass transport, specifically, reaction rate and local mass transfer (Weber *et al.*, 1991). Chemical reaction rates depend on the nature of specific interactions that occur between the solute and sorbent in the sorption process; on the other hand, local mass transfer is microscopic transfer, which refers to movement of solute under the influence of molecular or mass distribution by its concentration gradient. Equilibrium models have been widely developed to simulate sorption; however, work has shown that metal sorption processes cannot be successfully simulated only by equilibrium models and that transient processes must be included (Middelburg and Comans, 1991; Koeppenkastrop and De Carlo, 1993; Bruno *et al.*, 1995; Axe and Anderson, 1995 and 1997; Altin *et al.*, 1998; Scheidegger *et al.*, 1998; Thompson *et al.*, 1999; Trivedi and Axe, 1999 and 2000; Tonkin *et al.*, 2002). During local microscopic mass transfer in sorption, which refers to movement of solute under the influence of molecular or mass distribution by its concentration gradient, research has shown that three processes, film diffusion (Sparks, 1995; Jackman *et al.*, 2001), intraparticle diffusion (Fuller *et al.*, 1993; Papelis *et al.*, 1995; Trivedi and Axe, 1999, 2000, and 2001; Scheinost *et al.*, 2001; Manju *et al.*, 2002), and surface precipitation (Middelburg and Comans, 1991; Fendorf and Sparks, 1994; Ford *et al.*, 1999; Karthikeyan *et al.*, 1999; Thompson *et al.*, 1999; Scheckel *et al.*, 2000; Waychunas *et al.*, 2002), are the potential rate-limiting steps in sorption.

In the sorption of heavy metals to microporous hydrous oxides, numerous studies have demonstrated that this process is a two-step one (Benjamin and Leckie, 1981; Barrow *et al.*, 1989; Fuller *et al.*, 1993; Axe and Anderson, 1995, 1997; Holmen and

Gschwend, 1997; Jain and Ram, 1997; Merkle *et al.*, 1997; Strawn *et al.*, 1998; Roberts *et al.*, 1999; Trivedi and Axe, 1999, 2000, and 2001; Scheinost *et al.*, 2001; Manju *et al.*, 2002; Axe and Trivedi, 2002; Sen *et al.*, 2002): rapid adsorption of metal ions to the external surface is followed by slow intraparticle diffusion along the oxide micropore walls. The kinetics of the first step is quite fast where equilibrium is reached within minutes with sufficient mixing between the bulk aqueous phase and the adsorbent external surface. In the second step, the contaminant adsorbed at the surface slowly diffuses along sorption sites in the micropores of the oxide particle.

Studies with real systems emphasize that contributions from slower processes are needed for accurately depicting metal transport. Thus, models that often employ either equilibrium or reaction rate approaches (e.g., Gerard *et al.*, 1998; Yabusaki *et al.*, 1998; Clement, 2003) are inadequate for describing metal mobility in subsurface environments where amorphous oxides or oxide coatings are present (e.g., Gallo *et al.*, 1998; Baverman *et al.*, 1999; Zheng and Wang, 1999). To assess risks associated with contaminants to the surrounding environment and manage remedial activities requires accurate models and well-defined transport parameters. The objectives of this research are to model metal contaminant transport, fate, and subsequent impact on ecosystems, specifically to incorporate the intraparticle diffusion process into solute transport modeling, which supports advancing the ability of models to apply mobile and available concentrations found in the soil and subsurface environments and better quantify contaminant mobility and bioavailability.

This study first requires an understanding of metal speciation, which is a function of pH, ionic strength, reduction-oxidation potential, and other factors. Thus, a review of

geochemical equilibrium models to address metal speciation is presented in Chapter 2. Bioavailable species can be obtained through speciation models coupled with mechanistic models of metal distribution. A critical review in Chapter 3 demonstrates that equilibrium models are inadequate for simulating sorption and that transient processes are needed in transport modeling. Credibly simulating and predicting species mobility relies on accurate transport models. In Chapter 4, existing groundwater flow and solute transport models are evaluated and reviewed for addressing macroscopic transport. In Chapter 5, based on the review of previous chapters, objectives, hypotheses, and an overall transport modeling approach are developed. In Chapter 6, Pb sorption on microscopic amorphous oxides as discrete particles and coatings is studied, validating the transient natural attenuating process of intraparticle diffusion for not only discrete oxide particles but also oxide coatings. In Chapter 7, the method for coding the transient process, intraparticle diffusion, is presented for incorporation into the macroscopic transport model, Groundwater Modeling System (GMS), in depicting metal contaminant mobility. In Chapter 8, a case study of Sr^{90} transport at the Department of Energy Hanford Site, Washington, is presented using the newly developed package with GMS. Once bioavailable species are defined spatially and temporally, the information can be used to assess static or dynamic ecological risks resulting from exposure to different metals. A static ecological risk assessment was conducted for depleted uranium (DU) present at U.S. Army Aberdeen and Yuma Proving Grounds (APG and YPG) in Chapter 9. Finally, conclusions and recommendations for future work are outlined in Chapter 10.

CHAPTER 2

SPECIATION MODELING

The subsurface is among the most complex systems studied by scientists and engineers today, as discussed in the first chapter. Because of its complexity, geochemical modeling has gained widespread acceptance as a useful tool to interpret subsurface geochemical processes which affect the fate and transport of chemical components under varying conditions (Cheng and Yeh, 1998; Herbert, 2001). For example, these models are being used to predict the behavior of toxic and radioactive contaminants at proposed waste disposal sites (Oreskes *et al.*, 1994).

Geochemical modeling of natural aqueous systems was first introduced by Garrels and Thompson (1962) where they predicted the speciation of seawater. During the 1970's, rapid progress was made in the development of geochemical speciation models, which focused on mathematical modeling of geochemical reactions and the expansion of the number of species included in the models, but the models were often machine dependent and poorly documented (Herbert, 2001). Since the mid-1980's, the development of geochemical models has focused less on creation of new models and more on efforts to document and improve existing models. These efforts included the development of more complete thermodynamic databases, the ability to handle a wide range of physical and chemical conditions, such as high temperature, pressure, ionic strength, and improvement of the models' applicability to environmental and industrial systems (Bassett *et al.*, 1990; Brown *et al.*, 2000). However, since the 1990's, many new models, which have strong capabilities to deal with various systems, have been

developed; at the same time, great efforts have continued in improving thermodynamic databases and addressing distribution mechanisms.

2.1 Review of Speciation Models

Speciation modeling is the most common type of geochemical models, providing a quantitative description of the activities of different forms or species of a chemical. Speciation models have been developed to predict concentrations of the ions and complexes that will form, their thermodynamic activities, and the saturation state with respect to different species and minerals. (Rubin, 1983; Mangold and Tsang, 1991; Gavaskar *et al.*, 1997; Salmon 1999; Chilakapati, *et al.*, 2000). A competent speciation model should include a comprehensive thermodynamic database for aqueous complexes, solids, and gases of the elements of interest needed to adequately understand a given data set. These models also require a numerical method to solve the matrix for conservation and constitutive equations describing the system. Other important aspects of a model include an efficient solution method and the ability to model redox reactions and sorption. Additionally, integral to a model is the activity coefficient calculation and database modification ability.

This review on speciation models attempts to summarize several major numerical codes in a comparative evaluation based on published and unpublished reviews and the original documentation for individual codes (Yeh and Tripathi, 1989; Allison *et al.*, 1991; Mangold and Tsang, 1991; Wolery, 1992; Crawford, 1996; Butler and Cogley, 1998; Ganns, 1998; Schecher and McAvoy, 1998; HydroGeoLogic *et al.*, 1999; Parkhurst *et al.*,

1999; Lee and Windt, 2001; Post, 2001). In addition, in some cases, the code developers were directly consulted to get first-hand information.

There are many speciation models available, such as GEOCHEM (Sposito and Mattigod, 1980), EQUILIB (Morrey and Shannon, 1981), ECHEM (Morrey, 1988), SOLMINEQ (Kharaka *et al.*, 1988), SOILCHEM (Sposito and Coves, 1989), WATEQ4F (Ball and Nordstrom, 1991), EQ3/6 (Wolery, 1992), MINTEQA2 (Allison *et al.*, 1991; HydroGeoLogic *et al.*, 1999), OLI (OLI Systems, 1999), and PHREEQC (Parkhurst *et al.*, 1999; Post, 2001). Some models listed above include mass transfer calculations. The models reviewed were chosen on the basis of four criteria: (1) models are in the open literature with full descriptions and complete documentation; (2) models have been verified and validated; (3) models are widely used and updated; and (4) models are fully maintained and supported by organizations. After preliminary evaluation and screening of existing models, four models, MINEQL+, MINTEQA2, EQ3/6, and PHREEQC, were selected for critical review in this chapter. First, background and feature descriptions of the models are presented. Second, model evaluation is discussed. In the last section, recommended models are provided for the software tool development, which is the inclusion of speciation as well as transport modeling into the ecological risk assessment (ERA) software (Lu *et al.*, 2003).

2.1.1 MINEQL+

The model MINEQL+ descended from REDEQL, and is a refinement of Westall's model, MINEQL (Westall *et al.*, 1976). The MINEQL+ is an interactive data management system for chemical equilibrium modeling (Schecher and McAvoy, 1998). Since 1998, the model employed a Windows environment instead of DOS providing

simultaneous on-screen display of data entry screens, spreadsheet, and graphs. The features include: automatic highlighting of zero values for enthalpy and log *K*; input wizards to help users with data entry for pH and alkalinity; fixed ionic strength computation options; special reports where output can be summarized in a number of reports that perform additional data extraction or additional calculations on the output data; and autopilot that automates the progression of tools which are needed to solve a chemical equilibrium problem. Also, the temperature range of this version for model calculations has changed to 0-100°C instead of 0-50°C as provided in version 3.0.

The model MINEQL+ version 4.5 (Schecher and McAvoy, 2001) updates the thermodynamic database with 400 new species; this database is consistent with that used in MINTEQA2 (Allison *et al.*, 1991). It also includes full documentation for the database.

2.1.2 MINTEQA2

Like MINEQL+, MINTEQA2 has been derived from Westall's model, MINEQL (Westall *et al.* 1976). The MINTEQA2 and its documentation can be downloaded at no charge from the Center for Exposure Assessment Modeling (CEAM), U. S. EPA (Environmental Protection Agency) Environmental Research laboratory in Athens, Georgia (http://www.epa.gov/ceampubl/mmedia/minteq/index.htm, 2004). The CEAM software products are built using FORTRAN77, assembler, and operating system interface command languages (Butler and Cogley, 1998). The MINTEQA2 includes an extensive database of reliable thermodynamic data and an interactive program PRODEFA2 designed to be executed prior to MINTEQA2 for the purpose of creating the required input file (Allison *et al.*, 1991; HydroGeoLogic *et al.*, 1999). The version 4.02 was released in June 2000. Relative to MINEQL+, MINTEQA2 may be a little more

difficult to use because of the user interfaces operating in DOS. This code has been used in a number of applications, including groundwater analysis, simulation of reactive solute transport, restoration of an aquifer used for in situ uranium mining, and reactions among uranium mill tailings, clay liners, and natural sediments.

Visual MINTEQA which is a Windows version of MINTEQA2 ver 4.0 has been developed by Gustafsson (Gustafsson, 2001) and supported by the Swedish NFR (Natural Science Research Council) and MISTRA (Foundation for Strategic Environmental Research). This program is distributed via internet free of charge.

2.1.3 PHREEQC

The model PHREEQC was developed by Parkhurst and his colleagues at the U.S. Geological Survey (USGS) to focus on the application of computerized calculation methods for problems in geochemistry, including assessments of acid mine drainage in the western United States (Butler and Cogley, 1998). The PHREEQC is based on an ion-association aqueous model and has capabilities for (1) speciation and saturation-index calculation; (2) batch-reaction and one-dimensional (1D) transport calculations involving reversible and irreversible reactions; and (3) inverse modeling, which evaluates mineral and gas transfers that account for differences in composition between waters, within specified compositional uncertainty limits (Crawford, 1996; Parkhurst *et al.*, 1999). The new features in PHREEQC version 2 relative to version 1 include capabilities to simulate dispersion and stagnant zones in 1D-transport calculations, to model kinetics with user-defined rate expressions in Basic, and to model fixed-volume gas phases in addition to fixed-pressure gas phases (Parkhurst *et al.*, 1999). In reaction path calculations, this software is oriented more toward system equilibrium than just aqueous equilibrium.

Essentially, all the modes of each element in the system are distributed among the aqueous phase, pure solid and gas phases, exchange sites, and surface sites to attain system equilibrium (Butler and Cogley, 1998).

Inverse modeling attempts to account for the chemical changes that occur as a water evolves along a flow path. Assuming two water analyses which represent starting and ending water compositions along a flow path, inverse modeling is used to calculate the modes of minerals and gases that must enter or leave solution to account for the differences in composition. Inverse models that mix two or more waters to form a final water can also be calculated. The PHREEQC allows uncertainty limits to be defined for all analytical data, such that inverse models are constrained to satisfy mole balance for each element and valence states as well as charge balance for each solution, but only within these specified uncertainty limits (Parkhurst *et al.*, 1999).

The PHREEQC version 2.4.2 (Post, 2001) was released July 2001 for Windows, which is an extended version of PHREEQC version 2 (Parkhurst *et al.*, 1999). This software has the same familiar user interface as other common Windows programs. Newer features of PHREEQC for Windows include an input editor with some help features such as syntax highlight, a keyword index, and an output manager. Both PHREEQC version 2 and PHREEQC for Windows can be downloaded at no charge from USGS web site: http://wwwbrr.cr.usgs.gov/projects/GWC_coupled/phreeqc/index.html (2004). In the later section of evaluation models, the review will concentrate on the equilibrium speciation part of PHREEQC and compare it with other models.

2.1.4 EQ3/6

The EQ3/6 software package originated in the mid-1970s. It was originally developed by Wolery (1978) at Northwestern University to model seawater-basalt interactions in mid-ocean ridge hydrothermal systems. The model was brought to Lawrence Livermore National Laboratory in 1978 by the original author, and there underwent extensive development for modeling geological disposal of high-level nuclear waste (Wolery, 1992). Many of the refinements that have been incorporated into the code for use in nuclear waste applications are readily adaptable to applications in other environmental areas, such as the evaluation of acid mine waters, low-level radioactive waste, and chemical waste. Some of the more general processes that can be modeled using EQ3/6 include mineral dissolution, mineral precipitation, and waste leaching. Modeling can be accomplished over a temperature range from 0 to 300°C, a pressure range of 1 to approximately 100 atm, and an ionic strength range from dilute to greater than 10 molal (Wolery, 1992; Butler and Cogley, 1998).

The major components of the program are EQPT, EQ3NR, and EQ6. EQPT is the data file preprocessor used to prepare input files. The EQ3NR is the speciation solubility code and will be evaluated further with other speciation models in following section. EQ6 is the reaction path code that conducts calculations following the evolution of a reaction system. EQ3/6 version 7.2c has been released by LLNL (Lawrence Livermore National Laboratory). The comprehensive documentation for EQ3/6 version 7.0 (Wolery, 1992) is available at: http://eed.llnl.gov/geosciences/esd/geochem/eq36.html (2002).

2.1.5 Evaluation

In this section, the four models are comparatively evaluated, MINEQL+, MINTEQA2, EQ3/6, and PHREEQC, and based on this evaluation, model(s) will be recommended for use in the software tool development.

Before the discussion on model evaluation, model validation is considered. Geochemical model validation is important if model results are used in remediation decisions and policy formation, though the extent that numerical, geochemical models can be verified and validated has been questioned (Oreskes *et al.*, 1994). There are several definitions of model validation. Mangold and Tsang (1991) reported one definition adapted from the International Atomic Energy Agency (IAEA) "A conceptual model and the computer code derived from it are validated when it is confirmed that the conceptual model and the computer code provide a good representation of the actual processes occurring in the real system. Validation is thus carried out by comparison of calculations with experimental measurements and field observations." Another definition from Davis *et al.* (1991) in the Performance Assessment Plan for the proposed high-level nuclear waste repository at Yucca Mountain, Nevada, "the most common method of validation involves a comparison of the measured responses from in situ testing, lab testing, or natural analogs with the results of computational methods that embody the model assumptions that are being tested." From these definitions, it is shown that only through comparative analysis between lab data and model results are geochemical models validated. Other illustrations of models, such as model comparison, are generally called model evaluation.

Researchers at Battelle's Pacific Northwest Laboratory conducted an evaluation of the extent that geochemical codes could be used by the electric utility industry to study leachate migration from solid-waste sites (Kincaid *et al.*, 1984; Morrey *et al.*, 1986). The EQ3/6, MINTEQ (earlier version of MINTEQA2), PHREEQE, GEOCHEM, and EQUILIB were selected to be evaluated and several cases were tested, including comparison of solubility calculations for common minerals, evaluation of adsorption models, prediction of leachate from fly ash, and prediction of leachate composition in contact with soil. Morrey *et al.* (1986) concluded that PHREEQE, GEOCHEM, and EQUILIB were not as useful as the EQ3/6 and MINTEQ for several reasons. The EQUILIB model required adding additional species along with adsorption ability, which would necessitate significant restructuring of the code. The GEOCHEM has the most significant limitation where dissolution of finite quantities of solids is not feasible under most circumstances. The PHREEQE was not able to predict mineral precipitation that involved ones not initially specified in the problem configuration. The EQ3/6 and MINTEQ were further studied under comparison tests. EQ3/6 was found to be the most comprehensive available code for modeling the approach to equilibrium. The MINTEQ was selected because its convergence algorithm was mathematically compact and simple, its data were extensive, and it had the broadest ability to model adsorption. Subsequently, researchers completed five modeling tests of EQ3/6 and MINTEQ and concluded that both codes were valuable as standalone models, but were too slow and complex to be incorporated as a geochemistry code module in a transport code. As introduced in the previous section, MINTEQA2, an updated version of MINTEQ, became available in 1991 and has an interactive program used to create input files, which makes the model

more user oriented requiring less effort to set up a problem. Based on their review and available information on the equilibrium models, MINTEQA2 appeared be the most useful because it performed consistently in the geochemical test cases (Kincaid *et al.*, 1984; Morrey *et al.*, 1986) and it has been improved while other models have not been updated to the same degree. In the following, the review will critically evaluate the four models based on the following categories: activity coefficients, adsorption, and thermodynamic database.

Activity Coefficients

Geochemical equilibrium models predict the activities, activity coefficients, and concentrations of individual species based upon input values for the total concentrations of the chemical components present in the system. Most models rely on one of two theoretical approaches, the ion-association or the specific ion-interaction, to explain the relationship between activity and concentration under varying solution chemistry. These models are used to define mathematical relationships which define activity coefficients as a function of properties of the aqueous solutes (i.e., size and charge) as well as solution chemistry (i.e., ionic strength). Ion-association is the theoretical approach first used to predict activity coefficients based on the Debye-Hückel equation to relate aqueous activities to concentrations; this is one of the most common models used in speciation models (Herbert, 2001). One key assumption of the Debye-Hückel derivation is that ions can be treated as point charges. The ions interact with each other by coulombic forces (Bethke, 1996). Generally, the Debye-Hückel expressions do not account for all interactions among solutes. This limits the ability of the model to accurately predict activity coefficients of simple electrolytes at higher ionic strengths. A variety of

empirical and semi-empirical expressions have been proposed to extend the applicability of the Debye-Hückel equation to higher ionic strength systems. The Davies equation is one that improves the fit between the theoretical and experimental observations.

The other major approach describing ion interaction in aqueous solutions is the specific ion-interaction model. At higher ionic strengths both long-range electrostatic and short-range forces affect the complexation of ions in aqueous solutions. The specific ion-interaction model accounts for both of these types of forces through the use of a virial coefficient expansion of the Debye-Hückel equation. The Pitzer equation is used widely as the ion-interaction model, which applies empirical data to account for complexation and ion pair formation by describing the change in free ion activity with a series of experimentally defined virial coefficients. The ion-interaction model is superior to the ion-association model at calculating activity coefficients at high ionic strength, and can be used at low-ionic strengths as well. With this formulation, it is possible to compute the activities of many electrolytes at ionic strengths up to 20 M and temperatures up to 250°C (Benjamin, 2001; Herbert, 2001).

The MINTEQA2 and MINEQL+ models include both the Davies and the Debye-Hückel equations (Table 2.1). The EQ3NR has a more comprehensive set of models for predicting activity coefficients, and besides the Davies and Pitzer equation, the B-dot equation is also included in this code (Table 2.1). Few geochemical models incorporate activity coefficient calculations for solid-phase minerals. Most geochemical models assume that solid-phase minerals are in their standard states, and therefore, their activity coefficients are one. The EQ3NR is one geochemical model that can predict solid-phase activity coefficients as a function of mineral composition. There are two types of solid

Table 2.1 Equations for Predicting Activity Coefficients in Speciation Models

Name	Equation[a]	Definition	Ionic strength	MINEQL+	MINTEQA2	EQ3/6	PHREEQE
Debye-Hückel	$\log \gamma_i = -\frac{Az_i^2\sqrt{I}}{1+a_iB\sqrt{I}}$	$A = 1.82\times10^6(\varepsilon T)^{-3/2}$ where ε is the dielectric constant of the medium, z_i is ionic charge, I is ionic strength, $B = 50.3(\varepsilon T)^{1/2}$, a_i is ion size parameters,	<0.1	×	×		×
Davies	$\text{Log}\,\gamma_i = -Az_i^2\left(\frac{\sqrt{I}}{1+\sqrt{I}} - 0.2I\right)$		<0.5	×	×	×	
Pitzer	$\log \gamma_i = -\frac{Az_i^2\sqrt{I}}{1+a_i B\sqrt{I}} + \sum_j {}^{0}B_{ij}\ I\ m_j$	m_j is molality (mole/kg solution) of j, B_{ij} is specific interaction term between ions i and j,	<1			×	
B-dot	$\text{Log}\,\gamma_i = -\frac{Az_i^2\sqrt{I}}{1+a_i B\sqrt{I}} + \dot{B}I$	$\dot{B}$ is based on the mean salt activity concept and is linearized derivation function.	<1			×	

[a] Compiled from Bethke (1996) and Benjamin (2001)

phase activity coefficient models: molecular-mixing models and site-mixing models. EQ3NR use site-mixing models to describe the activity coefficient of mixed composition minerals (Wolery, 1992). Butler and Cogley (1998) reported that EQ3/6 is the computer program of choice for modeling complex geological phenomena with large numbers of components and potential solid phases, especially over a range of temperature and ionic strengths. EQ3/6 has the uncommon capability to model precipitation and dissolution of solid solutions. PHREEQC uses the Debye-Hückel equation to account for the non-ideality of aqueous solutions and approaches for the higher ionic strength issues are not incorporated in this software (Parkhurst *et al.*, 1999).

Adsorption

Sorption can be defined as the accumulation of a substance or materials at an interface between the solid surface and the bathing solution. Sorption is a general term that is used when the retention mechanism at a surface is unknown, and adsorption, surface precipitation, and polymerization are all examples of sorption (Sparks, 1995). As mentioned in the first chapter, sorption is considered significant for chemical transport, and is also the least well understood (Sposito, 1986; Mangold and Tsang, 1991). All speciation models only address adsorption; other processes like precipitation are kinetically limited. At equilibrium, there are three basic mathematical approaches to adsorption: distribution coefficient (isotherm equations), mass action models, and surface complexation models. Isotherm equations are simplest and most convenient models taking account of adsorption process, but they are unable to treat species having multiple oxidation states, variable degrees of complexation, or heterogeneous sorption sites. Mass action models handle ion exchange and heterogeneous sorption sites, which are widely

employed in existing codes and make use of thermodynamic databases. However, they lack full capability to model multiple oxidation states and specific adsorption, and additionally, the variation of adsorption with pH cannot be properly modeled. Surface complexation models, on the other hand, are sufficiently general to account for all the above variables, however, more data are needed (Sposito, 1989; Allison *et al.*, 1991; Mangold and Tsang, 1991; Marmier *et al.*, 1999). Weber *et al.* (1991) discussed concepts, models, and factors affecting contaminant fate and transport and presented a review of sorption phenomena in terms of adsorption, absorption, and precipitation, where absorption and precipitation are preceded by adsorption. The driving force for chemical equilibrium in adsorption processes is a reduction in surface energy. Adsorption is the accumulation of a species at a two-dimensional, solid-liquid interface; it strongly influences the transport of trace metals in subsurface systems and forms the basis for many remediation options.

There are a number of equations that are supported by many geochemical speciation programs including Freundlich, and Langmuir adsorption isotherms. Adsorption isotherms are commonly used to predict adsorption reactions because of their convenience and computational simplicity. On the other hand, these models are site specific and can be quite limited in reliably predicting adsorption under changing conditions. The most widely used models for describing sorption behavior are those based on the electric double-layer theory, such as the Gouy-Chapman model and the Stern model. A more sophisticated approach relies on surface complexation models, which include the constant capacitance, triple layer and modified triple layer, generalized two-layer, and the one-pK model (Sparks, 1995). These models describe adsorption based

on molecular descriptions of the process. Surface complexation models predict cation and anion adsorption in complex systems as a function of pH, ionic strength, complexing ligands, competition between ions, surface chemistry of particle surface, interaction between adsorbents, and effects of changing solution composition (Herbert, 2001). These characteristics make surface complexation models potentially invaluable for the prediction of adsorption reactions for different remediation methodologies, especially those techniques that affect solution or mineral surface chemistry. Unfortunately, as will be shown below, these models require knowledge of a number of different parameters which may not be available to the modeler.

Surface complexation models vary in how they describe the surface potential and where they allow the differing types of species to be sorbed. The constant capacitance model uses two layers to represent adsorption, where chemical adsorption occurs in the layer adjacent to the surface. In the triple layer model, specific adsorption occurs in the first two layers adjacent to the surface. However, only protonation or deprotonation is allowed in the first layer adjacent to the surface. Physically adsorbed species reside in the third layer extending out from the surface. This model uses two fitting parameters to describe the capacitance changes in the two outer layers (Allison *et al.*, 1991; Sparks, 1995).

Seven models are currently available in MINTEQA2 and MINEQL+ for modeling surface reactions and include: (1) the K_d, (2) the Langmuir (non-electrostatic model), (3) the Freundlich, (4) the ion exchange, (5) the constant capacitance, (6) the triple-layer, and (7) the diffuse-double layer. Thermodynamic databases of surface reactions are generally not complete for these models; the user often must provide the set of surface reactions

and their equilibrium constants. However, a database of several surface reactions relevant to the diffuse-double layer model for trace metal adsorption onto an iron oxide surface is included (Allison *et al.*, 1991; Schecher and McAvoy, 1998). During the 1990's, development of the database for diffuse-double layer sorption reactions at the hydrous ferric oxide (HFO) interface provided equilibrium speciation calculations for the Hazardous Waste Identification Rule (HWIR) (U. S. EPA, 1996). The contaminant metals and metalloids of interest in HWIR were arsenic, antimony, barium, beryllium, cadmium, chromium, cobalt, copper, lead, mercury, molybdenum, nickel, selenium, silver, thallium, tin, vanadium, and zinc. MINTEQA2 version 4.02 and MINEQL+ 4.5 include the most recent data for all HWIR contaminant metals pertinent to diffuse-double layer model adsorption reactions on HFO. EQ3NR does not include any adsorption model. PHREEQC incorporates ion exchange, diffusion-double layer, and non-electrostatic models such as the Langmuir and Freundlich isotherms. Table 2.2 provides an overview of adsorption models incorporated in each of software.

Thermodynamic Database

Much effort surrounding speciation model development is centered on the standardization of the associated thermodynamic databases. Variation in the thermodynamic constants can have a significant effect on variability in model predictions. Most databases used by speciation models contain algorithms that are used to estimate thermodynamic parameters at conditions of temperature and pressure other than the ones at which the data were collected. Many models use extrapolation techniques to determine equilibrium constants or Gibbs Free Energy values at higher temperatures and pressures. The extrapolation techniques generally do not include the ability to estimate error or uncertainty in the

Table 2.2 Adsorption Models in Speciation Software

Name	MINEQL+	MINTEQA2	EQ3/6	PHREEQC
K_d	×	×		
Langmuir	×	×		×
Freundlich	×	×		×
Ion exchange	×	×		×
Diffuse - double layer	×	×		×
Constant capacitance	×	×		
Triple - layer	×	×		

estimates. The uncertainty of these estimates can be large, especially at higher temperatures and pressures. If the accuracy of geochemical model predictions is critical, it is imperative that the modeler critiques the thermodynamic database in terms of parameter accuracy, error, and applicability to the conditions of the system being modeled (Bassett and Melchior, 1990; Herbert, 2001). The thermodynamic database used by MINTEQA2 version 3.0 (Allison *et al.*, 1991) contains over 1000 species and includes 31 organic ligands and associated reactions to represent complexation with trace metals. In version 4.0 (HydroGeoLogic *et al.*, 1999), all species involving the 31 organic ligand components have been reviewed and corrected. One organic component was found to have no corresponding species and was removed from the database. Of the 450 species associated with the other 30 organic ligands, 370 have been retained, most with updated thermodynamic constants or other parameters. Eighty of the original 450 have been deleted due to an absence of data within the necessary range of ionic strength and temperature. More than 200 new species involving these organic ligands have been added to the database. In addition to the correction of errors in the metal-organic complexes, the revised database for version 4.0 includes reactions for aqueous species of beryllium, cobalt, molybdenum, and tin. Compilations of stability constants have been used to verify and update the thermodynamic constants for inorganic species. Where possible, the source of the thermodynamic data has been cited in MINTEQA2 version 4.0 database. Data are mainly from the following organizations: (1) the Critical Stability Constants of Metal Complexes Database (CRITICAL) published by the National Institute of Standards and Technology (NIST), (2) Stability Constants Database (SC-DATABASE) published by the International Union of Pure and Applied Chemistry (IUPAC) and Academic Press,

(3) the U.S. Geological Survey equilibrium model WATEQ, and (4) other sources, including literature and other compilations.

The MINEQL+ bases its thermodynamic data on that of the MINTEQA2. In EQ3NR, there are five data files that are based on several data sources, such as SUPCRT92, Data Bank of the Nuclear Energy Agency of the European Community, and also some data summarized by Harvie *et al.* (1984) and Pitzer (1979). All data files are maintained at Lawrence Livermore National Laboratory (LLNL) in a relational database.

In PHREEQC, three database files are distributed within the program: phreeqc.dat, wateq4f.dat, and minteq.dat. The file named phreeqc.dat contains the thermodynamic data for aqueous species and gas and mineral phases that are essentially the same as those found in the program PHREEQE (Parkhurst *et al.*, 1980), which is the earlier version of PHREEQC. Only minor modifications have been made to make the data consistent with the tabulations in Nordstrom *et al.* (1990) and WATEQ4F (Ball and Nordstrom, 1991). The file named wateq4f.dat contains thermodynamic data for the aqueous species and gas and mineral phases that are essentially the same as WATEQ4F. In addition to data for the elements in the database file, phreeqc.dat, the database file wateq4f.dat contains data for the elements: arsenic, cesium, iodine, nickel, rubidium, selenium, silver, and uranium. The file named minteq.dat contains thermodynamic data for the aqueous species and gas and mineral phases that are derived from the database files of MINTEQA2 version 3.0 (Allison *et al.*, 1991). The user needs to select the aqueous species and thermodynamic database (Parkhurst *et al.*, 1999). In selecting the database, the software does not include preferences between the three.

2.1.6 Model Recommendation

From comparative evaluation of the four models MINEQL+, MINTEQA2, EQ3/6, and PHREEQC with respect to activity coefficients, adsorption, and thermodynamic database, we have a basis for selection. Considering activity coefficient calculations, EQ3/6 is the most robust one among the models, as it not only includes the Davies, Pitzer, and B-dot equations, but also incorporates activity coefficient models for solid-phase minerals and can predict solid-phase activity coefficients as a function of mineral composition. The MINEQL+ and MINTEQA2 include both the Davies and the Debye-Hückel equations, and are also robust in predicting activity coefficients up to an ionic strength of 0.5 molal. EQ3/6 does not include any adsorption model, which prevents its use for equilibrium adsorption, a very important mechanism in chemical transport. Although all these models are limited due to the lack of development of kinetically limited processes, MINEQL+ and MINTEQA2 are preferred, given that each has seven adsorption equilibrium models for surface reactions. The PHREEQC incorporates three kinds of adsorption models, ion exchange, double layer, and non-electrostatic ones such as the Langmuir and Freundlich isotherms.

The thermodynamic database has a great effect on speciation variability in model prediction. The MINTEQA2 and MINEQL+ have broader and more updated databases, and also have better documentation for the database compared with models EQ3/6 and PHREEQC. The thermodynamic data in MINEQL+ are based on that of the MINTEQA2. When evaluating models for software development, another important aspect, ease of use, should be considered as well. MINEQL+ is a Windows system based software. Although the Windows version of MINTEQA2, Visual MINTEQA (Gustafsson, 2001), has been

developed recently, validation is needed in using this program. In addition, the interface of Visual MINTEQA is not as user-friendly as that of MINEQL+, and also documentation as comprehensive as MINEQL+ is needed for this free software.

Recently, Meeussen (2003) developed an object-oriented structure for chemical equilibrium modeling, ORCHESTRA. The novel idea for this framework is that model equations are not hard-coded in the source code, but instead all equations are defined in text format and read by ORCHESTRA calculation kernel at run time. The advantages of this structure over other standard speciation algorithms are two fold. Model flexibility allows users to change or add model definitions without changing or recompiling the source code. Model compactness is achieved because the calculation kernel does not contain any information on chemical models. However, currently ORCHESTRA does not include a thermodynamic database, and also requires users be more knowledgeable with respect to equilibrium equations. In addition, this model does not have a user-friendly interface, which is an important aspect of new software development.

Overall, considering its comprehensive thermodynamic database, relatively strong ability to predict activity coefficients, more options for modeling adsorption at equilibrium, and user-friendly interface, MINEQL+ is recommended for our software development. This speciation model will be linked with other functioning sub-models.

2.2 Summary

Geochemical modeling is an attempt to interpret or predict the geochemical processes which occur in subsurface systems. To propose an appropriate model for aqueous speciation in our software development, speciation models were critically reviewed. After

preliminary evaluation and screening of existing models, four models, MINEQL+, MINTEQA2, EQ3/6, and PHREEQC, were selected for evaluation in this review. All four models have been verified and validated to some extent and are relatively widely used and updated. These models are readily available with full descriptions and complete documentation. The four models were compared for activity coefficients, adsorption, and thermodynamic database. Another important aspect, user-friendly interface, was also considered. The MINEQL+ is recommended because of its comprehensive thermodynamic database, relatively strong ability to predict activity coefficients, more options for modeling adsorption under equilibrium conditions, and user-friendly interface.

Through speciation modeling, MINEQL+, aqueous phase is obtained; however, credibly simulating and predicting metal contaminant species mobility relies on mechanistic models of metal distribution. In the next chapter, sorption processes are reviewed where intraparticle diffusion is demonstrated to be an important and rate-limiting step in the sorption. A subsequent review on existing solute transport models shows that either equilibrium or reaction rate approaches are often employed for describing metal sorption. Consequently, realistic solute transport models need to consider the intraparticle diffusion process.

CHAPTER 3

SLOW SORPTION PROCESS MODELING

Sorption processes at the mineral/water interface greatly affect the mobility and bioavailability of heavy metals in aquatic and soil environments. It is imperative that the kinetics and mechanisms of metal sorption be precisely understood. This chapter begins with a literature review on sorption, then will continue with a discussion on intraparticle diffusion and modeling the sorption process in existing solute transport codes. The review includes a discussion on the use of equilibrium models for sorption, which are generally found to be inadequate in simulating sorption. Secondly, the two-step process observed for metal sorption to microporous amorphous hydrous oxides is reviewed where rapid adsorption to the external surface is followed by slow intraparticle diffusion along the oxide micropore walls. Lastly, existing solute transport models often employ either equilibrium or reaction rate approaches for describing metal sorption processes. Therefore, realistic solute transport models need to consider the transient processes such as that observed for sorption to microporous sorbents.

3.1 Equilibrium Models

The fate and transport of heavy metals in soil and sediments are largely dependent upon the metal's interaction with mineral surfaces. As discussed in Chapter 1, amorphous oxide minerals of aluminum (HAO), iron (HFO), and manganese (HMO) are persistent in the subsurface and can control the distribution of metal contaminants in many aquatic environments. Sorption can be defined as the accumulation of a substance or material at

an interface between the solid surface and the bulk aqueous phase. It is a general term that is used when the retention mechanism at a surface is unknown, and adsorption, surface precipitation, and polymerization are all examples of sorption. Adsorption is the accumulation of a species at a two-dimensional, solid-liquid interface; it strongly influences the transport of trace metals in subsurface systems and forms the basis for many remediation options. At equilibrium, there are three basic mathematical approaches to adsorption: mass action models, distribution coefficient K_d (isotherm equations), and surface complexation models (Sparks, 1995; Jenne, 1998; Herbert, 2001), as presented in Chapter 2. Isotherm equations are simplest and often the most convenient, taking account of adsorption processes. There are a number of models supported by geochemical speciation programs including the linear, Freundlich, and Langmuir adsorption isotherms. Adsorption isotherms are commonly used to predict adsorption reactions because of their convenience and computational simplicity. However, these models are site specific and can be quite limited in reliably predicting adsorption under changing conditions. They are unable to treat species having multiple oxidation states, variable degrees of complexation, or heterogeneous sorption sites.

Mass action models handle ion exchange and heterogeneous sorption sites utilizing thermodynamic databases. However, they lack full capability to model multiple oxidation states and specific adsorption. In addition, the variation of adsorption with pH cannot be properly modeled. Surface complexation models, on the other hand, are sufficiently general to account for most of the above variables (Sposito, 1989; Mangold and Tsang, 1991). Surface complexation models include the constant capacitance, triple layer and modified triple layer, generalized two-layer, and the one-pK model (Sparks,

1995). These models describe adsorption based on molecular descriptions of the process. Surface complexation models predict cation and anion adsorption in complex systems as a function of pH, ionic strength, complexing ligands, competition between ions, surface chemistry of the particle surface, interaction between adsorbents, and effects of changing solution composition (Herbert, 2001). These characteristics make surface complexation models potentially invaluable for the prediction of adsorption reactions for different remediation methodologies, especially those techniques that affect solution or mineral surface chemistry. Unfortunately, these models require knowledge of a number of different parameters which may not be available to the modeler (Allison *et al.*, 1991; Marmier *et al.*, 1999).

Surface complexation models vary in how they describe the surface potential and where they allow different types of species to be sorbed. The constant capacitance model uses two layers to represent adsorption, where chemical adsorption occurs in the layer adjacent to the surface. Similarly with the constant capacitance model, the generalized two-layer model assumes that all surface complexes are inner-sphere. The difference between the constant capacitance and the generalized two-layer models is that the constant capacitance model assumes a linear relationship between surface charge and surface potential, and two-layer model describes this relationship by the Poisson-Boltzmann equation. In the triple layer model, specific adsorption occurs in the first two layers adjacent to the surface. However, only protonation or deprotonation is allowed in the first layer adjacent to the surface. Physically adsorbed species reside in the third layer extending out from the surface. This model uses two fitting parameters to describe the

capacitance changes in the two outer layers (Allison *et al.*, 1991; Bruno *et al.*, 1995; Sparks, 1995).

As shown above, many equilibrium models have been developed to model sorption; however, sorption processes generally cannot be successfully simulated by equilibrium models (Middelburg and Comans, 1991; Koeppenkastrop and Carlo, 1993; Bruno *et al.*, 1995; Altin *et al.*, 1998; Scheidegger *et al.*, 1998; Thompson *et al.*, 1999; Tonkin *et al.*, 2002). Middleburg and Comans (1991) studied sorption of cadmium on hydroxyapatite ($Ca_5(PO_4)_3(OH)$) where Cd adsorption displayed an initial rapid uptake followed by a relatively slow process that continued beyond 28 days. The high affinity of the hydroxyapatite surface for Cd is consistent with the enrichment of cadmium in phosphorite deposits. The Langmuir isotherm was used to model the first rapid step. The slow process may have resulted from surface precipitation and recrystallization. Middleburg and Comans used a time-dependent distribution ratio, K_d; however, this approach is based on equilibrium and does not reflect the mechanistic transient process. In addition, Koeppenkastrop and Carlo (1993) investigated rare earth element (REE), La, Sm, Ho, and Lu, uptake from solution by metal oxides. Their model development began with describing metal sorption the simplest way by assuming a one-step reversible reaction, which was inadequate as transient processes could not be ignored. This simple model did not fit experimental data successfully. They added parallel reactions and developed six different reaction paths, and then, finally obtained good fits to the experimental data. In these two examples, equilibrium could not describe sorption process and reactions kinetics was employed. However, complementary microscopic investigations are needed to support their proposed mechanisms.

Altin *et al.* (1998) used general purpose adsorption isotherm equations to fit the sorption data of Pb and Cd on both unmodified and Ca-saturated kaolinite and montmorillonite. In the case of Cd sorption, a single site Langmuir isotherm was not successful; the experimental data could be divided into two linear portions, potentially illustrating adsorption of Cd ion at the two different surfaces, kaolinite and montmorillonite. Tonkin *et al.* (2002) used the equilibrium speciation computer program PHREEQC along with the diffuse double-layer surface complexation model to simulate metals, such as Pb, Cu, As, Mo, and Sb, removal onto natural oxide particles formed during the mixing of acid rock drainage with ambient surface water. The equilibrium sorption model, with a single set of surface parameters and surface complexation constants, predicted the partitioning of Pb and Cu on iron oxides. However, they found that the use of this simple model did not work for metals like As, Mo, and Sb, and suggested there may be additional removal mechanisms that are not represented by the equilibrium model.

Bruno *et al.* (1995) experimentally studied and modeled U(VI)-$Fe(OH)_3$ surface precipitation/coprecipitation equilibrium. They differentiated the various phenomena that occur after metal ions are adsorbed onto the surface of the hydrous oxide: surface precipitation, then surface/structure diffusion, finally solid solution formation. They considered that as the diffusion in this solid matrix is a very slow process, surface precipitation is the process expected to take place at room temperature. The experiment indicated a very fast sorption of U(VI) in the amorphous Fe(III)-oxyhydroxide initially followed by a slow surface precipitation process. The model based on surface complexation was developed and resulted in a clear overestimation of the calculated

concentration of uranium in solution with respect to the measurements. They applied two alternative models by assuming another surface coordination and varying site density and obtained a better fit with experimental data. Alternatively, using spectroscopy Thompson *et al.* (1999) investigated the dynamic interactions of mineral dissolution, cation surface adsorption, and precipitation in an aging Co(II)-clay-water system. Long-term Co(II) sorption experiments were continued for up to 7,000 h, during which time samples were collected periodically. The two-step uptake was described as surface adsorption rapidly occurring initially followed by precipitation of cobalt hydrotalcite during most of the 7,000 h. The rate varied considerably with the availability of dissolved Al. Surface precipitation was the rate-limiting process and equilibrium could not describe the mechanism. Therefore, non-equilibrium models are needed to describe the phenomenon.

Scheidegger *et al.* (1998) also conducted short-term and long-term Ni sorption studies on clay and aluminum oxide minerals to determine the sorption mechanisms. Their studies are not solely based on a macroscopic analysis, but combine kinetic and spectroscopic investigations, X-ray Absorption Fine Structure (XAFS) measurements. The experiments showed that the Ni sorption kinetics strongly depend on the mineral surface present. For the Ni/pyrophyllite system, Ni uptake is nearly completed within 24 h; for the Ni/gibbsite and Ni/montmorillonite systems the uptake reactions were much slower where 1-2 months were required until most of the Ni was removed from solution. The XAFS analysis revealed that as the reaction time increased, the number of Ni second-neighbor (N) atoms increased in all sorption systems, suggesting the continuous growth of a mixed Ni/Al hydroxide phase. Roberts *et al.* (1999) monitored the effect of time of Ni sorption to soil clay at pH 6.0, 6.8, and 7.5. Sorption increased as a function of

time. Specifically, at pH 6.8, Ni sorption proceeded quite rapidly initially within 10 h, followed by a more gradual sorption period of 800 hours. The kinetics at pH 7.5 were characterized by an extremely rapid initial step occurring over 12 h, then by a much slower sorption region where Ni was nearly completely removed from solution within 200 hours. These phenomena clearly demonstrate that kinetics is important. Based on the review above, equilibrium models alone cannot accurately simulate sorption, and non-equilibrium models are indeed needed.

During local microscopic mass transfer in sorption, which refers to movement of solute under the influence of molecular or mass distribution by its chemical gradient, research shows that film diffusion (Sparks, 1995; Jackman *et al.*, 2001), intraparticle diffusion (Fuller *et al.*, 1993; Papelis *et al.*, 1995; Trivedi and Axe, 1999, 2000, and 2001; Scheinost *et al.*, 2001; Manju *et al.*, 2002), and surface precipitation (Middelburg and Comans, 1991; Fendorf and Sparks, 1994; Ford *et al.*, 1999; Karthikeyan *et al.*, 1999; Tompson *et al.*, 1999; Scheckel *et al.*, 2000; Waychunas *et al.*, 2002), are the potential rate-limiting steps in sorption. Film diffusion involves transport of metal ions through a boundary layer of film that surrounds the particle surface. Intraparticle diffusion involves transport of ions along pore-wall surfaces and/or within the pores of microporous sorbents. As the amount of a metal ion sorbed on a surface increases to some maximum or limiting surface coverage, a surface precipitate may form (Sparks, 1995).

Film diffusion and intraparticle diffusion are rate-limiting processes under different circumstances. Axe and Anderson (1998) examined the hydraulic regime along with the adsorbate diffusivity and estimated the Biot number (Bi), which is the ratio of external to internal mass transfer. They concluded that external film mass transfer is not

an important resistance for systems when intraparticle diffusivities are much smaller than bulk values. Under these conditions the Biot number is greater than 1 and intraparticle diffusion controls mechanism. On the other hand, when diffusion is equal to bulk values, film diffusion becomes important in groundwater systems. In the next section, the review focuses on the intraparticle diffusion, which has been demonstrated to be a rate-limiting process in sorption by a number of researchers.

3.2 Intraparticle Diffusion

Among various sorts of sorption substrates, amorphous oxide minerals of aluminum, iron, and manganese can control the distribution of inorganic contaminants in many aquatic environments. These oxides are not only persistent in aquatic environments, but are also important adsorbents for metal ion contaminants (Jenne and Zachara, 1987; Axe and Anderson, 1995, 1998). Many studies have shown that sorption of heavy metals to hydrous oxides is a two-step process (Benjamin and Leckie, 1981; Barrow *et al.*, 1989; Fuller *et al.*, 1993; Papelis *et al.*, 1995; Axe and Anderson, 1995, 1997; Strawn *et al.*, 1998; Roberts *et al.*, 1999; Trivedi and Axe, 1999, 2000, and 2001; Scheinost *et al.*, 2001; Manju *et al.*, 2002; Axe and Trivedi, 2002; Sen *et al.*, 2002): a rapid adsorption of metal ions to the external surface is followed by slow intraparticle diffusion along the oxide micropore walls. The kinetics of the first step are quite fast where equilibrium is reached within minutes with sufficient mixing between the bulk aqueous phase and the adsorbent external surface. In the second step, the contaminant adsorbed at the surface slowly diffuses along sorption sites in the micropores of the oxide particle.

In the 1980's, Benjamin and Leckie (1981) observed that adsorption of Cd, Zn, Cu and Pb on amorphous iron oxyhydroxide was initially fast followed by a much slower second step. Barrow *et al.* (1989) studied adsorption kinetics of Ni, Zn, and Cd on goethite and concluded that the observed two-step kinetics corresponded to an initial rapid reaction followed by slow diffusion of the metal ions into goethite. Fuller *et al.* (1993) found that sorption of arsenate on hydrous ferric oxide proceeded in two steps with a fast uptake on the exterior of the aggregate and a slow uptake limited by the rate of intraparticle diffusion. Papelis *et al.* (1995) investigated cadmium and selenite adsorption on aluminum hydroxides and found that the sorption data were consistent with diffusion, assuming solute diffusion in a sphere with limited volume.

Recently, Axe and co-workers (Axe and Anderson, 1995 and 1997; Trivedi and Axe, 1999, 2000, and 2001; Axe and Trivedi, 2002) conducted series of sorption studies with Sr, Cd, Zn, and Ni on amorphous HAO, HFO, and HMO oxides. Besides adsorption edge and isotherms, they used constant boundary batch (CBC) experiments, where the bulk adsorbate concentration was maintained approximately constant for all times. They found intraparticle diffusion is an important and rate-limiting process in the sorption. In aquatic systems representative of natural environments, the internal micropore surfaces of HAO, HFO, and HMO can account for 40 to 90% of the sorption sites. Their research also demonstrated that thermodynamic and transport parameters can be predicted based on theoretical methods. Strawn *et al.* (1998) studied kinetics and mechanisms of Pb(II) sorption and desorption at the aluminum oxide-water interface. They observed that adsorption kinetics were initially fast, resulting in 76% of total sorption occurring within 15 min, followed by a slow continuous sorption reaction. There are three possible

explanations for the slow sorption: diffusion to internal sites, surface precipitation, or slow reactions with aluminol sites. They ruled out surface precipitation based on XAFS results. Consequently, slow sorption was attributed to intraparticle diffusion through micropores. They also suggested that slow reactions with aluminaol sites might occur because different types of ligand sites exist on γ-Al_2O_3 and sorption onto sites with large activation energies is possible resulting in slower kinetics.

Scheinost *et al.* (2001) measured Cu and Pb sorption as a function of ferrihydrite morphology, reaction temperature, metal competition, and fulvic acid concentration over a period of two months, in which surface diffusion was recognized as the limiting process. Manju *et al.* (2002) conducted an investigation into the sorption of heavy metals, including Pb, Hg, and Cd, from wastewater by polyacrylamide-grafted iron (III) oxide. Intraparticle diffusion of metal ions through pores in the adsorbent was shown to be the rate-limiting step. Sen *et al.* (2002) studied kinetics and adsorption of Cu and Ni metal ions from their aqueous solutions on iron oxide, kaolin, and sand. Their kinetic experiments indicated that the adsorption of Cu and Ni metal ions on oxides is a two-step process: a rapid adsorption of metal ions to the external surface is followed by potentially slow intraparticle diffusion in the interior of the particles. They reported that in the case of kaolin, intraparticle diffusion occurs through the space between the lattice layers; while in the case of iron oxide, it occurs in the micropores of the oxide particles.

Based on previous studies, intraparticle diffusion of heavy metals on hydrous oxides is a critical step in sorption and plays an important role in fate and transport of metal contaminants in subsurface environments. Thus, realistic transport models should consider this diffusion process, as models that often employ either equilibrium or reaction

rate approaches (e.g., Gerard *et al.*, 1998; Yabusaki *et al.*, 1998; Clement, 2003) are inadequate for describing metal mobility in subsurface environments where amorphous oxides or oxide coatings are present (e.g., Gallo *et al.*, 1998; Baverman *et al.*, 1999; Zheng and Wang, 1999). In the following section, a review of applying sorption processes in existing solute transport modeling is presented.

3.3 Sorption Process in Solute Transport Modeling

A comprehensive review on groundwater flow and transport models is provided in the next chapter. In this section, sorption processes in existing solute transport modeling are reviewed.

Mangold and Tsang (1991) give a thorough summary of solute transport models developed during the 1970's and 1980's. Most of them simulate sorption processes based on the local equilibrium assumption, such as Groundwater Package (Marlon-Lambert, 1978), KONBRED (Konikow and Bredehoeft, 1978), GWTHERM (Runchal *et al.*, 1979), SHALT (Pickens and Grisak, 1979), MAGNUM 2D-CHAINT (Baca *et al.*, 1981), CFEST (Gupta *et al.*, 1982), FTRANS (GeoTrans, 1982), PORFLOW (Runchal, 1985), SWIFT II (Reeves *et al.*, 1986), HST3D (Kipp, 1987), and NEFTRAN (Longsine *et al.*, 1987). In addition, some transport models do not incorporate sorption, for example, Grove/Galerkin (1977), SALTRP (Frind and Trudeau, 1980), RESTOR (Warner, 1981), and PTC (Lai *et al.*, 1986). Since 1990, solute transport models have been developed for various scenarios; however, like counterparts developed earlier, many apply a local equilibrium assumption for sorption. However, there are some models which use kinetic

approaches when the local equilibrium assumption is not valid. Further discussion regarding specific models follows.

Engesgaard and Kipp (1992) developed a one-dimensional solute transport model MST1D using finite difference techniques, which can simulate multispecies solute transport in groundwater systems, with precipitation-dissolution and oxidation-reduction reactions under local chemical equilibrium. Its equilibrium-sorption process simulation is based on the PHREEQC code (Parkhurst and Appelo, 1999) and incorporates ion exchange, diffuse-double layer, and Langmuir and Freundlich isotherms. The PHREEQC was presented in detail in Chapter 2. The MINTRAN (Walter *et al.*, 1994) applies the thermodynamic approach in modeling transport of multiple chemical substances in groundwater systems. Its sorption processes make use of MINTEQA2 (Allison *et al.*, 1991), a well-known speciation model discussed earlier. The transport module, PLUME2D accounts for advection and dispersion and does not include sorption kinetics. The mobility of potentially toxic dissolved metals, Cr, Pb, and Mn, discharged from mine tailing sources into an aquifer in northern Ontario was investigated with MINTRAN (Walter *et al.*, 1994). In the case of a 12-year old source, the model showed most metals were immobilized through precipitation, where the groundwater was expected to meet drinking water standards without costly remediation measures. The accuracy of this model remains to be investigated. The 3D-HYDROGEOCHEM (Cheng and Yeh, 1998) and its precursor HYDROGEOCHEM (Yeh and Tripathi, 1991) are coupled models of subsurface flow, heat transfer, and reactive chemical transport. The sorption process is dealt with by ion-exchange, the Langmuir isotherm, surface complexation, and triple-layer models where local equilibrium is assumed. Cheng and Yeh (1998) emphasized that

sorption processes could be simulated more adequately by incorporating chemical kinetics into 3DHYDROGEOCHEM model, which they proposed is the first task needed in improving the model.

Many significant groundwater pollution problems involve complex reactive mixtures of inorganic and organic pollutants, such that of the co-disposal of a radionuclide and organic ligands, in a metal oxide-coated sand aquifer. The FEREACT (Tebes-Stevens *et al.*, 1998) is a reactive transport model which handles such interacting processes. Considering the sorption processes, this code has advantages over previous models. It treats heterogeneous reactions as reaction kinetics controlled. Specifically, FEREACT was developed using a module structure so that users could define the reactions. The subroutines for computing the rate terms are external to the code and they can be thought of as reaction modules to be added for any particular application. Although using reaction kinetics would not accurately describe intraparticle diffusion, the model does attempt to include transient processes. The FEREACT has been applied to simulate the migration of a radionuclide, ^{60}Co, and an organic ligand, EDTA, through a sandy aquifer. The BIORXNTRN (Hunter *et al.*, 1998) is another reactive transport model which was developed for biogeochemical transport systems. Similar to FEREACT, BIORXNTRN focuses on inorganic and organic transport and microbially-driven reactions. The model incorporates kinetic descriptions for the microbial degradation pathways of organic matter; on the other hand, the treatment of heterogeneous sorption processes was kept relatively simple and only local equilibrium was applied to this process. Hunter *et al.* (1998) used BIORXNTRN to simulate the distribution of chemical species and reaction rates along flow paths in subsurface environments, in which a

pristine aquifer is contaminated by an organic-rich leachate from a landfill. The microbial oxidation of organic matter resulted in the degradation of dissolved and solid oxidants and the appearance of reduced species. They believed that the reactivity, or biodegradability, of the organic matter is shown to be a major factor governing the biogeochemical dynamics in the plume. The model predicted different distributions of the biodegradation pathways, depending on whether the organics of the leachate have uniform or variable reactivity. However, Hunter *et al.* did not consider intraparticle diffusion processes, which may affect the concentration profiles as well. Provided that this mechanism could be simulated, coupled with other biogeochemical processes, predictions would have more credibility and dependability.

The KIRMAT (Gerard *et al.*, 1998) is a 1D multi-solute mass transport system and treats multi-components in advective transport, subjected to several equilibrium-controlled dissolution and precipitation reactions. However, this model does not give much attention to the sorption process. Baverman *et al.* (1999) developed a geochemical and transport simulation tool, CHEMFRONTS, used to calculate mass transport and fluid rock interactions. This model is based on the quasi-stationary approximation which describes the evolution of geochemical processes occurring in a sequence of stationary states. The model focuses the mineral dissolution and precipitation using a kinetic expression and does not consider sorption processes in the overall mass transport. The CHEMFRONTS has been applied to predict geochemical transformations in unsaturated porous media in subsurface from the Aitik site in northern Sweden. They simulated the breakthrough of Cu in drainage water from mining waste and the release of dissolved Cu. Considering the many geochemical processes, pH conditions were regarded as the most

influential factor affecting the mobility of copper. The breakthrough curves showed that the peak concentration of copper was obtained between 14 and 15 years, due to the release of previously accumulated copper. In accounting for the sorption process in this model simulation, it is reasonable to predict that this will happen even later.

The MT3DMS (Zheng and Wang, 1999) superseded by RT3D (Clement, 2003) is a 3D solute transport model for simulating advection, dispersion, and chemical reaction in groundwater. Three types of adsorption isotherms, linear, Freundlich, and Langmuir, are considered. In addition, the code simulates first-order reversible reaction kinetics. Zheng and Wang (1999) applied the MT3DMS to investigate the effectiveness and performance of various remedial scenarios for a 1,2-dichloroethane plume. The unconfined aquifer consisted of an upper zone of fine and medium grain sands and a lower zone of medium sands. For sorption, they compared the linear isotherm to a first-order reaction kinetics expression and while the equilibrium assumption was inadequate, a first-order reaction was also unsuccessful in addressing the transient process(es). Studies with real and model systems emphasize that contributions from slower processes should be included together with equilibrium models for accurately depicting contaminant sorption processes.

Based on the review of existing solute transport models, either equilibrium models or reaction rate approaches are often employed for describing metal sorption processes. However, many studies have demonstrated that intraparticle diffusion is an important and rate-limiting process in the sorption, which needs to be considered in realistic solute transport modeling. In the next chapter, groundwater flow and solute transport models will be reviewed for addressing macroscopic transport in developing a

comprehensive evaluation of contaminant transport and fate. Transient processes can then be simulated and incorporated into the selected model for accurately depicting metal contaminant mobility.

CHAPTER 4

GROUNDWATER FLOW AND TRANSPORT MODELING

Numerical simulation in space and time is an established method in hydrological transport studies. Different codes address different aspects of fluid flow and mass transport. Flow of groundwater is governed by the principles of conservation of mass and momentum. Conservation of mass for the fluid is expressed as the equation of continuity, and the conservation of momentum is expressed in the Navier-Stokes equation. Microscopic movement through pores and fractures may be averaged over a sufficiently large volume of the medium to obtain a macroscopic description of the flow. Solute transport is governed by the conservation of mass and the processes of advection, molecular diffusion, and kinematic dispersion. Advection describes the movement of solutes carried by groundwater flow. The process of molecular diffusion is the spread of the solute molecules throughout the fluid by virtue of their kinetic motion. Kinematic dispersion (diffusion imposed on advection) is the spreading of solute due to the heterogeneity of the microscopic velocities in the motion of the fluid (Mangold and Tsang, 1991). This chapter is focused on a review and evaluation of existing groundwater flow and solute transport models, one of which is proposed for addressing macroscopic solute transport and incorporation of mechanistic transport processes such as intraparticle diffusion.

4.1 Background

The use of hydrological transport models is prevalent in the field of environmental science and engineering. Models have been applied to investigate a wide variety of hydrogeologic conditions and are being applied to predict the fate and transport of contaminants for risk evaluation. In this section, background of groundwater flow and solute transport models is reviewed with the objective of selecting one for incorporation of intraparticle diffusion.

A groundwater flow model is intended to calculate the bulk rate and direction of groundwater through aquifers and confining units in the subsurface. These calculations are referred to as simulations. The simulation of groundwater flow requires a thorough understanding of the hydrogeologic characteristics of the site. The hydrogeologic investigation should include complete characterization, such as thickness of aquifers and confining units, hydrologic boundaries, hydraulic properties, distribution of hydraulic head, and distribution and magnitude of groundwater recharge, pumping, or leakage to or from surface water bodies. These characteristics may be constant or may change with time. The output from model simulations is the hydraulic heads and groundwater flow rates which are in equilibrium with the hydrogeologic conditions defined for the modeled area. The model can also be used to simulate possible future changes to hydraulic head or groundwater flow rates as a result of changes in characteristics of the aquifer system. Overall, hydraulic head gradients and hydraulic conductivity determine the direction and magnitude of groundwater flow (MIDEQ, 2001).

A transport model simulates the movement of a solute via groundwater. As mentioned previously, the transport of solutes is a process governed by the principle of

conservation of mass and the processes of advection, molecular diffusion, and kinematic dispersion. Transport models require the development of a calibrated groundwater flow model. In addition to a thorough hydrogeological investigation like in groundwater flow modeling, the simulation of solute transport processes requires further characterization, such as boundary conditions for the solute, initial distribution of solute, location, history and mass loading rate of chemical sources or sinks, effective porosity and soil bulk density, and longitudinal and transverse dispersivity (MIDEQ, 2001). Output from the model simulations are contaminant concentrations that exist in the groundwater flow system under the geochemical conditions defined for the modeled area.

Transport models describe the groundwater flow and fate using mathematical equations based on certain simplifying assumptions. The governing hydrological equations are briefly presented as follows. For a more in depth discussion, Mangold and Tsang (1991) and Yeh and Tripathi (1989) provide excellent reviews and illustrations.

4.1.1 Flow Equations

As discussed previously, the flow of groundwater is governed by the principles of conservation of mass and momentum; the conservation of mass for the fluid is expressed as the equation of continuity, and the conservation of momentum is expressed in the Navier-Stokes equation for the flow of a compressible fluid. To obtain a macroscopic description of the flow in terms of measurable attributes of the fluid and the rock matrix, the microscopic movement through the subsurface may be averaged over a sufficiently large volume of the medium. Darcy's law is a macroscopic equation of motion for the flux of a unit mass of fluid, v (L/T), flowing relative to the rock under the fluid potential (mechanical energy per unit fluid mass) (Hubbert, 1940).

$$v = -\frac{k}{\mu} \cdot (\nabla p - \rho g \nabla z) = -K \cdot \nabla h \tag{4.1}$$

where k is the permeability tensor (L^2); μ is the dynamic viscosity of the fluid (M/LT); ∇ is the gradient operator; p is the fluid pressure (M/LT^2); ρ is the fluid density (M/L^3); g is the acceleration due to gravity (L/T^2); z is vertical distance (L) above a datum level (positive upward); K is the hydraulic conductivity tensor (L/T); and h is the total head (L). Darcy's law describes a linear relationship between groundwater flow and the hydraulic gradient, which holds under a broad range of conditions common in hydrogeological environments.

The equation of continuity (mass conservation) for the fluid is

$$\nabla \cdot (\rho v) + \frac{\partial}{\partial t}(\rho \phi) + \rho Q = 0 \tag{4.2}$$

where t is the time (T); ϕ is the porosity of the medium (dimensionless, $0 \le \phi \le 1$); and Q is a prescribed source or sink of volumetric fluid flow (positive for fluid withdrawn) per unit volume (1/T). The equation applies either to a porous medium ($\phi < 1$) or a fracture ($\phi \approx 1$); it describes the rate of accumulation of fluid mass within a given volume of the medium and accounts for transient effects from changes in storage, due to the compressibilities of both the rock matrix, α (LT^2/M), and the fluid, β (LT^2/M). The effect of the second term in Equation 4.2 may be written as $S_s(\partial h / \partial t)$, where $S_s = \rho g(\alpha + \phi\beta)$ is the coefficient of specific storage (1/L) that describes the volume of fluid released from storage under a unit decline in hydraulic head.

The governing equation of groundwater flow may thus be derived from the equation of continuity by expanding the first term of Equation 4.2 and assuming terms

involving changes in fluid density ($\nu \cdot \nabla \rho$) to be negligible when compared to terms involving changes in velocity ($\rho \nabla \cdot \nu$) over the volume of a spatial mesh element. Now, substituting Darcy's law for ν and the specific storage term for $\partial(\rho\phi)/\partial t$, the governing equation may be given as

$$-\nabla \cdot \nu = \nabla \cdot (K \cdot \nabla h) = \frac{\partial}{\partial x}\left(K_x \frac{\partial h}{\partial x}\right) + \frac{\partial}{\partial y}\left(K_y \frac{\partial h}{\partial y}\right) + \frac{\partial}{\partial z}\left(K_z \frac{\partial h}{\partial z}\right) = S_s \frac{\partial h}{\partial t} + Q \qquad (4.3)$$

This is an equation describing the transient flow of groundwater as a function of hydraulic head in the presence of fluid sinks or sources in an anisotropic saturated medium. Steady state exists when $\partial h / \partial t = 0$. Many simplifications are possible, and various models use the above equation at steady state $(\partial h/\partial t = 0)$ or with isotropic media $(K_x = K_y = K_z = K)$. However, there is an increasing trend for models to retain the full generality in order to accurately simulate complex hydrogeological environments.

4.1.2 Solute Transport Equations

The transport of solutes is a process governed by the principle of conservation of mass and the processes of advection, molecular diffusion, and kinematic dispersion. The governing equation of solute transport is given by:

$$\nabla \cdot (\nu C_j) - \nabla \cdot (D \cdot \nabla C_j) = \phi \frac{\partial C_j}{\partial t} + Q_{c_j} \qquad j = 1 \cdots, N_c \qquad (4.4)$$

where ν is the Darcian flow velocity (L/T) from Equation 4.1; C_j is the volumetric concentration of the jth substance (M/L^3); D is the dispersivity tensor (L^2/T); ϕ is the porosity; Q_c is a source/sink term (M/L^{3}T); and N_c is the number of independent chemical entities. The first term describes transport of substance j due to advection, and

the second term gives transport due to hydrodynamic dispersion (including diffusion). Together they yield the change in flux. The microscopic balances addressing sorption and other chemical reactions in solute transport will be illustrated in the next section.

This section reviewed groundwater general flow and transport equations, which are used to set up the hydrological solute transport models. By mathematically representing a hydrogeological system, reasonable alternative scenarios can be predicted, tested, and compared. The applicability or usefulness of a model depends on how closely the mathematical equations approximate the physical system being modeled. In order to evaluate the applicability or usefulness of a model, it is necessary to have a thorough understanding of the physical system and the assumptions embedded in the derivation of the mathematical equations. In the next section, transport model evaluation will be presented with recommendations for use in addressing transient processes.

4.2 Review and Evaluation of Groundwater Flow and Transport Models

There are many transport models existing as commercial products, and some models are available in the open literature. Tables 4.1 and 4.2 show a relatively comprehensive model list. Among them, transport models reviewed and evaluated were chosen on the basis of four criteria: (1) models are in the open literature or commercial products with full descriptions and complete documentation; (2) models have been verified, validated, and are updated; (3) models not only have been applied to specific field problems, but also can deal with other circumstances; and (4) models are fully maintained and supported by organizations. Based on the above criteria, six models, WinTran (ESI, 2002), FLOWPATHII (Waterloo Hydrogeologic, 2002), Visual MODFLOW (Visual

Table 4.1 Transport and Integrated[a] Models

Category	Model (Transport module)	Property	Reference
Transport	SARIP	1D	Thiez and Lemonnier (1990).
	PLUME2D	1, 2D	Walter *et al.* (1994).
	TOUGH2^{w}	1, 2, 3D	Pruess (1991).
Integrated	BIORXNTRN	1D	Hunter *et al.* (1998).
	CHEMFRONTS	1D	Baverman *et al.* (1999).
	CHEQMATE	1D	Cross *et al.* (1991).
	CHMTRNS	1D	Noorishad *et al.* (1989).
	DIAPHORE (SARIP)	1D	Gallo *et al.* (1998).
	DYNAMIX	1D	Liu and Narashimhan (1989).
	FEREACT	1, 2D	Tebes-Stevens *et al.* (1998).
	HYDROGEOCHEM	1D	Yeh and Tripathi (1991).
	3DHYDROGEOCHEM	1, 2, 3D	Cheng and Yeh (1998).
	KIRMAT	1D	Gerard *et al.* (1998).
	MCTRACKER	1, 2, 3D	Yabusaki *et al.* (1998).
	MINTRAN (PLUME2D)	1, 2D	Walter *et al.* (1994).
	MST1D	1D	Engesgaard and Kipp (1992).
	PHREEQC	1D	Parkhurst and Appelo (1999).
	RAFT	1, 2, 3D	Chilakapati *et al.* (2000).
	TOUGHREACT (TOUGH2^{w})	1, 2, 3D	Xu *et al.* (1999).
	XT	1, 2D	Bethke (1997).
	A solute transport model	1, 2D	Runkel *et al.* (1996).

[a] Integrated refers to transport, speciation, and biodegradation.

Table 4.2 Transport Models (Commercial Products)

Name	Property	Price	Distributor (Company)
3DFEMFAT	3-D finite-element model of flow and transport	$1,000	Scientific Software Group
AQUA3D	3-D groundwater flow and contaminant transport model	$900	Scientific Software Group
AT123D	3-D long-term pollutant fate and migration in groundwater model	$495	Scientific Software Group
BIOF&T 2-D/3-D	Biodegradation, flow and transport model	BIOF&T 2-D - $ 950; BIOF&T 3-D (includes 2-D) - $ 1,900	Scientific Software Group
FLOWPATH II	2-D groundwater modeling including contaminant transport	Academic 5 User License, 1 Set Manuals $442.50	Rockware Inc.
GMS	3-D groundwater flow and transport modelling	Academic License $2,990	Environmental Modeling Systems, Inc.
Groundwater Vistas 3.0	3-D groundwater flow and transport modelling	Single license- standard version $900.00 Single license- advanced version $1,425.00	Rockware Inc.
HYDROGEOCHEM	2-D hydrologic transport and geochemical reaction model	$1,500	Scientific Software Group
HYDROGEOCHEM 2	2-D reactive multispecies multicomponent chemical transport model	$5,000	Scientific Software Group
MOC	2-D solute transport and dispersion in ground water	MOC Report/Doc (Original & Modification): $20 MOC:$300; MOCGRAF: $250; MOCTIME: $250; all Three Programs - $ 700	Scientific Software Group
MODFLOW-SURFACT 2.2	3-D flow and contaminant transport modeling	Academic Single License $2,188.75	Rockware Inc.

Table 4.2 Transport Models (Commercial Products) (Continued)

SOLUTRANS	3-D solute transport modeling	Academic single license: $195.00	Rockware Inc.
Visual MODFLOW	3-D groundwater flow and contaminant transport	MODFLOW, MODPATH, MT3DMS, and RT3D: $990.00	Rockware Inc.
Visual MODFLOW Pro	3-D groundwater flow and contaminant transport modeling	Academic 5 user license (includes Visual MODFLOW, 3D Explorer and WinPEST): $1,490.00	Rockware Inc.
WinTran	2-D groundwater flow and contaminant transport model	Single License $540.00	Rockware Inc.

MODFLOW Pro) (Waterloo Hydrogeologic, 2002), Groundwater Vistas (GV) (ESI, 2002), HYDROGEOCHEM 2 (Yeh and Salvage, 1997), and GMS (Groundwater Modeling System) (BYU, 2002) were selected for further review in this chapter.

In the following sections, background and descriptions of the above models are presented. Model evaluation is then discussed. Finally, the recommended transport models are provided for use in this research.

4.2.1 WinTran

WinTran is a 2D groundwater flow and contaminant transport model, which couples the steady-state groundwater flow model from WinFlow (ESI, 2002) with a contaminant transport model. Both WinFlow and WinTran are developed by ESI (Environmental Simulation International, Inc.). The transport model is an embedded finite-element simulator, which is constructed automatically by the software but displays numerical criteria to allow the user to avoid numerical or mass balance problems. In this model, contaminant mass may be injected or extracted using any of the analytic elements, including wells, ponds, and linesinks. WinTran displays both head and concentration contours, and concentration may be plotted versus time at selected monitoring locations. This model can (1) simulate steady-state flow and transient transport in confined and unconfined aquifers; (2) simulate effects of wells, linesinks, ponds, and constant concentration sources; (3) display mass balance error during simulation; (4) contour concentration at user-specified time steps during simulation; and (5) compute velocities either analytically or using the finite-element flow model (ESI, 2002).

4.2.2 Visual MODFLOW

Visual MODFLOW is a 3D groundwater flow and contaminant transport model. Visual MODFLOW was first released in August 1994 by Waterloo Hydrogeologic, Inc. and is currently being used by over 3,000 consultants, regulators and educators worldwide (Guigual and Franz, 2002). In addition, it is the featured software package in many continuing education courses offered around the world (Guigual and Franz, 2002). Visual MODFLOW is based on MODFLOW (Harbaugh *et al.*, 2000) with an incorporated contaminant transport model. MODFLOW is the U.S. Geological Survey (USGS) modular 3D finite difference groundwater flow model that was first published in 1984 by USGS (McDonald and Harbaugh, 1984). It has a modular structure that allows it to be easily modified to adapt the code for a particular application. Many new capabilities have been added to the original model. Further discussion about the MODFLOW model will be provided in Section 4.2.7.

The Visual MODFLOW interface has been specifically designed to increase modeling productivity and decrease the complexities. Three modules control the program: the input, the run, and the output modules. When opening or creating a file, the code switches between these modules to build or modify the input parameters, run the simulations, and display results (Waterloo Hydrogeologic, 2002). Recently, Visual MODFLOW Pro has been further developed to combine the standard Visual MODFLOW package with WinPest (Waterloo Hydrogeologic, 1999) and the Visual MODFLOW 3D-Explorer. WinPEST is a Windows version of the PEST program (Water Numerical Computing, 2000), which is a model-independent parameter estimator. With its inversion engine, WinPEST sets bounds on parameters while minimizing the discrepancy between

model results and field observations and has achieved good results in the calibration of large and complex models (Waterloo Hydrogeologic, 2002). The Visual MODFLOW 3D-Explorer is a built-in 3D visualization system for displaying and animating Visual MODFLOW models using 3D graphics technology.

4.2.3 Groundwater Vistas

Groundwater Vistas (GV), developed by ESI (Environmental Simulation International, Inc.), is a sophisticated Windows graphical user interface for 3D groundwater flow and transport modeling. Groundwater Vistas incorporates MODFLOW, MT3D (Zheng, 1990), and MODPATH (Pollock, 1994), and supports PEST and UCODE (Poeter and Hill, 1998), both of which are model-independent calibration software tools.

Calibration is one of the most complex parts of applying groundwater models. Groundwater Vistas has advantages over other models and can assist model calibration in four ways: (1) calibration statistics for head, drawdown, concentration, or flux; (2) automated parameter sensitivity analysis; (3) automatic model calibration using a nonlinear least-squares technique built into the GV interface; and (4) support for the PEST model. The sensitivity analysis tests the model parameters or boundary conditions where the resulting effect on model calibration statistics is observed. By producing a series of simulations with different values for a single model parameter, the model demonstrates how a parameter may be modified in order to achieve a better calibration. This analysis is a tedious process because many simulations are required for each parameter and there are often many parameters to analyze. GV provides an automated way of performing a sensitivity analysis that improves the process. In 2002, an advanced

version of Groundwater Vistas was released by ESI, called Stochastic MODFLOW (ESI, 2002). The changes include Monte Carlo simulations that can be launched directly from GV and hydraulic conductivity can use geostatistical simulation results.

4.2.4 FLOWPATHII

The FLOWPATH was first released in 1989 by Waterloo Hydrogeologic, Inc. At that time, it was an integrated groundwater flow and pathline modeling software package. FLOWPATH II for Windows, the latest version of FLOWPATH, is the 2D groundwater model and includes contaminant transport, which has graphical display for flexibility and control (Waterloo Hydrogeologic, 2002).

The FLOWPATH II uses a finite difference modeling scheme to simulate confined, leaky, or unconfined flow in both heterogeneous and anisotropic porous media with spatially varying thickness and/or bottom elevation. The program can account for multiple pumping and injection wells; spatially variable groundwater recharge and evapotranspiration; variable leakage characteristics of underlying and overlying aquitrads, ditches and drains; and interaction between groundwater aquifers and surface water bodies. The program will also perform a water balance to check how well solutions converged. The model: (1) imports all previous FLOWPATH model files; (2) provides grid rotation over the site map; (3) includes an expandable model domain; (4) has fully object-oriented wells, properties and boundary conditions; (5) allows for cell-by-cell anisotropy for hydraulic conductivity properties; (6) applies customizable display of contoured results, pathlines and overlay priorities; (7) plots concentration versus distance

at each output time step; and (8) animates particle tracking and contaminant transport simulations (Waterloo Hydrogeologic, 2002).

4.2.5 HYDROGEOCHEM 2

The HYDROGEOCHEM 2 is a modification of HYDROGEOCHEM 1.0 (Yeh and Tripathi, 1991), developed by Yeh and Tripathi at the Pennsylvania State University. This computer program is designed to solve coupled hydrologic transport and geochemical equilibrium problems. This modification includes replacement of chemical equilibrium subroutines by a mixed chemical kinetic and equilibrium model to deal with species whose concentrations are controlled by either thermodynamics or kinetics (The Scientific Software Group, 2002). The HYDROGEOCHEM 2 is 2D hydrologic transport and geochemical reaction model for saturated and unsaturated media. It comprises two basic modules: the transport module and the geochemical reaction module which are solved iteratively with three options: (1) a complete iteration, (2) an operator splitting, and (3) a predictor-corrector method. The transport module includes advection, hydrodynamic dispersion, and diffusion. In the geochemical reaction module, nine types of reactions are included to generate eight types of product species, such as complex, adsorbed, and precipitated ones.

The HYDROGEOCHEM 2 is reported to be flexible and versatile in modeling a relatively wide range of problems (The Scientific Software Group, 2002). Specifically, the model can: (1) treat heterogeneous and anisotropic media, (2) consider spatially and temporally-distributed as well as point sources/sinks, (3) accept the prescribed initial conditions or obtain initial conditions by simulating the steady-state version of the system

under consideration, (4) handle time-dependent fluxes over variable boundaries, (5) deal with time-dependent total fluxes over Cauchy boundaries, (6) include the off-diagonal dispersion coefficient tensor components in the governing equation for dealing with cases when the coordinate system does not coincide with the principal directions of the dispersion coefficient tensor, (7) give three options (exact relaxation, under- and over-relaxation) for estimating the nonlinear matrix, and (8) include two options (direct solution with Gaussian elimination method and successive point iterations) for solving the linearized matrix equations.

4.2.6 GMS

GMS (Groundwater Modeling System) is a comprehensive groundwater modeling software developed by Environmental Modeling Research Laboratory at Brigham Young University (BYU, 2002). GMS is a widely used package that provides tools for most groundwater simulation phases including site characterization, model development, post-processing, calibration, and visualization. GMS is the only system that supports TINs (Triangulated Irregular Networks), solids, borehole data, 2D and 3D geostatistics, and both finite element and finite difference models in 2D and 3D (EMS, 2002). Environmental Modeling System and BOSS International give a relatively comprehensive description about GMS software. Further information can be found at: http://www.ems-i.com/GMS/gms.html and http://www.bossintl.com (2004).

The GMS provides complete support for the USGS MODFLOW finite difference, MODPATH particle tracking (Pollock, 1994), MT3DMS multi-species contaminant transport (Zheng and Wang, 1999), RT3D solute transport (Clement and Jones, 2000;

Clement, 2003), the recently released SEAM3D bioremediation transport (Waddill and Widdowson, 1997), the Army Corps SEEP2D finite element (Tracy, 2002), and FEMWATER finite element groundwater models (Yeh *et al.*, 1992) (Table 4.3). Tools are provided for site characterization, model conceptualization, mesh and grid generation, geostatistics, telescopic model refinement, automated model calibration, and output post-processing. The modular design of GMS enables the user to select modules in custom combinations choosing only those groundwater modeling capabilities the user requires. GMS is composed of several modules (EMS, 2002):

(1) Map module allows the user to develop a conceptual model and a corresponding numerical model for the area being studied where boundary conditions and parameter values can then be directly assigned to these graphical entities.

(2) Grid module is used to construct both 2D and 3D Cartesian grids. These grids can be used for 3D interpolation, iso-surface rendering, cross-sections, and finite difference modeling.

(3) Finite element mesh module is used to construct both 2D and 3D finite element meshes. A variety of tools are provided for automated mesh generation and mesh editing.

(4) Subsurface characterization module is used to construct TINs (Triangulated Irregular Networks) and solid models and to display borehole data. TINs are formed by connecting a set of x-y-z points with edges to form a network of triangles. TINs can be used to represent the surface of a geologic stratum, and can be displayed in oblique view with hidden surfaces removed. Solid models of stratigraphy can also be constructed, allowing cross-sections to be cut anywhere in the model.

Table 4.3 Models Supported by GMS

Model	Function	Reference
MODFLOW	Groundwater flow	Harbaugh and McDonald (1996)
MODPATH	A particle tracking code that is used in conjunction with MODFLOW. After running a MODFLOW simulation, the user can designate the location of a set of particles. The particles are then tracked through time using the flow field computed by MODFLOW.	Pollock (1994)
MT3DMS	A modular 3D transport model for the simulation of advection, dispersion, and chemical reactions of dissolved constituents in groundwater systems.	Zheng and Wang (1999)
RT3D	A multi-species reactive transport model and modified version of MT3DMS. Numerous pre-defined reactions are available.	Clement (2003)
SEAM3D	A reactive transport model used to simulate complex biodegradation problems involving multiple substrates and multiple electron acceptors. It is based on the MT3DMS code.	Waddill and Widdowson (1997)
SEEP2D	A 2D finite element groundwater model, which is designed to be used on profile models such as cross-sections of earth dams or levees.	Tracy (2002)
FEMWATER	A 3D finite element flow and transport model. GMS supports a coupled version of the original FEMWATER model (which is for flow only) with the transport model LEWASTE.	Yeh *et al.* (1992)

4.2.7 Model Evaluation

In the previous section, background and features of six groundwater flow and transport models were presented. Among them, Visual MODFLOW (Visual MODFLOW Pro), Groundwater Vistas (GV), and GMS (Groundwater Modeling System) use the USGS MODFLOW model as the groundwater flow module and incorporate solute transport. MODFLOW-2000 (Harbaugh *et al.*, 2000) released by the USGS is the latest version of MODFLOW, which simulates steady and non-steady state flow in an irregularly shaped flow system where aquifer layers can be confined, unconfined, or a combination of confined and unconfined. Flow from external stresses, such as flow to wells, evapo-transpiration, flow to drains, and flow through riverbeds, can be simulated. Hydraulic conductivities or transmissivities for any layer may be anisotropic, and the storage coefficient may be heterogeneous. The MODFLOW was designed to have a modular structure that facilitates ease of understanding and ease of enhancing. Ease of understanding means that modelers should understand how a model works in order to use it properly. Ease of enhancement was an objective because experience showed that there was a continuing need for new capabilities (Harbaugh *et al.*, 2000).

The groundwater flow equation of MODFLOW is solved using the finite difference approximation. Because of its ability to simulate a wide variety of systems, its extensive publicly available documentation (Hill, 1992; Harbaugh and McDonald, 1996; Hill, 1998; Hill *et al.*, 2000; Harbaugh *et al.*, 2000; Mehl and Hill, 2001), and its wide application (Rhee *et al.*, 1993; Osiensky and Williams, 1996; Wang and Zheng, 1997; Lasserre *et al.*, 1999; Chu *et al.*, 2000; York *et al.*, 2000; Anderson *et al.*, 2002; Mattson *et al.*, 2002), MODFLOW is currently the most used groundwater flow model in the

USGS (Osiensky and Williams, 1996; USGS, 2002). With repect to the accuracy of MODFLOW, developers (Konikow and Harbaugh, 2002) were consulted and associated literature was reviewed (Konikow and Bredehoeft, 1992; Lasserre *et al.*, 1999; Chu *et al.*, 2000; Mattson *et al.*, 2002). Konikow and Bredehoeft (1992) illustrate that groundwater models, such as MODFLOW, cannot be validated by comparison with field data because of significant uncertainty in defining field parameters. In personal communication, Konikow (2002) stated: "The model can be made to match the field observations using any of an infinite set of combinations of values for the model parameters. This nonuniqueness makes validation with field data a fruitless exercise." On the other hand, Konikow (2002) also reported that there are many examples of successful validation studies. MODFLOW has been used as predictive tool (Rhee *et al.*, 1993; Osiensky and Williams, 1996; Wang and Zheng, 1997; Lasserre *et al.*, 1999; Chu *et al.*, 2000; York *et al.*, 2000; Anderson *et al.*, 2002; Mattson *et al.*, 2002). Lasserre *et al.* (1999) tested the GIS-model and MODFLOW on a 20-km^2 hydrogeological catchment, particularly vulnerable to agricultural nitrate pollution. The results indicated that the simulated nitrate concentrations were consistent with measured values. Because nitrate is relatively stable in the subsurface, bulk transport modeling should be sufficient in describing mobility. Therefore, Lasserre *et al.* successfully modeled the field data. Chu *et al.* (2000) applied MODFLOW to simulate pesticide transport in the subsurface and detected groundwater vulnerability to aldicarb pollution. Compared with the other analytical models, aldicarb residual concentrations in soil and in aquifer were in good agreement. Aldicarb is very soluble in water and is highly mobile in soil (Koc: 8-37); therefore, the pesticide can be modeled well by MODFLOW without considering complicated sorption mechanisms.

Mattson *et al.* (2002) studied electro-kinetic transport of acetate through an unsaturated heterogeneous soil and compared the field data with that observed in numerical modeling predictions by MODFLOW and MT3D. The model predictions using a three-layer electrical conductivity/moisture content profile were in agreement qualitatively with the observed acetate distribution.

Another important feature of MODFLOW is the ability to model 3D in the subsurface; on the other hand, models, such as WinTran, FLOWPATHII, and HYDROGEOCHEM 2, are 2D groundwater flow and transport models. Therefore, this review will focus on the three 3D models, Visual MODFLOW, GV, and GMS. The following review will critically evaluate these based on groundwater flow, solute transport, and model presentation, new versions and costs.

Groundwater Flow

As introduced previously, the three models under review incorporate groundwater flow and transport to simulate the subsurface. The groundwater flow module in the Visual MODFLOW, GV, and GMS are all based on the USGS MODFLOW model. Specifically, GMS version 3.1 and earlier Visual MODFLOW versions both use MODFLOW 96; GV supports MODFLOW 2000. Compared with the 96 version, MODFLOW 2000 is designed to accommodate two additional equations, including solute transport and equations for estimating parameters that produce the closest agreement between model-calculated heads and flows and measured values. In the earlier MODFLOW versions, two other models as extensions of MODFLOW, MODFLOWP (Hill, 1992) and MOC3D (Konikow *et al.*, 1996), were developed to solve parameter calibration and solute transport problems in addition to the groundwater flow equation. MODFLOWP solves a

MODFLOW calibration problem by using nonlinear regression to calculate values of selected input data that result in agreement between measured and model calculated values, and MOC3D uses the method of characteristics (Abbott, 1966) to solve the solute transport equation for concentration. Users can add both modules into MODFLOW 96. Therefore, MODFLOW 2000 has been developed to facilitate the addition of multiple types of equations without the complexity of selecting appropriate modules (Harbaugh *et al.*, 2000).

Environmental Modeling Systems and Waterloo Hydrogeological Inc. released GMS version 4.0 and Visual MODFLOW 3.1, both with integration of MODFLOW 2000. For calibration tools, GMS supports two other models, PEST and UCODE. The PEST is a general purpose parameter estimation utility developed by Watermark Numerical Computing (2000). The purpose of PEST is to assist in data interpretation, model calibration, and predictive analysis. The UCODE is another parameter estimation utility developed by Poeter and Hill (1998). In addition to evaluating estimated parameters, UCODE can be used to evaluate model representation, diagnose inadequate data, and quantify the likely uncertainty of model simulated values (Poeter and Hill, 1998). The objective of both PEST and UCODE is to run a model as many times as needed in minimizing the variance using least squares analysis. In Visual MODFLOW, WinPEST is a functional version of the PEST program that has been compiled and optimized to run as a Windows application.

As discussed earlier, the groundwater flow module in Visual MODFLOW, GV, and GMS is based on the USGS MODFLOW model. Currently, they all integrate MODFLOW-2000. The GMS and Visual MODFLOW have capabilities of model

calibration by UCODE, PEST, and WinPEST and also simulating solute transport, which will be addressed in the following section.

Solute Transport

The MT3DMS (Zheng and Wang, 1999) superseded by RT3D (Clement and Jones, 2000; Clement, 2003) is a solute transport model in GMS. The precursor of MT3DMS is MT3D, a 3D solute transport model for simulation of advection, dispersion, and chemical reactions of contaminants in groundwater systems. The governing equation including advection and dispersion was presented in the Section 4.1 Equation 4.4. The mass balance addresses fluid sinks/sources, equilibrium adsorption, and first-order irreversible rate reactions (Zheng and Bennett, 2002):

$$\theta R\frac{\partial S}{\partial t}=\frac{\partial}{\partial x_i}\left(\theta D_{ij}\frac{\partial S}{\partial x_i}\right)-\frac{\partial}{\partial x_i}(q_i S)+q_s S_s-\lambda_1\theta S-\lambda_2\rho_b C \tag{4.5}$$

where the retardation factor is defined as

$$R=1+\frac{\rho_b}{\theta}\frac{\partial C}{\partial S} \tag{4.6}$$

and S is the dissolved concentration (M/L^3); C is the sorbed concentration (M/M), a function of the dissolved concentration S, as defined by a sorption isotherm; q_i is the Darcy velocity (L/T); D_{ij} is the dispersion coefficient tensor (L^2/T); q_s is the flow rate of a fluid source or sink per unit aquifer volume (1/T); S_s is the concentration of the fluid source or sink flux (M/L^3); λ_1 is the reaction rate constant for the dissolved phase (1/T); λ_2 is the reaction rate constant for the sorbed phase (1/T); θ is the porosity; and ρ_b is the bulk density of the porous medium (M/L^3). If local equilibrium cannot be assumed for

the adsorption process, Zheng and Bennett (2002) use a first-order reversible kinetic expression to represent the sorption process.

The MT3D was first developed by Zheng (1990) with partial support from the U.S. EPA. Since 1990, MT3D has been available in the pubic domain from the U.S. EPA. MT3D is based on a modular structure to permit simulation of transport components independently or jointly. The MT3DMS is the enhanced version that retains the modular structure of the original code and is used in conjunction with MODFLOW in a two-step flow and transport simulation. Heads and flux terms are computed by MODFLOW on a cell by cell basis during the flow simulation and are written to a formatted file. This file is then read by MT3DMS and utilized as the flow field for the transport portion of the simulation. The MT3DMS differs from MT3D in that it has multi-species structure for accommodating add-on reaction packages, supports additional solvers, and allows for cell by cell input of all model parameters.

The RT3D is a multispecies reactive transport model developed by the Battelle Pacific Northwest National Laboratory (Clement and Jones, 2000; Clement, 2003); it employs a set of chemical reaction packages including BETX (benzene-toluene-xylene mixture) degradation, sorption of organics, a double-monod model, sequential decay, and aerobic/anaerobic model for PCE (tetrachloroethene)/TCE (trichloroethene) degradation. In GMS, RT3D also allows the user to define reactions that are not pre-defined. The user-defined reaction packages can be created by two approaches: the dynamically linked library option and the linked subroutine option (Clement and Jones, 2000). The user can predict reactions and build a set of partial differential equations, then code their own functioning part. The functioning part can be linked to RT3D and executed when RT3D

is launched. This feature gives the user more flexibility to build their model to simulate different scenarios. In addition, Environmental Modeling System hosts training courses annually to present instructions for using RT3D with GMS. This is another important advantage for users.

Like GMS, GV and Visual MODFLOW both have transport modules, MT3DMS and RT3D. Although general functions of MT3DMS and RT3D can be found in GV and Visual MODFLOW, neither supports the user-defined reaction packages of RT3D. Clement and co-workers (Clement and Jones, 2000; Clement, 2003), developers of RT3D, have an ongoing collaboration with GMS developers (Johnson, 2002). Therefore, GMS can simulate solute transport under more varying scenarios with greater capabilities than the two others. In the next section, model presentation, new versions, and costs of three models will be reviewed.

Model Presentation, New Versions, and Costs

Besides groundwater flow and transport, the three software described above have other important features as well. In this section, model overview, new versions, and costs will be presented.

In GMS, the map module can be used to construct a conceptual model directly on an actual site map using the GIS (Geographic Information System) object. The boundary conditions and parameter values can be assigned directly to the GIS object. This map can be defined and edited in MODFLOW at the conceptual level or on a cell-by-cell basis at the grid level (EMS, 2002). Another characteristic of GMS is that FEMWATER and SEEP2D are supported, which are finite element models to simulate flow in both the saturated and unsaturated zones. Visualization animation of transient simulation results

and transient data sets can be converted into an animation film loop. For an academic license, GMS costs $2, 990 and Environmental Modeling Systems provides free updates within a major version.

As discussed in Section 4.2.2, Visual MODFLOW Pro is the updated version of Visual MODFLOW, which has some advanced features. Among them, the Visual MODFLOW 3D-Explorer has a built-in 3D visualization system for displaying transient groundwater flow and contaminant transport modeling results. The animation tool automatically steps through the entire sequence of output time steps for the selected model parameters (heads, drawdowns, or concentrations). Other features include automated model calibration using WinPEST and natural attenuation by RT3D. The natural attenuation by RT3D includes BETX degradation, sequential decay, aerobic/anaerobic degradation, and rate-limited sorption represented by a first-order reversible reaction. Visual MODFLOW costs $1,490 for academic license and the user is charged for model upgrades. Groundwater Vistas also has its advanced version, Stochastic MODFLOW. The new features of this model are that Monte Carlo simulations for model parameters may be launched directly from GV and hydraulic conductivity can use geostatistical simulation results. For this advanced version and single license, GV costs $1,425 and the updates of GV are free within the major version.

4.2.8 Model Recommendation

In the previous section, the three models were evaluated, GMS, GV, and Visual MODFLOW (Pro) with respect to groundwater flow, transport, and model presentation, new versions, and costs (Table 4.4). In all models, groundwater flow is based on the

USGS MODFLOW, and currently, they all integrate the MODFLOW-2000, which is designed to accommodate two additional equations compared with MODFLOW 96, including solute transport and equations for estimating parameters that produce the closest agreement between model-calculated heads and flows and measured values.

The MT3DMS and RT3D are two solute transport models incorporated by all three models. Most functions of the two transport models can be found in GMS, GV, and Visual MODFLOW. The only advantage provided by GMS over the others is that the user-defined reaction subroutine can be linked and automatically launched with the RT3D package. Therefore, GMS gives users more flexibility for building their model to simulate various scenarios. The GMS also includes finite element models, FEMWATER and SEEP2D, to simulate flow in the saturated and unsaturated zones, the map module using GIS objects, and visualization animation of transient simulation results. Visual MODFLOW provides visualization capabilities of 3D representations.

Overall, considering its extensive ability to address groundwater flow and solute transport in the subsurface, its flexibility for user modeling under various scenarios, and its comprehensive model presentation, GMS is recommended as the transport routine to be linked with other functioning parts in this research.

4.3 Summary

Groundwater flow and solute transport models are used widely to help understand complex hydrogeological processes during solute transport in the subsurface. The models of reactive transport employ two basic sets of equations, flow and solute transport equations. There are many hydrological transport models available commercially, and

Table 4.4 Major Comparison with GMS, Visual MODFLOW, and Groundwater Vistas

Category	GMS	Visual MODFLOW	Groundwater Vistas
Groundwater flow	MODFOLW 2000	MODFOLW 2000	MODFLOW 2000
Solute transport	MT3DMS, RT3D; RT3D supports user-defined package	MT3DMS, RT3D; RT3D does not support user-defined package	MT3DMS, RT3D; RT3D does not support user-defined package
Model presentation and new versions	Map module construct conceptual model using GIS object; FEMWATER and SEEP2D are supported, which are finite element models to simulate flow in both saturated and unsaturated zone; Excellent visualization animation of transient simulation results; Free updated during minor upgrades.	Updated version Visual MODFLOW Pro includes Visual MODLFOW 3D-Explorer, a visualization system for viewing transient groundwater flow and contaminant transport modeling results; Automated calibration model using WinPEST; User needs to pay model update.	Updated version Stochastic MODFLOW supports the Monte Carlo model launched directly from GV; Automated model calibration using a nonlinear least-squares technique; Updates are free within a major version.

some models are in the open literature. To propose an appropriate model for solute transport in software development, groundwater flow and solute transport models were critically reviewed. After preliminary evaluation and screening, six models, WinTran, FLOWPATHII, Visual MODFLOW (Visual MODFLOW Pro), Groundwater Vistas, HYDROGEOCHEM 2, and GMS were selected for further review. The USGS code MODFLOW is currently the most widely used numerical model in the USGS for groundwater flow problems (Osiensky and Williams, 1996; USGS, 2002). Because Visual MODFLOW, Groundwater Vistas, and GMS all use MODFLOW for groundwater flow and include contaminant transport codes, these were further evaluated for groundwater flow, solute transport, model presentation, new versions, and costs. GMS is selected for its extensive ability to address groundwater flow and solute transport, its flexibility for user modeling under various scenarios, and its comprehensive model presentation.

Based on review and evaluation above, GMS will be employed as the macroscopic transport model in this research where the intraparticle diffusion process will be incorporated. This process is a critical step in sorption and plays an important role in fate and transport of metal contaminants in subsurface environments. In the next chapter, objectives, hypotheses, and the approach are overviewed.

CHAPTER 5

OVERVIEW OF OBJECTIVES, HYPOTHESES, AND APPROACH

Assessing risks associated with heavy metals to the surrounding environment and managing remedial activities requires simulation tools that depict speciation and risk with accurate mechanistic models and well-defined transport parameters. Such tools need to address the following processes: (1) aqueous speciation, (2) distribution mechanisms, (3) transport, and (4) ecological risk. The primary objective of this research is to develop a simulation tool that accounts for these processes. Speciation in the aqueous phase is a function of pH, ionic strength, and redox potential. Once the chemical form is understood, its mobility can be addressed through sorption modeling. Based on the review of geochemical equilibrium models, MINEQL+ is proposed for considering metal speciation in the aqueous phase because of its comprehensive thermodynamic database, relatively strong ability to predict activity coefficients, more options for modeling adsorption under equilibrium conditions, and user-friendly interface.

Sorption or distribution processes greatly affect metal mobility and bioavailability in aquatic and soil environments. Based on the review presented in Chapter 3, kinetics and mechanisms of metal sorption in the subsurface environments have been widely investigated. Numerous studies have demonstrated that sorption of heavy metals to hydrous Al, Mn, and Fe oxides is a two-step process: a rapid adsorption of metal ions to the external surface is followed by slow intraparticle diffusion along the oxide micropore walls. Intraparticle diffusion is the rate-limiting step. Equilibrium models for simulating the sorption process are generally found to be inadequate and transient processes are

indeed important. Nevertheless, current solute transport models often employ either equilibrium models or reaction rate approaches for describing metal sorption. Therefore, an objective of this research is to include intraparticle diffusion in addressing solute transport in macro scale codes to accurately describe metal contaminant transport and fate in the soil and subsurface environments.

Once metal distribution is addressed mechanistically, accurate bulk transport modeling is needed. An evaluation and review of existing groundwater flow and transport models in Chapter 4 resulted in identifying GMS (Groundwater Modeling System) for addressing macroscopic solute transport. The advantages of GMS over other transport models lie in its extensive ability to address groundwater flow and solute transport, the flexibility for user modeling under various scenarios, and the comprehensive model presentation. In GMS, RT3D is the reactive transport module that allows users to define reactions for different processes. The user-defined reaction packages in RT3D are amenable for linking the microscopic intraparticle diffusion with the macroscopic advection and dispersion transport in GMS. Modeling intraparticle diffusion requires balance of definition and solution given the initial and boundary conditions, code development into the RT3D reaction module, and lastly, execution of the intraparticle diffusion package within GMS.

The hypotheses for this research center on the presented modeling approach for simulating metal contaminant speciation, mobility, and bioavailability, and that this approach can be applied in conducting ecological risk assessment. Specifically

(1) Solute mobility based on transport modeling (micro- and macro-transport) can be simulated and validated through field studies and laboratory studies.

(2) Intraparticle surface diffusion can be coded into a macroscopic transport model for depicting sorption of heavy metals to microporous amorphous Al, Mn, and Fe oxides as discrete particles and coatings under variable boundary conditions.

(3) Bioavailable species can be used to assess static or dynamic ecological risks resulting from exposure to contaminants.

To address these hypotheses and the research objectives in developing mechanistic and accurate simulation tools, the approach includes first validating the slow sorption process on a system of discrete and coated minerals with the contaminant Pb (Chapter 6). Then in an effort to account for these surfaces, intraparticle diffusion is incorporated into a macroscopic solute transport code (Chapter 7) and subsequently tested on a field-scale level for the Hanford site with Sr^{90} (Chapter 8). Lastly, this research demonstrates that once the bioavailable form of a contaminant is understood, static and/or dynamic ecological risk assessments can be conducted. This phase of the research focused on depleted uranium and its presence at the Aberdeen and Yuma Proving Grounds (Chapter 9). Overall, this work contributes to applying a holistic approach to addressing contaminant transport and fate.

CHAPTER 6

MODELING Pb SORPTION TO MICROPOROUS AMORPHOUS OXIDES AS DISCRETE PARTICLES AND COATINGS

Heavy metals such as Pb released into the subsurface pose a threat to human health and the surrounding environment. Concerns about the detrimental effects have resulted in extensive research efforts to better understand processes involved in the fate and transport of these contaminants in subsurface systems. Substantial studies have shown that trace metals are strongly associated with the particulate phases in aquatic environments (Turekian, 1977; Brewer, 1975; Lion, 1982; Jackson and Inch, 1989; Dong, *et al.*, 2000; Weng *et al.*, 2001). These particulate phases are comprised of a diverse mixture of clay minerals, metal oxides, and organic matter. Therefore, the sorption of metals in natural aquatic and/or soil environments is expected to be complicated given the varying composition of the interfaces.

Amorphous oxide minerals of aluminum, iron, and manganese occur as coatings on other mineral surfaces or as discrete particles, and are persistent in aquatic environments (Jenne and Zachara, 1987; McLaren *et al.*, 1996; Stumm and Morgan, 1996; Dong *et al.*, 2000 and 2003). They have large surface areas, porous structures, and an abundance of binding sites; therefore, they have a significant impact on contaminant mobility (Jenne, 1968; Coughlin and Stone, 1995). In the sorption of heavy metals to hydrous oxides, numerous studies have demonstrated that this process is a two-step one (Benjamin and Leckie, 1981; Barrow *et al.*, 1989; Fuller *et al.*, 1993; Waychunas *et al.*, 1993; Papelis *et al.*, 1995; Axe and Anderson, 1995, 1997; Strawn *et al.*, 1998; Roberts *et al.*, 1999; Trivedi and Axe, 1999, 2000, and 2001; Scheinost *et al.*, 2001; Manju *et al.*,

2002; Axe and Trivedi, 2002; Sen *et al.*, 2002): rapid adsorption of metal ions to the external surface is followed by slow intraparticle diffusion along the micropore walls of the oxide. Benjamin and Leckie (1981) observed that adsorption of Cd, Zn, Cu, and Pb on amorphous iron oxyhydroxide was initially fast followed by a much slower second step. Barrow *et al.* (1989) studied adsorption kinetics of Ni, Zn, and Cd on goethite and concluded that the observed two-step kinetics corresponded to a fast initial adsorption reaction followed by slow diffusion of the metal ions into the goethite. Fuller *et al.* (1993) found that sorption of arsenate on hydrous ferric oxide proceeded in two steps with a fast uptake on the exterior of the aggregate and a slow uptake limited by the rate of intraparticle diffusion. Papelis *et al.* (1995) investigated cadmium and selenite adsorption on aluminum hydroxides and found uptake is controlled by intraparticle diffusion. Recently, Axe and co-workers (Axe and Anderson, 1995 and 1997; Trivedi and Axe, 1999, 2000, and 2001; Axe and Trivedi, 2002) conducted a series of sorption studies that included Sr, Cd, Zn, and Ni on amorphous HAO, HFO, and HMO. In addition to adsorption edges and isotherms, they used constant boundary condition (CBC) semi-batch experiments, where the bulk adsorbate concentration was maintained approximately constant at all times. They found intraparticle diffusion was an important and rate-limiting process in sorption. Scheinost *et al.* (2001) measured Cu and Pb sorption as a function of ferrihydrite morphology, temperature, metal competition, and fulvic acid concentration over a period of two months, in which surface diffusion was recognized as the limiting process. Manju *et al.* (2002) conducted an investigation into the sorption of heavy metals, including Pb, Hg, and Cd, from wastewater by polyacrylamide-grafted iron (III) oxide. Intraparticle diffusion of metal ions through

pores was shown to be the rate-limiting step. For porous surfaces such as Al, Fe, and Mn oxides, where the average pore size is greater than or equal to 1.9 nm (Axe and Anderson, 1995; Trivedi and Axe, 1999), the distribution falls into the IUPAC classification of micro- and meso-pores which is based on gas-solid systems. However, in the aqueous phase, pore surfaces are hydrated, resulting in potentially layers of water adsorbed to these pore walls (Karger and Ruthven, 1992). Therefore, the mesopores may act as micropores. Based on previous studies, intraparticle diffusion of heavy metals in hydrous oxides is a critical step in sorption and plays an important role in fate and transport of metal contaminants in subsurface environments.

In addition to discrete systems, many studies have also revealed that hydrous iron, manganese, and aluminum oxide coatings substantially affect sorption behavior (Levy and Tamura, 1973; Lion *et al.*, 1982; Knocke *et al.*, 1988; Edwards and Benjamin, 1989; Jackson and Inch, 1989; Van Benschoten *et al.*, 1994; Rybicke *et al.*, 1995; Lothenbach *et al.*, 1997; Naidja *et al.*, 1997; Dong, *et al.*, 2000 and 2003; Zhuang *et al.*, 2000; Papini *et al.*, 2002). For example, Levy and Tamura (1973) observed that aluminum oxide-coated montmorillonite exhibited calcium-magnesium exchange properties different from those of pure montmorillonite. Lion *et al.* (1982) found Fe/Mn hydrous oxides and organic coatings controlled Cd and Pb sorption in the South San Francisco Bay estuary. Knocke *et al.* (1988) reported in a review that Mn oxide potentially deposits on filtration media in water treatment facilities increasing Mn removal. Edwards and Benjamin (1989) found that iron oxide-coated sand had properties similar to discrete Fe oxide in removing metals over a wide pH range. Van Benschoten *et al.* (1994) observed that iron oxide surface coatings reduce metal extraction efficiency from sandy soils. Lothenbach *et al.*

(1997) showed that at pH > 6 aluminum-coated montmorillonite was more efficient in immobilizing heavy metals than untreated montmorillonite, while in more acidic soils (pH < 5), untreated montmorillonite was expected to be a dominant surface. Naidja *et al.* (1997) found tyrosinase sorption on hydroxyaluminum-montmorillonite increased with increasing coating from 1 to 5 mmol Al g^{-1} clay.

In this chapter, systematic studies were conducted to assess Pb sorption to microporous Al, Fe, and Mn oxides. Studies included long-term ones to investigate intraparticle surface diffusivities. In addition, Pb sorption on montmorillonite and HAO-coated montmorillonite was evaluated in an effort to better simulate the subsurface. Montmorillonite is one of the most prevalent clays in soils and sediments and possesses a large specific surface area (Schlegel *et al.*, 1999; Strawn and Spark, 1999). A number of studies have been conducted with montmorillonite coated with Al or Fe oxyhydroxide (Green-Pederson and Pind, 2000; Celis *et al.*, 1997; Helmy *et al.*, 1994) to simulate natural settings; however, long-term sorption processes have not been investigated to the same extent as in discrete oxide systems. Therefore, Pb sorption was investigated for HAO-coated montmorillonite and compared to that of discrete oxide systems.

6.1 Materials and Methods

Sorption studies were conducted with freshly precipitated oxides at 25 °C. All chemicals used in oxide precipitation were reagent grade and only Millipore-Q Type I deionized water was employed. All systems were prepared in carbonate-free environment by purging with N_2. HAO was synthesized according to the method described by Gadde and Laitinen (1974) and others (Anderson and Benjamin, 1990; McPhail *et al.*, 1972;

Shuman, 1977), by drop-wise addition of stoichiometric amounts of NaOH to aluminum nitrate solution which was aged for 4 h prior to the sorption experiment. Using the method detailed by Gadde and Laitinen (1974), HMO was prepared by slowly adding manganese nitrate to alkaline sodium permanganate solution. The HMO suspension was then centrifuged, rinsed, and redispersed in sodium nitrate solution at pH 7 where it was aged for 16 hours. HFO was precipitated as described by Dzombak and Morel (1986); briefly, NaOH is slowly added to $Fe(NO_3)_3$ solution. The suspension is aged with constant mixing for 4 h at a pH of 7 to 7.5. Additional details for synthesizing HAO, HFO, and HMO are described elsewhere (Axe and Anderson, 1995; Trivedi and Axe, 1999). Montmorillonite used in the study has been treated (Swy-2, Clay Mineral Society), and included removal of carbonate, iron and manganese oxides, and organic matter in accordance with Kunze and Dixon (1986) and O'Day *et al.* (1994). HAO-coated montmorillonite was prepared by drop-wise addition of an $Al(NO_3)_3$ solution to the montmorillonite suspension, which was followed by pH adjustment to 7.0 with 0.5 M NaOH. The suspension was mixed for 2 h, centrifuged, washed repeatedly with deionized water, and then freeze-dried. In an effort to assess the capacity of montmorillonite for the coating, a range of Al loadings (0.09, 0.18, 0.27, 0.54, 0.81, and 1.08 g Al g^{-1} clay) were applied. Acidic ammonium oxalate was used to extract noncrystalline aluminum oxide (Blume and Schwertmann, 1969; Dzombak and Morel, 1990); the extractant was filtered and analyzed with atomic absorption spectrometry (AA) for total Al. Based on the extraction analysis, the loading of 0.18 g Al g^{-1} montmorillonite (or 0.35 g HAO g^{-1} montmorillonite) was selected as it represents a maximum coating capacity on montmorillonite.

Characterization of the hydrous amorphous oxides, montmorillonite, and HAO-coated montmorillonite included particle size analyses (PSA) using a Beckman-Coulter LS 230 analyzer, surface area evaluation by N_2-BET (Brunauer-Emmett-Teller), and potentiometric titration to assess the pH point of zero charge (pH_{PZC}). Oxide mineralogy was characterized by a Philips X'Pert x-ray diffraction (XRD) with Ni-filtered Cu K-α radiation. Morphology of the oxides was studied by a Philips Electroscan 2020 environmental scanning electron microscope (ESEM) and a LEO 1530 VP field emission scanning electron microscope (FE-SEM). In addition, energy dispersive x-ray analysis (EDX) was used for elemental mapping of the mineral surfaces.

Two types of sorption experiments were conducted: (i) conventional short-term ones, and (ii) long-term studies designed to evaluate diffusivities. Stock solutions were tagged with ^{210}Pb; its activity in the samples of suspensions and filtrates were measured with a Beckman LS6500 multipurpose scintillation counter. Turbulent hydraulic conditions (Reynolds number > 10^4 with respect to the reactor diameter) were maintained by rapid stirring in all experiments to minimize the external mass-transfer resistance. Procedures for short-term studies involved adsorption edges and isotherms to evaluate the effect of pH, ionic strength, and concentration. A $NaNO_3$ electrolyte was used to maintain the ionic strength of solutions, which ranged from 1.0×10^{-3} to 1.0×10^{-1}. Short-term adsorption studies were conducted in 250-ml Nalgene® containers with a contact time of 4 hours. In these experiments, contact times from less than 1 to 72 h revealed no change in the amount sorbed, indicating equilibrium or pseudo-equilibrium between the lead adsorbed to external surface of the oxides and that in the bulk aqueous phase. The long-term or constant boundary condition (CBC) experiments were used to study the slow

sorption process of intraparticle surface diffusion. In these studies, the Pb ion concentration in the bulk aqueous phase was maintained approximately constant by continuously monitoring and adding adsorbate as needed (Axe and Anderson, 1995 and 1997; Trivedi and Axe, 1999). Therefore, the adsorbate concentration on the external surface of the particle was maintained constant. All aqueous concentrations of Pb were below saturation based on MINEQL+.

6.2 Results and Discussion

6.2.1 Oxide Characteristics

Earlier studies (Axe and Anderson, 1995; Trivedi and Axe, 1999) revealed discrete oxide aggregates were generally spherical with irregular topography. The coating shows increased aggregation as compared to discrete aluminum oxide and montmorillonite (Figure 6.1). An analysis for Al and Si reveals that Al appears to be more abundant on the HAO-coated montmorillonite than the montmorillonite surface; on the other hand, the coating has less Si than montmorillonite (Figure 6.2). XRD also confirms the presence of the HAO coating; although the montmorillonite structure was observed, its intensity decreased as the degree of coating increased. Furthermore, discrete HAO and montmorillonite systems have smaller modes in the particle size distribution (PSD) than the coated system (Figure 6.3). The pH_{PZC} of the HAO-coated montmorillonite is 5.0 ± 0.5 (Table 1), which is consistent with Zhuang and Yu (2002). Avena and De Pauli (1998) observed a pH_{PZC} of 8.5 for the edge sites of montmorillonite, where most of the pH-dependent charge is located (Chang and Sposito, 1996; Sposito, 1989). The difference

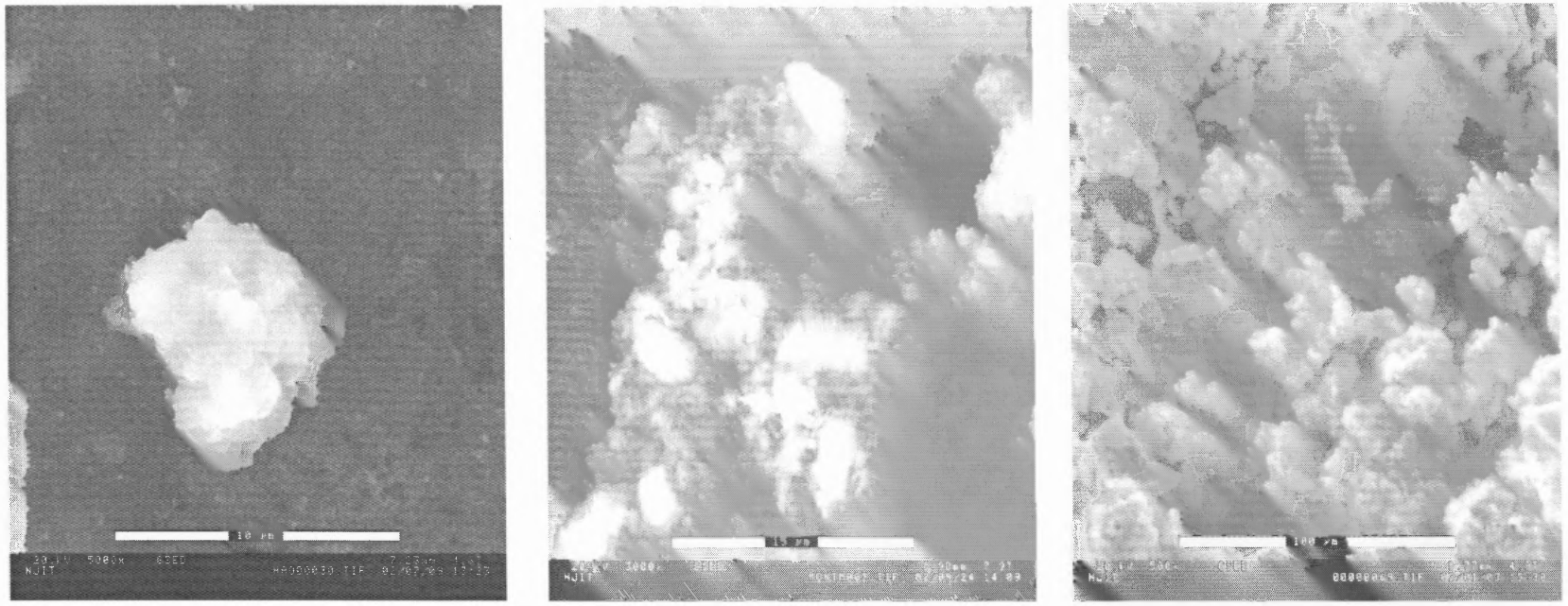

(a) HAO (b) montmorillonite (c) HAO-coated montmorillonite

Figure 6.1 SEM photographs of HAO, montmorillonite, and HAO-coated montmorillonite

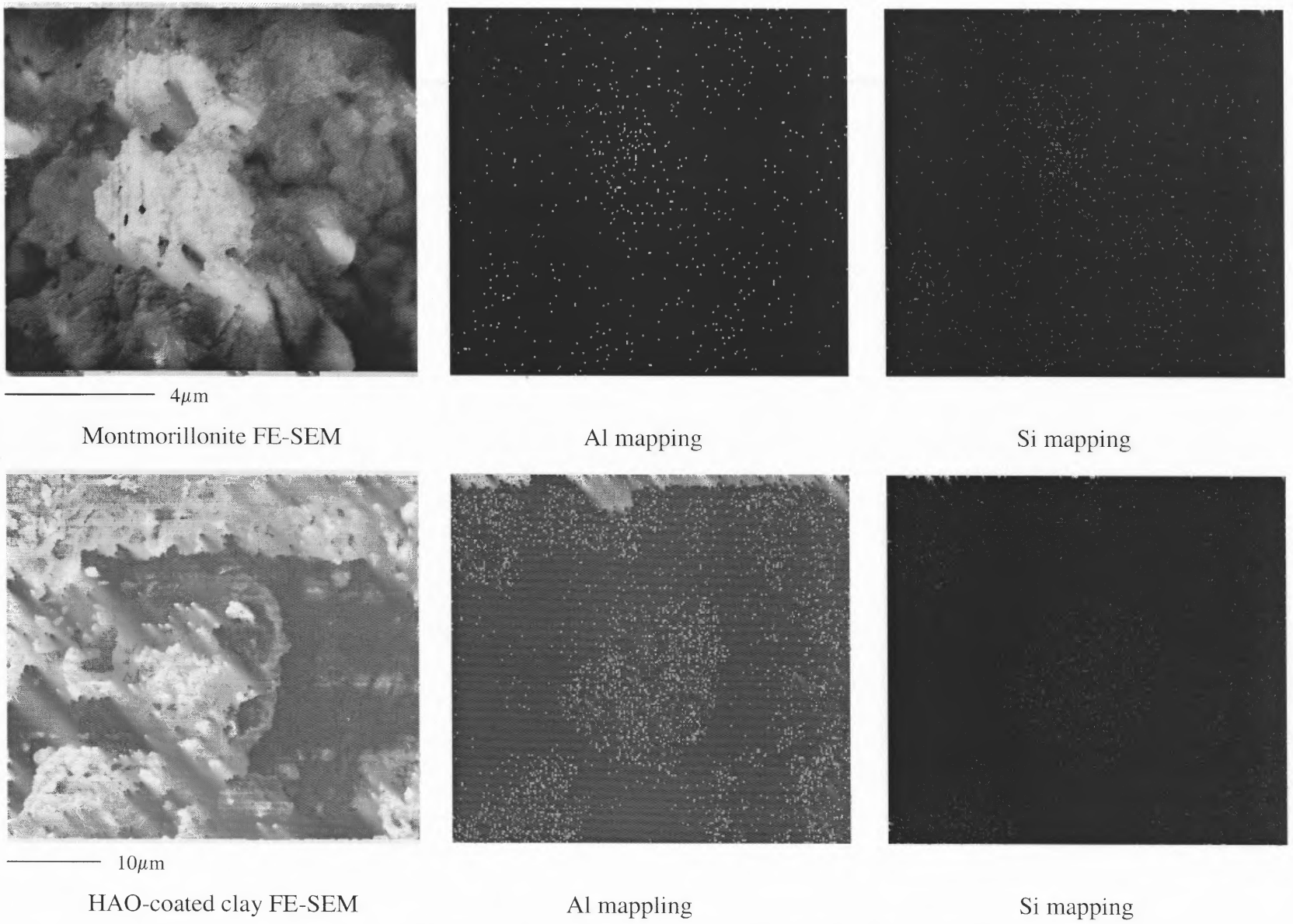

Figure 6.2 EDX mapping of silicon and aluminum on HAO-coated montmorillonite and montmorillonite

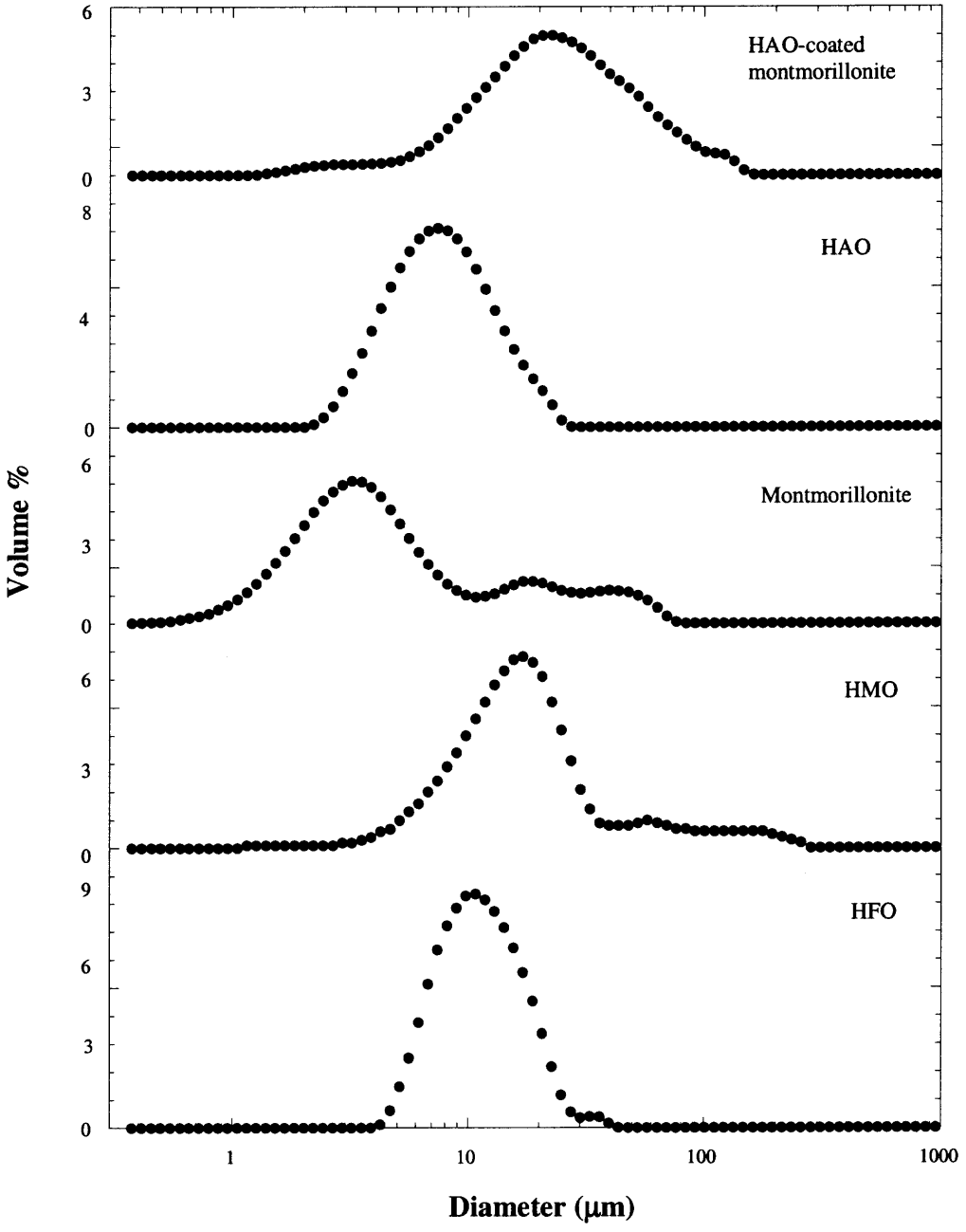

Figure 6.3 Particle size distributions of HAO, HFO, HMO, montmorillonite, and HAO-coated montmorillonite at pH 5, ionic strength 1.0×10^{-2} M with $NaNO_3$, and 25°C

Table 6.1 Characteristics of HAO, HFO, HMO, Montmorillonite, and HAO-coated Montmorillonite

Materials	Surface area ($m^2 g^{-1}$)	Porosity	Mode pore diameter (nm)	Mean diameter (μm)	Bulk density ($g\ cm^{-3}$)	pH_{PZC}	K_d (Pb adsorption) ($L\ g^{-1}$)
HAO	411 [a]	0.45	1.9	7.5	1.54	8.6 ± 0.5	8.6
HFO	600 [b]	0.50	3.8	13.0	1.75	7.6 ± 0.5	596.4
HMO	359 [a]	0.35	2.1, 6.1 (Bimodal)	19.6	1.75	2.4 ± 0.5	13253.0
Montmorillonite	27.8	0.51	12.3	8.7	1.48	4.2 ± 0.5	5742.3
HAO-coated montmorillonite	10.1	0.72	56.6	21.8	1.03	5.0 ± 0.5	324.6

[a] Based on Trivedi and Axe (1999).
[b] Based on Dzombak and Morel (1986).

between our results and others lies in that edge sites only account for less than 4% of the overall montmorillonite surface area. Given the pH_{PZC} of 8.6 for HAO and 4.2 for montmorillonite determined experimentally, montmorillonite still plays a critical role in the surface charge of the coating system; this is most likely because of the non-uniform nature of the coating, which can be observed in the FE-SEM micrograph (Figure 6.2). Other characteristics such as porosity, bulk density, and surface area are presented in Table 6.1. Montmorillonite has a large internal surface area that may not be accounted for in using N_2-BET; however, this does not significantly impact our modeling as sorption and the associated parameters were normalized to the mass present.

6.2.2 Sorption Studies

In adsorption edge experiments (Figure 6.4), for HFO there was no effect of ionic strength, suggesting Pb ions may form inner-sphere complexes with this surface, which is consistent with other studies (Swallow *et al.*, 1980; Trivedi *et al.*, 2003). Swallow *et al.* (1980) reported that sorption of Cu^{2+} and Pb^{2+} to hydrous ferric oxide was unaffected by variations in ionic strength from 0.005 to 0.5 M $NaClO_4$, or by changes in the nature of the background electrolyte from $NaClO_4$ to a complex artificial seawater mixture. Trivedi *et al.* (2003) observed that Pb sorption to ferrihydrite did not vary with ionic strength between 10^{-3} and 10^{-1} M $NaNO_3$. The adsorption edge for HAO begins at pH 4.5, a lower pH condition may result in dissolution; therefore, given the degree of adsorption, the effect of ionic strength may not be discernible. For Pb adsorption on HMO, montmorillonite, and HAO-coated montmorillonite, our results showed Pb sorption decreased with increasing ionic strength. Pb ions may form outer-sphere complexes on these surfaces. Other researchers (Trivedi and Axe, 1999 and 2000; Baeyers and

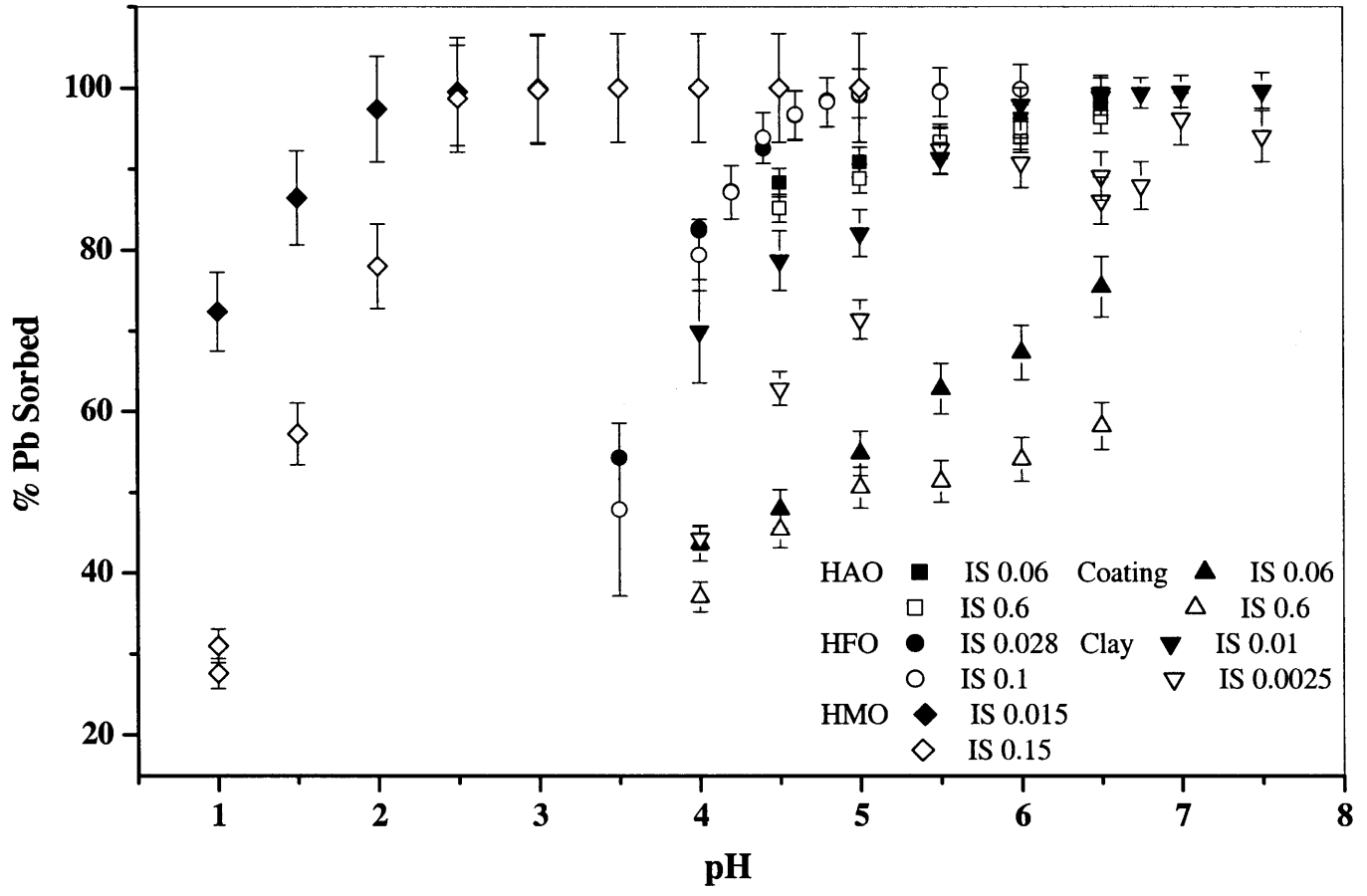

Figure 6.4 Pb adsorption edges on HFO, HMO, HAO, montmorillonite, and HAO-coated montmorillonite, at 25°C as a function of ionic strength with $NaNO_3$. For all Pb studies, the initial concentration was 10^{-5} M. HAO and HFO concentrations were 1 g L^{-1}, HMO concentration was 0.5 g L^{-1}, montmorillonite concentration was 0.001 g L^{-1}, and HAO-coated montmorillonite concentration was 0.005 g L^{-1}.

Bradbury, 1997; Kraepiel *et al.*, 1999) have found similar results. Among them, Trivedi and Axe (2000) reported that Cd and Zn ions may retain their waters of hydration upon sorption to HAO, HFO, and HMO; compared with our investigations, amorphous oxides can form inner- or outer-sphere complexes with different metal ions. Other studies, for example, revealed Ni adsorption to Na-montmorillonite decreased with an increase in ionic strength (Baeyers and Bradbury, 1997). Furthermore, using XAFS (X-ray absorption fine structure spectroscopy), Strawn and Sparks (1999) found Pb adsorption on montmorillonite varies from primarily outer-sphere complexation at low ionic strength and pH to a mixture of outer- and inner-sphere complexation as pH and ionic strength increase. Pb adsorption at high ionic strength (>0.1 M) may be associated with the permanently charged surface sites on the clay edges (Strawn and Sparks, 1999). Because we observed an ionic strength effect suggesting outer-sphere complexation, Pb adsorption on montmorillonite at a relatively low ionic strength may involve ion exchange sites.

Isotherms for Pb adsorption to the three oxides, montmorillonite, and HAO-coated montmorillonite show a linear relationship between that sorbed to the external surface of the mineral and the bulk aqueous concentration (Figure 6.5) suggesting adsorption can be described with one average type of site. Based on Langmuir-Hinshelwood kinetics and given that the available sites are approximately equivalent to the total sites, the Langmuir isotherm reduces to the linear distribution model (Fogler, 1992). The distribution coefficient K_d (L g^{-1}) is simply the product of the total sites and the equilibrium constant. This approach is useful for describing adsorption in modeling the long-term sorption process (discussed below). Among a number of macroscopic studies, Hiemstra *et al.* (1989) used a single type of surface site to describe the titration

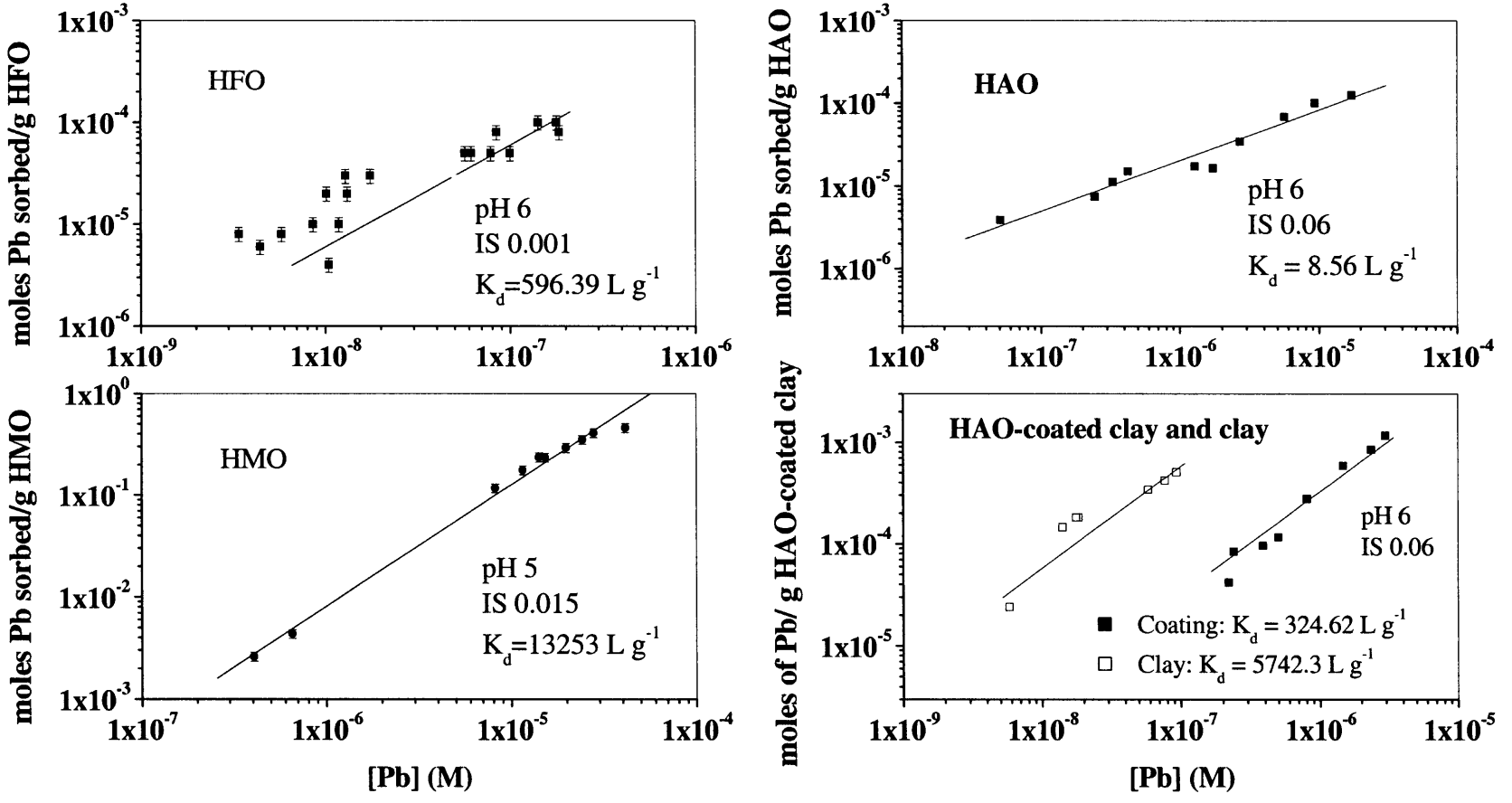

Figure 6.5 Isotherms of Pb adsorption to HFO, HMO, HAO, montmorillonite, and HAO-coated montmorillonite at 25°C with $NaNO_3$ electrolyte. HAO concentration was 0.5 g L^{-1}, HFO concentration was 0.3 g L^{-1}, HMO concentration was 0.5 g L^{-1}, montmorillonite concentration was 0.001 g L^{-1}, and HAO-coated montmorillonite concentration was 0.005 g L^{-1}.

behavior of hematite that exhibited poorly developed crystal planes. Christal and Kretzschmar (1999) showed that the titration behavior as well as the adsorption of Cu and Pb to hematite could be described very well with a single surface site. Through XAFS, Manceau *et al.* (1992) observed lead adsorbed to HFO by one mechanism, a mononuclear edge-sharing bidentate complex. Trivedi *et al.* (2003) found the configuration of the sorption complex is independent of the adsorbate concentration at constant pH. Therefore, they concluded that Pb sorption to ferrihydrite may be described with one average type of mechanism. Based on our isotherms of Pb sorption on montmorillonite and HAO-coated montmorillonite, Pb sorption to the montmorillonite surface is greater than that for the coated one. On the other hand, Zhuang and Yu (2002) also investigated similar systems but did not observe an effect of the Al oxide coating on sorption; this difference may be due to the degree of coating and that the isotherm was conducted at a different pH, 6.5. While edges and isotherms reveal effects of pH and concentration, they are short-term (4 h contact time) experiments resulting from adsorption to the external surface. For microporous sorbents, long-term studies are needed as well.

In these alternative experiments, a constant boundary condition was maintained, where the initial amount of Pb sorbed represents adsorption to the external surface. Pb concentrations employed in these experiments are within the linear range studied in the isotherm studies. Subsequently, the amount of Pb ion sorbed to the oxide gradually increased due to intraparticle surface diffusion. Initially, pore diffusion was considered in modeling sorption; however, predictions only accounted for 20% of the total sorbed when the bulk concentration at pore entrance is used as the boundary condition. Furthermore, the variance did not converge and therefore, pore diffusion cannot describe the

experimental data. On the other hand, when adsorption is significant, transport in pores is dominated by surface diffusion (Froment and Bischoff, 1990). For spherical particle geometry, a linear isotherm, and insignificant pore diffusion, the species mass balance for Pb is

$$\frac{\partial C}{\partial t} = \frac{D}{r^2}\frac{\partial\left[r^2\left(\frac{\partial C}{\partial r}\right)\right]}{\partial r} \tag{6.1}$$

where

$$D = \frac{D_s}{1+\left(\frac{\varepsilon_p}{\rho K_i}\right)} \tag{6.2}$$

In this expression, C is the contaminant concentration sorbed; D_s is the surface diffusivity and fitting parameter in the model; ε_p is the oxide porosity; ρ is the bulk density; and K_i is the distribution coefficient representing the product of the equilibrium constant and the internal site density. The assumption that internal sites are no different than external ones has also been observed in recent work with XAFS, for example, in Zn sorption to HMO the local structure from long-term samples was consistent with that from short-term samples (Trivedi *et al*, 2001). In addition, XAFS work with Sr sorption to HMO (Axe *et al.*, 2000) as well as HFO (Axe *et al.*, 1998) further corroborates this assumption. Applying this assumption here for Pb sorption, the analytical solution to Equation 6.1 integrated over the volume of a sphere based on the following initial and boundary conditions

$$C(r,0) = 0 \tag{6.3}$$

$$\frac{\partial C}{\partial r}(0,t)=0 \tag{6.4}$$

$$C(R,t)=C_s \tag{6.5}$$

results in the mass sorbed per particle at a given time:

$$M=4\pi C_s\frac{R^3}{3}\left[1-\frac{6}{\pi^2}\sum_{n=1}^{\infty}\frac{1}{n^2}\exp\left(-\frac{Dn^2\pi^2t}{R^2}\right)\right] \tag{6.6}$$

where C_s is the metal concentration sorbed on the oxide external surface. The amount sorbed to the internal surface of a single particle times the number of particles present for given radius (R) was summed over the entire particle size distribution to obtain the concentration sorbed internally. This total plus that sorbed to the external surface found from the short-term sorption studies provides the theoretical concentration. By minimizing the variance, the only fitting parameter is surface diffusivity; modeling results are shown in Figures 6.6 and 6.7. Errors associated with the experiments were calculated from the propagation of errors (POE) method (Ku, 1966) and range from 7 to 10%. Errors associated with the model from POE method are also shown, which accounts for standard deviations in the number of particles as well as the error in the distribution coefficient describing the mass adsorbed to the surface. All data fall within two standard deviations of the model, which demonstrates the model describes the data reasonably well. Furthermore, substantial evidence supports intraparticle diffusion as the rate-limiting mechanism in sorption to microporous oxides: Sr sorption to HFO (Axe and Anderson, 1995) and HAO and HMO (Trivedi and Axe, 1999), Cu and Pb sorption to ferrihydrite (Scheinost *et al.*, 2001), and Ni, Cd, and Zn sorption to HAO, HFO, and HMO (Trivedi and Axe, 2000 and 2001). Based on our adsorption isotherms and recent

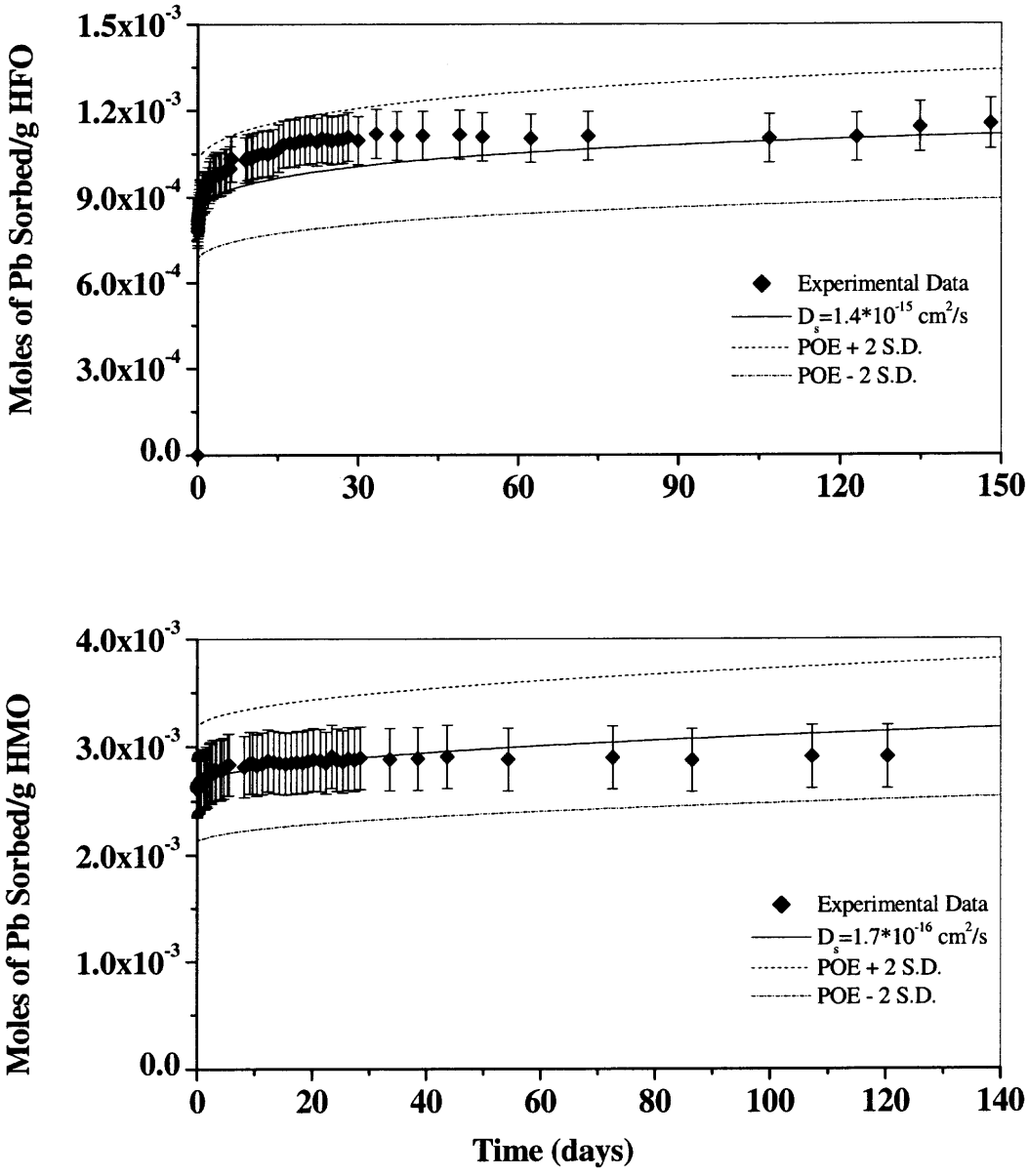

Figure 6.6 CBC studies of Pb sorption to HFO and HMO at 25°C with an ionic strength of 1.5×10^{-2} M ($NaNO_3$). For HFO, $[Pb]_{bulk} = 5.2\times10^{-5}$ M at pH 5 and 0.3 g L^{-1} HFO; and, for HMO, $[Pb]_{bulk} = 4.4\times10^{-4}$ M at pH 4 and 0.1 g L^{-1} HMO.

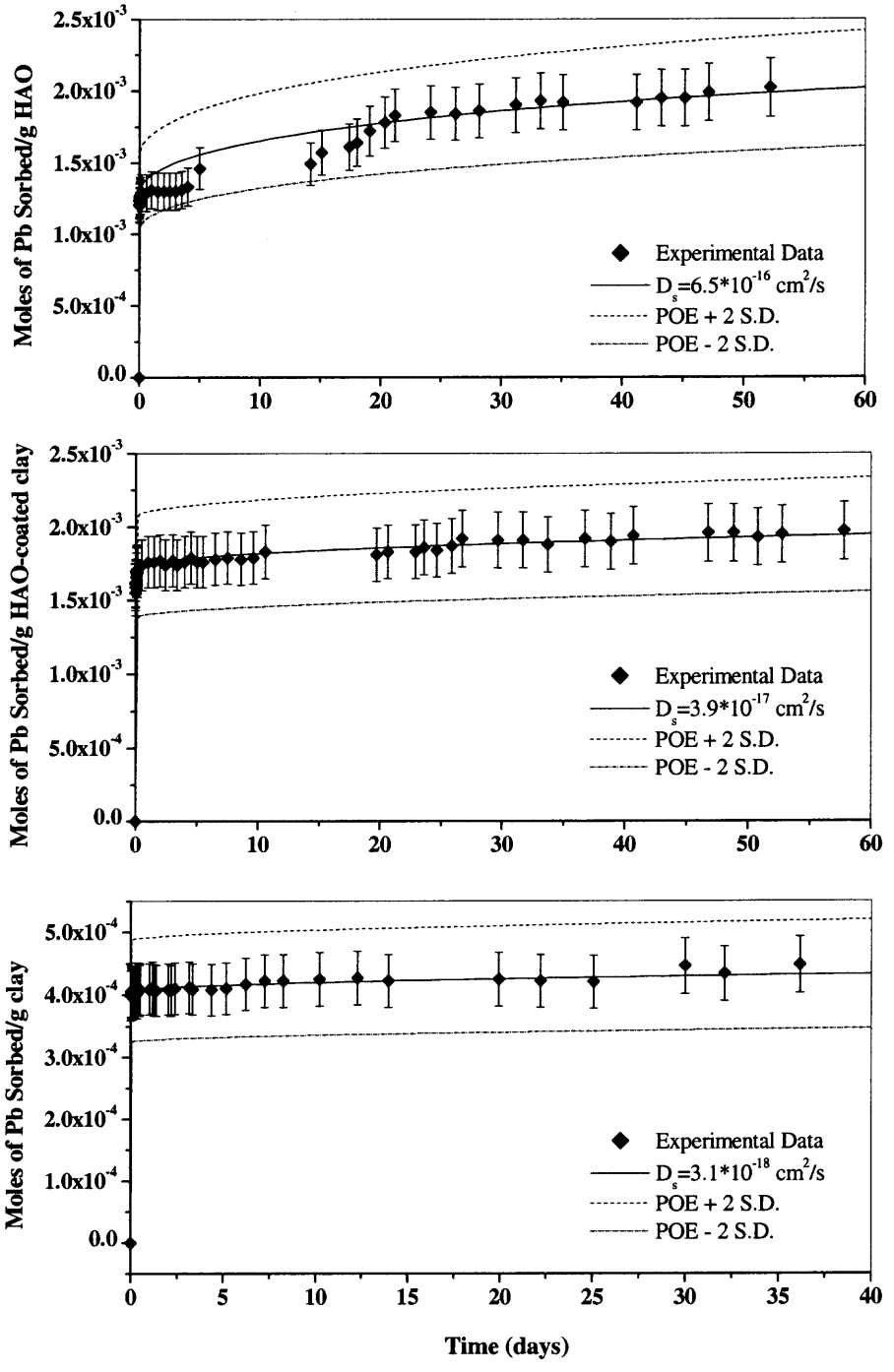

Figure 6.7 CBC studies of Pb sorption to HAO, montmorillonite, and HAO-coated montmorillonite at 25°C and an ionic strength of 1.0×10^{-2} M with $NaNO_3$. For HAO, $[Pb]_{bulk} = 8.3\times10^{-6}$ M at pH 6 and 0.02 g L^{-1} HAO; for HAO-coated montmorillonite, $[Pb]_{bulk} = 1.7\times10^{-4}$ M at pH 5 and 0.2 g L^{-1} coatings; and, for montmorillonite, $[Pb]_{bulk} = 9.5\times10^{-6}$ M at pH 6 and 0.1 g L^{-1} montmorillonite.

work with XAFS (Axe *et al.*, 1998 and 2000; Trivedi and Axe, 2001), there is no evidence of either surface precipitation or solid-solid solution formation; long-term studies suggested that internal surface sites were no different than external ones. In addition, given the presence of microporosity, intraparticle diffusion is expected and is therefore modeled as the rate-limiting process in Pb sorption to these oxides and coatings.

Studies with Pb sorption to HFO, HMO, HAO, montmorillonite, and HAO-coated montmorillonite (Figures 6.6 and 6.7) demonstrate that surface diffusivities range from 10^{-18} to 10^{-15} cm^2 s^{-1}. These diffusivities clearly show that diffusion is a slow and rate-limiting process in sorption. After running the model to equilibrium, which takes approximately 15 to 30 years, internal sites were found to be responsible for approximately 45-90% of the total metal uptake to these oxides. For discrete oxides, surface diffusion is the dominant mode of intraparticle transport, which is consistent with others (Axe and Anderson, 1995, 1997; Misak *et al.*, 1996; Trivedi and Axe, 1999, 2000, and 2001). For sorption to montmorillonite, Morrissey and Grismer (1996) studied sorption of acetone, benzene, and toluene to pure clay minerals including kaolinite, illite, and Ca-montmorillonite; they found the process was limited by diffusion. Gemeay *et al.* (2002) observed adsorption kinetics of metanil yellow dye, *p*-aminodiphenylamine (*p*-NH2-DPA), and benzidine by Na-montmorillonte, where again intraparticle diffusion was the rate-limiting mechanism. Furthermore, Fadali (2003) reported the sorption of basic dyes (Basic Red) onto montmorillonite was intraparticle diffusion-controlled. For sorption to oxide coatings, intraparticle diffusion has also been observed in a number of studies (Holmen and Gschwend, 1997; Jain and Ram, 1997; Merkle *et al.*, 1997; Lai *et al.*, 2000; Stefanove, 2001). Among them, Holmen and Gschwend (1997) observed that

slow diffusion controls the rate of sorption of hydrophobic organic compounds on quartzitic aquifer sands with iron oxyhydroxide and aluminosilicate (clay) coatings. Jain and Ram (1997) investigated lead and zinc sorption on sediment which was mainly composed of sand and Fe/Mn oxides; they observed very slow diffusion of the adsorbed metals from the surface into the micropores. Merkle *et al.* (1997) studied soluble Mn (II) removal by oxide-coated media including synthetically coated and naturally coated, in which surface diffusion was also the rate-limiting mechanism.

Based on the resultant diffusivities for discrete aluminum oxide, aluminum oxide-coated montmorillonite, and montmorillonite, specifically 10^{-16}, 10^{-17}, and 10^{-18} cm^2 s^{-1} (Figure 6.7), respectively, substrate surface characteristics influence metal ion mobility. The smallest diffusivity reflects the surface characteristics of montmorillonite, which exhibited the greatest affinity for Pb ions among the three systems. When Pb ions sorbed on aluminum oxide-coated montmorillonite, surface diffusion is affected by both the discrete oxide and clay. Based on the FE-SEM micrograph (Figure 6.1), diffusion occurs in both aluminum oxide and montmorilllonite. Furthermore, based on this diffusivity, the contribution from discrete aluminum oxide and clay can be evaluated by employing their individual particle size distributions and concentrations. The results suggest 0.82 g amorphous oxide g^{-1} clay contributes the overall diffusivity. Compared with that initially applied, 0.35 g HAO g^{-1} clay, the amorphous oxide appears to have a greater impact than that based on stoichiometry. Montmorillonite is comprised of Al (18% by weight), Si (23%), Fe (7%), and O (45%) based on XRF analyses. During the coating process, the system was initially at about pH 2 for 2 h and then adjusted to pH 7. We hypothesize that alumina in montmorillonite partially dissolves, then reforms as amorphous oxides, which

can be demonstrated by the montmorillonite solubility. Al solubility in montmorillonite is controlled by gibbsite or amorphous aluminum hydroxide (May *et al.*, 1986). At pH 2-3, Ganor *et al.* (1999) found that gibbsite dissolved at a rate of 2.2×10^{-12} mole m^{-2} s^{-1} based on column studies and therefore, this rate may include mass transfer limitations. However, we maintained a turbulent regime in the batch system, thus the dissolution rate may be greater than that observed in column studies. Furthermore, Lydersen *et al.* (1991) found amorphous aluminum oxide dissolution can be described as a two-step process at pH 4.5: the dissolution was relatively fast during the first 2.7 h, and then a far slower rate followed for the remaining 24 hours. Based on their model, $C(t) = C_0 e^{-0.45t}$, where $C(t)$ is concentration of $Al(OH)_{3(s)}$ present at time t, C_0 is initial concentration of $Al(OH)_{3(s)}$, approximately 50-60% of the amorphous aluminum oxide dissolves in the first 2 hours. Given that 0.15 g of montmorillonite were present in the studies, the coating system is projected to exhibit a 17-20% increase in the amorphous aluminum oxide from alumina dissolution, which is consistent with our estimation based on concentrations and particle size distributions. This result also demonstrates that oxides control Pb sorption in coated areas, while montmorillonite is the dominant surface at uncoated edge areas.

Because these long-term studies are time-consuming, theoretically based methods to predict diffusivities may be useful. Based on previous work (Axe and Anderson, 1997; Trivedi and Axe, 1999, 2000, and 2001), site activation theory can be applied for this purpose, where the sorbed ion or molecule vibrates at a site until it has sufficient energy, E_A (activation energy), to jump to the neighboring site. Accordingly, assuming a sinusoidal potential field along the pore surface, the surface diffusivity is a function of E_A and the mean distance between the sites (λ)

$$D_s = \lambda\left(\frac{E_A}{2m}\right)^{1/2} \exp\left(\frac{-E_A}{RT}\right) \tag{6.7}$$

where m is the molecular mass of the sorbing species and $\exp(-E_A/RT)$ is the Boltzmann factor. From the polanyi relation, E_A is linearly related to adsorption enthalpy, ΔH^0, through the proportionality constant α which was studied for transition and alkaline earth metals (Trivedi and Axe, 2000 and 2001). Using the experimental diffusivity, E_A was estimated by Equation 6.7 and employing the polanyi relation, α for HAO, HFO, and HMO was obtained (Table 6.2). The results show that the polanyi constant for Pb adsorption to the three oxides is equivalent. This constant is expected to be equivalent for metals from the same group of the Periodic Table because of potentially similar sorption complexes formed with the oxides. Using the α obtained through this study, activation energies of other metals from Group 14 (IVA) may be calculated, and theoretical diffusivities can be predicted.

6.3 Summary

Lead sorption to hydrous amorphous Al, Fe, and Mn oxides as well as to montmorillonite and HAO-coated montmorillonite can be described by a two-step process: rapid adsorption of metal ions to the external surface is followed by slow intraparticle diffusion along the micropore walls. Best-fit surface diffusivities ranged from 10^{-18} to 10^{-15} cm^2 s^{-1}. Specifically for Pb sorption on discrete aluminum oxide, aluminum oxide-coated montmorillonite, and montmorillonite, diffusivities of 10^{-16}, 10^{-17}, and 10^{-18} cm^2 s^{-1}, respectively, were observed. The results indicate substrate surface characteristics influence metal ion mobility, where diffusivity increased as affinity decreased. These

Table 6.2 Theoretical Parameters of Pb Sorbed to Hydrous Metal Oxides

Oxide	λ **(nm)**[a]	C_t **(Site Density) (mol g^{-1})**[b]	ΔH^0 **(kcal mol^{-1})**[c]	**Exp.** D_s **(cm^2 s^{-1})**	E_A **(kcal mol^{-1})**	α[d]
HAO	0.35	0.012	38.2	6.5×10^{-16}	16.8	0.4
HFO	0.24	0.025	41.4	1.4×10^{-15}	16.1	0.4
HMO	0.15	0.034	42.3	1.7×10^{-16}	17.1	0.4

[a] Calculated from oxide surface area and site density.
[b] Based on Trivedi and Axe (1999).
[c] Based on correlation between ΔH^0_{ads} and R_H (hydrated radius) developed by Trivedi and Axe (2001).
[d] α for transition metals is 0.80 for HAO, 0.68 for HFO, and 0.60 for HMO (Trivedi and Axe, 2001).

studies demonstrate transient natural attenuating processes such as intraparticle diffusion need to be included in accurately describing the migration of heavy metals in subsurface environments.

In the next chapter, the approach for incorporating the diffuse model into GMS for accurately depicting metal contaminant mobility is discussed.

CHAPTER 7

MODELING MICROSCOPIC TRANSPORT – INTRAPARTICLE DIFFUSION

As intraparticle diffusion is a rate-limiting mechanism in sorption for metal contaminant sorption to microporous amorphous oxide minerals, this microscopic transport process will be included into a macroscopic solute transport code to accurately describe metal contaminant mobility. As discussed in Chapter 4, RT3D (Clement, 2003), developed by the Battelle Pacific Northwest National Laboratory, is a multispecies reactive transport model. In the Groundwater Modeling System (GMS), RT3D allows users to define reactions with greater flexibility in simulating different scenarios. The user-defined reaction packages in RT3D are amenable for linking the microscopic intraparticle diffusion model with the macroscopic advection and dispersion transport in GMS. A flow chart of the intraparticle diffusion modeling process is shown in Figure 7.1.

7.1 Intraparticle Diffusion Equation Setup for Solute Transport

Transport of an adsorbate through interior pores of an amorphous oxide is intraparticle diffusion. Species flux, N, can be described by Fick's law,

$$N = -D\nabla\overline{C} \tag{7.1}$$

where D is diffusion coefficient and $\overline{C}$ is the ion concentration. The species mass balance for a porous, spherical oxide particle yields the following equation (Axe and Anderson, 1995):

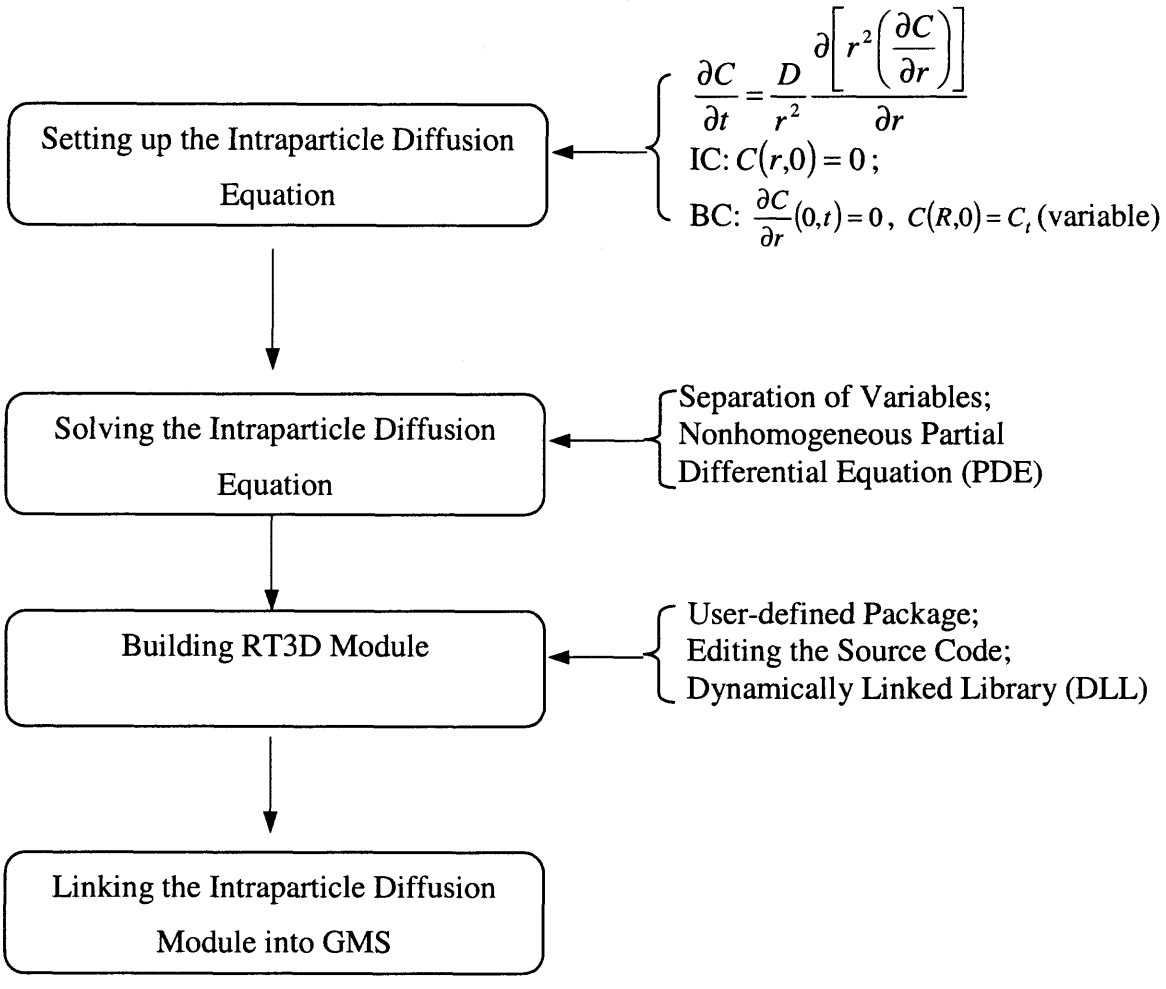

Figure 7.1 Flow chart of intraparticle diffusion modeling

$$\varepsilon_p \frac{\partial S}{\partial t} + \rho \frac{\partial C}{\partial t} = \frac{\rho}{r^2} \frac{\partial \left(D_s r^2 \frac{\partial C}{\partial r} \right)}{\partial r} + \frac{1}{r^2} \frac{\partial \left(D_e r^2 \frac{\partial S}{\partial r} \right)}{\partial r} \tag{7.2}$$

In this expression, S is the contaminant concentration in the aqueous phase; C is the contaminant concentration in the sorbed phase; r is the radial position within the sphere; ε_p is the porosity of the particle; D_s is the surface diffusion coefficient within the sorbent particle; ρ is the oxide bulk density; and D_e is the pore diffusion coefficient within the sorbent. For instantaneous adsorption and constant diffusivities (for dilute contaminant concentrations or no adsorbate-adsorbate interaction) (Axe and Anderson, 1995), the balance can be written as

$$\frac{\partial C}{\partial t} = \frac{\left[D_s + \left(D_e \frac{dS}{\rho dC} \right) \right]}{\left[1 + \left(\varepsilon_p \frac{dS}{\rho dC} \right) \right]} \frac{1}{r^2} \frac{\partial \left[r^2 \left(\frac{\partial C}{\partial r} \right) \right]}{\partial r} \tag{7.3}$$

where adsorption equilibrium is described by a linear isotherm. Because of the strong affinity between the adsorbate and the surface, pore diffusion as a transport process through the oxide micropores is insignificant (Axe and Anderson, 1995). Therefore, Equation 7.3 becomes

$$\frac{\partial C}{\partial t} = \frac{D}{r^2} \frac{\partial \left[r^2 \left(\frac{\partial C}{\partial r} \right) \right]}{\partial r} \tag{7.4}$$

where

$$D = \frac{D_s}{1 + \left(\frac{\varepsilon_p}{\rho K_i} \right)} \tag{7.5}$$

where K_i is the distribution coefficient sorption to internal sites.

The macroscopic, advective-dispersive solute transport is described as (Zheng and Bennett, 2002),

$$\theta\frac{\partial S}{\partial t}=\theta\frac{\partial}{\partial x_i}\left(D_{ij}\frac{\partial S}{\partial x_j}\right)-\frac{\partial}{\partial x_i}(q_i S)+q_s S_s \tag{7.6}$$

where q_i is the Darcy velocity, D_{ij} is the dispersion coefficient tensor, q_s is the flow rate of a fluid source or sink per unit aquifer volume, S_s is the concentration of the fluid source or sink flux, and θ is the porosity. For a volume without source(s), Equation 7.6 can be reduced to

$$\theta\frac{\partial S}{\partial t}=\theta\frac{\partial}{\partial x_i}\left(D_{ij}\frac{\partial S}{\partial x_j}\right)-\frac{\partial}{\partial x_i}(q_i S) \tag{7.7}$$

Sorption of heavy metals to hydrous oxides is a two-step process as discussed and shown previously: a rapid adsorption of metal ions to the external surface is followed by slow intraparticle diffusion along the oxide micropore walls. Considering the first step of the process, rapid adsorption that can be described as an equilibrium process, mass accumulates along the oxide micropores and is removed from the aqueous phase; thus, solute transport becomes

$$\theta\frac{\partial S}{\partial t}=\theta\frac{\partial}{\partial x_i}\left(D_{ij}\frac{\partial S}{\partial x_j}\right)-\frac{\partial}{\partial x_i}(q_i S)-\rho_b\frac{\partial C_t}{\partial t} \tag{7.8}$$

For a linear isotherm,

$$\frac{\partial C_t}{\partial t}=\frac{\partial C_t}{\partial S}\frac{\partial S}{\partial t}=K_d\frac{\partial S}{\partial t} \tag{7.9}$$

where C_t is the sorbed concentration on the external surface and ρ_b is the bulk density of the porous medium. Substituting Equation 7.9 into Equation 7.8, the following is obtained

$$\theta\frac{\partial S}{\partial t}=\theta\frac{\partial}{\partial x_i}\left(D_{ij}\frac{\partial S}{\partial x_j}\right)-\frac{\partial}{\partial x_i}(q_i S)-\rho_b K_d\frac{\partial S}{\partial t} \tag{7.10}$$

Considering slow intraparticle diffusion is an attenuating mechanism, which is illustrated by Equation 7.4, the governing equations describing intraparticle diffusion coupled with advection and dispersion processes are as follows:

$$\theta\frac{\partial S}{\partial t}=\theta\frac{\partial}{\partial x_i}\left(D_{ij}\frac{\partial S}{\partial x_j}\right)-\frac{\partial}{\partial x_i}(q_i S)-\rho_b K_d\frac{\partial S}{\partial t}-\rho_b\frac{\partial C}{\partial t} \tag{7.11}$$

$$\frac{\partial C}{\partial t}=\frac{D}{r^2}\frac{\partial\left[r^2\left(\frac{\partial C}{\partial r}\right)\right]}{\partial r} \tag{7.4}$$

Equations above describe macroscopic transport processes as well as the intraparticle diffusion. Macroscopic solute transport models which employ Equation 7.10 have been widely applied to predict the fate and transport of contaminants, as discussed in Chapter 4. Based on review of existing transport models, GMS is selected for incorporating microscopic intraparticle diffusion modeling in accurately describing metal contaminant mobility in the presence of microporous amorphous Fe, Al, and Mn oxides. In the following section, modeling of the intraparticle diffusion process is presented and includes solving the non-homogeneous partial differential equation and building the user-defined package for microscopic transport in RT3D, the multispecies reactive transport module in GMS.

7.2 Modeling for Intraparticle Diffusion

Given the initial and boundary conditions, intraparticle diffusion of metal ions in microscopic amorphous oxides can be described by the following:

$$\frac{\partial C}{\partial t} = \frac{D}{r^2}\frac{\partial\left[r^2\left(\frac{\partial C}{\partial r}\right)\right]}{\partial r} \tag{7.4}$$

$$C(r,0) = 0 \tag{7.12}$$

$$\frac{\partial C}{\partial r}(0,t) = 0 \tag{7.13}$$

$$C(R,t) = C_t \tag{7.14}$$

where R is the radius of oxide particle. The microscopic diffusion Equation 7.4 is a parabolic equation, with Dirichlet and Neumann boundary conditions, Equation 7.12 and Equation 7.13, respectively. Separation of variables, which is one of the most widely used solution techniques for second order partial differential equations, can be employed to solve this type of equation. By applying this analytical method, the solution to Equation 7.4 applying Equations 7.12-14 is:

$$C = C_t + \sum_{n=1}^{\infty}(-1)^n \frac{2RC_t}{nr\pi}\exp\left(-\frac{n^2\pi^2 Dt}{R^2}\right)\sin\frac{n\pi r}{R} \tag{7.15}$$

Integrating the concentration profile over the volume of a spherical particle yields the mass of species sorbed internally for a given particle size:

$$M = 4\pi\rho C_t\frac{R^3}{3} - \sum_{n=1}^{\infty}\frac{8R^3\rho C_t}{n^2\pi}\exp\left(-\frac{n^2\pi^2 Dt}{R^2}\right) \tag{7.16}$$

where M is the mass of species sorbed to the particle.

This diffusion model was validated by experimental data in this research (Chapter 6) as well as by others (Axe and Anderson, 1995 and 1997; Trivedi and Axe, 1999, 2000, and 2001), as shown in Figures 7.2-7.6 (Details for experiments and fitting methods are outlined in Chapter 6). The experimental data included heavy metal, Zn, Ni, Cd, Sr, and Pb, sorption on amorphous Al (HAO), Fe (HFO), and Mn (HMO) oxides, which occur as coatings on other mineral surfaces or as discrete particles and are persistent in soil and the subsurface environments, as discussed in the previous chapter. Errors associated with the model from the propagation of errors (POE) method (Ku, 1966) are also included in the figures. The POE analysis accounts for errors that include the standard deviations in the number of particles as well as the error in the distribution coefficient describing the mass adsorbed to the surface. The results show that all data fall within one or two standard deviations of the model and are consistent with the diffusion model describing intraparticle diffusion in microporous amorphous oxide minerals. Furthermore, running the model to equilibrium reveals the process ranges from one to more than thirty years (Figures 7.7-7.11).

Groundwater flow can be characterized as laminar (e.g., Freeze and Cherry, 1979; Todd, 1980; Bowen, 1986), and therefore mass transfer from bulk solution to the surface of microporous particles needs to be considered. As a result, the following boundary condition is used (Crank, 1975)

$$D\rho\frac{\partial C}{\partial r}(R,t)=k(S-S_t) \tag{7.18}$$

where k is the external mass transfer coefficient of metal ions, S_t is the metal ion concentration along the particle surface related to C_t by $C_t = K_d S_t$ assuming a linear

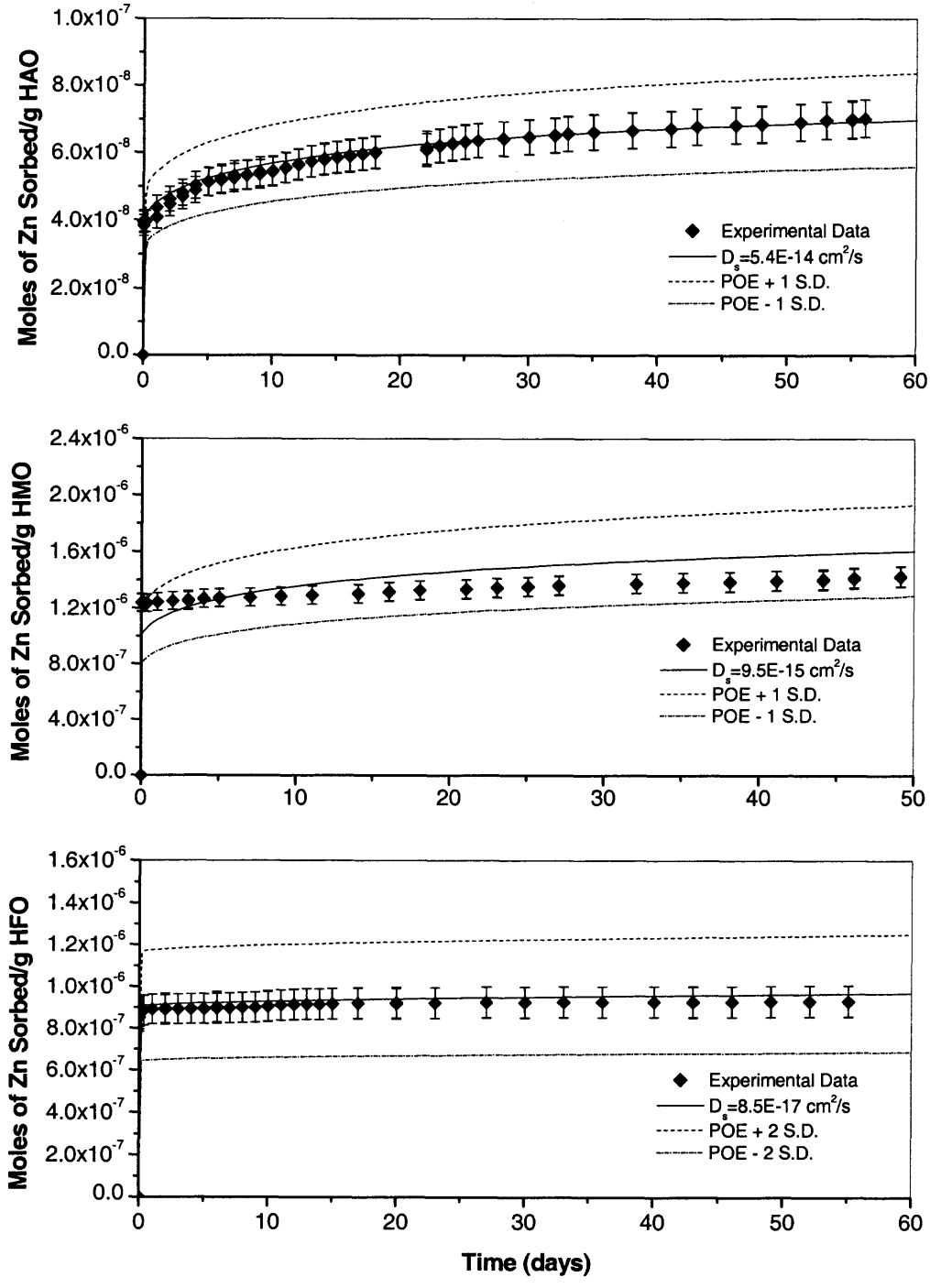

Figure 7.2 Zn sorption to HAO, HMO, and HFO as a function of time in constant boundary condition studies

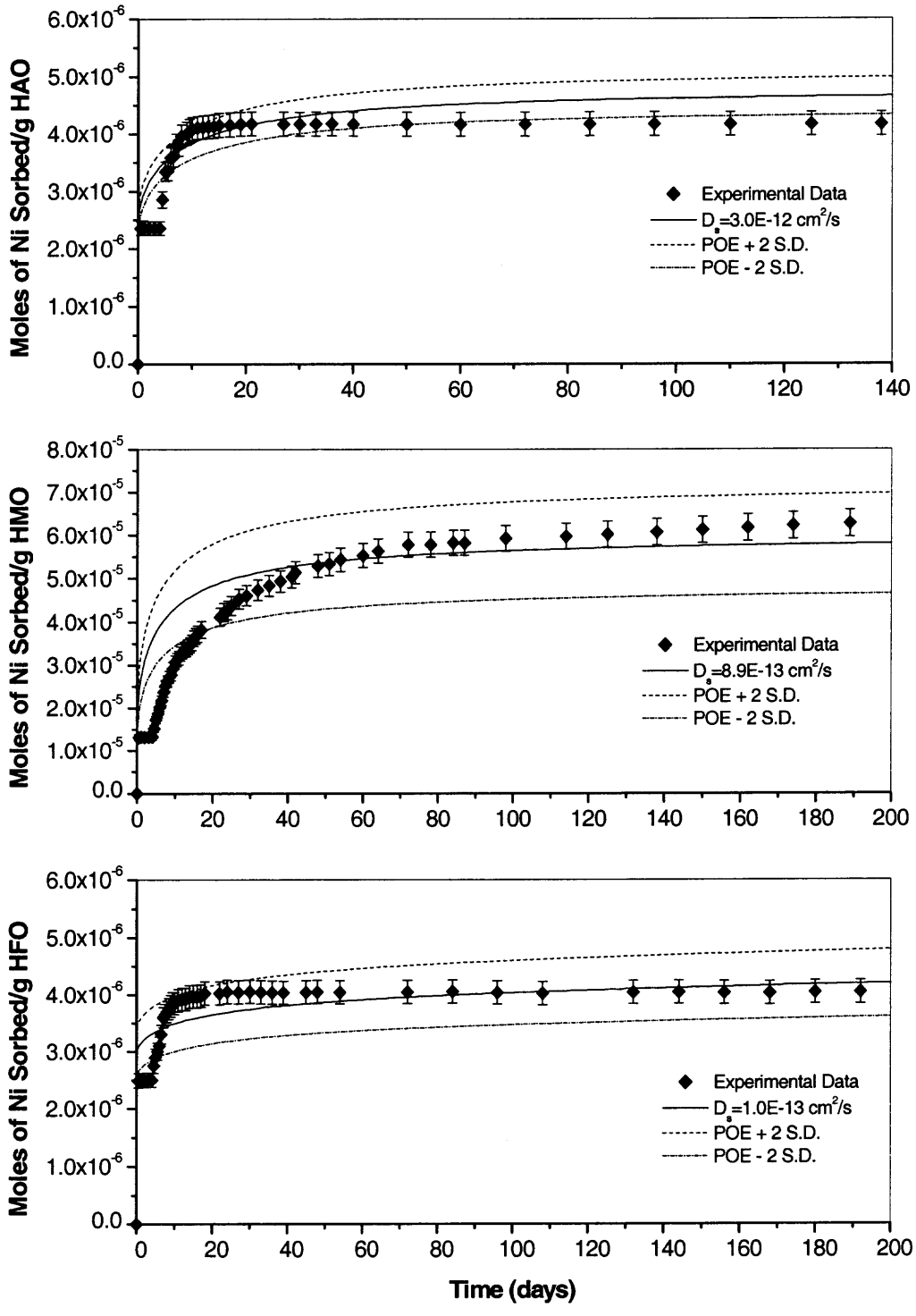

Figure 7.3 Ni sorption to HAO, HMO, and HFO as a function of time in constant boundary condition studies

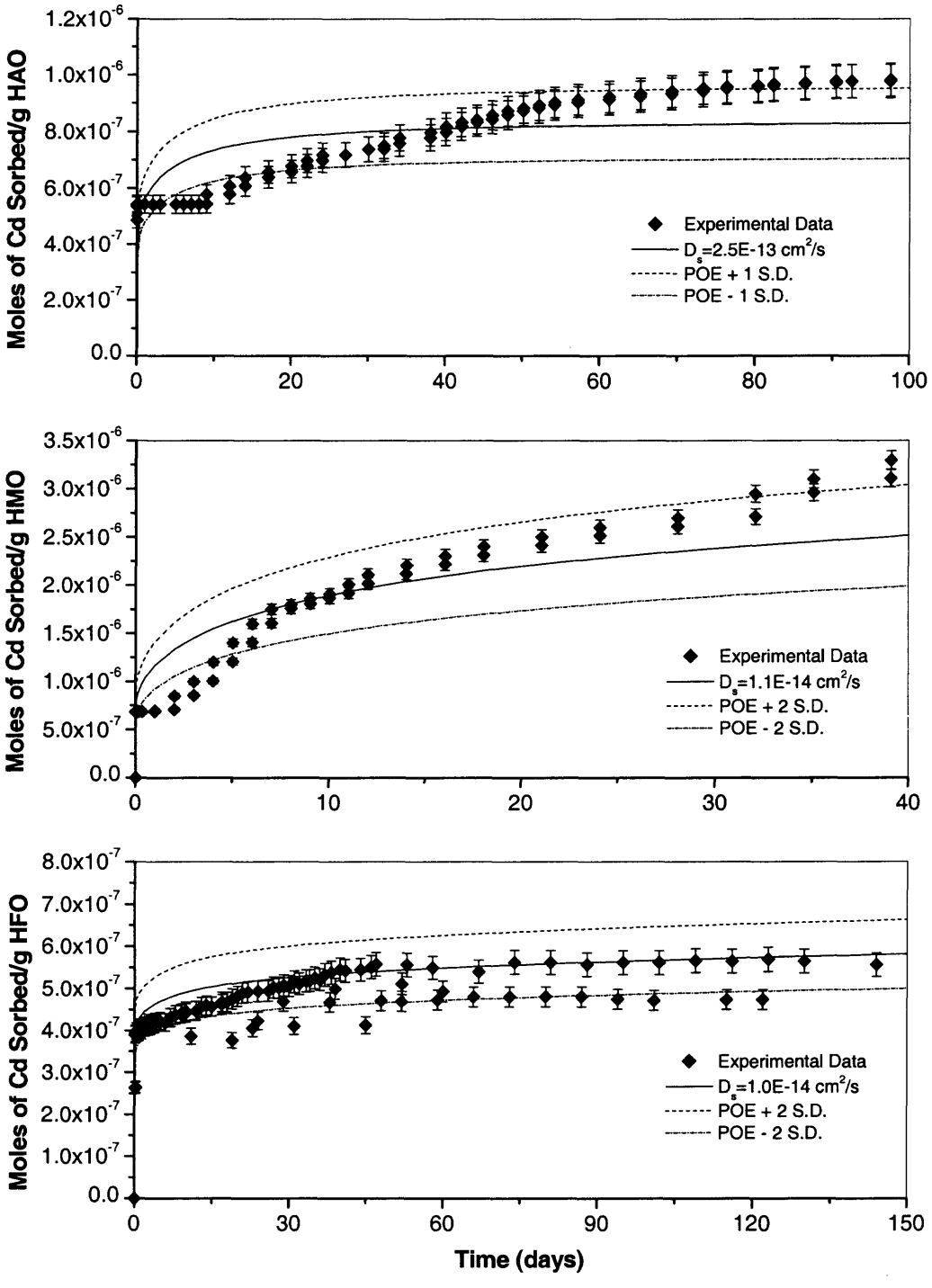

Figure 7.4 Cd sorption to HAO, HMO, and HFO as a function of time in constant boundary condition studies

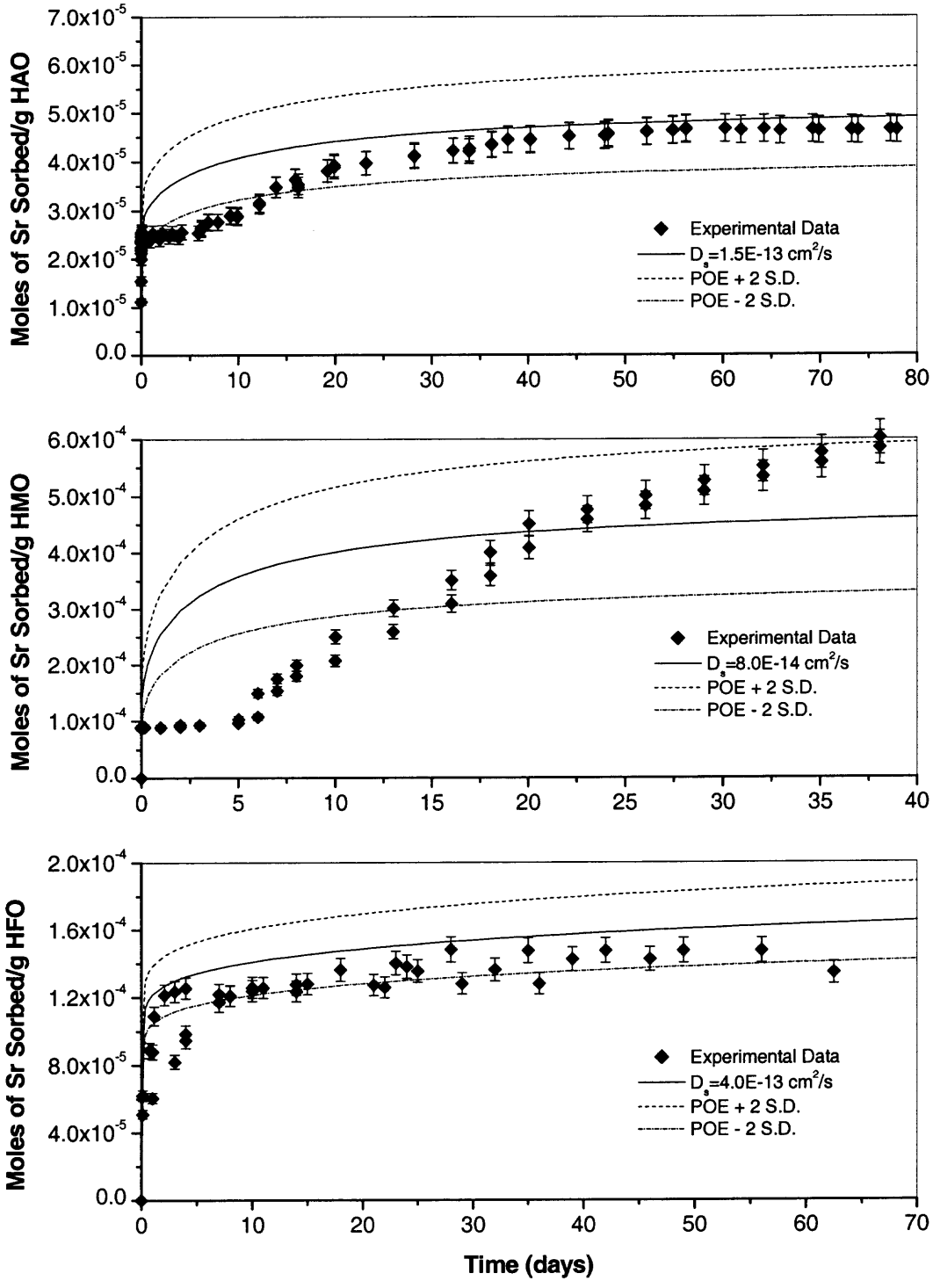

Figure 7.5 Sr sorption to HAO, HMO, and HFO as a function of time in constant boundary condition studies

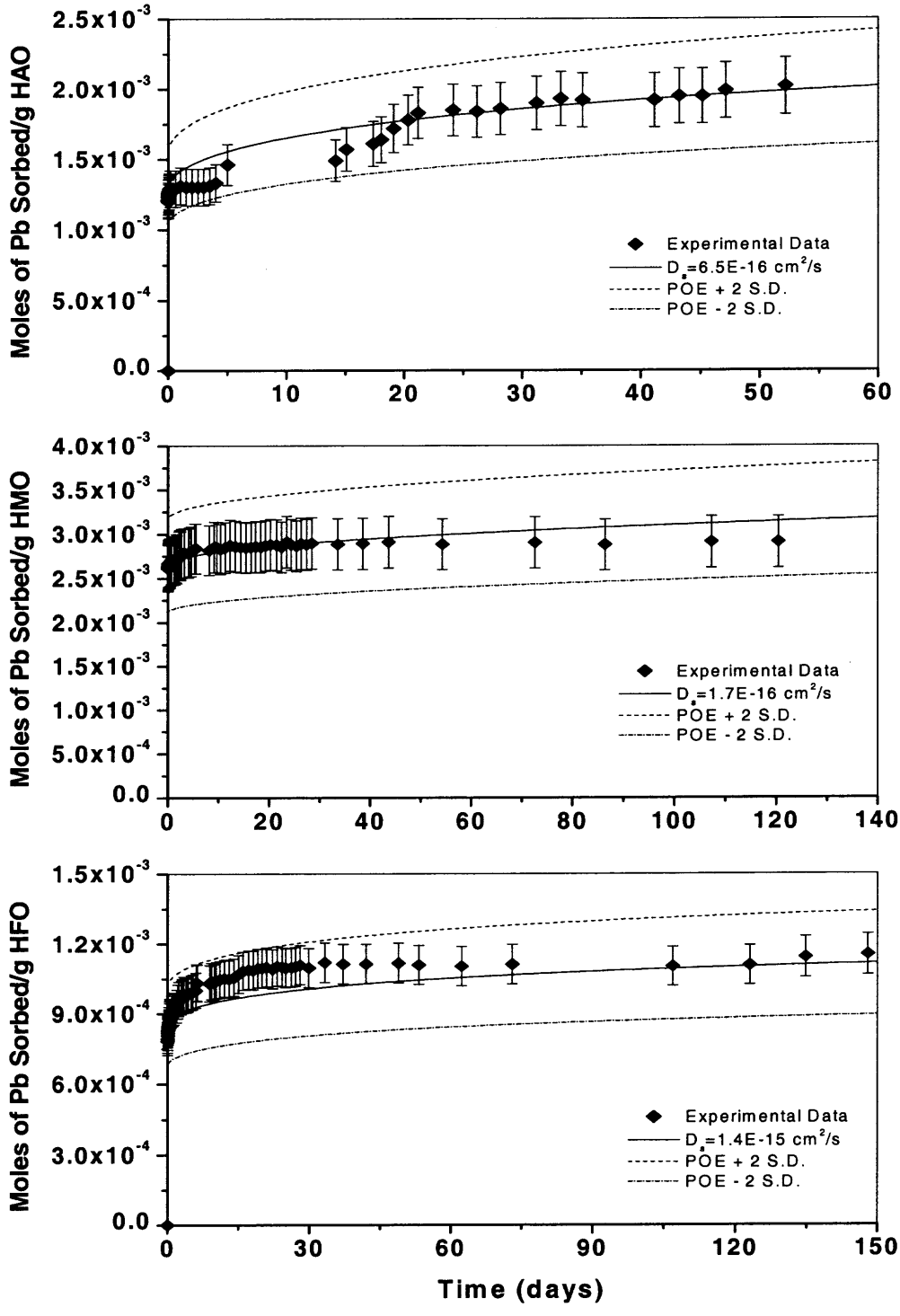

Figure 7.6 Pb sorption to HAO, HMO, and HFO as a function of time in constant boundary condition studies

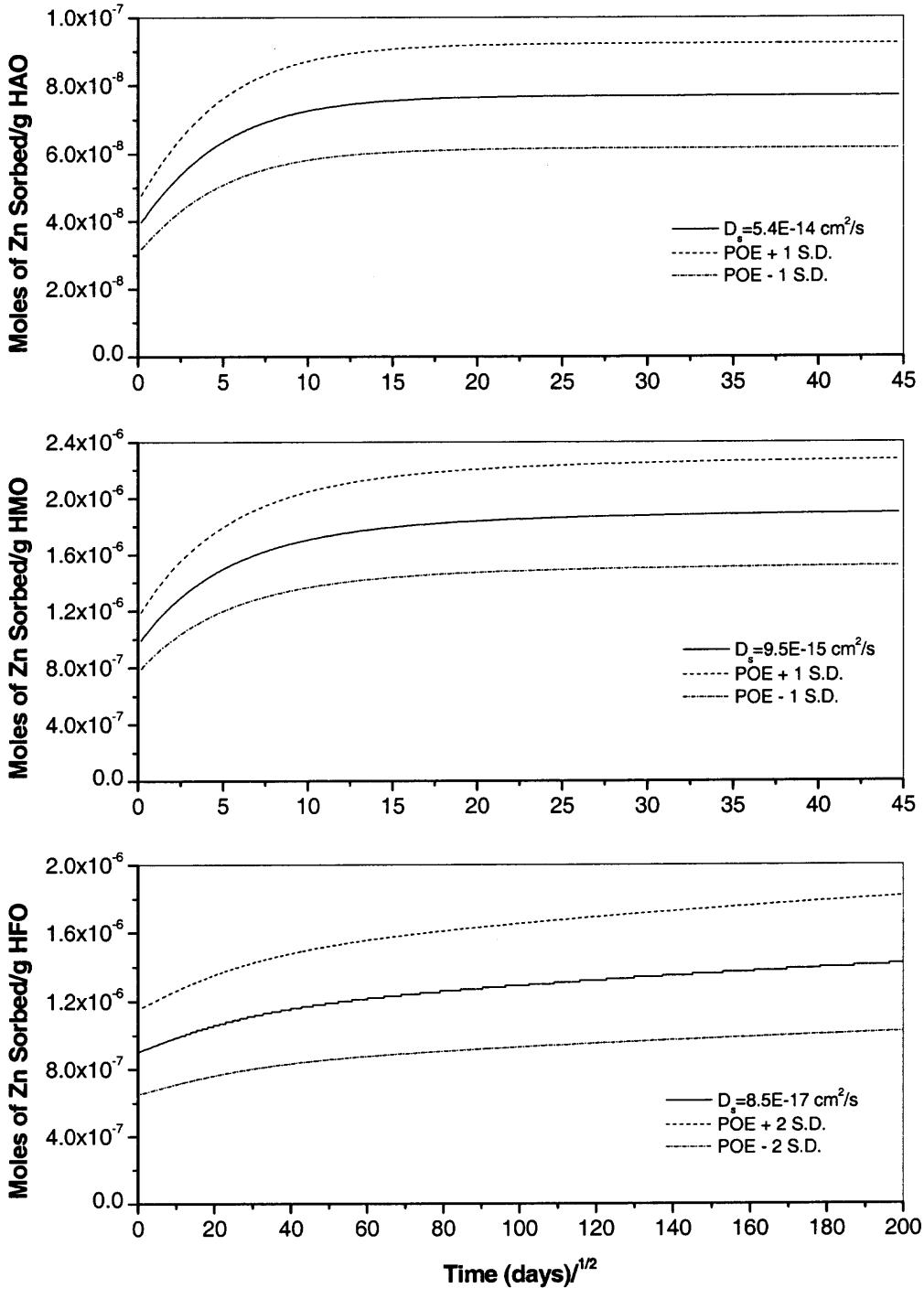

Figure 7.7 Zn sorption to HAO, HMO, and HFO as a function of time till equilibrium

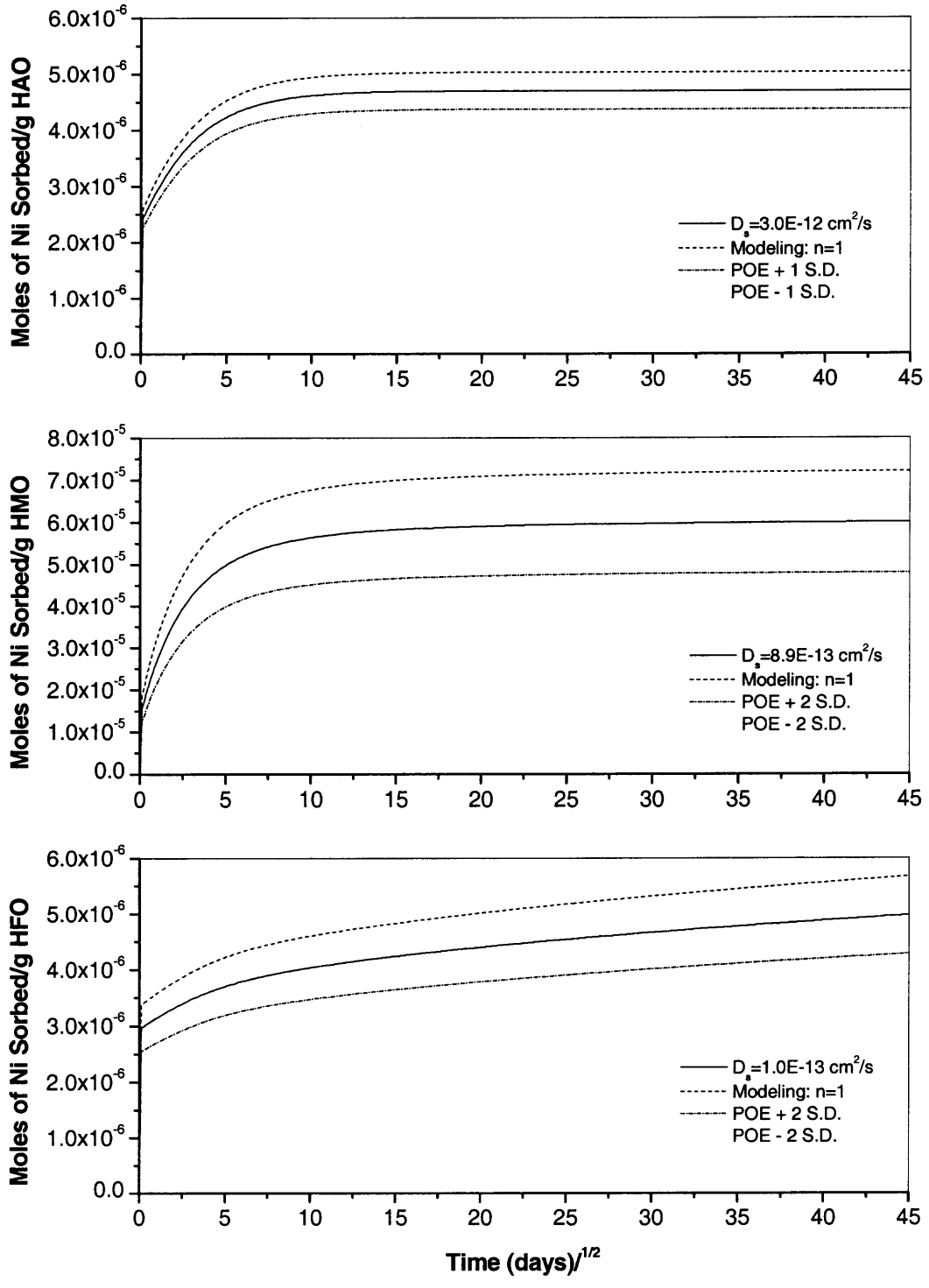

Figure 7.8 Ni sorption to HAO, HMO, and HFO as a function of time till equilibrium

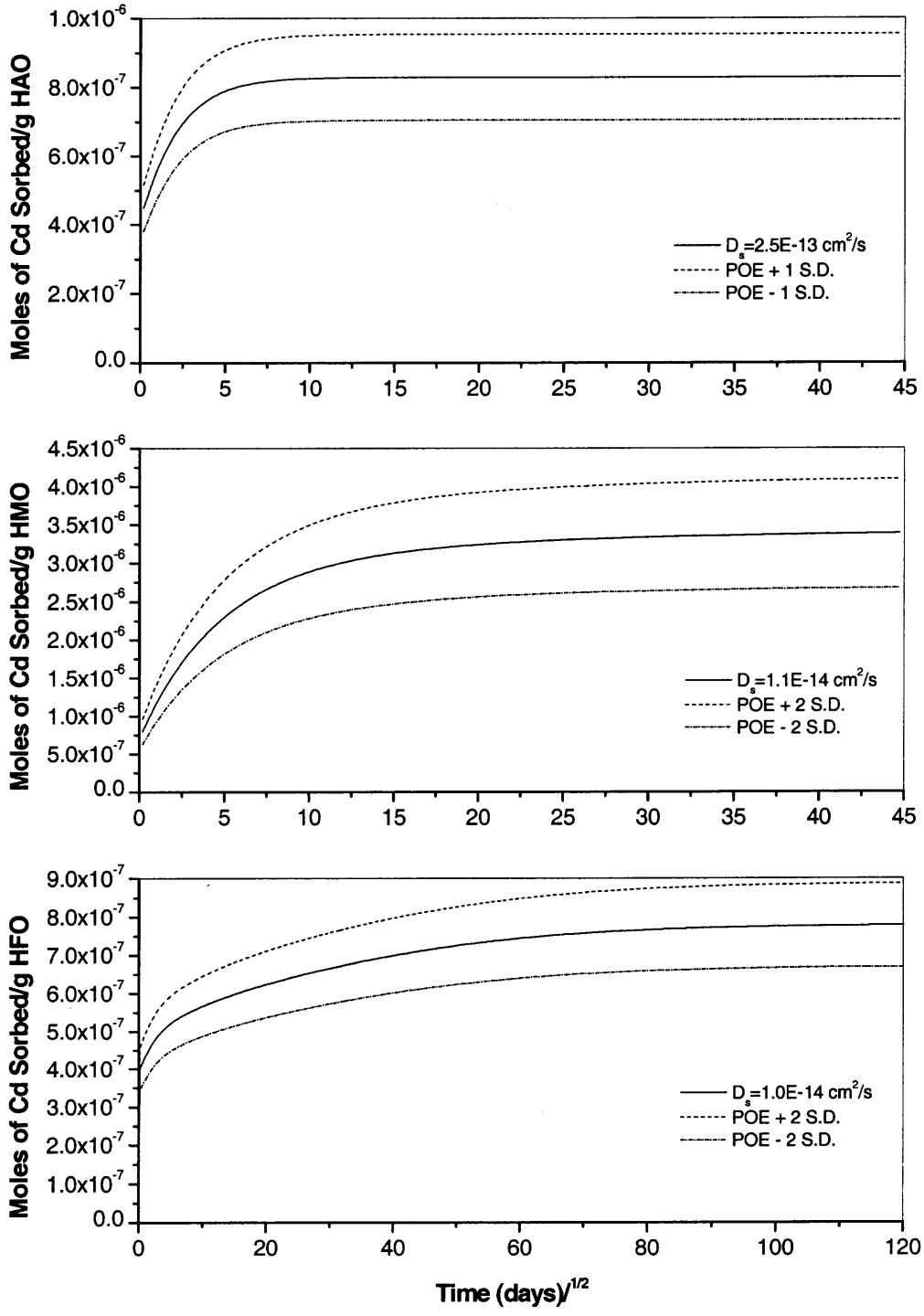

Figure 7.9 Cd sorption to HAO, HMO, and HFO as a function of time till equilibrium

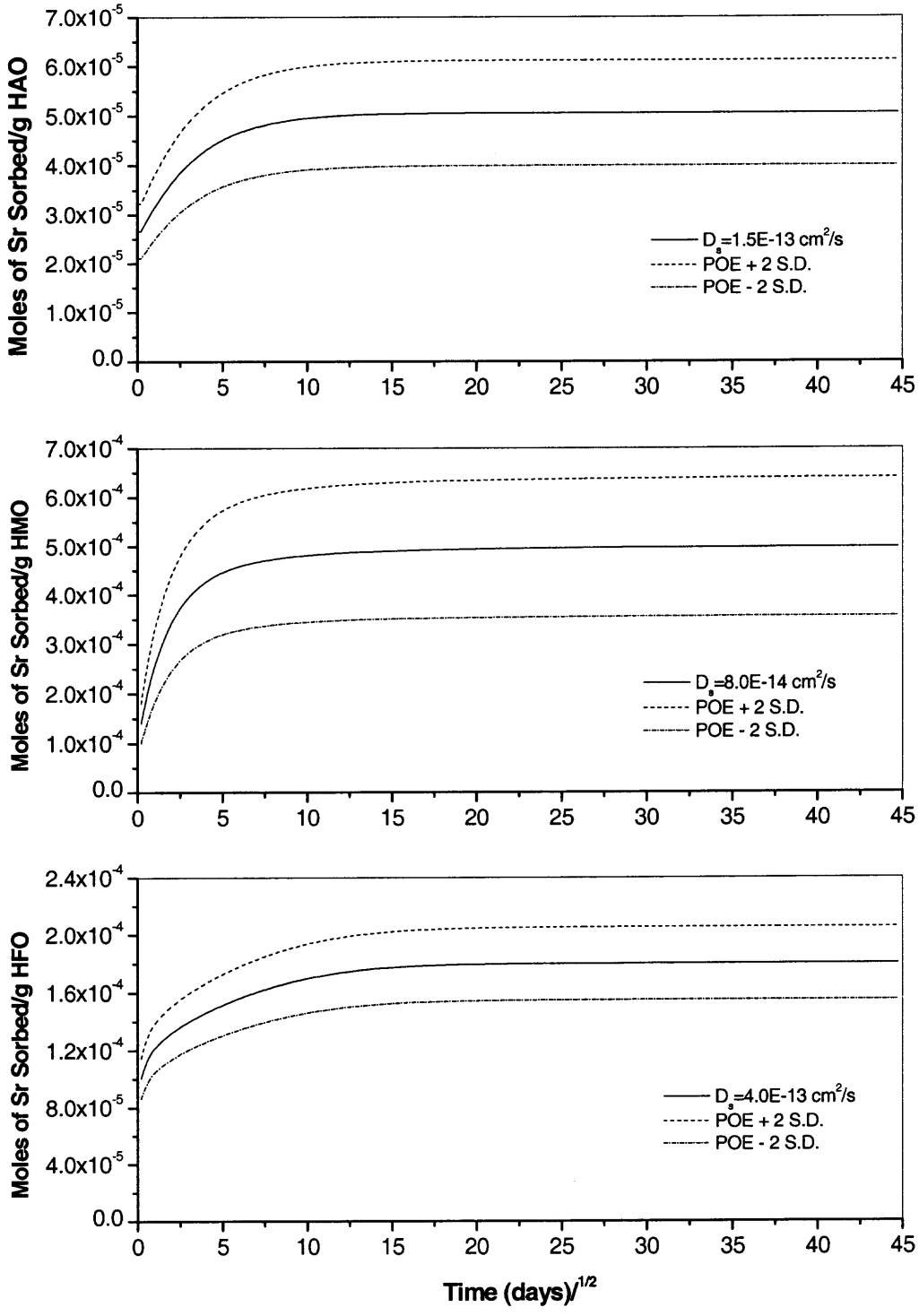

Figure 7.10 Sr sorption to HAO, HMO, and HFO as a function of time till equilibrium

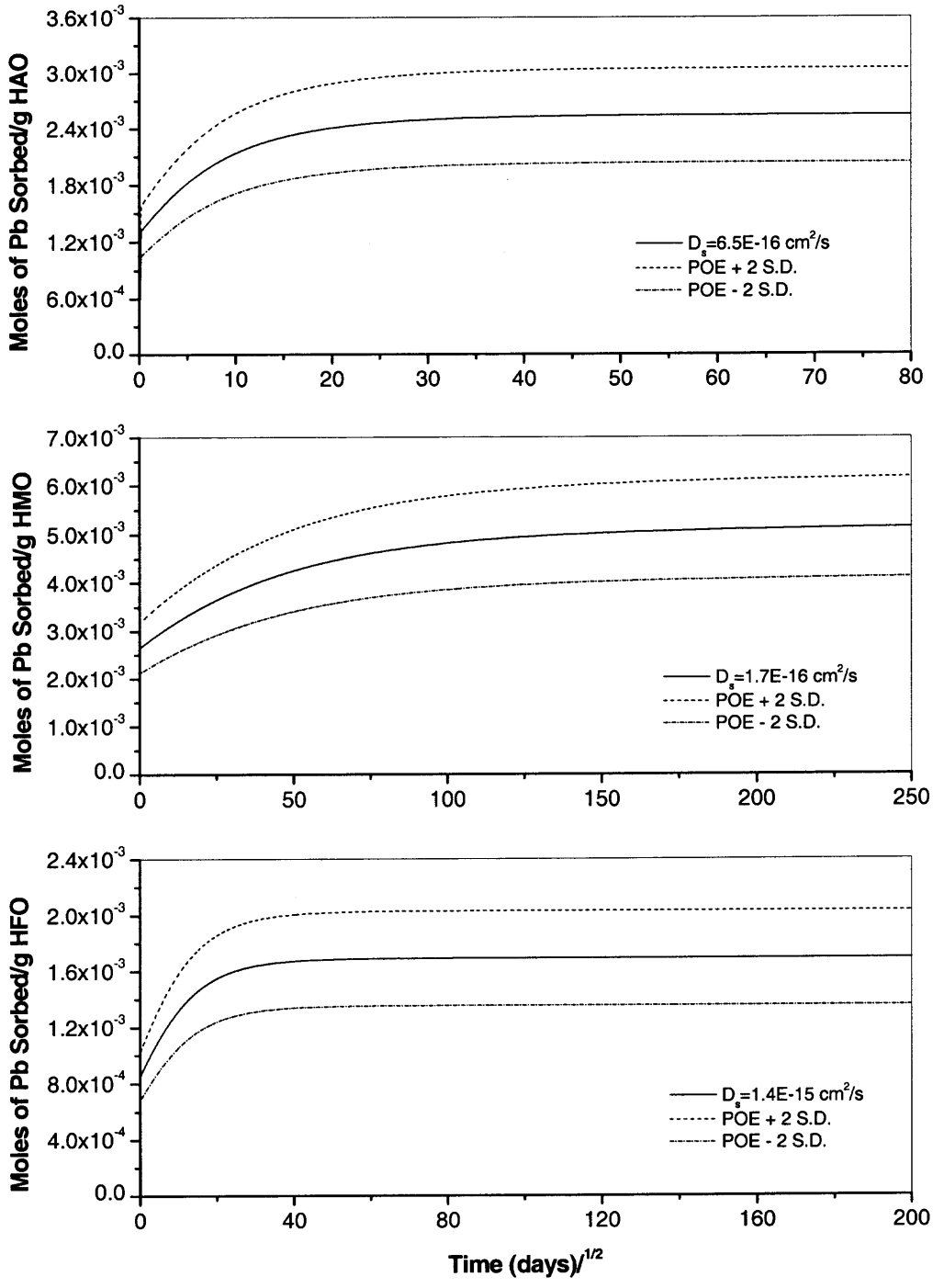

Figure 7.11 Pb sorption to HAO, HMO, and HFO as a function of time till equilibrium

isotherm, and S is the bulk concentration. To solve Equation 7.4 combined with boundary condition Equations 7.13 and 7.18, first, these equations are transformed to

$$\frac{\partial C}{\partial \tau} = \frac{1}{x^2} \frac{\partial \left[x^2 \left(\frac{\partial C}{\partial x} \right) \right]}{\partial x} \tag{7.19}$$

$$C(x,0) = 0 \tag{7.20}$$

$$\frac{\partial C}{\partial x}(0,\tau) = 0 \tag{7.21}$$

$$\frac{\partial C}{\partial x}(1,\tau) = B(S - S_t) \tag{7.22}$$

where

$$\tau = \frac{D}{R^2} t, \; x = \frac{r}{R}, \text{ and } B = \frac{Rk}{D\rho} \tag{7.23}$$

Specifically, B lies in the range of 0.1-100 based on ranges of parameters, D, 10^{-12} to 10^{-18} cm^2/s, k, 10^{-8} to 10^{-14} cm/s, and R, 0.13 to 78.3 μm. Then, the method of parabolic concentration layer approximation (Yao and Tien, 1992) is applied. The derivations were made by assuming that the concentration profile within particle may be represented by a parabolic expression over a spatial domain with time. The intraparticle concentration profile is as follows:

$$C = C_0 = \begin{cases} a + bx + dx^2, & 1 - \delta \le x \le 1 \\ 0, & 0 \le x \le 1 - \delta \end{cases} \tag{7.24}$$

where δ is the concentration layer thickness and a, b, and d are time-varying coefficients to be determined, and C_0 is the initial value of C. From continuous function,

$$C = C_0 \text{ and } \frac{\partial C}{\partial x} = 0 \text{ at } x = 1 - \delta \tag{7.25}$$

From Equations 7.24 and 7.25, a, b, and d can be solved. Then, given a vanishing average residual and assuming δ is much less than unity, the following equation is derived (Yao and Tien, 1992):

$$\frac{dC}{d\tau} = 6\left(\frac{C_t - C_0}{C - C_0} + \frac{1}{2}\right)(C_t - C) \tag{7.26}$$

where

$$C_t = \frac{(1 - B/K_d)C}{4} + \frac{1}{2}\left[\frac{1}{4}(1 - B/K_d)^2 C^2 + 2C(C + BS)\right]^{1/2} \tag{7.27}$$

with $C_0 = 0$, equation becomes

$$\frac{dC}{d\tau} = 6\left(\frac{C_t}{C} + \frac{1}{2}\right)(C_t - C) \tag{7.28}$$

replacing τ by t,

$$\frac{dC}{dt} = \frac{6D}{R^2}\left(\frac{C_t}{C} + \frac{1}{2}\right)(C_t - C) \tag{7.29}$$

In order to assess the accuracy of the above approximation method, Yao and Tien (1992) obtained the numerical solution by applying the orthogonal collocation method for intraparticle diffusion. The solution is exact in the sense that the number of collocation points is symmetrically increased until there is no discernible change in the solution. The method of parabolic concentration layer approximation is accurate when comparing the results with the numerical solution. Based on the example from Yao and Tien (1992), demonstration and validation of the approximation method with numerical methods are provided in Appendix A.

Substituting Equation 7.29 into Equation 7.11,

$$\theta\frac{\partial S}{\partial t}=\theta\frac{\partial}{\partial x_i}\left(D_{ij}\frac{\partial S}{\partial x_j}\right)-\frac{\partial}{\partial x_i}(q_i S)-\rho_b K_d\frac{\partial S}{\partial t}-\frac{6\rho_b D}{R^2}\left(\frac{C_t}{C}+\frac{1}{2}\right)(C_t-C) \qquad (7.30)$$

By rearranging terms, the governing equation describing microscopic intraparticle diffusion coupled with advection and dispersion is the following

$$R_1\frac{\partial S}{\partial t}=\frac{\partial}{\partial x_i}\left(D_{ij}\frac{\partial S}{\partial x_j}\right)-\frac{1}{\theta}\frac{\partial}{\partial x_i}(q_i S)-\frac{6\rho_b D}{\theta R^2}\left(\frac{C_t}{C}+\frac{1}{2}\right)(C_t-C) \qquad (7.31)$$

where the retardation factor is defined as

$$R_1=1+\frac{\rho_b K_d}{\theta} \qquad (7.32)$$

To solve coupled transport equations, such as Equation 7.31, the operator split (OS) method (Yanenko, 1971) is an efficient numerical strategy. The OS is a decoupling technique for solving flow problems involving coupled chemical transport and reaction processes, and is widely used for the numerical computation of reactive flow (Zheng, 1990; Clement, 1997; Barry *et al.*, 1997; Lu *et al.*, 1999; Clement *et al.*, 2000; Sportisse *et al.*, 2000; Diaw *et al.*, 2001; Islam and Singhal, 2002). The reasons for implementing such an approach to reactive transport problems are as follows: first, existing transport codes can be used to incorporate new transport modules; and, secondly, computational requirements are reduced (Barry *et al.*, 1996; Sportisse *et al.*, 2000). Specific examples for applying the OS are presented below.

Zheng (1990) utilized this operator-split strategy to develop a general numerical solution scheme for solving the coupled partial/ordinary differential equations, which described single-species transport with a first-order reaction. Clement and coworkers (1997 and 2000) applied an OS method to develop a general numerical solution scheme

for solving the coupled partial/ordinary differential equations for fate and transport of aqueous and solid phase species in multi-dimensional saturated porous media. They developed a reactive model to aid in the analysis of a natural attenuating system for chlorinated solvent sites. Lu *et al.* (1999) used the operator-splitting method to solve a set of reactive transport equations that describe hydrocarbon decay and transport under aerobic and sequential-anaerobic environments. Sportisse *et al.* (2000) performed numerical tests by the OS method in one-dimensional case with diffusion, chemical kinetics, dry deposition, and emission. Diaw *et al.* (2001) used operator splitting to solve the one dimensional solute transport equation in saturated-unsaturated porous media, with the discontinuous finite element method for discretization of the advective term. Islam and Singhal (2002) employed a two-step sequential operator splitting method to solve a coupled transport model and biogeochemical reaction equation, which simulates one-dimensional multi-component landfill leachate transport.

In operator splitting, the intraparticle diffusion process can be separated from the governing equations and assembled into a set of differential equations:

$$\frac{dS}{dt} = -\frac{6\rho_b D}{\theta R_1 R^2}\left(\frac{C_t}{C} + \frac{1}{2}\right)(C_t - C) \tag{7.33}$$

$$\frac{dC}{dt} = \frac{6D}{R^2}\left(\frac{C_t}{C} + \frac{1}{2}\right)(C_t - C) \tag{7.34}$$

A new user-defined package is developed to setup these equations, which is presented as following.

7.3 Coding Process

To simulate the intraparticle diffusion in a solute transport system, the process is coded into the RT3D reaction module, where a user-defined reaction package is developed. RT3D's user-defined reaction packages can be created using one of two approaches: the dynamically linked library (DLL) option or the linked subroutine option. With the DLL option, the subroutine for the reaction package is compiled as a stand-alone DLL, automatically launched by RT3D when RT3D is executed. With the linked subroutine option, the code for the new reaction subroutine is compiled and linked with the RT3D source code. The RT3D executable must be recompiled each time the reaction package is modified (Clement and Jones, 2000). Because of the need for portability of the developed reaction package, the DLL option is the more convenient of the two options. Therefore, the intraparticle diffusion package is created using the dynamically linked library (DLL) approach.

Furthermore, in the DLL approach, three methods can be used for coding the intraparticle diffusion package. The difference between these methods lies in the ways to treat the process parameters. In the first method, all parameter values are explicitly assigned within the diffusion module prior to compilation. This is not an efficient method since it requires recompilation of the diffusion routine whenever a parameter is modified. In the second method, all of the parameter values are spatially constant but are assigned and modified externally as input data. In the third method, some parameters are treated as spatially variable and assigned to each cell. Others are externally assigned and modified as input data, in a similar fashion to the second method. However, this option requires more computer resources, both execution time and memory. The third method is the most

viable one to treat different process parameters, however, initially the first method was used to reduce the need for debugging. After creating the intraparticle diffusion process package and linking it to RT3D, the process can run a full-fledged simulation with GMS.

7.4 Summary

In this chapter, an approach was presented for incorporating the diffusion process into RT3D module of GMS, which is a macroscopic transport code. A case study of implementing the new intraparticle diffusion package with bulk transport in GMS is presented in the next chapter.

CHAPTER 8

INCORPORATING INTRAPARTICLE SURFACE DIFFUSION INTO A BULK TRANSPORT CODE FOR GROUNDWATER MODELING: CASE STUDY FOR Sr^{90} AT THE HANFORD SITE

Based on the review of existing solute transport models, either equilibrium or reaction rate approaches are often employed for describing metal sorption. However, many studies have demonstrated that intraparticle diffusion is an important and rate-limiting process in the sorption, and therefore needs to be considered in realistic solute transport modeling. This work is focused on incorporating intraparticle surface diffusion into a bulk transport code for groundwater flow and solute transport. Based on earlier work (Trivedi and Axe, 1999, 2000, and 2001), correlations were developed for predicting theoretical diffusivities; in this chapter an approach for assessing both surface diffusion and distribution coefficients is presented. The diffusion model was coded into the Groundwater Modeling System (GMS) (BYU, 2002), where MODFLOW-2000 (Harbaugh *et al.*, 2000) handles groundwater flow, and RT3D addresses solute transport. The resulting model was employed for simulating and predicting Sr^{90} mobility at the U.S. DOE Hanford Site, Washington.

8.1 Case Study

The Hanford Site, a facility in the U.S. DOE nuclear weapons complex, encompasses 586 square miles and is located along the Columbia River in southeastern Washington State (Figure 8.1). The site was acquired by the federal government in 1943, and until the

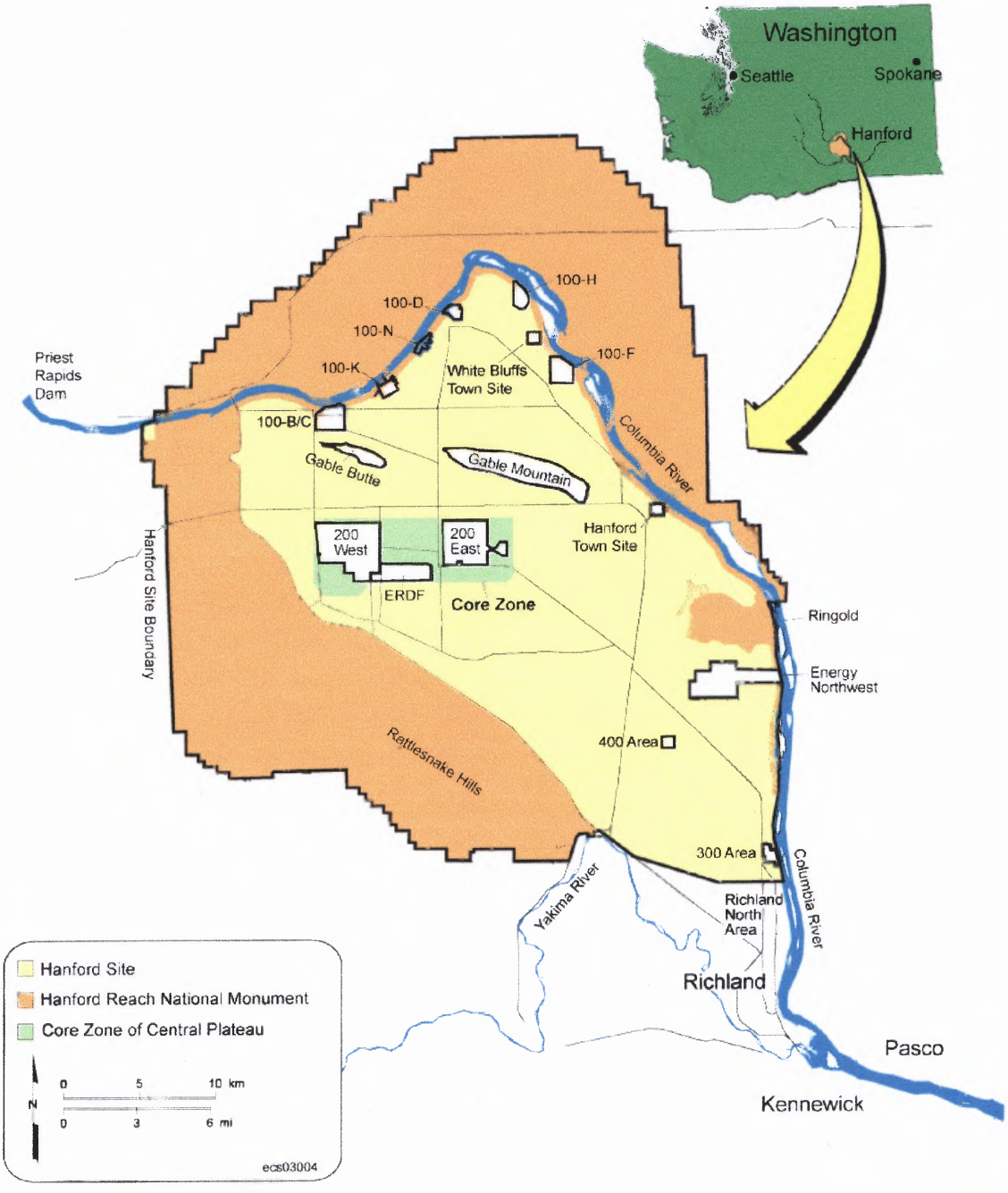

Figure 8.1 Map of the Hanford Site (adapted from Hartman *et al.* (2003))

1980s was dedicated primarily to the production of plutonium for national defense and the management of resulting waste. Today, under the direction of the U.S. DOE, Hanford is engaged in the world's largest environmental cleanup project, with a number of technical, political, regulatory, financial, and cultural issues (Hartman *et al.*, 2003). Sr^{90} is a major radionuclide in spent nuclear fuel (from nuclear reactors) and high-level radioactive wastes associated with weapons production. Sr^{90} is a known carcinogen due to its emission of ionizing radiation and confirmed by epidemiological studies on radiation-induced tumors (U.S. EPA, 1994). Contamination has been observed in the 100-N area adjacent to the Columbia River. This plume originates from two liquid waste disposal facilities, 116-N-1 and 116-N-3, which are still in operation; other wastes include nitrate, sulfate, and petroleum hydrocarbons (Hartman *et al.*, 2002 and 2003).

In GMS, the grid approach or the conceptual model approach can be used to construct a groundwater simulation; the latter is usually employed for an irregular and complex hydrogeological system such as the 100-N area. Based on data availability, an aquifer can be built by either scatter points or stratigraphy: the scatter points approach is a simpler method for defining layer elevations, while stratigraphy modeling is implemented through borehole interpretation based on a set of TINs (Triangulated Irregular Network) and is best suited for complex systems. Therefore, for the Hanford Site, the stratigraphy approach is employed where the conceptual model converts the system into the 3D grid MODFLOW (Harbaugh *et al.*, 2000).

The Hanford Site lies within the Pasco Basin, a structural depression that has accumulated a relatively thick sequence of fluvial, lacustrine, and glaciofluvial sediments. The sedimentary deposits comprise an unconfined aquifer system. Based on

site characterization (Vermeul *et al.*, 2003), 16 boreholes at Hanford are used and assist in representing the different types of hydrogeologic units: the Hanford Formation, the Ringold Formation, and the Basalt Formation (Table 8.1). A set of TINs is constructed representing the interfaces between adjacent layers according the vertices along the boundary (Figure 8.2). After creating the aquifer model, a conceptual model bounded by the Columbia River is constructed including the local coverage of sources/sinks and recharge. Further, the conceptual model is converted to the groundwater grid model with the active and inactive zones as well as assigned layer ranges to stratigraphic units representing consecutive sequences coinciding with the aquifer model. After parameters are defined, the groundwater model is launched to acquire head profiles for the Hanford Site (Figure 8.3).

As discussed above, the Sr^{90} plume originates from two disposal facilities, 116-N-1 and 116-N-3, in the 100-N area (Figure 8.1). Based on the Hanford Site model, a local model is developed through a regional to local model conversion, and is used to simulate Sr^{90} transport in and around the 100-N area. This conversion is often referred to as telescopic grid refinement and can be implemented through GMS. During this stage, groundwater elevations computed from the regional model are applied as specified head boundary conditions to the local scale model. After the conversion process, a local model is developed (Figure 8.4).

To address Sr^{90} mobility, distribution and diffusion coefficients were calculated based on the composition of sediments, which are predominantly quartz with iron and manganese oxide coatings (Barnett *et al.*, 2002; Pace *et al.*, 2003). Specifically, the

Table 8.1 Summary of Hydrogeological Units at the Hanford Site

Hydrogeological Unit	Lithologic Description	Horizontal Hydraulic Conductivity (m/d)	Vertical Hydraulic Conductivity (m/d)	Specific Yield	Effective Porosity
Hanford Formation	Fluvial gravel and coarse sands	50	2.5	0.15	0.31
Ringold Formation	Fluvial gravel, sands, and silts	1.0	0.05	0.15	0.33
Basalt Formation	Basalt	1.4×10^{-5}	7×10^{-7}	0.15	0.015

[a] Data collected from Cole *et al.* (2001)

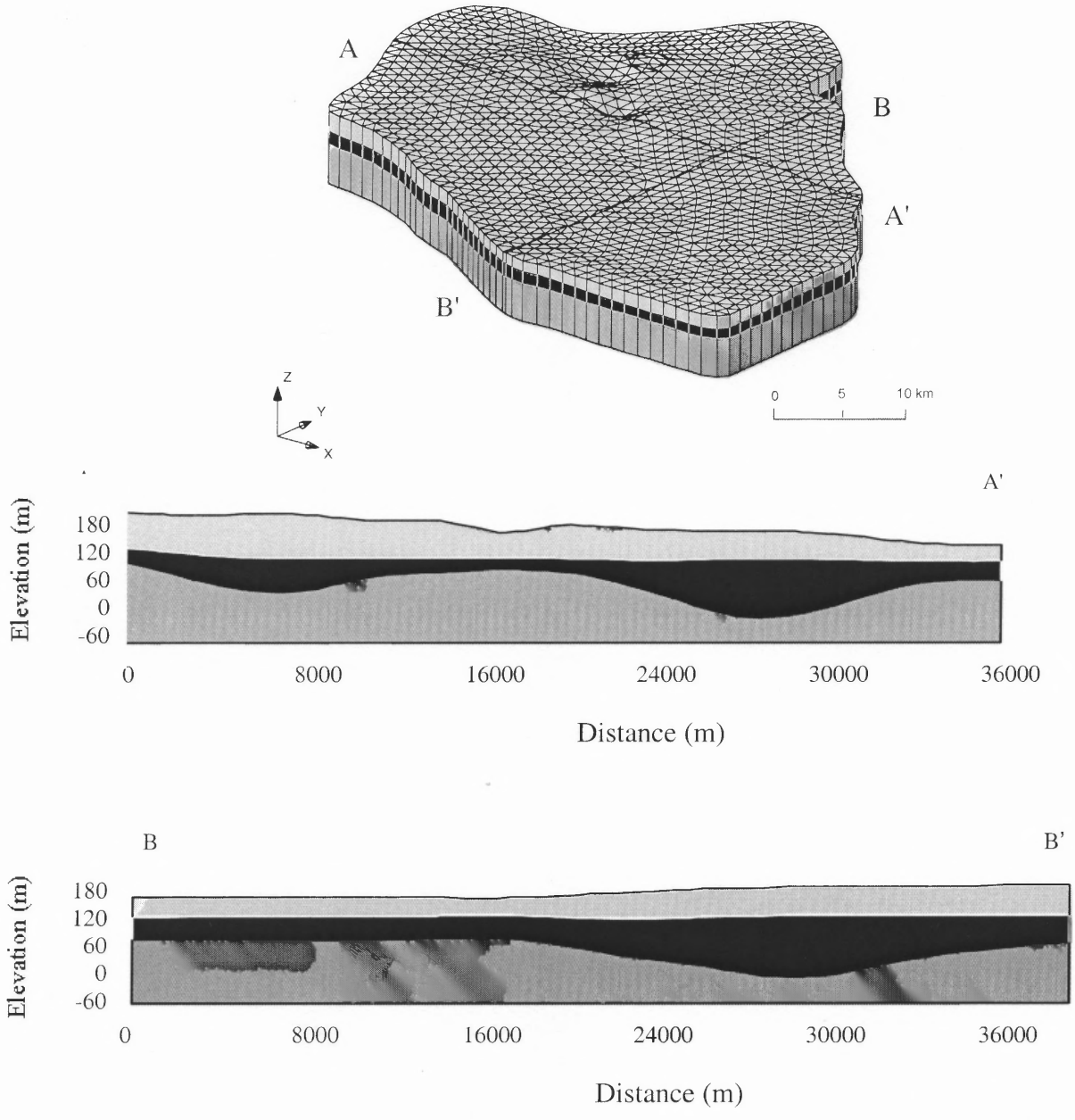

Figure 8.2 Aquifer model of the Hanford Site (light grey: the Hanford Formation, black: the Ringold Formation, and dark grey: the Basalt Formation), where the Ringold Formation is the primary aquifer (developed based on Vermeul *et al.* (2003))

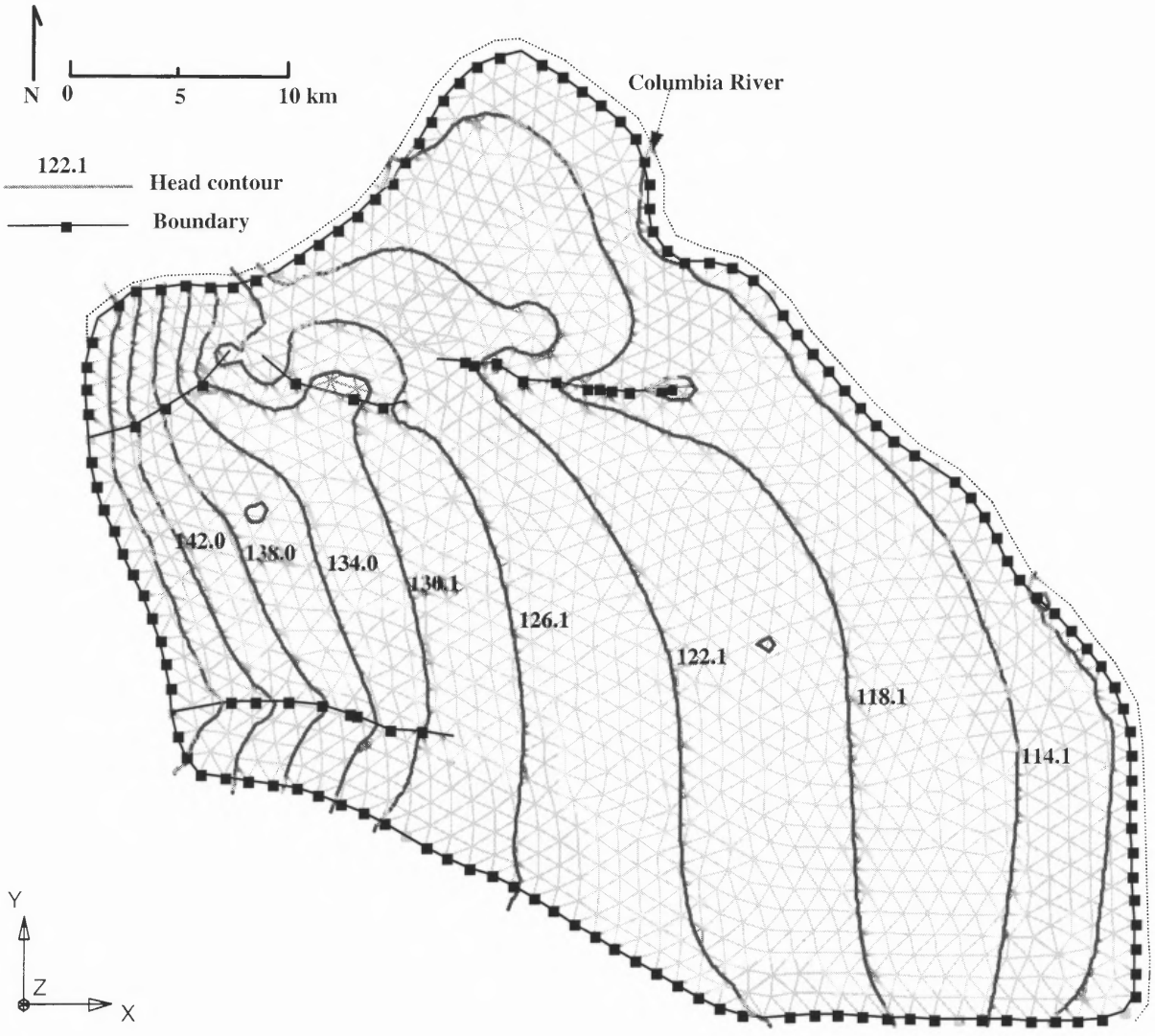

Figure 8.3 Groundwater head profile of the Hanford Site (Unit: m)

principal aquifer or the Ringold Formation is composed of quartz with the iron oxide, 25.3 g kg^{-1}, and the manganese oxide, 4.0 g kg^{-1} (Barnett et al., 2002); and the Hanford Formation consists for the most part of quartz with iron oxide, 5.4 g kg^{-1} (Pace et al., 2003). As the Ringold Formation, Layer 2 in our model, controls groundwater flow, its mineralogy is used exclusively to calculate distribution and diffusion coefficients. Based on correlations for predicting thermodynamic and transport parameters (Trivedi and Axe, 1999, 2000, and 2001), relationships for distribution and diffusion coefficients as a function of pH were developed for Sr^{90} sorption to aluminum, iron, and manganese oxides (Figure 8.5). In addressing the transient sorption process as well as surface affinity, hydrous oxides are assumed dominant (Axe and Anderson, 1995; Trivedi and Axe, 1999) with respect to interactions with Sr^{90}. As the Ringold Formation pH has been observed to be on average 6.8 ± 0.6 (Barnett et al., 2002), distribution and surface diffusion coefficients were estimated based on the mass fraction of oxides (Table 8.2). Barnett et al. (2002) collected samples from the Ringold Formation and found 98% sand, 2% silt, and less than 1% clay (wt/wt) with an associated size range of 0.0625-2 mm for sand, 0.002-0.0625 mm for silt, and less than 0.002 mm for clay (USGS, 2004). Using Monte Carlo simulations with 10,000 iterations, the mean is given a Gaussian distribution and the particle size range of Ringold Formation. The oxide particle size was evaluated based on the mass present (Table 8.2).

For the boundary condition, the correlation (Bird *et al.*, 2002)

$$Sh_m = \frac{kd}{D} = 0.991(\mathrm{Re\ Sc})^{1/3} \tag{8.11}$$

was used to obtain the external mass transfer coefficient, where d is the particle diameter; Sh_m, 79, is the Sherwood number; $\mathrm{Re} = dv/\nu$, 7.2×10^{-5}, is the Reynolds number (ν is the

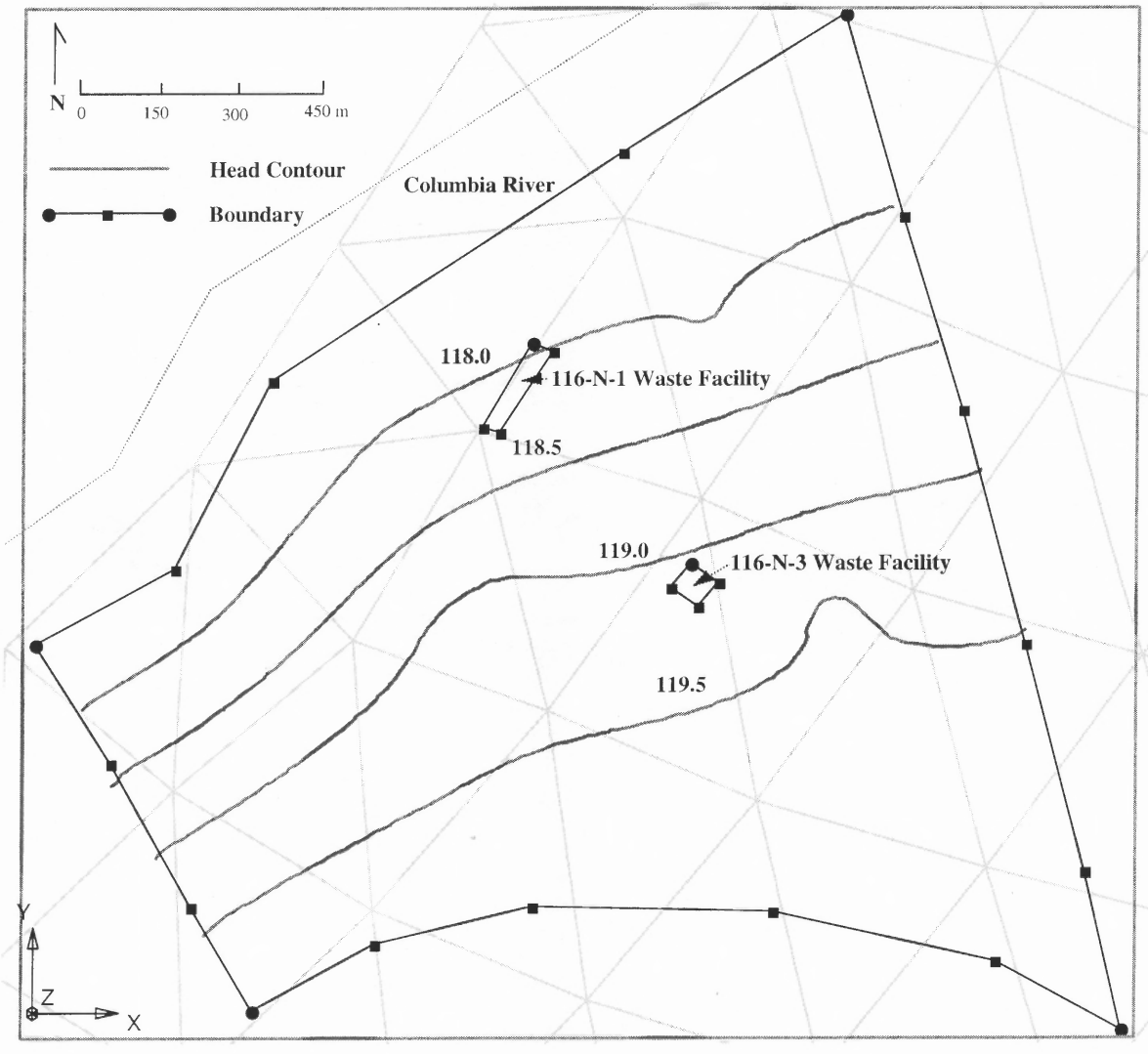

Figure 8.4 Local model of the 100-N area converted from the regional model of the Hanford Site (Unit: m) (developed based on Hartman *et al.* (2002 and 2003))

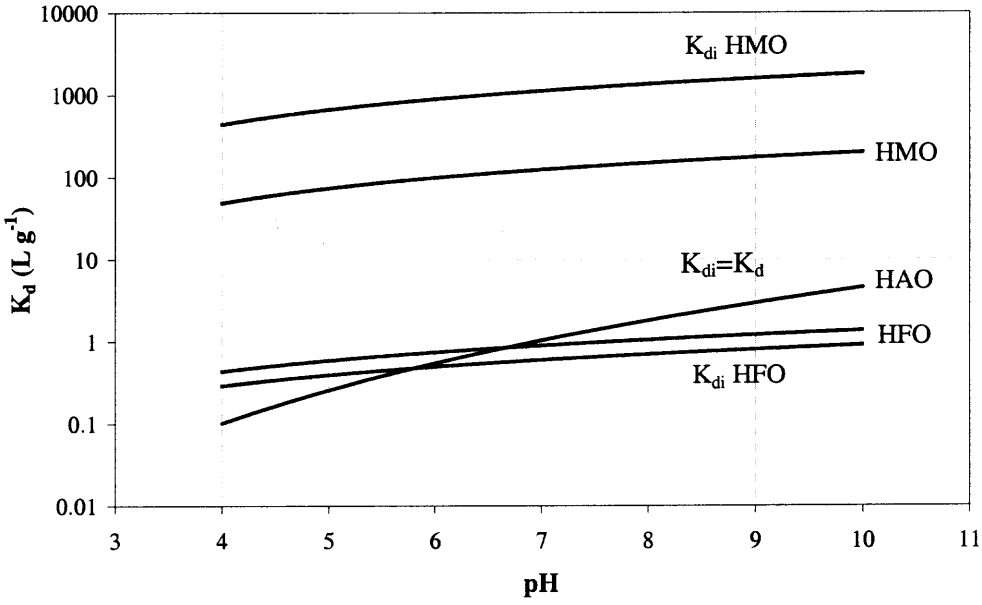

(a) Distribution coefficient vs. pH

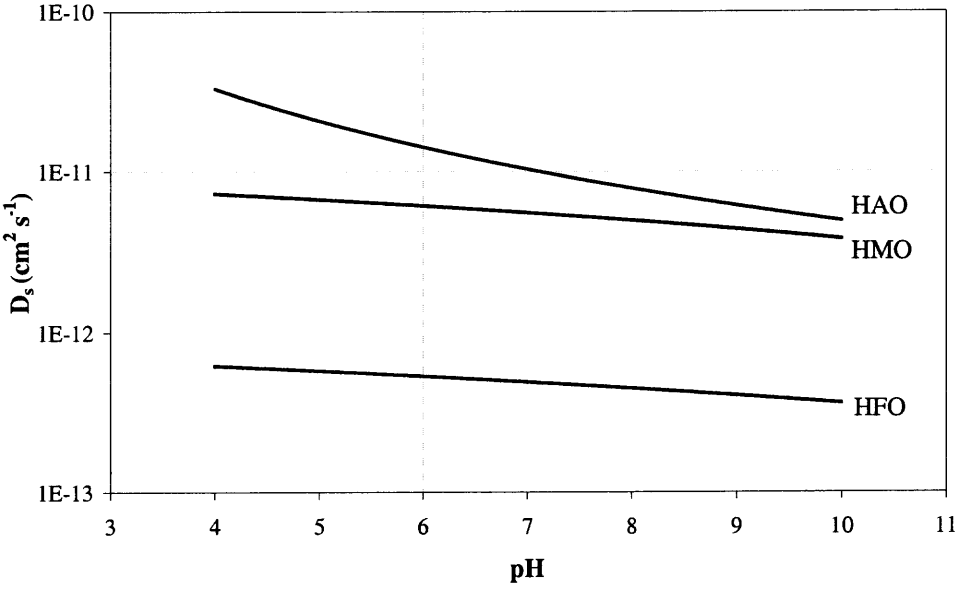

(b) Surface diffusivity vs. pH

Figure 8.5 Sr^{90} distribution and diffusion coefficients vs. pH for HAO, HFO, and HMO at 25°C based on Trivedi and Axe (1999, 2000, and 2001). K_{di} is the internal distribution coefficient representing the product of the equilibrium constant and internal site density; K_d is the external distribution coefficient and is the product of the equilibrium constant and external surface site density. For HAO, K_{di} is equivalent to K_d as internal sites constitute approximately 50% of the total sites.

Table 8.2 Input Data for the Modeling of Sr^{90} at the Hanford Site

Site Specific Data	Hydrogeological Unit	Longitudinal Dispersivity[a] (m)	Transverse Dispersivity[a] (m)	Vertical Dispersivity[a] (m)	Mean Particle Size (μm)	Bulk Density (g cm^{-3})
Layer 1	Hanford Formation	6.0	1.8	1.8	1,233	1.5
Layer 2	Ringold Formation	30.5	9.2	9.2	967	1.3
Layer 3, 4	Basalt Formation	30.5	9.2	9.2	967	1.3

Oxide Mass Fraction[b] (g kg^{-1})		Oxide Particle Size (μm)	Distribution Coefficient (L g^{-1})	Diffusion Coefficient (cm^2 s^{-1})	External Mass Transfer Coefficient (cm s^{-1})	Simulation Time (Years)
Fe	Mn					
25.3	4.0	28	16.4	1.1×10^{-12}	1.8×10^{-8}	14

[a] Data adapted from Cole *et al.* (2001).
[b] Data adapted from Barnett *et al.* (2002).

bulk velocity and ν is the kinematic viscosity); and $Sc = \nu/D$, 7.1×10^9, is the Schmidt number.

Like many other sites, the recharge rate is an unknown quantity. This is a common impediment that usually limits the use of transport models in realistic field simulations. To circumvent this limitation, the recharge rate was quantified through a model calibration process, which in turn was constrained by measured field-scale data, aquifer characteristics, and groundwater quality (Table 8.2). Vermeul *et al.* (2003) reported the rate ranged between 0.0026 and 0.127 m/year; the average 0.073 m/year was employed in this work. However, during the calibration process, varying the rate did not significantly affect the model results. Source concentration is a more sensitive parameter, which needed to be qualified and assessed. Samples collected between 1993 and 2002 (Hartman *et al.*, 2003) show Sr^{90} concentrations in the liquid waste disposal facilities, 116-N-1 and 116-N-3 (Figure 8.6), ranging between 8 and 95 mg L^{-1}. Calibrating with varying concentrations revealed that 90.0 and 45.0 mg L^{-1} of Sr^{90} in the two facilities were required to simulate measured conditions in 2001 and 2002 (Figure 8.7). Sr^{90} transport was then simulated from 1990 to 2002 (Figure 8.8); the front contour (minimum plotted) reflects the concentration of 0.0024 mg L^{-1}, which is one tenth of the drinking water standard for Sr^{90} (U.S. EPA, 1996). Over 12 years, the Sr^{90} plume extended in and around 100-N area. This contour provides a clear picture of the area adversely impacted and can assist those individuals assessing remediation and control activities. Furthermore, Sr^{90} transport is simulated for 2003 and 2004 (Figure 8.9); the most recently available data of 2003 (Hartman *et al.*, 2004) validated observed modeling results. Sr^{90} continues to migrate within the 100-N area and will potentially extend into other areas of the Hanford

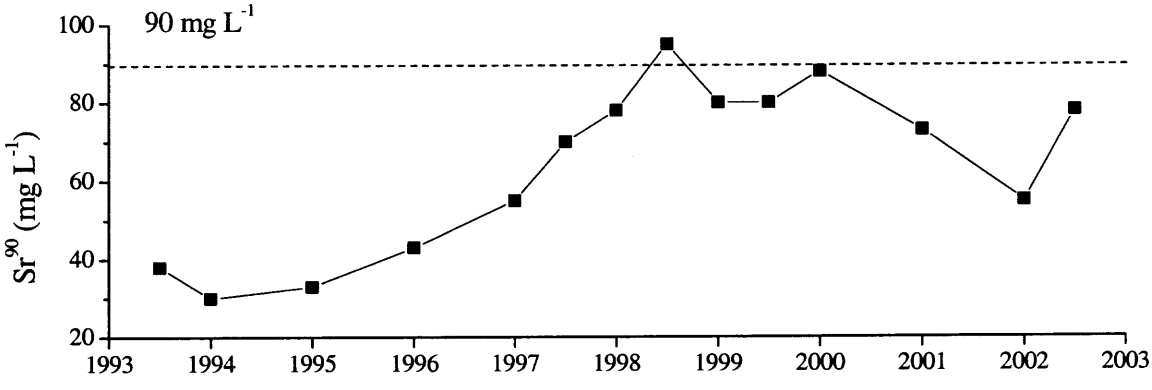

(a) 116-N-1 Waste Disposal Facility

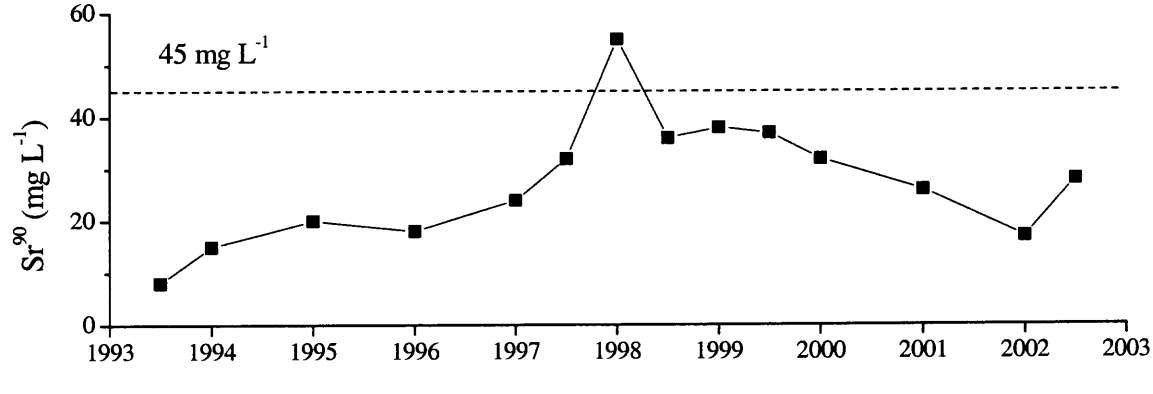

(b) 116-N-3 Waste Disposal Facility

Figure 8.6 Sr^{90} concentrations in the liquid waste disposal facilities of the 100-N area, Hanford Site

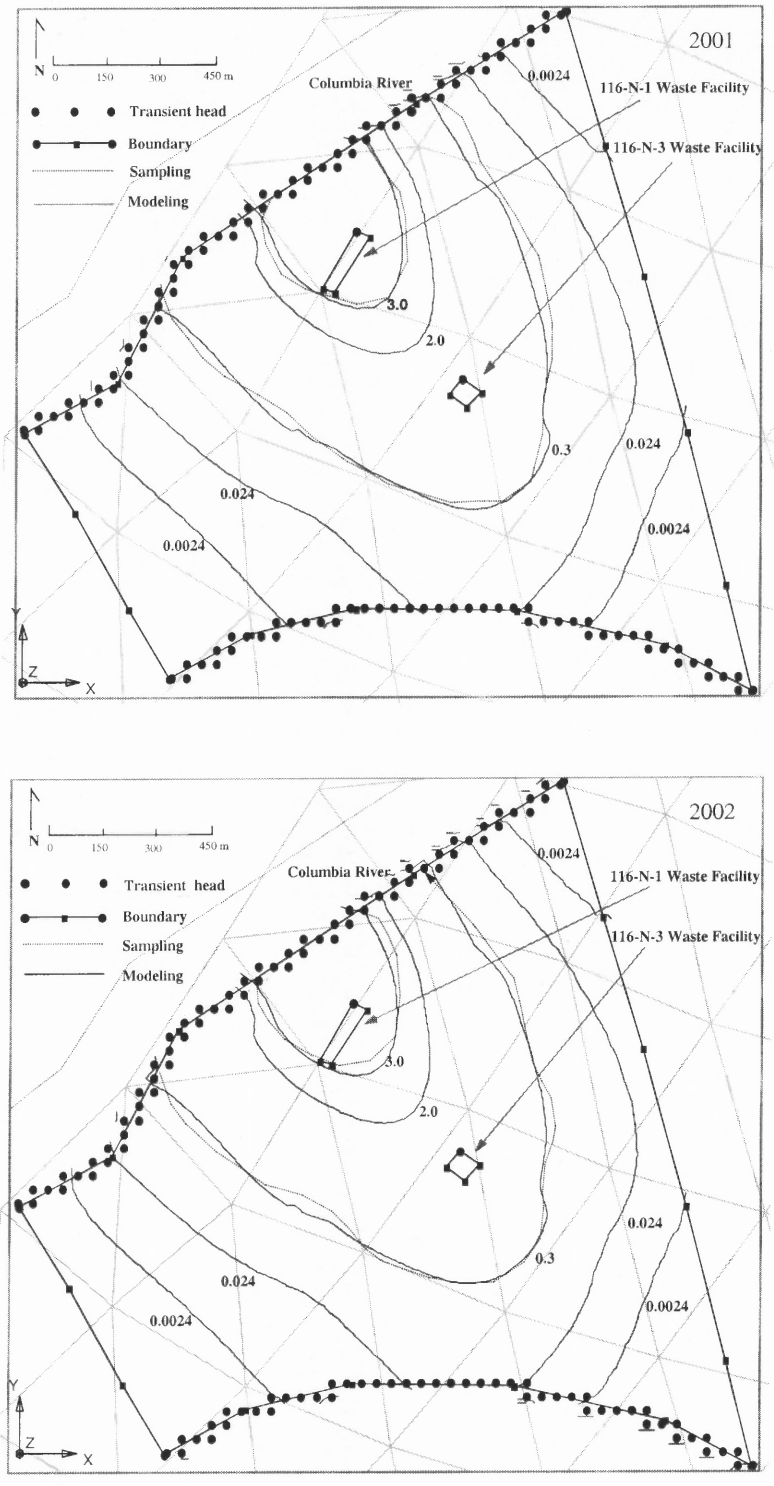

Figure 8.7 Calibration results with sampling contours of the Sr^{90} plume for 2001 and 2002 over the 100-N area, Hanford Site (Unit: mg L^{-1})

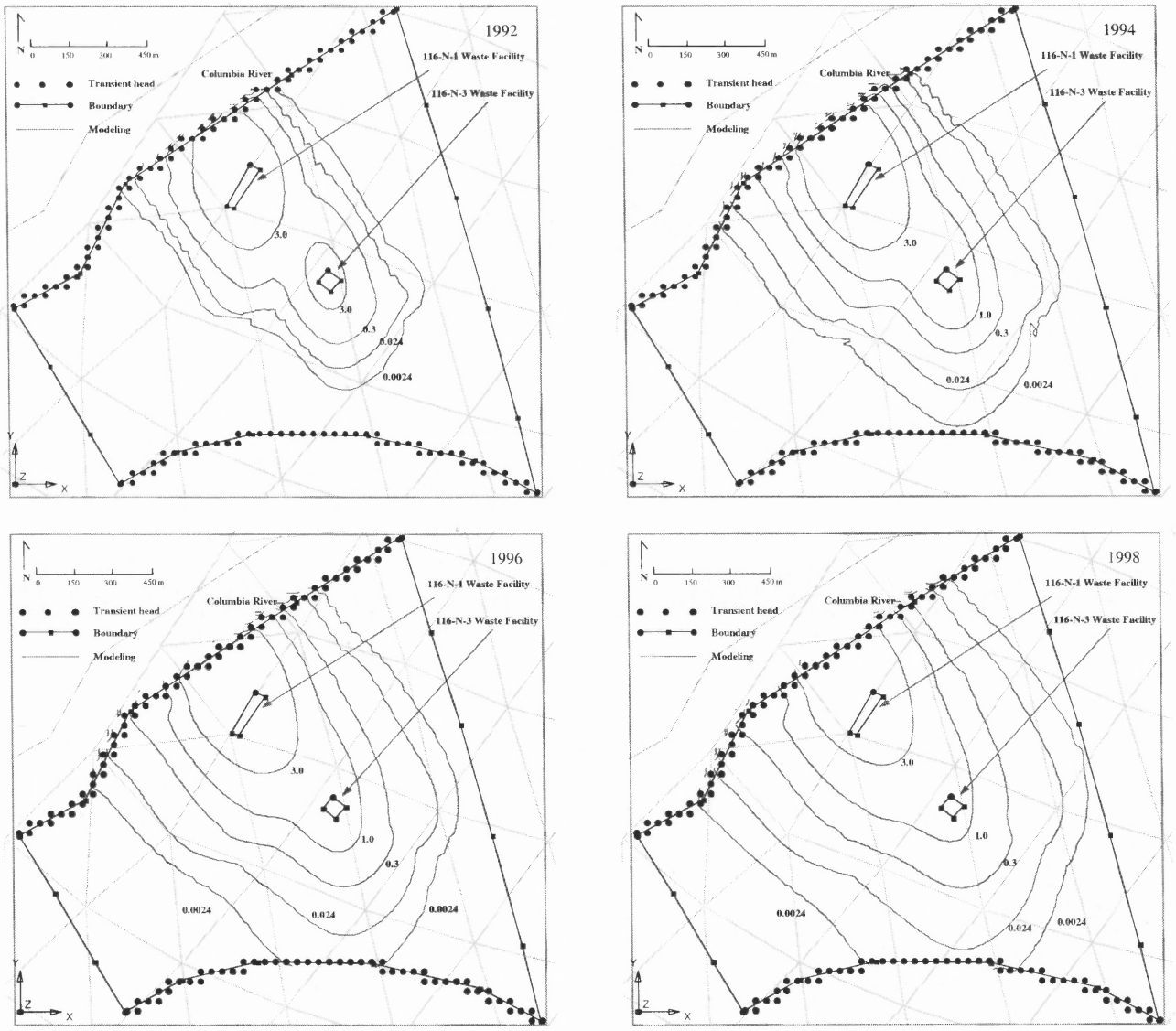

Figure 8.8 Modeling results of the Sr^{90} plume for 1992, 1994, 1996, and 1998 over the 100-N area, Hanford Site (Unit: mg L^{-1})

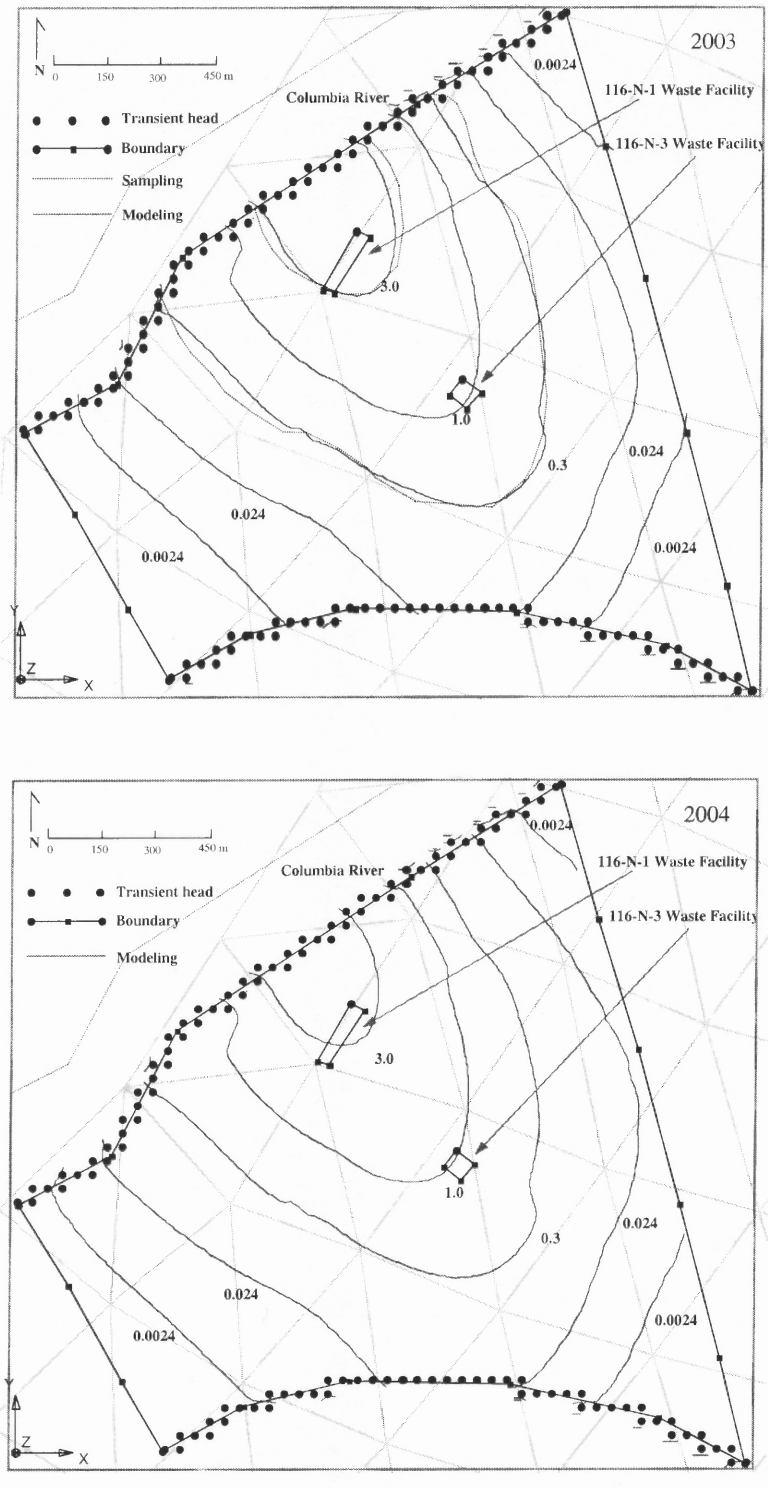

Figure 8.9 Prediction and validation of the Sr^{90} plume for 2003 and 2004 over the 100-N area, Hanford Site (Unit: mg L^{-1})

Site and beyond.

8.2 Summary

Intraparticle surface diffusion, which is the rate-limiting process for metal sorption to amorphous oxides as discrete particles and coatings, was incorporated into GMS to accurately simulate metal contaminant transport and fate. In the model development, the parabolic concentration layer approximation was employed, and the operator split technique was used to solve the microscopic diffusion equation coupled with macroscopic advection and dispersion. The resulting model was employed for simulating Sr^{90} mobility at the U.S. DOE Hanford Site, Washington. During the simulation, the conceptual model approach along with stratigraphy modeling based on borehole data was applied. The methods for addressing the distribution coefficient as well as the surface diffusivity are outlined and can be applied easily to other sites. Furthermore, the local model developed to simulate Sr^{90} transport in and around the 100-N area from 1990 to 2004, indicates the contaminant plume is slowly extending beyond this area and into the adjacent areas.

For understanding risks associated with heavy metals to the surrounding environment, bioavailable species can be used to assess static or dynamic ecological risks resulting from exposure to different metals. A static ecological risk assessment is conducted for depleted uranium (DU) present at Aberdeen and Yuma Proving Grounds in the next chapter.

CHAPTER 9

USING A PROBABILISTIC APPROACH IN AN ECOLOGICAL RISK ASSESSMENT SIMULATION TOOL: TEST CASE FOR DEPLETED URANIUM (DU)

Once mobile and bioavailable species are known, the last step in the simulation process is to address risk. An ecological risk assessment is a process that evaluates the likelihood that adverse ecological effects may occur or are occurring as a result of exposure to one or more stressors (U.S. EPA, 1992a). The process is used to systematically evaluate and organize data, information, assumptions, and uncertainties to help understand and predict the relationships between stressors and ecological effects in a way that is useful for environmental decision-making. Ecological risks can be assessed through field studies; however, performing a large number of these studies may be inappropriate because of the expense in sacrificing receptors and the overall cost in obtaining field data. Because of the variety of habitats and species in an ecosystem and the associated interactions between biota and physical-chemical conditions, risk assessment is a complex process. Therefore, computer simulation tools are needed for risk assessment and they have become a powerful, cost-effective tool for understanding and managing ecological risks (Carbonell *et al.*, 2000; Sydelko *et al.*, 2001; Naito *et al.*, 2002; Lu *et al.*, 2003).

A computer simulation tool, the ERA model, has been developed for conducting ecological risk assessments (Lu *et al.*, 2003). This tool is based on a preliminary evaluation of existing eco-risk models and includes a Windows-based interface, an interactive database management system (DBMS), and a comprehensive evaluation of exposure pathways addressing site- and species- specific estimation of chemical uptake

from abiotic and biotic media. Monte Carlo simulations are used for characterizing parameter and risk uncertainty as probabilistic distributions. In the past, risk assessment methods have focused on a single indicator for risk. While this approach has found its usefulness as a screening tool, it does not consider the full range of available information, nor does it explicitly account for important sources of uncertainty in estimating risks (Lahkim *et al.*, 1999; Yegnan *et al.*, 2002). In addition, point estimates of risk may convey an inaccurate sense of accuracy and can lead to inconsistencies in making comparisons among risks (Thompson and Graham, 1996). Furthermore, relying on a single value estimate of risk for remedial activity typically results in an over estimation of costs (U.S. EPA, 1992a; Lahkim *et al.*, 1999).

Probabilistic risk assessment differs from the deterministic approach by allowing a value to be chosen from a distribution of plausible values for an exposure variable. Variables that can assume different values for different receptors are referred to as random variables. In probabilistic risk assessment, one or more (random) variables in the risk equation are defined mathematically by probability distributions. Similarly, the output of a probabilistic risk assessment is a range or distribution of risks experienced by the various members of the population of concern (Warren-Hicks and Moore, 1998). Probabilistic distribution methods have been employed in human (Vermeire *et al.*, 2001), ecological (Jager *et al.*, 2001), and technological risk assessments (Schumacher *et al.*, 2001) to quantify uncertainties in predictions of risks.

When performing an uncertainty analysis with probabilistic distributions generated with Monte Carlo simulations in ecological or human risk assessment, several commercial software packages are widely employed (Morgan and Henrion, 1998;

Lohman *et al.*, 2000; Moschandreas and Karuchit, 2002). For example, Crystal Ball® was employed in a probabilistic analysis of regional mercury impacts on wildlife. Another software, @Risk® was used as a screening level for a probabilistic assessment of mercury risks in the Florida Everglades food web (Lohman *et al.*, 2000). These tools are not specific for ecological risk assessment and have been widely applied to assess risks in other fields, such as financial consulting, cost estimate consulting, market research, engineering cost analysis, and insurance. Therefore, the user needs to be aware of how to apply software functions and recreate model equations, input parameters, and the foodweb for a given application. These procedures are relatively time consuming. In a comprehensive risk assessment, where exposure is addressed via the trophic levels of the food web, a spreadsheet approach for performing an uncertainty analysis is not practical as the result is only useful for the one condition studied. The risk assessment model with probabilistic distributions generated through Monte Carlo simulations addresses parameters and data (including the food web) are stored in the modifiable DBMS. In this study, the ERA simulation tool is used to assess risk of depleted uranium (DU) at two U.S. Army sites, Aberdeen and Yuma Proving Grounds (APG and YPG). Concerns have been raised at these two sites about the potential exposure to the associated ecosystems and adverse health effects of DU.

Depleted uranium is a by-product from processing natural uranium to produce the enriched form used as fuel for nuclear reactors or military applications (Hartmann *et al.*, 2000). Health risk of exposure to DU is a complex issue. Due to the low specific radioactivity and the dominance of α-radiation, no acute risk is likely from external exposure (Bleise *et al.*, 2003). However, internalized DU has a greater potential for

adverse impacts on body than that externalized, such as mutagenesis from radiological effects where risks are a function of the particle characteristics. Renal, reproductive, and developmental effects from chemical impacts are a function of the route of exposure, duration of exposure, and speciation (Fulco *et al.*, 2000). McClain *et al.* (2001) studied the primary transport route of DU through wounds and confirmed mutagenic behavior of DU, which transformed human osteoblast cells to a tumorigenic phenotype. The non-radioactive or chemical effect associated with exposure to uranium and its compounds involves renal toxicity, detected by the presence of protein and cell casts in the urine. Additionally, the chemical and radiological impacts of uranium can act synergistically to cause tissue damage. Therefore, it cannot be assumed that cancer is due solely to the radiological effects of uranium or that organ damage is exclusively due to its heavy-metal properties (Fulco *et al.*, 2000).

Since the 1950s, DU has been used as a penetrator in munitions and testing programs at APG, which is located in the western shore of Chesapeake Bay, a productive and complex ecosystem. The facility provides design and testing of ordnance material in close proximity to the nation's industrial and shipping centers. As a result of the program, DU has been deposited on over 1500 acres. Most penetrator impacts occurred within about 500 m of the firing axis after the DU munitions passed through soft targets used to check accuracy and performance. Penetrators strike the ground, trees, and wetlands after hitting soft targets and eventually come to rest in the impact area (Ebinger *et al.*, 1996). A second-highly used test area is located at YPG near the Arizona-California border and in the vicinity of the Colorado River, Squaw Lake, and Mittry Lake. YPG began testing DU munitions against soft targets in the 1980s, and the test area comprises 12,000 acres

(Oxenberg, 1997). Ebinger *et al.* (1996) reported that redistribution in the arid environment at YPG was mainly due to erosion of DU fragments and redeposition in washes that drain the area. Ingestion of DU by wildlife is likely from consuming DU-contaminated soil accumulated on vegetation or pelts.

In this chapter, the components of the ERA model are discussed and include along with exposure pathways, the relation-based food web, ecosystem receptors, risk characterization, and uncertainty analysis. The process for conducting the DU risk assessment is presented, which includes selecting reference values, obtaining concentrations in media, and identifying exposure parameters. The risk assessment is then presented and validated.

9.1 ERA Model

Based on a review by Weiss (1999) and Lu *et al.* (2003), existing ecological risk assessment models are often site-specific. These models are therefore useful in addressing site-specific issues. However, when databases exist and are limited to site-specific conditions and not modifiable, applications have limited use. General models, which can be easily adapted to other sites, remain few, and are often simple and associated with significant uncertainties. The ERA model (Lu *et al.*, 2003) is a generic screening tool for ecological risk assessment that can be modified for varying site conditions and ecosystems through a Windows-based interface and interactive modifiable DBMS. Based on trophic sources, a food web has been integrated into the framework of the DBMS.

9.1.1 Exposure Pathways and the Food Web

Following U.S. EPA and other guidelines (U.S. EPA, 1992b and 1993a; Thomann *et al.*, 1992; Hope, 1995; Cheng, 1998; PNNL, 1998), the ERA model addresses potential exposure pathways of ingestion, inhalation, and dermal absorption for terrestrial animals; root and foliar uptake for plants; and direct absorption for aquatic species. Each mathematical equation for exposure incorporates species-specific information on diet composition, body weight, home range, food and water ingestion rates, and incidental ingestion rates of environmental media. Given a specified set of possible exposure pathways and routes, these equations can be combined to produce site- and species-specific estimates of chemical uptake from abiotic and biotic media. The exposure algorithms applied to the ERA model are based on a compilation of studies (Maughan, 1993; U.S. EPA, 1993a and 1993b; Farago, 1994; Hope, 1995; Cheng, 1998; PNNL, 1998). All equations applied in the ERA model are provided in Appendix B. These exposure models for terrestrial and aquatic plants and animals are used in software developed with Visual Basic 6.0. The DBMS provides robust storage and retrieval capabilities and can solve problems, such as data redundancy and inconsistency, data relationship definition, and security problems. Based on these advantages, Microsoft Access DBMS was selected to handle data in this model (Lu *et al.*, 2003). The parameters associated with exposure models including benchmarks, site characteristics, chemical properties, and exposure parameters are stored in the database. Furthermore, the DBMS is linked to external databases such as the U.S. EPA ECOTOX to address site-specific applications.

9.1.2 Animal and Plant Receptors at APG and YPG

Generally, assessment endpoints are explicit expressions of the environmental value that is to be protected, operationally defined by an ecological entity and its attributes (U.S. EPA, 1998). Various endpoints may be used for predictive assessments, but the final selection is often affected by the availability of toxicity data in the literature and the quality of the data. Criteria were identified to provide guidance for defining the endpoint receptors (U.S. EPA, 1992a; PNNL, 1998): (1) Commercial or recreational importance; (2) Protection status under the Endangered Species Act or similar state legislation; (3) Critical component of either the terrestrial or aquatic, ecosystem: key predator or prey; (4) High potential exposure to contaminants; (5) Availability of toxicological information for the species; and (6) Representatives of a foraging guild. In addition, the species listed as "threatened, endangered, and sensitive species on DOD lands" by the U.S. Army (Martin and Fischer, 2000) have also been included (Lu *et al.*, 2003).

APG and YPG were identified as baseline ecosystems for the ERA model, which represent coastal and desert ecosystems, respectively. Considering the diversity of the APG ecosystem and the large area of YPG, a significant number of wildlife species live within the two sites. Following U.S. EPA (1998) guidance and criteria above and considering databases and records maintained by the federal and state agencies including those associated with the two proving grounds (Lu *et al.*, 2003), the list of receptors are shown in Table 9.1.

Table 9.1 Selected Receptors of APG and YPG (adapted from Lu *et al.* (2003))

Species Category	Aberdeen Proving Ground	Yuma Proving Ground
Birds	Mallard, American kestrel, barred owl, bald eagle	Mexican spotted owl, loggerhead shrike, gamble's quail
Mammals	White-tailed deer, beaver, white-footed mouse, cottontail rabbit, Indiana bat	Kit fox, cactus mouse, black-tailed jackrabbit, mule deer, lesser long-nosed bat
Reptiles & Amphibians	Eastern garter snake, lizards, woodhouse's toad	Desert tortoises, sonoran whipsnake, desert spiny lizard
Aquatic Animals	Whitefish, pacific lamprey, white sturgeon, rainbow trout	NA [a]
Aquatic Plants	Water millfoil, phytoplankton, periphyton	NA
Terrestrial Plants	Fern, rushes, slender blue flag	Creosote bush, foothill paloverde trees, saguaro cactus

[a] NA: Not Applicable.

9.1.3 Risk Characterization and Uncertainty Analysis

Once the ecosystem and site characteristics are fully understood, the applied daily dose (ADD) or body burden can be estimated for an individual receptor. An ecological hazard quotient (EHQ) is then calculated by dividing the $ADD_{pathway}$ (or body burden) by the reference value:

$$EHQ = ADD_{pathway} \div reference\ \ value \tag{9.1}$$

The reference value recommended in this model is the no observed adverse effect level (NOAEL) or no observed adverse effect concentration (NOAEC) for terrestrial and aquatic species, respectively. The NOAEL and NOAEC are derived from experiments conducted on laboratory species, and represent the highest dose or contaminant concentration applied that did not result in a measurable adverse effect (Cockerham and Shane, 1994; Sample *et al.*, 1996; Weiss, 1999). For example, uranium reference values for terrestrial animals represent doses that did not adversely affect the receptor's reproductive system; for terrestrial plants the benchmark represents reduction in the plant's root weight. Reference values for aquatic species are the highest doses that did not increase mortality.

Based on the selected reference values, the EHQ represents varying levels of risk or measures of levels of concern (Tannenbaum *et al.*, 2003). Although risk categories are outlined here, receptor risk should be evaluated individually based on the endpoint. An EHQ less than 1 suggests the toxicological effects are unlikely to occur and hence the potential for unacceptable risk is minimal (Tannenbaum *et al.*, 2003). A NOAEL-based EHQ greater than 1 but less than the LOAEL (lowest observed adverse effect level)

indicates that effects are possible but uncertain. Finally a LOAEL-based EHQ>1 indicates that effects are probable and exposure exceeded the lowest dose associated with effects. The EHQ value provides an indication of level of risk to a receptor.

In the risk assessment, as discussed previously, uncertainties are an inherent part because the data and understanding of ecosystem may be limited. Therefore, probability density functions were sampled using Monte Carlo simulations. By applying the simulation, distribution characteristics were studied and convergence revealed a minimum iteration of 500 based on the 95^{th} confidence level, which is in agreement with Tellinghuisen (2000). However, in this study, the selected iteration is based on a 99^{th} confidence level, as we are interested in the lower probability outcomes at the tails of the distributions. In this case, 1000 iterations were selected (Frey and Rhodes, 1998).

Probabilistic distributions have been used as a tool to qualify uncertainty in prediction of risks to humans and ecological receptors (Frey and Rhodes, 1998). The distributions characterize the degree of belief that the true but unknown value of a parameter lies within a specified range of values for that parameter (Warren-Hicks *et al.*, 2002). Criteria for selecting a distribution are based on National Council on Radiation Protection and Measurements (NCRP, 1996) and U.S. EPA (1998) guidelines. The distribution should represent site-specific uncertainty and variation in that parameter (Schumacher *et al.*, 2001). Also, the distribution must represent the range of values for that parameter in a given system. The selected distribution should be consistent between sites for specific parameters (Warren-Hicks *et al.*, 2002). Moreover, the form of the distribution should reflect the magnitude, range, and interpretation of the parameter (NCRP, 1996). For example, contaminant concentration cannot be negative; therefore,

the sampling distribution should reflect the restricted range. The probabilistic distributions of the exposure parameters were gathered from a number of studies and are summarized in Table 9.2. As the lognormal distribution has a longer tail than other distributions, it is widely used in environmental analysis to represent positively valued data exhibiting positive skewness (NCRP, 1999; Cullen and Frey, 1999). Pollutant concentration tends to be lognormally distributed, which has been explained by the theory of successive random dilutions (Ott, 1990). After the pollutants are emitted by the source, they undergo successive mixing and dilution, resulting in a lognormal frequency distribution. Furthermore, a goodness of fit test was conducted to assess the appropriateness of the lognormal distribution for sampling data at both APG and YPG sites. By using the Anderson-Darling (A) test, the lognormal distribution was found to be the most appropriate for the DU data. Therefore, in this study, the lognormal distribution is selected to represent the distribution form for the DU concentrations in the media. Both aquatic species bio-concentration factors and soil to plant uptake factors are defined as the ratio of contaminant concentration at equilibrium in tissues to that in the water or soil where values were generated from field and/or laboratory data (Jorgensen *et al.*, 1991; PNNL, 1998; Sample *et al.*, 1998). The associated distributions have been observed as skewed, which has led to the use of the logarithmic transformation of the parameter to obtain the lognormal distribution (Traas *et al*, 1996; Verhaar *et al.*, 1999; Samsoe-Petersen *et al.*, 2002; Liao *et al.*, 2003).

Physiological parameters such as body weight, surface area, and ingestion and inhalation rates in terrestrial animals may vary seasonally, geographically, and by age. These parameters typically follow a Gaussian distribution (U.S. EPA, 1993a and 1997b).

Table 9.2 Input Variables Used in the Monte Carlo Simulation for DU Case Study

Parameter	Definition	Unit	Distribution	References
EC	Contaminant concentration	mg/L (water), mg/kg (soil), mg/m^3 (air)	lognormal	1-9
BW	Body weight	kg	normal	2, 3, 10-14
IR_f	Food ingestion rate	kg/day	normal	3, 10, 12, 13
IR_{dw}	Ingestion rate of drinking water	L/day	normal	3, 12, 13
IR_i	Inhalation rate	M^3/day	normal	2, 13
SA	Surface area	cm^2	normal	3, 13
AF	Soil-to-skin adherence factor	mg/ cm^2	default value: 1	15, 16
α_d	Contaminant-specific dermal absorption factor	mg/kg (body burden) / mg/kg (daily dose)	default value: 0.01	15, 16
P_{cs}	Fraction of receptor surface area in contact with soil per day	d^{-1}	default value: 0.22	11, 15, 16
θ	Site use factor	Ratio of contaminant area to home range	default value: 1	11, 15
ψ	Seasonal factor	fraction of time per year receptor occurs at site	default value: 1	11, 15
BCF	bio-concentration factor	L/kg	lognormal	3, 11, 17-21
B_v,	Bio-concentration factor for vegetative plant parts	mg/kg (soil)/mg/kg (vegetative plant)	lognormal	15, 16, 21, 22, 23
B_r	Bio-concentration factor for non-vegetative plant parts	mg/kg (soil)/mg/kg (vegetative plant)	lognormal	15, 16, 21, 22, 23

References:

1. Hattis *et al* (2001)
2. Hertwich *et al.* (1999)
3. McKone (1993)
4. Ott (1990)
5. Polder *et al.* (1998)
6. Smith (1994)
7. Stow and Qian (1998)
8. Travis and Arms (1988)
9. Veith *et al.* (1980)
10. Briggs *et al.* (1983)
11. Kenaga and Goring (1980)
12. MacIntosh *et al.* (1994)
13. U.S. EPA (1997a)
14. Wiwatanadate and Claycamp (2000)
15. Hope (1999)
16. U.S. EPA (1993a)
17. Hope (1995)
18. Lahkim *et al.* (1999)
19. McKone (1994)
20. Nayak *et al.* (2001)
21. West and Kodel (1999)
22. Absallom *et al.* (1999)
23. Finley *et al.* (1994)

The normal distribution is commonly used to represent uncertainty resulting from unbiased measurement errors (Morgan and Henrion, 1998). Because the normally distributed random variable takes on values over the entire range of real data, the standard deviation is a measure of the population variance. Surface area, ingestion, and inhalation rates are a function of the body weight and are often estimated using allometric equations (U.S. EPA, 1993a).

With limited field or laboratory data, default values are recommended (Hope, 1995 and 1999). The U.S. EPA applied such an approach for soil to skin adherence factors and the contaminant specific dermal absorption factor (U.S. EPA, 1989; U.S. EPA, 1993a; U.S. EPA, 2001). Moreover, because of limited data, these values were based on exposure for humans not terrestrial animals to which they were applied (U.S. EPA, 1989; Hope, 1995). Therefore, in the study, a similar approach was used for parameters related to dermal contact (Table 9.2): soil to skin adherence factor, contaminant specific dermal absorption factor, soil contact fraction factor, and site use factor.

9.2 Risk Assessment

Once the ecosystem was defined along with the food web, the process for conducting the DU risk assessment included selecting reference values, obtaining concentrations in media, identifying exposure parameters, and validating model results. Among them, exposure parameters have been discussed previously; in the following, reference value selection, DU concentrations in media, and model and validation results are presented.

9.2.1 Reference Value

The relevant NOAEL and NOAEC data were identified from multiple sources for the terrestrial and aquatic receptors of the case study (Sample *et al.*, 1996; Efroymson *et al.*, 1997; U.S. EPA, 2003). In instances where toxicological data for receptors were unavailable, surrogate species were selected based on taxonomy, life style, and/or toxicological response similarity. Surrogate application requires applying a conversion method based on test species and the receptor's body weights. Wildlife NOAELs can be estimated for an untested species by the following equation (Sample and Arenal, 1999):

$$NOAEL_{wildlife} = NOAEL_{test}\left(\frac{bw_{test}}{bw_{wildlife}}\right)^{1-b} \tag{9.2}$$

Where the $NOAEL_{wildlife}$ represents the ecosystem receptor of concern, the $NOAEL_{test}$ is the surrogate test species for which the *NOAEL* is available, *bw* represents their respective body weights, and *b* is an allometric scaling factor. From Sample and Arenal (1999), scaling factors of 1.2 and 0.94 should be used for birds and mammals, respectively. NOAEL data on test species, mouse and black duck, were used to calculate other untested species NOAEL values based on Equation 9.2. (Toxicological data are available in Appendix C).

9.2.2 DU Concentrations in Media

As discussed previously, the lognormal distribution was applied to describe DU concentrations in both water and soil for APG and YPG. Sampling data on uranium concentrations in surface water, groundwater, and soils from APG and YPG were collected by Ebinger *et al.* (1996) and stored in a database developed and maintained by

Los Alamos National Laboratory (Ebinger, 2002). At APG, uranium concentrations in the surface- and ground-water samples were analyzed based on nine samples near the western shore of Chesapeake Bay. Potentially impacted soils were sampled mainly in conjunction with well water sampling and were collected over 1,500 acres; a total of 35 samples were collected representing an extremely limited data set. (See Appendix D for sampling area and associated data.)

YPG is characterized as a typical desert ecosystem; therefore field studies were conducted, for the most part, on soil samples. Ebinger *et al.* (1996) established sample plots on two firing ranges at YPG. Plots were distributed nonrandomly along the area of 12,000 acres, where first penetrator impacts were closely clustered and had been identified as exhibiting elevated levels of DU contamination (Price, 1991; Ebinger *et al.*, 1996; Oxenberg, 1997). These areas were situated along the axis of the firing line and could be identified by impact craters, recently displaced soils, and DU fragments. Locations for sample plots varied along the firing line and from observable impact craters and according to Ebinger *et al.* (1996) were assumed to cover a range of contaminant levels for each firing line. According to U.S. EPA's soil sampling protocol (U.S. EPA, 1992c), when a plume is suspected and the orientation of the plume can be estimated, the sampling grid should be oriented in such a manner that the extending axis of the grid is parallel to the suspected plume center line; however, this is not necessary and a square or rectangular grid is one of the most useful for reconnaissance. DU concentrations in soil were based on 22 samples, again a very limited data set for the impacted area. (See Appendix D for sampling area and associated data.)

9.2.3 Risk Results

Based on speciation, $UO_2CO_3^0{}_{(AQ)}$ and $UO_2(OH)^+$ are the two dominant and mobile species at pH 6-7 and pE 5-15 that may adversely affect receptors from exposure (see Appendix E for further review of DU Chemistry) . For YPG terrestrial plants (Figure 9.1), because of high DU concentration in soil, the overall distributions for DU uptake for the creosote bush, foothill paloverde trees, and saguaro cactus suggested a 90% likelihood of a reduction in root weight. For most terrestrial animals at YPG, given DU concentration in soil, the dose is less than that resulting in a decrease offspring in weight and size. However, for the lesser long-nosed bat, reproduction effects are expected to occur through the reduction in size and weight of offspring. Among the different exposure pathways for the bat, including ingestion, inhalation, and dermal absorption, the dominant pathway is through insect ingestion, which accounts for 97% of its diet. Furthermore, insect exposure includes all the concerned ingestion pathways -- soil, water, and food (plants), and also dermal and inhalation exposure. Based on the characteristics of terrestrial animals and their responses to DU exposure, the bat is more vulnerable than other terrestrial species. The positive skewness of EHQ distribution on the bat exemplifies the sensitivity (Figure 9.2).

From the field studies (Ebinger *et al.*, 1996), pocket mice, kangaroo rat, and white-throated woodrat samples were analyzed for uranium concentrations to estimate risk levels at YPG. Samples of carcasses, kidneys, and livers from these animals were collected for identifying uranium concentrations. For pocket mice, the greatest uranium concentration was found in carcass samples, 115.4 mg kg^{-1}; for kangaroo rat, the worst case was observed in kidney samples 4.3 mg kg^{-1}; and for white-throated woodrat, the

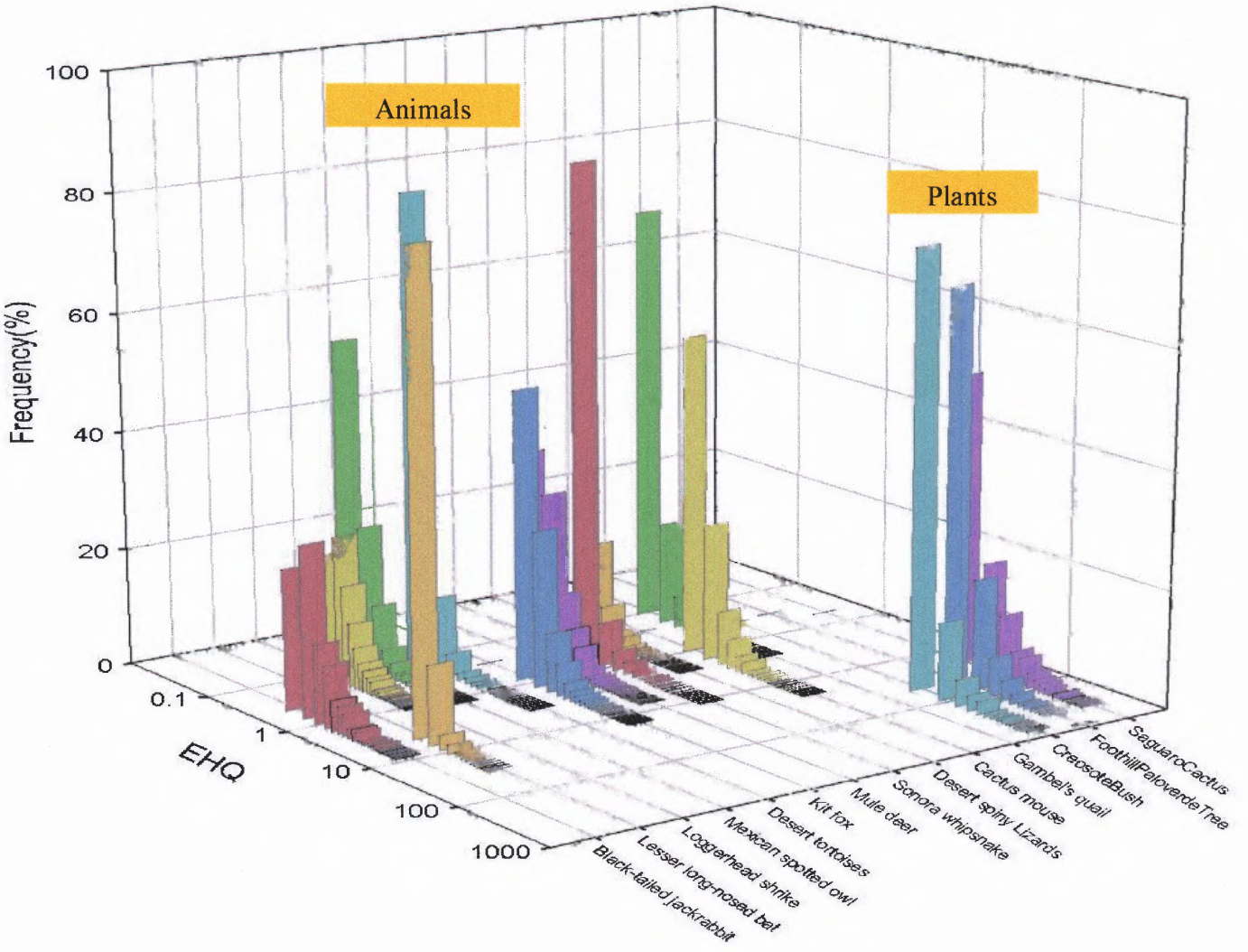

Figure 9.1 EHQ distributions for YPG terrestrial receptors

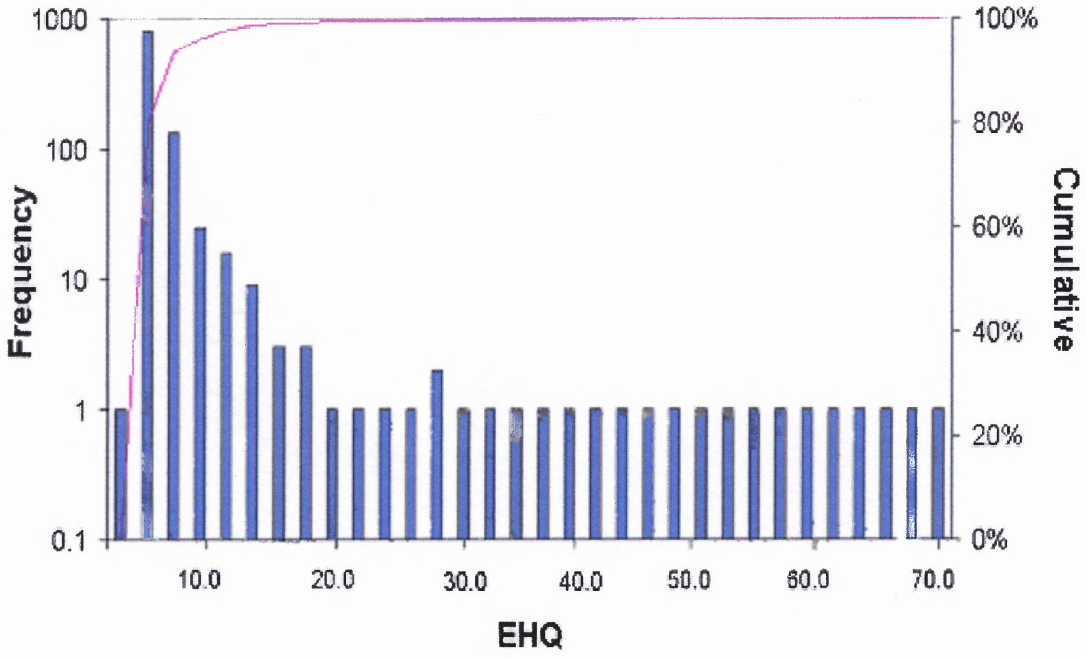

Statistical data	
Mean	3.86E+00
Standard Error	1.08E-01
Median	3.05E+00
Standard Deviation	3.41E+00
Sample Variance	1.16E+01
Kurtosis	1.68E+02
Skewness	1.07E+01
Range	6.77E+01
Minimum	2.18E+00
Maximum	6.99E+01
Sum	3.86E+03
Count	1.00E+03
Confidence Level(95.0%)	2.11E-01

Figure 9.2 Statistical data for EHQ (Lesser long-nosed bat)

greatest concentration of uranium was 76.7 mg kg^{-1} in carcass samples. Based on our risk assessment, a receptor from the same family Murid, cactus mouse, exhibited a uranium concentration of 2.46 to 224.6 mg kg^{-1}. Sampling data from Murid receptors, pocket mice, kangaroo rat, and white-throated woodrat, fall into the distribution predicted in the ERA tool (Figure 9.3).

At APG, based on limited DU data, exposure potentially poses little risk for terrestrial animals (Figure 9.4), representing the likelihood that there is no observable impact on receptor's reproduction or development. Ebinger *et al.* (1996) collected deer samples to evaluate potential DU uptake and transfer to humans who consume deer. They analyzed kidney, livers, muscle, and bone samples, and found that the greatest uranium concentration among those samples was 0.0051 mg kg^{-1}, which falls in the distribution observed here of 0.0042 to 7.3 mg kg^{-1} for the receptor, white-tailed deer (Figure 9.3). For APG terrestrial plants (Figure 9.4), modeling results of risk showed that the 90^{th} percentiles for rushes, slender blue flag, and fern may result in a reduction in root weight.

Compared with terrestrial plants at APG, uranium potentially poses lower risks to aquatic plants and again this is based on a very limited set of data (Figure 9.5). Considering DU exposure to aquatic animals at APG, uranium uptake is potentially not expected to increase mortality. For the aquatic plant, milfoil, two samples were collected (Ebinger *et al.*, 1996) from field studies, where 2.1 and 0.8 mg kg^{-1} of uranium were observed. Our modeling results showed that the uranium concentration in milfoil ranged from 6.4×10^{-3} to 18.6 mg kg^{-1}, and are consistent with field data (Figure 9.3). In addition, their results (Ebinger *et al.*, 1996) indicated that the presence of DU was confirmed by isotopic ratios observed in the cattail and pickerel weed, representing

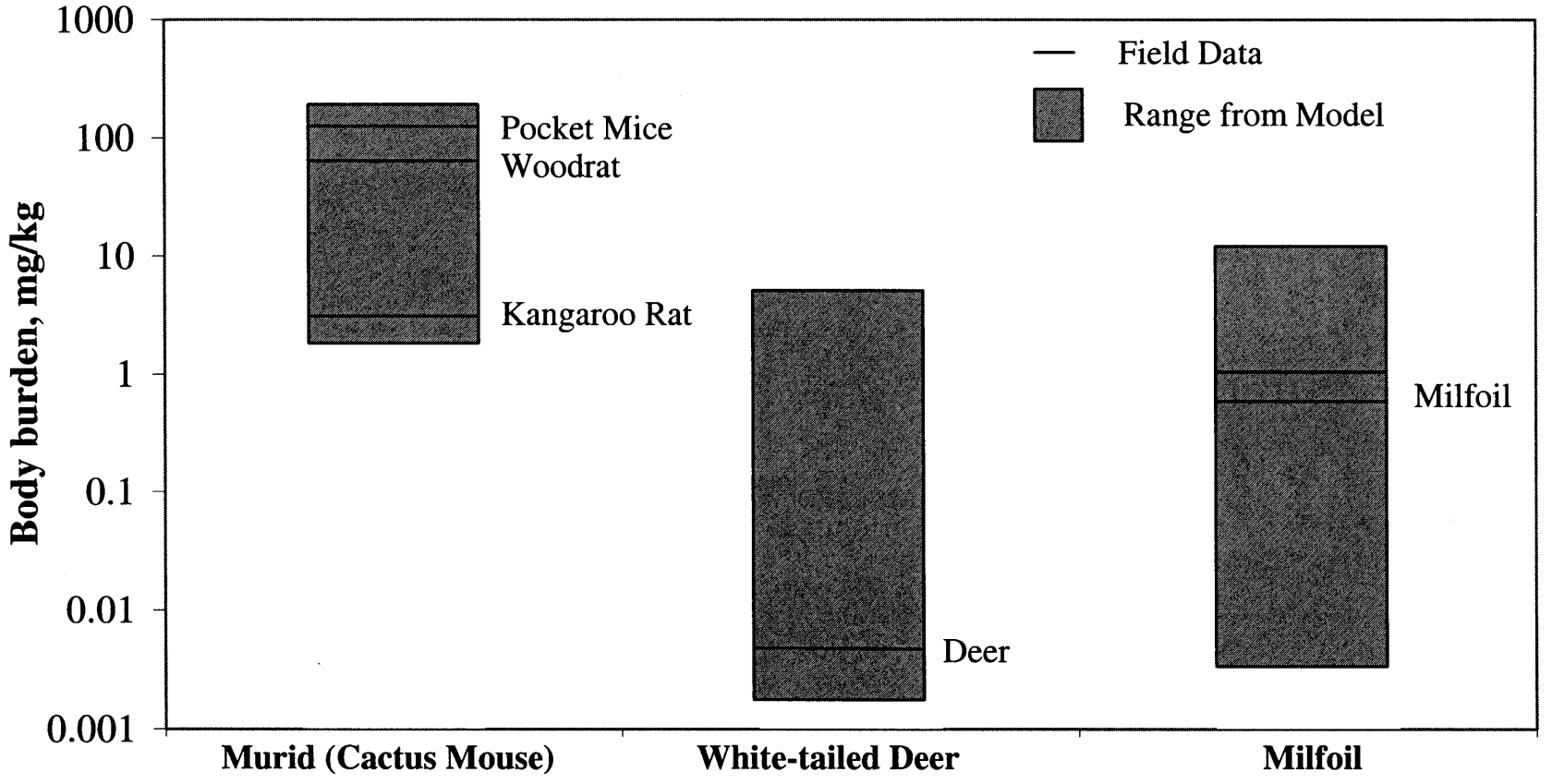

Figure 9.3 ERA modeling validation on DU

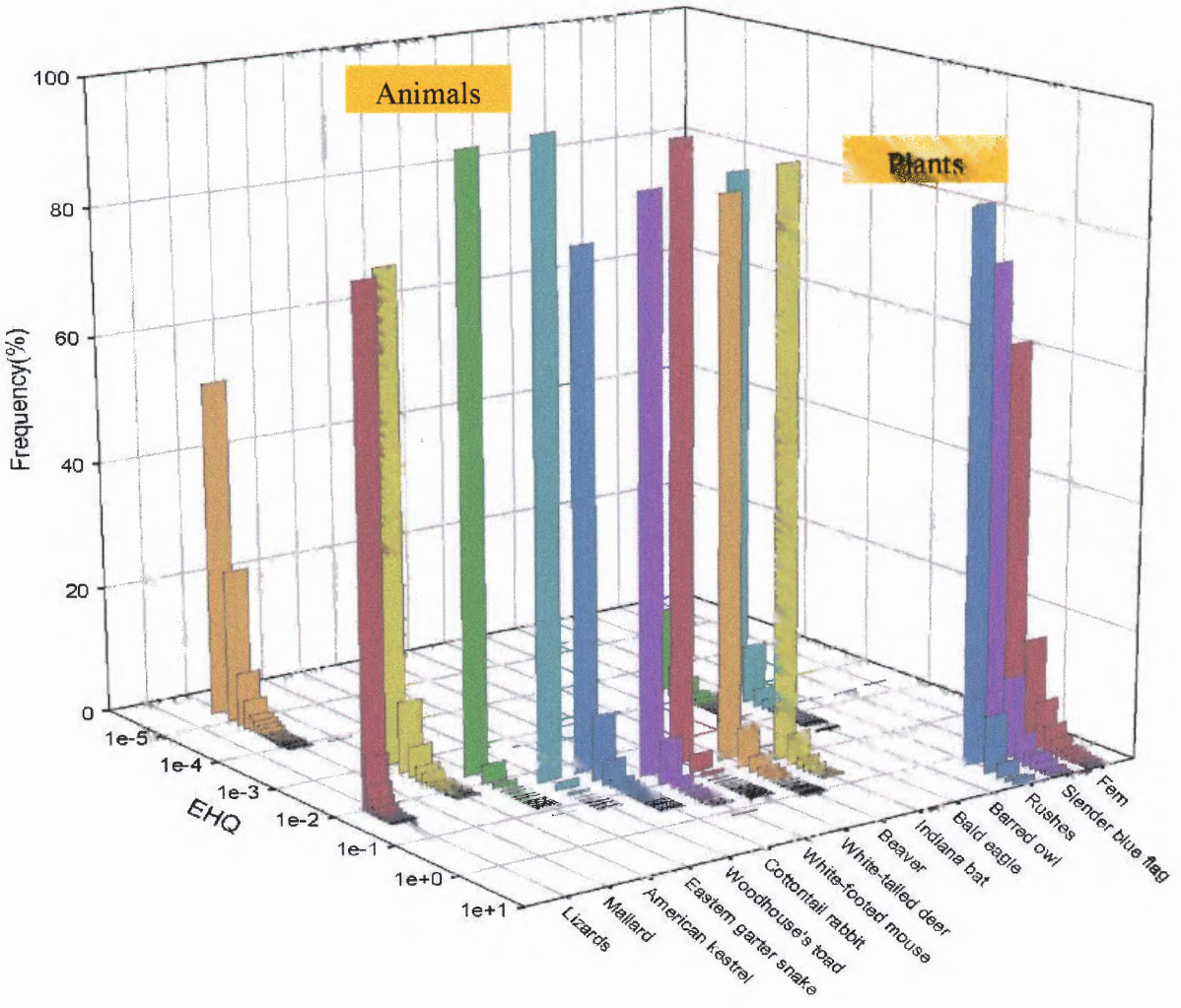

Figure 9.4 EHQ distributions for APG terrestrial receptors

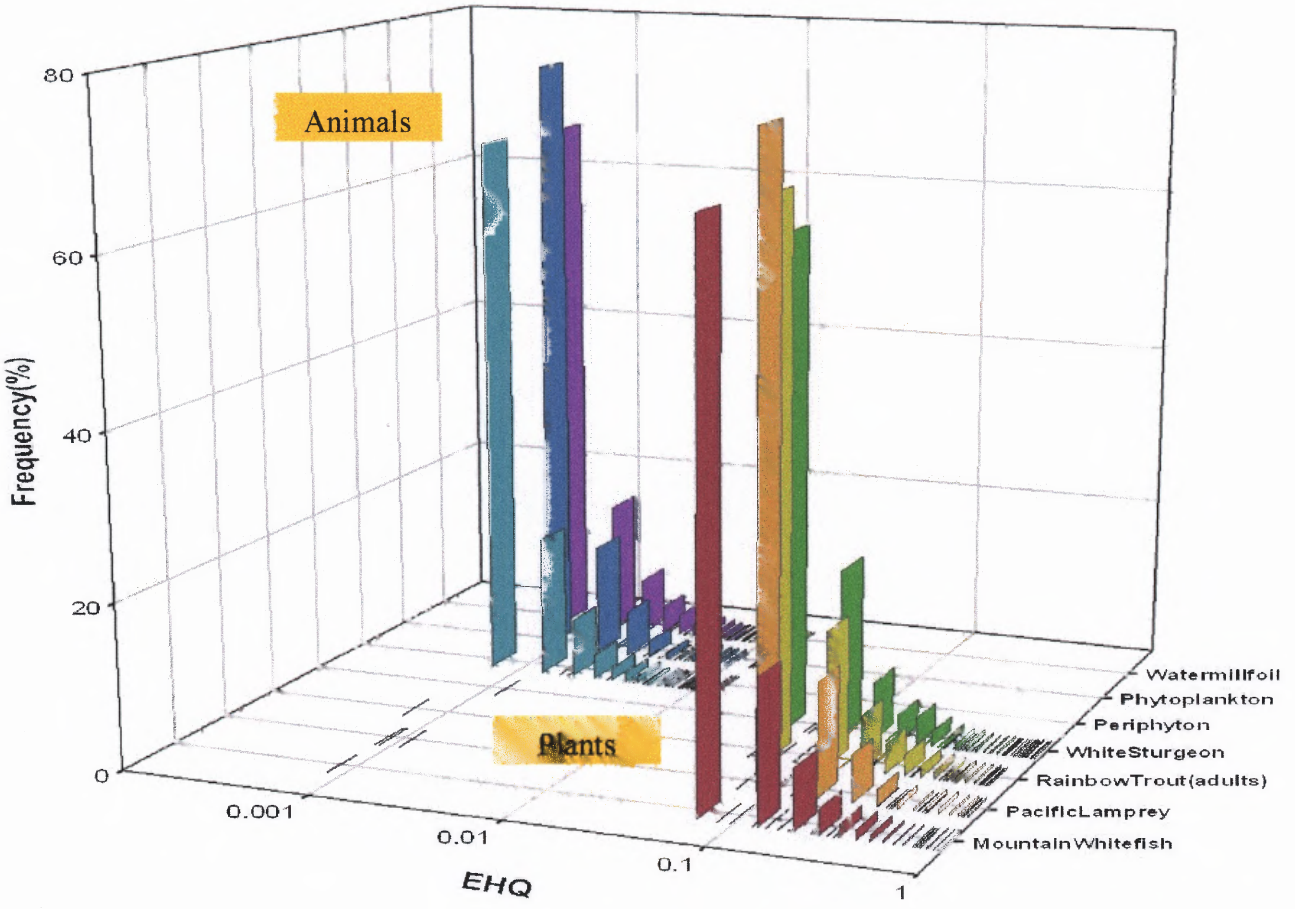

Figure 9.5 EHQ distributions for APG aquatic receptors

uptake, attachment, or adsorption of DU from water or sediments where these aquatic organisms grow.

9.3 Summary

Risks from exposure to DU at two U.S Army sites, APG and YPG, were characterized based on the data available. Exposure pathways for terrestrial and aquatic plants and animals were applied in software developed using Visual Basic 6.0 with associated parameters stored in the Microsoft Access DBMS. To characterize risk and address uncertainty, the model employs Monte Carlo simulations for assessing parameter and risks as probabilistic distributions. Results from the ERA model suggest that a reduction in plant root weight is considered likely to occur from exposure to uranium at YPG and APG. For most terrestrial animals at YPG, the predicted DU dose is less than that resulting in a decrease offspring in weight and size. However, for the lesser long-nosed bat, reproductive effects are expected to occur through the reduction in size and weight of offspring. At APG, uranium uptake will not likely affect survival of aquatic plants and animals. However, data were limited reflecting the risk observed and further field investigations at both sites are recommended. Through model validation, the results from the ERA model are consistent with sampling data from field studies of Ebinger *et al.* (1996). This static risk assessment provides solid background for applying the dynamic approach. In the next chapter, conclusions and recommendations for future work are outlined.

CHAPTER 10

CONCLUSIONS AND RECOMMENDATIONS FOR FUTURE WORK

10.1 Conclusions

Metals such as lead, strontium, and depleted uranium released into the subsurface pose a threat to human health and the environment. To assess risks associated with heavy metals to the surrounding environment and manage remedial activities requires simulation tools that depict speciation and risk with accurate mechanistic models and well-defined transport parameters. The aim of this research was to develop a comprehensive modeling approach or simulation tool for contaminant speciation, distribution, transport, and risk. In simulating metal contaminant mobility in the subsurface, speciation is required. Once the chemical form is understood, its mobility and bioavailability can be addressed. MINEQL+ was selected and employed for addressing metal speciation in the aqueous phase because of its comprehensive thermodynamic database, relatively strong ability to predict activity coefficients, more options for modeling adsorption under equilibrium conditions, and user-friendly interface.

Once speciation in the aqueous phase is understood, its distribution with subsurface minerals needs to be accurately depicted. Amorphous oxide minerals are important and prevalent surfaces affecting metal mobility as of Al, Fe, and Mn occur as coatings on other mineral surfaces or as discrete particles, and are persistent in aquatic environments. They have large surface areas, porous structures, and an abundance of binding sites. Numerous studies have demonstrated that this sorption process is a two-step one: rapid adsorption of metal ions to the external surface is followed by slow

intraparticle diffusion along the micropore walls of the oxide. Through experiments on Pb sorption to HAO, HFO, and HMO, as well as to montmorillonite and HAO-coated montmorillonite, intraparticle diffusion was observed to be the rate-limiting mechanism in the sorption process, where best-fit surface diffusivities ranged from 10^{-18} to 10^{-15} cm^2 s^{-1}. The results suggest oxide coatings and montmorillonite are effective sinks for heavy metal ions. Therefore, hydrous oxides and oxide coatings greatly affect the metal bioavailability.

Contributions from slower processes such as intraparticle diffusion should be included in bulk transport models for accurately depicting metal contaminant sorption processes. Thus, transport models that often employ either equilibrium or reaction rate approaches are inadequate for describing metal mobility in subsurface environments. Therefore, intraparticle diffusion of metal contaminants has been incorporated into transport modeling. Evaluation and review of existing groundwater flow and transport models resulted in identifying GMS (Groundwater Modeling System) for addressing macroscopic solute transport. Diffusion was coded into GMS through the solute transport module RT3D. The method of parabolic concentration layer approximation was employed in the diffusion model development. The operator split technique was used to solve microscopic diffusion equation coupled with macroscopic advection and dispersion transport. The resulting package in RT3D was linked through DLL with the advection and dispersion components. Subsequently, Sr^{90} mobility at the U.S. Department of Energy Hanford Site was simulated. Methods for addressing the distribution coefficient as well as the surface diffusivity were outlined in the research. Based on the Hanford Site model, a local model was developed to simulate Sr^{90} transport in and around the 100-N

area from 1990 to 2004. Results revealed Sr^{90} continues to migrate within the 100-N area and will potentially extend into other areas of the Hanford Site and beyond.

In the last phase, once the bioavailable species is defined, it can be used to assess static or dynamic ecological risks resulting from exposure to different metals. Employing the ERA model, a static ecological risk assessment was conducted for depleted uranium (DU) present at U.S. Army YPG and APG. A probabilistic approach employing Monte Carlo simulations for assessing parameters and risks as distributions was used in the ERA model to characterize risk and address uncertainty. Results suggest that a reduction in plant root weight is considered likely to occur from exposure to uranium at YPG and APG. For most terrestrial animals at YPG, the predicted DU dose is less than that resulting in a decrease offspring in weight and size. However, for the lesser long-nosed bat, reproductive effects are expected to occur through the reduction in size and weight of offspring. At APG, based on a very limited data, uranium uptake will not likely affect survival of terrestrial animals and aquatic species. In a model validation exercise, based on field and laboratory studies, sampling data collected at APG and YPG of pocket mice, kangaroo rat, white-throated woodrat, deer, and milfoil revealed that body burden concentrations fall into the distributions simulated at both sites. This static risk assessment provides solid background for applying the dynamic approach.

The tool developed is available here at NJIT and includes the ERA software with links to MINEQL+, external databases, and the modified GMS code.

10.2 Recommendations for Future Work

Based on this research, the following are recommended for future work on contaminant transport, fate, and ecological risk assessment.

(1) To further address contaminant mobility and bioavailability, GMS with the intraparticle diffusion package can be linked with surface water or watershed models to fully describe contaminant spatial and temporal aspects beyond groundwater systems.

(2) To fully utilize the GIS tool, ArcGIS or ArcView tools in implementing GMS for importing and converting GIS data from external sources.

(3) To combine the ecological risk assessment with a life cycle approach taking into account the overall cradle to grave perspective for sustainable development.

(4) To qualify the magnitude of potential impacts to ecosystems from exposure to single as well as multiple contaminants requires better toxicological data addressing communities verses individual receptors.

APPENDIX A

VALIDATION ON THE PARABOLIC CONCENTRATION LAYER APPROXIMATION METHOD

The purpose of this example is to demonstrate and validate the accuracy of the parabolic concentration layer approximation method (Yao and Tien, 1992) by applying the orthogonal collocation and finite difference methods.

From the method of parabolic concentration layer approximation as discussed in Chapter 7

$$\frac{dC}{d\tau} = 6\left(\frac{C_t}{C} + \frac{1}{2}\right)(C_t - C) \tag{A-1}$$

$$C_t = \frac{(1-B)C}{4} + \frac{1}{2}\left[\frac{1}{4}(1-B)^2 C^2 + 2C(C+BS)\right]^{1/2} \tag{A-2}$$

where C is sorbed concentration, C_t is the variable concentration sorbed on the oxide external surface, S is the aqueous concentration, $\tau = \frac{D}{R^2}t$, and $B = \frac{Rk}{D}$ as defined in the Chapter 7.

From mass balance in the bulk phase, one has

$$V_f(S_0 - S) = V_s \rho C \tag{A-3}$$

where S_0 is the initial concentration of the species in the aqueous phase, and V_f and V_s are, respectively, the volumes of bulk fluid and of adsorbent. As this is a validation based on Yao and Tien (1992), their data are used here and S_0 is set equal to 1, and then define

$$\alpha = \frac{V_f}{V_s \rho} \tag{A-4}$$

Then, Equation A-3 becomes

$$S = 1 - \frac{C}{\alpha} \tag{A-5}$$

Substituting Equation A-5 into Equation A-2 yields

$$C_t = \frac{(1-B)C}{4} + \frac{1}{2}\left[\frac{1}{4}(1-B)^2 C^2 + 2C\left(C + B\left(1 - \frac{C}{\alpha}\right)\right)\right]^{1/2} \tag{A-6}$$

Equation A-1 can be integrated numerically in conjunction with Equation A-6 with the initial condition $C = 0$ at $\tau = 0$, and results are shown in Table A-1. Solutions by the orthogonal collocation (Yao and Tien, 1992) and the finite difference are also shown in the following table.

Table A-1 Value of C as Function of τ Obtained by Different Methods ($\alpha = 1$, $B = 100$)

τ		**0.001**	**0.002**	**0.005**	**0.01**	**0.02**	**0.05**	**0.1**	**0.2**	**1**
Model[a]	(1)[b]	0.0760	0.112	0.179	0.243	0.316	0.413	0.468	0.495	0.500
	(2)[c]	0.0760	0.112	0.178	0.243	0.316	0.413	0.467	0.495	0.500
Orthogonal Collocation		0.0750	0.112	0.174	0.233	0.300	0.390	0.450	0.488	0.500
Finite difference		0.0762	0.111	0.174	0.233	0.300	0.390	0.450	0.488	0.500

[a] The parabolic concentration layer approximation method.
[b] Results from Yao and Tien (1992).
[c] Results from recalculation based on the approximation method.

APPENDIX B

EXPOSURE ALGORITHMS (ADAPTED FROM LU *et al.* (2003))

Following U.S. EPA Guidelines (U.S. EPA, 1998), quantitative exposure estimations address the pathways of ingestion, inhalation, and dermal absorption for terrestrial animals; root and foliar uptake for plants; and direct absorption for aquatic species (Cheng, 1998; Hope, 1995; PNNL and CRCIA MTR, 1998; Thomann and Parkerton, 1992; U.S. EPA, 1993a and 1992b). Each exposure equation incorporates species-specific information on diet composition, body weight, home range, food and water ingestion rates, and incidental ingestion rates of environmental media, as available. Given a specified set of possible exposure pathways and routes, these equations can be combined to produce site- and species- specific estimation of chemical uptake from abiotic media. The body burden of plants is based on contaminant uptake from air, soil, pore water, and groundwater. Uptake may be through either the roots or transport across aboveground membranes of aerial contaminants. Herbivores and omnivores consume primary sources of contaminants such as soil and water and secondary ones like that of contaminated plants. Omnivores and carnivores consume animal prey that has also received some degree of exposure. Besides the level of contamination present in the various pathways of exposure, the fractional absorption of these contaminants controls both the resulting concentrations in the organism and its toxicological response to those absorbed doses. The predator-prey food web is relationally imbedded within the database structure. This method allows for any number of organisms to be included without increasing the mathematical complexity. Compared with a matrix structure method introduced by

Sharpe and Mackay (2000), the trophic levels expressed by a relational database are more flexible and easily modified for a specific food web. Furthermore, it is not restricted to one receptor per species. The exposure algorithms applied to the ERA model are described as follows.

Uptake of contaminants by plants is complex and involves processes such as adsorption, complexation, and precipitation, which are not yet mechanistically understood for modeling purposes (Farago, 1994; Ross, 1994). However, an approach based on plant-soil (K_{ps}), plant-soil solution (K_{pw}), and plant-air (K_{pa}) partition coefficients can provide a simple and useful method for assessing uptake and risk. For the three exposure pathways, Equation (1) is applied:

$$C_i = EC_i \times K_{pi} \quad \text{(B-1)}$$

$$C_{total} = \Sigma C_i \quad \text{(B-2)}$$

where

C_i = contaminant concentration in the receptor from the i^{th} pathway (mg/kg)

C_{total} = total contaminant concentration from exposure to soil, water, and air (mg/kg)

EC_i = contaminant concentration in medium (mg/kg for soil EC_s, mg/L for water EC_w, and mg/ m^3 for air EC_a)

K_{pi} = plant-medium partition coefficient ([mg/kg] soil / [mg/kg] roots for plant-soil K_{ps}, L/kg for plant-solution K_{pw}, and m^3/kg for plant-air K_{pa})

In the event a partition coefficient is not available, estimation methods include those for organics based on, for example, the octanol-water partition coefficient (K_{ow}) (Lyman, Reehl and Rosenblatt, 1990). For inorganics, the geometric mean of bioconcentration

factors for leafy and root vegetables can be applied to represent above- and below-ground plants, respectively (Hope, 1995; Strenge and Peterson, 1989). Model validation assists in affirming the resulting effects.

Ingestion, inhalation, and dermal absorption present the principal means by which terrestrial wildlife receptors are exposed to contamination. As mentioned above, these receptors may receive exposure through direct contact (primary pathway) with abiotic media and through consumption (secondary pathway) of contaminated food. Exposure estimation for these species must, therefore, include consideration of contaminant body burdens in the lower trophic level forage or prey, based on the food web. Because using a food web model requires ecological information with respect to historical data and site-specific feeding relationships, the process introduces a crucial ecological perspective into what might otherwise be a purely toxicological exercise (Hope, 1995).

Dermal exposure can be a significant exposure route for animals that are in frequent contact with contaminated water, sediment, or soil. However, the estimation of contaminant uptake via dermal absorption is also problematic for ecological resources, primarily because many of the required parameters have not been measured for terrestrial biota (Hope, 1995). The following model is developed to evaluate exposure based on an estimate of the mass of soil or sediment adhering to a surface area of a receptor:

$$ADD_i = [(SA \times AF \times P_{cs} \times EC_s \times CF \times \alpha_i)/BW] \times \theta \times \psi \quad \text{(B-3)}$$

$$C_i = ADD_i / k_e \quad \text{(B-4)}$$

where

ADD_i = applied daily dose through the i^{th} exposure pathway (mg contaminant/kg of receptor body weight)

SA = surface area of ecological receptor (cm^2)

AF = soil-to-skin adherence factor (mg/ cm^2)

P_{cs} = fraction of receptor surface area in contact with soil per day (d^{-1})

α_i = contaminant-specific absorption factor (mass fraction absorbed into blood)

k_e = contaminant-specific depuration rate (d^{-1})

BW = body weight of receptor (kg)

CF = conversion factor (1×10^{-6} kg/mg)

θ = site use factor

ψ = seasonality factor; percentage of time per year receptor dwells at site

Exposure via inhalation of volatilized contaminants and fugitive dust is evaluated with the following equation (Hope, 1995):

$$ADD_i = [(IR_a \times EC_a)/BW] \times \theta \times \psi \quad \text{(B-5)}$$

$$C_i = ADD_i \times (\alpha_i / k_e) \quad \text{(B-6)}$$

where

IR_a = inhalation rate (m^3/day)

Ingestion of contaminants is typically the most significant route of exposure in assessing risks to terrestrial animals. Ingestion includes both secondary exposure, where contaminated forage or prey is consumed, and primary exposure, where contaminated water, sediments, or soil are consumed. The associated algorithms are

$$ADD_i = [(EC_s \times FS \times IR_i) / BW] \times \theta \times \psi \quad \text{(B-7)}$$

$$ADD_i = [(EC_w \times IR_{iw}) / BW] \times \theta \times \psi \quad \text{(B-8)}$$

$$ADD_i = \sum [(C_k \times FR_{fk} \times IR_i) / BW] \times \theta \times \psi \quad \text{(B-9)}$$

where

FS = mass fraction of soil or sediment in the diet (as percentage of diet on dry weight basis)

IR_i = ingestion rate on dry-weight basis (kg/day)

IR_{iw} = ingestion rate of drinking water (mg/day)

FR_{fk} = wet weight fraction of the k^{th} food item in receptor diet (kg food/kg diet)

The sum of Equations B7–B9 is the applied daily dose through all the concerned ingestion exposure pathways – namely ingestion of soil, water, and food (mg contaminant/kg of receptor body weight). These three equations are derived from the Wildlife Exposure Factors Handbook (U.S. EPA, 1993a) and Hope (Hope, 1995), and have been applied to wildlife ingestion of contaminated soil, water, and food. The exposure parameters were obtained from literature (Maughan, 1993; Owen, 1990) and peer-reviewed databases (i.e., ECOTOX, (U.S. EPA, 2003) and MEPAS (Strenge and Peterson, 1989)) or estimated with empirical equations recommended by for example, the U.S. EPA (U.S. EPA, 1993a).

In the ERA model, aquatic receptors are defined as non-rooted, free-floating aquatic macrophytes and free-swimming aquatic animals. Total uptake for these species is represented by partitioning or absorption from surface water (Hope, 1995):

$$C_{aq} = EC_{sw} \times BCF \quad \text{(B-10)}$$

where

C_{aq} = contaminant body burden in aquatic receptor (mg/kg)

BCF = contaminant-specific bioconcentration factor (L/kg)

The contaminant-specific bioconcentration factor (BCF) can be obtained from literature (Lyman *et al.*, 1990; U.S. EPA, 2000). Factors not available for inorganic contaminants (e.g., metals) may be estimated from empirical equations using, for example, the solubility constant (K_{so}). Generally, exposure for aquatic receptors will be dominated by bioconcentration (partitioning from water) mechanisms as opposed to bioaccumulation (uptake through food and water consumption) ones, unless the contaminant has a log (BCF) greater than five in which case dietary uptake may play an important role in the overall exposure of aquatic animals (Thomann, 1992). Because of the lack of data on aquatic animal uptake through ingestion, this model includes only direct absorption.

APPENDIX C

MORE DATA IN DU RISK ASSESSMENT

Table C-1 Uranium Toxicological Data for Terrestrial Wildlife

Analyte	Form[a]	Test Species	Test NOAEL[b] (mg/kg/d)	Endpoint	Estimated NOAEL[c, d] (mg/kg/d)
$UO_2(CH_2COOH)_2$	$UO_2CO_{3(AQ)}$ $UO_2(OH)^+$	mouse	3.07	Little Brown Bat	3.322
$UO_2(CH_2COOH)_2$	$UO_2CO_{3(AQ)}$ $UO_2(OH)^+$	mouse	3.07	Short-tailed Shrew	3.187
$UO_2(CH_2COOH)_2$	$UO_2CO_{3(AQ)}$ $UO_2(OH)^+$	mouse	3.07	White-footed Mouse	3.115
$UO_2(CH_2COOH)_2$	$UO_2CO_{3(AQ)}$ $UO_2(OH)^+$	mouse	3.07	Meadow Vole	2.988
$UO_2(CH_2COOH)_2$	$UO_2CO_{3(AQ)}$ $UO_2(OH)^+$	mouse	3.07	Mink	2.477
$UO_2(CH_2COOH)_2$	$UO_2CO_{3(AQ)}$ $UO_2(OH)^+$	mouse	3.07	Cottontail Rabbit	2.45
$UO_2(CH_2COOH)_2$	$UO_2CO_{3(AQ)}$ $UO_2(OH)^+$	mouse	3.07	Red Fox	2.263
$UO_2(CH_2COOH)_2$	$UO_2CO_{3(AQ)}$ $UO_2(OH)^+$	mouse	3.07	River Otter	2.187
$UO_2(CH_2COOH)_2$	$UO_2CO_{3(AQ)}$ $UO_2(OH)^+$	mouse	3.07	White-tail Deer	1.945
$U_{(s)}$	$DU_{(s)}$	black duck	16	Rough-winged Swallow	6.684
$U_{(s)}$	$DU_{(s)}$	black duck	16	American Robin	9.163
$U_{(s)}$	$DU_{(s)}$	black duck	16	Belted Kingfisher	10.442
$U_{(s)}$	$DU_{(s)}$	black duck	16	American Woodcock	11.068
$U_{(s)}$	$DU_{(s)}$	black duck	16	Cooper's Hawk	12.979
$U_{(s)}$	$DU_{(s)}$	black duck	16	Barn Owl	13.135
$U_{(s)}$	$DU_{(s)}$	black duck	16	Barred Owl	14.317
$U_{(s)}$	$DU_{(s)}$	black duck	16	Red-tailed Hawk	15.669
$U_{(s)}$	$DU_{(s)}$	black duck	16	Osprey	16.594
$U_{(s)}$	$DU_{(s)}$	black duck	16	Great Blue Heron	18.215

[a] pH: 6-7.
[b] Sample *et al.* (1996).
[c] b=0.94 mammals and 1.2 birds (Sample and Arenal, 1999).
[d] NOAEL: 0.9 (mg/kg/d) (for Lizards (side-blotched), Western aquatic garter snake, Woodhouse's toad (adult)) (PNNL, 1998).

Table C-2 Uranium Toxicological Data for Terrestrial Plants

Analyte	Form[a]	Test Species[b]	Test LOEC (mg/kg)	Endpoint
$UO_2(NO_3)_2$	$UO_2CO_{3(AQ)}$ $UO_2(OH)^+$	Swiss chard	5	Fern
$UO_2(NO_3)_2$	$UO_2CO_{3(AQ)}$ $UO_2(OH)^+$	Swiss chard	5	Rushes
$UO_2(NO_3)_2$	$UO_2CO_{3(AQ)}$ $UO_2(OH)^+$	Swiss chard	5	Slender blue flag
$UO_2(NO_3)_2$	$UO_2CO_{3(AQ)}$ $UO_2(OH)^+$	Swiss chard	5	Creosote bush,
$UO_2(NO_3)_2$	$UO_2CO_{3(AQ)}$ $UO_2(OH)^+$	Swiss chard	5	Foothill paloverde trees
$UO_2(NO_3)_2$	$UO_2CO_{3(AQ)}$ $UO_2(OH)^+$	Swiss chard	5	Saguaro cactus

[a] pH: 6-7.
[b] Efroymson *et al.* (1997).

Table C-3 Uranium Toxicological Data for Aquatic Species

Analyte	Form[a]	Species	Test NOAEC[b] (mg/L)	Aquatic species
$UO_2(NO_3)_2$	$UO_2CO_{3(AQ)}$ $UO_2(OH)^+$	Periphyton	2	Aquatic plants[c]
$UO_2(NO_3)_2$	$UO_2CO_{3(AQ)}$ $UO_2(OH)^+$	Phytoplankton	2	
$UO_2(NO_3)_2$	$UO_2CO_{3(AQ)}$ $UO_2(OH)^+$	Water milfoil	2	
$UO_2(NO_3)_2$	$UO_2CO_{3(AQ)}$ $UO_2(OH)^+$	Mountain whitefish	0.021	Aquatic animals[d]
$UO_2(NO_3)_2$	$UO_2CO_{3(AQ)}$ $UO_2(OH)^+$	Pacific lamprey	0.021	
$UO_2(NO_3)_2$	$UO_2CO_{3(AQ)}$ $UO_2(OH)^+$	Rainbow trout (adults) Rainbow trout (edds) Rainbow trout (larvae)	0.021	
$UO_2(NO_3)_2$	$UO_2CO_{3(AQ)}$ $UO_2(OH)^+$	White sturgeon	0.021	

[a] pH 6-7.
[b] Ecological Toxicity Database (U.S. EPA, 2003).
[c] Surrogate aquatic plants are Chlorella vulgaris and Green algae.
[d] Surrogate aquatic animals are Fathead minnow.

APPENDIX D

DEPLETED URANIUM (DU) SAMPLING MAPS AND ASSOCIATED DATA

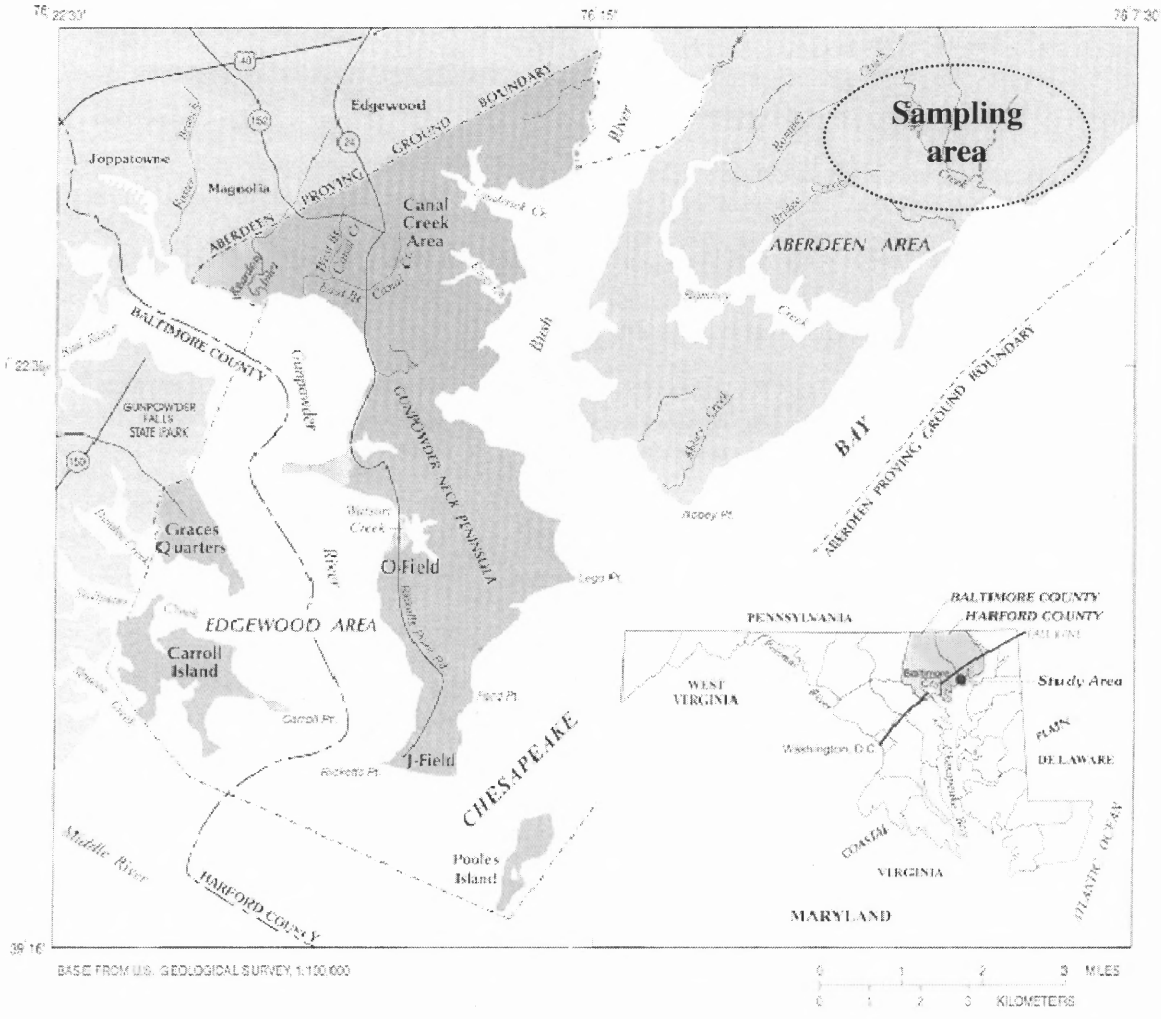

Figure D-1 APG area, Maryland (adapted from Donnelly *et al.*, 1998)

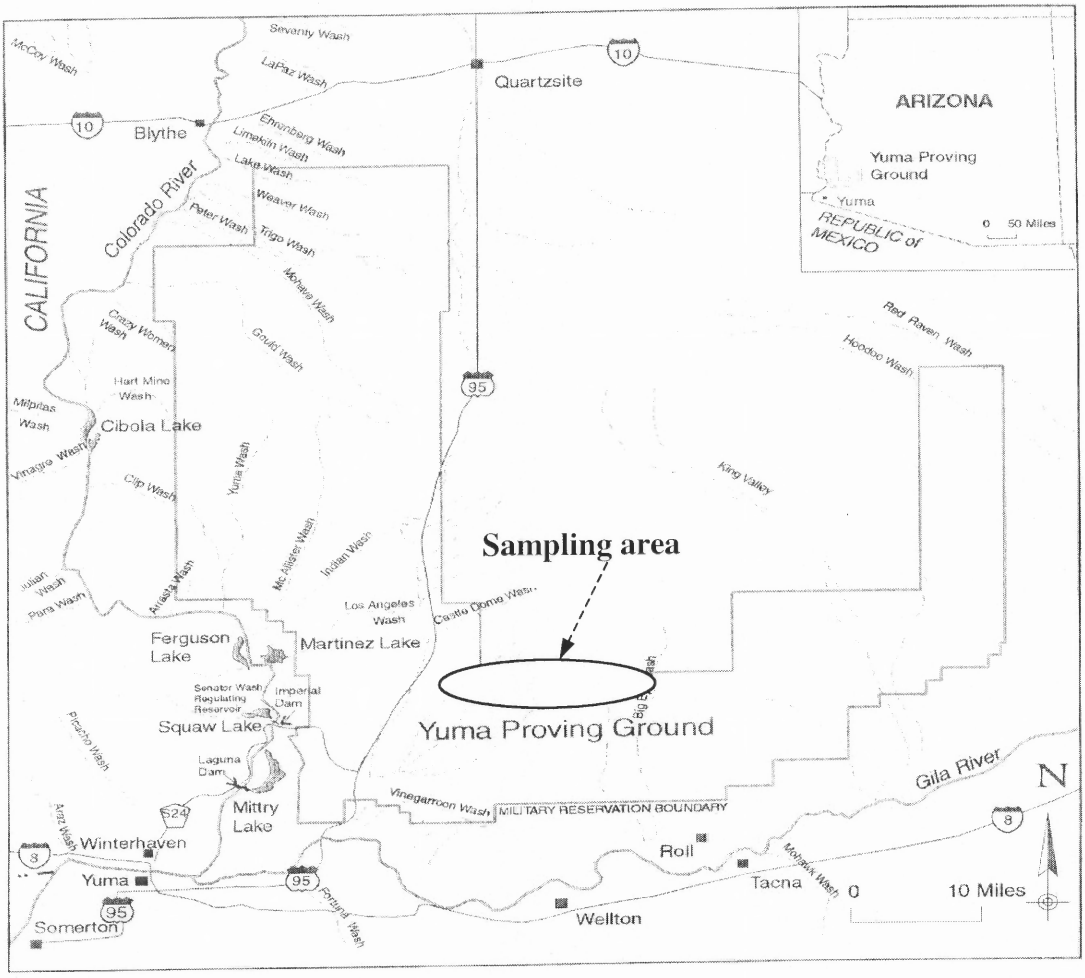

Figure D-2 YPG area, Arizona (adapted from Entech Engineers, Inc., 1998)

Table D-1 Uranium Concentrations in Media at APG and YPG (adapted from Ebinger *et al.*, 1996)

Sample No.	YPG	APG	
	in soil (mg/kg)	in soil (mg/kg)	in water (mg/L)
1	220.6	17.28	1.71×10^{-4}
2	43.22	2.7	9.90×10^{-4}
3	110.42	5.94	5.10×10^{-4}
4	140.6	86.4	3.30×10^{-5}
5	21.05	9.18	1.86×10^{-4}
6	43.22	7.29	9.90×10^{-4}
7	602.6	5.13	9.60×10^{-4}
8	822.8	11.07	1.03×10^{-2}
9	55.26	1.19	1.01×10^{-3}
10	21.15	0.95	
11	1205.6	4.05	
12	1404.2	0.84	
13	24.12	0.81	
14	41.27	0.54	
15	2.7	0.27	
16	0.21	7.56	
17	25.04	5.4	
18	13.47	0.27	
19	26.94	1.81	
20	38.11	0.27	
21	0.0025	1.0	
22	100.44	0.19	
23		1.11	
24		0.3	
25		2.19	
26		0.49	
27		0.54	
28		0.27	
29		2.7	
30		0.38	
31		1.4	
32		0.65	
33		0.43	
34		0.35	
35		2.19	

APPENDIX E

CHEMISTRY OF DEPLETED URANIUM (DU)

Naturally uranium (U) is a radioactive element with three principal isotopes: ^{238}U, ^{235}U, and ^{234}U. These isotopes are alpha particle emitters (Fulco *et al.*, 2000). DU is a by-product from the processing of natural uranium to produce enriched uranium that is used as fuel for nuclear reactors or military applications. The use of uranium in these applications requires increasing the proportion of the ^{235}U isotope found in natural uranium ores (Hartmann *et al.*, 2000). Uranium is enriched to facilitate its use in reactors and weapons. DU, the byproduct of this process, cannot sustain a nuclear reaction or be used as the fuel for nuclear weapons because it contains less ^{234}U and ^{235}U, but its high density (18.9 g/cm^3) and metallurgical properties make it useful in kinetic energy weapons and armor systems (AEPI, 1995).

Natural uranium is 99.2746% ^{238}U, 0.7200% ^{235}U, and 0.0054% ^{234}U, while depleted uranium is 99.7956% ^{238}U, 0.2002% ^{235}U, and 0.0007% ^{234}U (Ebinger *et al.*, 1996) (Table E-1). The DU isotopic composition ($^{238}U/^{235}U$ ~500) is therefore different from natural uranium, which has a ratio of $^{238}U/^{235}U$ ~137.88 (Ketterer *et al.*, 2000). Because the ^{235}U and ^{234}U are present at much less concentrations in DU as compared to natural uranium, the term "depleted" is used. The comparison of natural uranium, DU, and enriched uranium is shown at Table E-1.

The great effort stimulated by the importance of uranium in nuclear chemistry and technology has generated relatively thorough knowledge of the aqueous chemistry of uranium (Baes *et al.*, 1986). Uranium occurs in the +4, +5, and +6 oxidation states or

Table E-1 Comparison of Natural, Enriched, and Depleted Uranium

	^{238}U	^{235}U	^{234}U	**Total Activity (Bq/g)**
α Emitters (MeV)	4.2	4.2	4.8	
γ Emitters (MeV)	0.048		0.053	
Half-life (year)	4.5×10^{9}	7.1×10^{8}	2.5×10^{5}	
Specific activity (Bq/g)[a]	12,445	80,011	2.313×10^{8}	
Uranium (%)	99.2746	0.7200	0.0054	25,280
Enriched Uranium (%)	96.471	3.5	0.02884	81,508
Depleted Uranium (%)	99.7956	0.2002	0.0007	14,656

[a]1Bq (Becquerel) = 1.000 disintegration per second (dps), 1pCi = 10^{-12}Ci = 0.037Bq.

U(IV), U(V) and U(VI), respectively. The most important species in nature are those of uranous [U(IV)] and uranyl [U(VI)]. The uranous ion [U^{+4}]and its aqueous complexes predominate in ground water of low Eh. U(IV) is the most stable oxidation state in common uranium ore minerals, where uraninite [$UO_{2(c)}$] dominates. For the U(V) oxidation state, uranium occurs as the UO_2^+ ion, which forms relatively weak complexes. This species is only found at intermediate oxidation potentials, low pHs, and is generally unstable relative to U(IV) and U(VI) (Langmuir, 1997). In oxidizing environments, uranium is highly soluble as the uranyl ion [UO_2^{2+}] and its complexes (Langmuir, 1997).

A pe-pH diagram at 25°C with a uranium concentration of 10^{-8} M is given in Figure E-1. This plot offers a convenient way to describe the major changes in uranium speciation in redox-active systems and shows the dominant uranium forms in the presence of the uraninite [$UO_{2(c)}$]. Given the stability of water, the typical uranium speciation in natural bodies of water includes the uranyl ion [UO_2^{2+}] and its complexes under oxidizing conditions. On the other hand, in reducing environments, uraninite [$UO_{2(c)}$] dominates. For a pH of 7 and total uranium concentration of 10^{-8} M at atmospheric CO_2 pressure ($10^{-3.5}$ bar), the c (concentraton)-pe diagram (Figure E-2) shows the aqueous complexes like $UO_2CO_3^o$ predominate under oxidizing conditions, and under reducing environments, uraninite [$UO_{2(c)}$] is stable. The solubility of uraninite [$UO_{2(c)}$] is shown in Figure E-3 where under typical aqueous pHs the solubility ranges from 10^{-13} M to 10^{-8} M. Therefore, the U(IV) concentrations in groundwater at low Eh are usually much less than 10^{-8} M. Figure E-4 illustrates U(IV) speciation, which is dominated by hydroxyl complexes with a U concentration of 10^{-14} M.

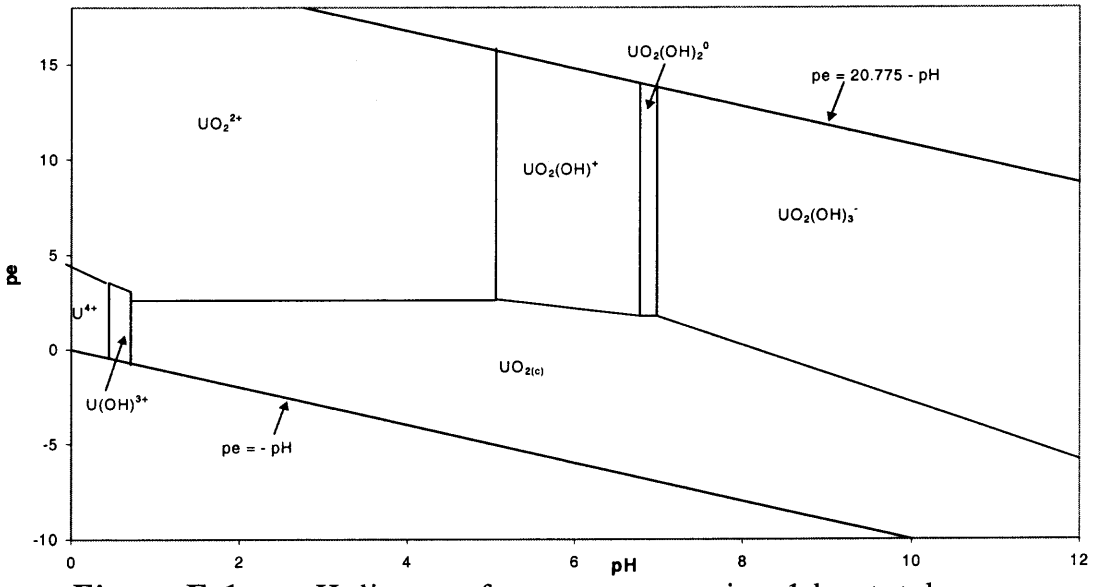

Figure E-1 pe-pH diagram for aqueous species, 1 bar total pressure, and total $U=10^{-8}M$ (typical groundwater uranium concentration).

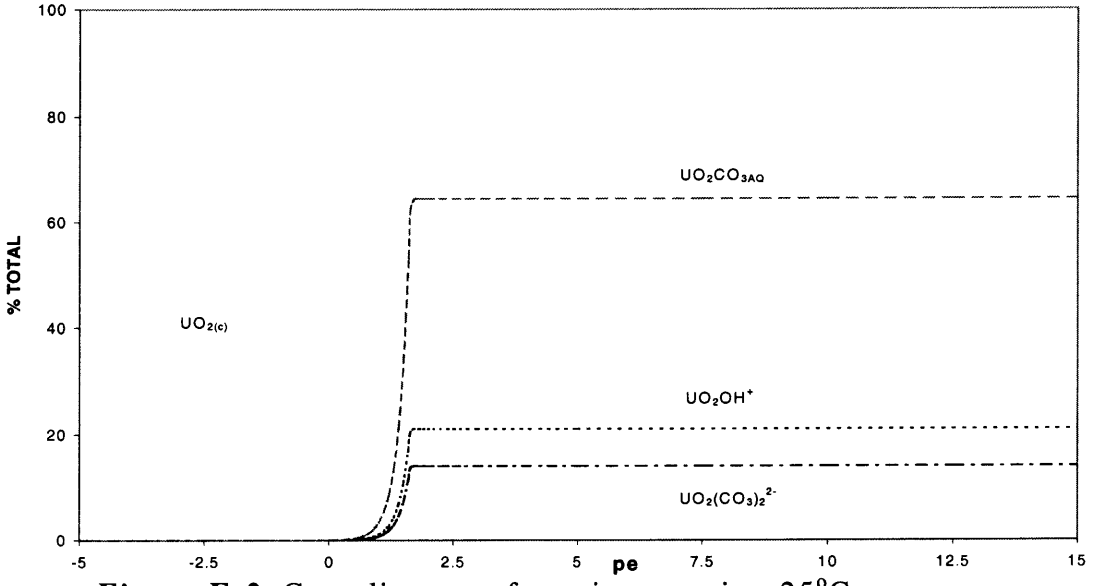

Figure E-2 C-pe diagram of uranium species, 25°C, total $U=10^{-8}M$ (typical groundwater uranium concentration), pH=7, and $P_{CO2}=10^{-3.5}$atm.

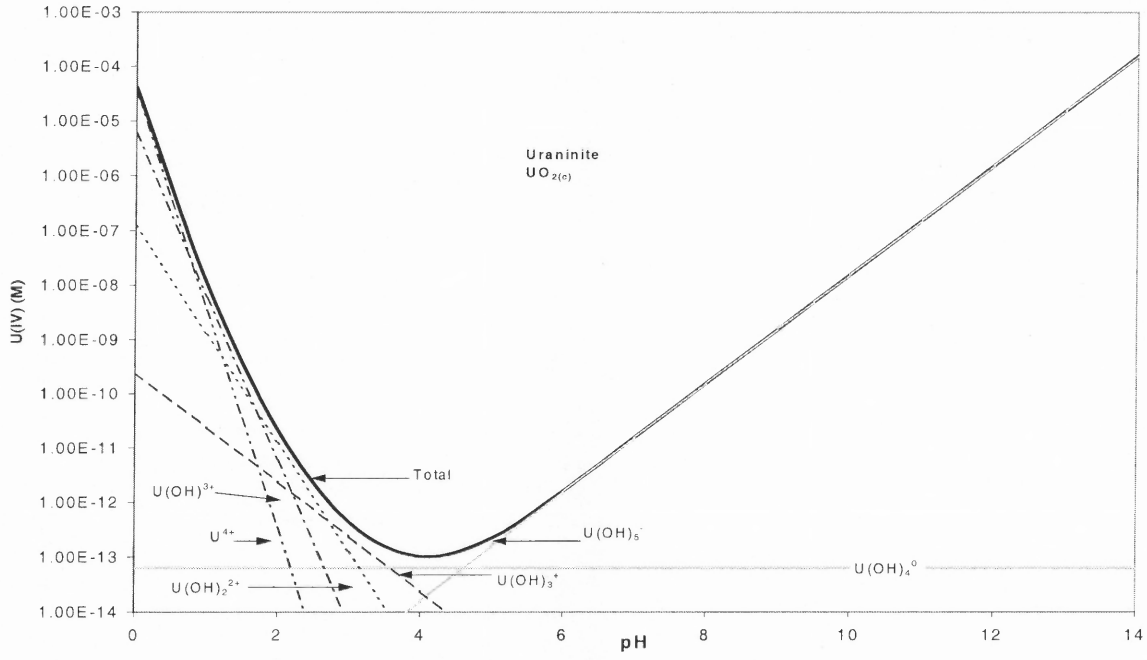

Figure E-3 Solubility of uraninite ($UO_{2(c)}$), 25°C, I=0.001M, and $P_{CO2}=10^{-3.5}$atm.

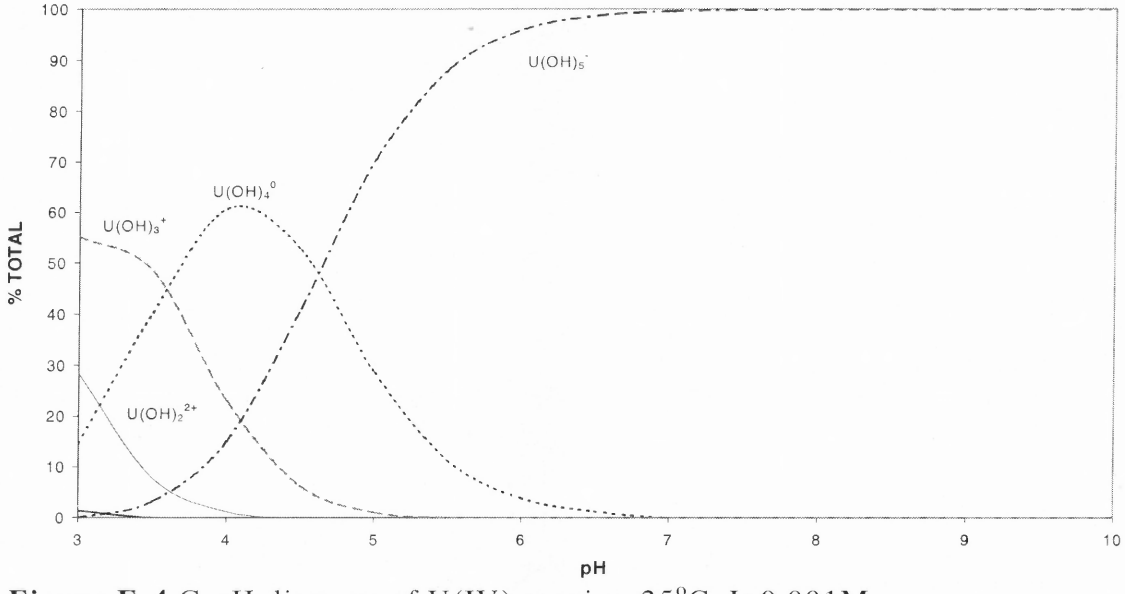

Figure E-4 C-pH diagram of U(IV) species, 25°C, I=0.001M, total $U=10^{-14}$M, and $P_{CO2}=10^{-3.5}$atm.

With respect to U(VI), the uranyl ion forms strong carbonate complexes in most natural waters. Their importance as a function of pH at atmospheric CO_2 pressure ($10^{-3.5}$ bar) is shown in Figure E-5, which indicates that these complexes largely outweigh the hydroxo- U(VI)- complexes above pH 6. The carbonate complexes are extremely important because they greatly increase the solubility of uranium minerals, and also limit the extent of uranium adsorption in oxidized waters, thus increasing uranium mobility. Other important U(VI) complexes are formed with fluoride, phosphate, and sulfate ligands (Langmuir, 1997). The effect of the carbonate complexes on schoepite (β-$UO_3 \cdot 2H_2O$) solubility is evident from Figure E-6, which shows the solubility as a function of pH at atmospheric CO_2 pressure. Uranium U(VI) minerals are most often products of the oxidation and weathering of nearby primary U(IV) ore minerals such as uraninite [$UO_{2(c)}$] and coffinite [$USiO_{4(c)}$] (Langmuir, 1997).

Uranium is the most abundant actinide element, which averages 1.2 to 1.3 μg/g in sedimentary rocks, 2.2 to 15 μg/g in granites, and 20 to 120 μg/g in phosphate minerals. According to Bertell (1999), natural uranium in soil is about 1 to 3 μg/g, whereas in uranium ore it is about 1,000 times more concentrated, reaching about 0.05 to 0.2% of the total weight. Uranium concentrations are usually between 0.1 and 7 μg/L in streams where uranium mineral deposits exists. Seawater contains 2 to 3.7 μg/L uranium, and generally groundwaters in granite have some of the highest uranium concentrations, although they rarely exceed 20 μg/L (Langmuir, 1997).

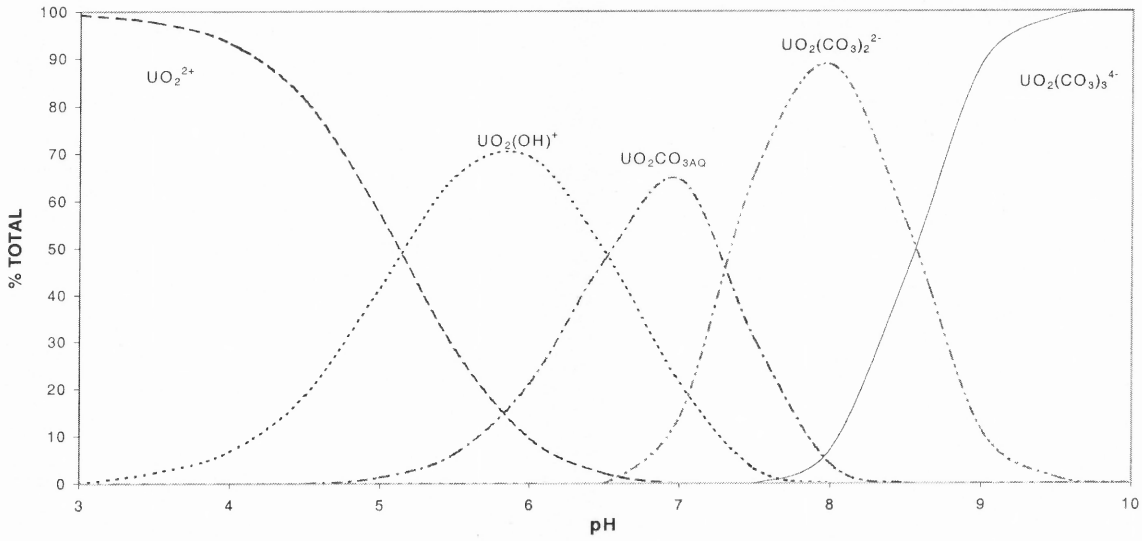

Figure E-5 C-pH diagram of U(VI) species, 25°C, I=0.001M, total U = 10^{-8}M (typical groundwater uranium concentration), and $P_{CO2}=10^{-3.5}$atm.

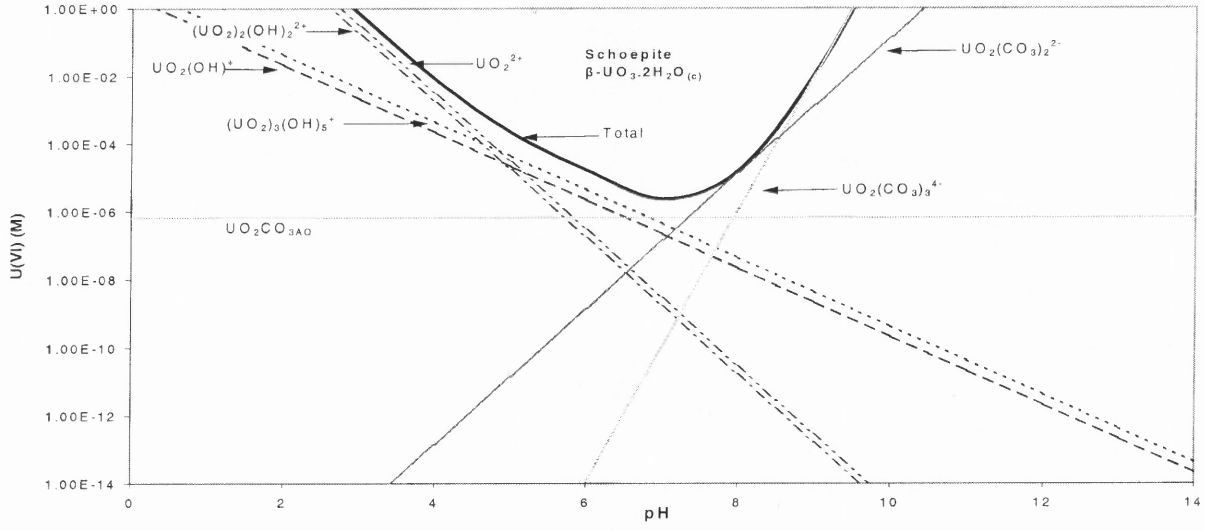

Figure E-6 Solubility of schoepite (β-$UO_3.2H_2O_{(c)}$), 25°C, I=0.001M, and $P_{CO2}=10^{-3.5}$atm.

Isotopes of uranium have the same chemical properties because they all have the same number of protons, 92. However, variation in the number of neutrons gives the isotopes different radiological properties (Fulco *et al.*, 2000). In both DU and natural uranium, ^{238}U consitutes more than 99%. Natural uranium contains three isotopes of atomic masses 234, 235, and 238 (Table E-1) and DU contains these three plus a trace amount of 236. These isotopes, ^{234}U, ^{235}U, and ^{236}U, vary in their ability to undergo nuclear fission, interactions with nuclear particles, radioactive decay rates, and the types of radiation they emit upon radioactive decay (AEPI, 1995). ^{236}U is not a naturally occurring uranium isotope, but is sometimes present as a byproduct of nuclear fission derived from nuclear fuel. The radioactivity of DU is roughly 60% that of natural uranium and 20% of enriched uranium. The reasons for this are the reduction in the ^{234}U and ^{235}U isotopes of DU substantially lowers specific activity. The presence of trace amounts of ^{236}U does not significantly increase DU's radioactivity because the specific activity of ^{236}U (63.6 Ci/g) is only about 1 percent of that of ^{234}U (6,200 Ci/g) (AEPI, 1995).

The hazard from the radioactivity of the uranium compounds depends somewhat on the isotopic composition of the uranium. The ^{234}U and ^{235}U isotopes are more of a radiological hazard than the ^{238}U isotope because of their higher specific activities (Table E-1). In DU, most of the ^{234}U and ^{235}U isotopes have been selectively removed through industrial processing, the radiological hazard from DU is therefore less than that from natural or enriched uranium (Hartmann *et al.*, 2000). However, DU has radiological health risk from exposure to low-level radiation, and this is a complex issue. Alpha particles are primary emitters in these isotopes with low penetrating ability. The radiation

emitted by DU results in health risks from both external and internal exposure. According to U.S. AEPI (1995), potential radiological health effects from external DU exposure are small and the radioactive properties of DU have a greater potential for health impacts when DU is internalized. DU can be internalized through inhalation or ingestion. Internalized DU delivers radiation wherever it migrates into the body. The health risks of internal DU exposure are a function of the particle characteristics, route of exposure, duration of exposure, and the speciation.

As previously indicated, DU and natural uranium have the same chemical behavior and physical properties. Therefore, chemical toxicity data developed for any isotope of uranium are applicable to DU. Uranium is categorized as a heavy metal (i.e., any metal with a specific gravity of 5.0 or greater). The chemical toxicity of a uranium compound varies depending on the nature of the compound, its solubility, and its route of exposure (Fulco *et al.*, 2000). The main chemical effect associated with exposure to uranium and its compounds is renal toxicity, detected by the presence of protein and cell casts in the urine. When DU is incorporated in the body, the soluble components migrate throughout the body. The kidney is the most sensitive organ to DU toxicity. Human epidemiological studies of workers in the uranium mining and milling industries suggest that nephrotoxicity is of primary concern. Other organ systems are less sensitive to the effects of uranium than the kidney (Hartmann *et al.*, 2000). Rostker (1998) found that once dissolved in the blood, about 90% of the uranium present will be excreted by the kidney in urine within 24-48 hours. The remaining 10% is retained by the body, and can deposit in bones, lungs, liver, kidney, fat, and muscle. Insoluble uranium oxides, if inhaled, can remain in the lungs for years, where they are slowly taken into the blood.

The Agency for Toxic Substances and Disease Registry (ATSDR) also found DU's chemical toxicity presents acute effects on the respiratory system when the health effects of DU to exposed Gulf War veterans were studied (ATSDR, 1990; McDiarmid *et al.*, 2000).

Additionally, the chemical and radiological properties of uranium could act synergistically to cause tissue damage, and therefore, it cannot be assumed that cancer would be due solely to the radiological effects of uranium or that organ damage is exclusively due to its heavy-metal properties (Fulco *et al.*, 2000).

APPENDIX F

STEPS IN MODELING APPLICATION ON CONTAMINATED SITES

In this research, a simulation tool (ERA model) was developed with a comprehensive modeling approach for assessing risks and impacts associated with contaminants to the surrounding environment. To apply this approach, contaminant speciation, distribution mechanism, transport, and ecological risks need to be addressed. The steps in applying this tool to contaminated sites are outlined as follows:

(1) In simulating contaminant mobility in the subsurface, speciation is required. Once the chemical form is understood, its mobility and bioavailability can be addressed. Contaminant speciation in the aqueous phase can be obtained by thermodynamic models, such as MINEQL+ (linked to ERA model).

(2) Contaminant distribution with subsurface minerals needs to be accurately depicted. Employing GMS along with the transient process package in RT3D, contaminant mobility can be simulated. During this process, parameters on aquifer geology and hydrogeology (Table F-1) need to be obtained based on site specific data. Although defining hydrology requires field data, modeling the transient sorption process does not involve the need for laboratory studies. The simulation begins with groundwater flow development. Stratigraphy modeling is implemented by borehole interpretation based on a set of TINs (Triangulated Irregular Network) to setup the aquifer model; then the conceptual model is constructed using featured objects in the Map module of GMS. Groundwater using MODFLOW-2000 is converted from the conceptual model providing head profiles.

(3) Based on the regional groundwater flow model, a local model is developed through a regional to local model conversion, and is used to simulate solute transport in and around the local area. To address contaminant mobility, transport parameters (Table F-1) can be calculated based on the approach outlined in this research (Chapter 8). Relationships developed for distribution and diffusion coefficients as a function of pH to aluminum, iron, and manganese oxides can be applied and accounted for by the mass fraction of oxides (Figure F-1). Specifically, for example, a sandy aquifer with 25.3 g kg^{-1} iron oxide and 4.0 g kg^{-1} manganese oxide,

$$K_d = K_{d(HFO)} \frac{25.3}{29.3} + K_{d(HMO)} \frac{4.0}{29.3} = 16.4 \text{ L g}^{-1}$$

The boundary condition correlation developed by Bird *et al.* (2002)

$$Sh_m = \frac{kd}{D} = 0.991(\text{Re Sc})^{1/3}$$

is used to obtain the external mass transfer coefficient, where d is the particle diameter. For example, in Sr^{90} transport simulation at the Hanford Site, Re, the Reynolds number, is 7.2×10^{-5}; the Schmidt number, Sc, is 7.1×10^{9}; therefore, the Sherwood number, Sh_m, is 79. Based on D ($D = D_s/(1+\varepsilon_p/\rho K_i)$, Chapter 6 Equation 6.2), 1.1×10^{-12} cm^2 s^{-1}, and d, 28 μm, k is calculated to be 1.8×10^{-8} cm s^{-1}.

(4) Lastly, once the bioavailable species is defined spatially and temporally, it is used to assess static or dynamic ecological risks resulting from exposure to different contaminants. A probabilistic approach employing Monte Carlo simulations for assessing parameters and risks as distributions is used in the ERA model (Lu *et al.*, 2003) to characterize risk and address uncertainty. After conducting risk assessment, model validation is needed based on field sampling data.

Table F-1 Parameters for Transport Simulation

	Parameters	Symbol	Unit
Aquifer geology	Aquifer elevation	L	m
and hydrogeology	Thickness	d	m
	Sediment composition	c	g kg^{-1}
	Hydraulic conductivity	K	m d^{-1}
	Dispersivity	D_{ij}	m
	Effective porosity	ε	cm^{-3} pore/cm^{-3} solid
	Specific yield	Y	cm^{-3} water/ cm^{-3} soild
	Particle size	R	mm
	Bulk density	ρ	g cm^{-3}
Transport	Distribution coefficient	K_d	L g^{-1}
	Surface diffusivity	D	cm^2 s^{-1}
	External mass transfer coefficient	k	cm s^{-1}

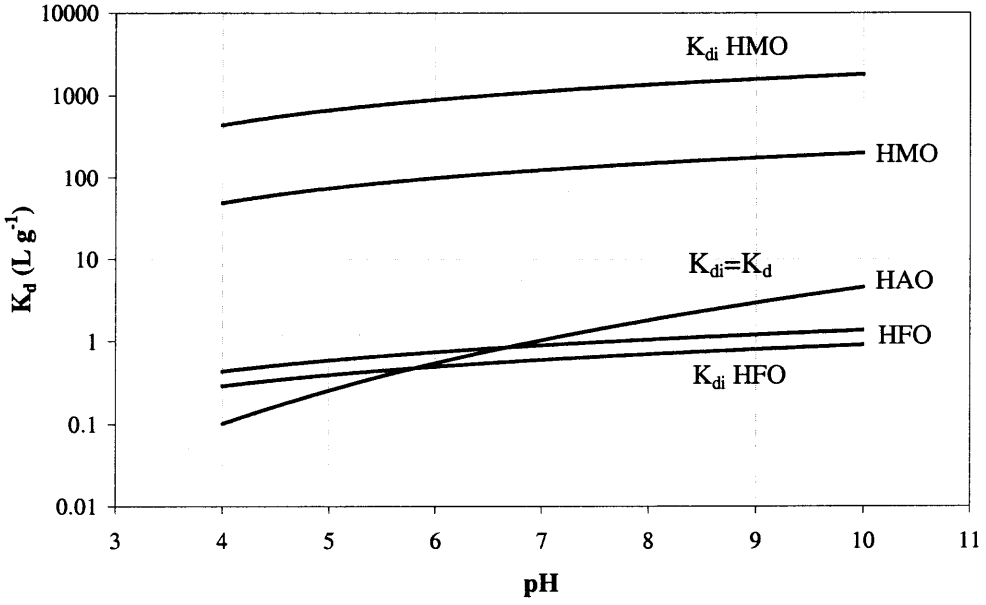

(a) Distribution coefficient vs. pH

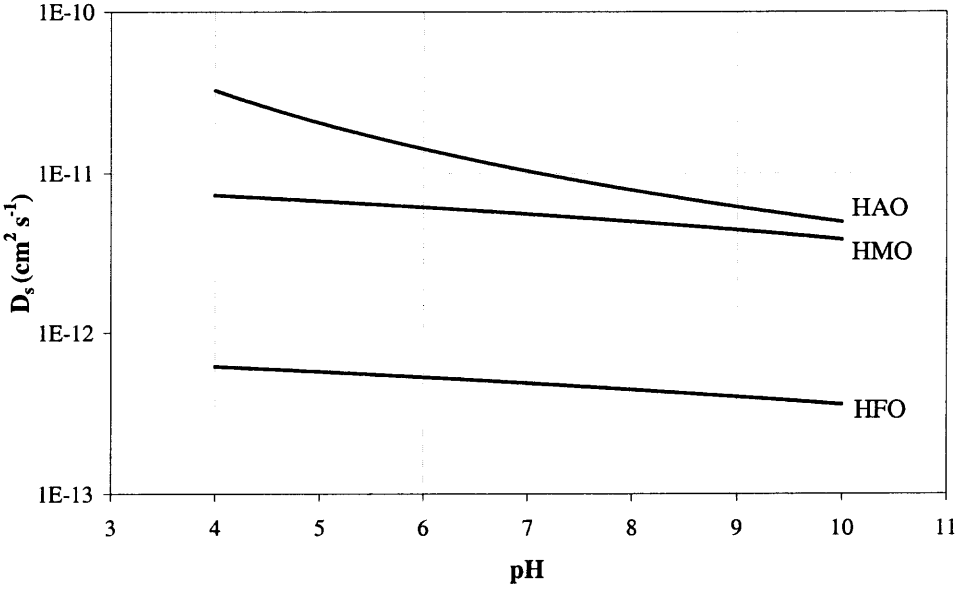

(b) Surface diffusivity vs. pH

Figure F-1 Sr^{90} distribution and diffusion coefficients vs. pH for HAO, HFO, and HMO at 25°C based on Trivedi and Axe (1999, 2000, and 2001). K_{di} is the internal distribution coefficient representing the product of the equilibrium constant and internal site density; K_d is the external distribution coefficient and is the product of the equilibrium constant and external surface site density. For HAO, K_{di} is equivalent to K_d as internal sites constitute approximately 50% of the total sites.

APPENDIX G

COMPUTER CODES

Intraparticle Surface Diffusion Code with RT3D

```
c INTRAPARTICLE DIFFUSION MODULE

c New Jersey Institute of Technology

c Should be used as a user-defined module with RT3D inside Groundwater Modeling
System (GMS)


      SUBROUTINE Rxns(ncomp,nvrxndata,j,i,k,y,dydt,
     &      poros,rhob,reta,rc,nlay,nrow,ncol,vrc)
C*Block 1:*************************************************************

c List of calling arguments
c ncomp - Total number of components
c nvrxndata - Total number of variable reaction parameters to be input via RCT file
c J, I, K - node location (used if reaction parameters are spatially variable)
c y - Concentration value of all component at the node [array variable y(ncomp)]
c dydt - Computed RHS of your differential equation [array variable dydt(ncomp)]
c poros - porosity of the node
c reta -  Retardation factor
c rhob -  bulk density of the node
c rc - Stores spatially constant reaction parameters (can dimension upto 100 values)
c nlay, nrow, ncol - Grid size (used only for dimensioning purposes)
c vrc - Array variable that stores spatially variable reaction parameters

C*End of Block 1*******************************************************

C*Block 2:*************************************************************

c*   *Define parameters inside RT3D with standard interface block*

    !MS$ATTRIBUTES DLLEXPORT :: rxns
    IMPLICIT NONE
    INTEGER ncol,nrow,nlay
    INTEGER ncomp,nvrxndata,j,i,k
    INTEGER, SAVE :: First_time=1
    DOUBLE PRECISION y,dydt,poros,rhob,reta
    DOUBLE PRECISION rc,vrc
    DIMENSION y(ncomp),dydt(ncomp),rc(100)
    DIMENSION vrc(ncol,nrow,nlay,nvrxndata),reta(ncomp)
```

```
C*End of block 2*********************************************************

C*Block 3:***************************************************************

c     *Declare intraparticle surface diffusion-specific new variables*

c     R = Particle size (cm)
c     P = Bulk density (g/cm3)
c     D = Diffusivity (cm2/s)
c     Kd = Partitioning coefficient(l/g)
c     Ct = Sorbed concentration in the particle surface (mg/g)
c     S = Bulk concentration (mg/l)
c     C = sorbed concentration (mg/g)
c     A, Ctc, Cpc,B = Defined variables in the equations (A: cm2.l/cm3, Ctc and Cpc are
dimentionless, and B: cm3/g)

      DOUBLE PRECISION R, P, D, Kd, A, B, Ctc, Cpc, S, C, Ct

C*End of block 3*********************************************************

C*Block 4:***************************************************************

c     *Initialize reaction parameters here, if required*

      IF (First_time .EQ. 1) THEN

          P=rhob

        First_time = 0 !reset First_time to skip this block later

      END IF

C*End of block 4*********************************************************

C*Block 5:***************************************************************

c     *Assign or compute values for new variables, if required*

      S = y(1)
      C = y(2)
      Kd=vrc(j, i, k, 1)
      R=vrc(j, i, k, 2)
      D=vrc(j, i, k, 3)
      Kd=vrc(j, i, k, 4)

C*End of block 5*********************************************************
```

```
C*Block 6:*****************************************************************

c     *Differential Equations -- Intraparticle diffusion*

      Cpc=0.5*sqrt(0.25*((1-B*0.001/Kd)**2)+2*(1+B*P))
      Ctc=(1-B*0.001/Kd)/4+Cpc

      Ct=S*Kd
      A=poros*(1+P*Kd/poros)*R*R

     dydt(1) = -(Ctc+0.5)*(6.0*P*D)/A*(Ct-C)
     dydt(2) = (Ctc+0.5)*(6.0*D)/(R*R)*(Ct-C)

C*End of block 6***********************************************************

       RETURN
       END
```

Code for Estimating Intraparticle Surface Diffusivity

```
#include <stdlib.h>
#include <iostream.h>
#include <fstream.h>
#include <math.h>
#include <string>
#include <iomanip.h>

#define STRLEN 30
#define FIRSTDELIMITER ','
#define SECONDDELIMITER '\n'

void main ()
{
        // define all variables and parameters
        /*Ds: surface diffusivity, Cs: bulk concentration, E: porosity, Kd: external
        distribution coefficient, Ki: internal distribution coefficient, mass: mass sorbed
        per particle, summ: overall mass sorbed per particle, var: variance, sd: standard
        deviation, diff: differences between experimental data and modeling, rad: particle
        radius, num: numbers of specific particle, n, nn, nnn, a, sum, sum1, sum2, diff2,
        persum, percent, and aveer: variables defined in loops*/

        double pi=3.14159, Ds=8.7e-17, Cs=1.71e-4, p=1.03, E=0.45, Kd, sd;
        double mass[310], Ki, sum, D, a, rad[100], num[100], Ct, summ[300], t[100],

        data[100], sum1, sum2, diff, diff2, percent, persum, var, aveer;

        int n=100, i, j, k, nn=0, nnn=0, ii;
        char string[2][STRLEN], string1[2][STRLEN];

        //build files connections

        ofstream f2("result.txt");
        ofstream f3("new3.txt");
        ifstream f4("psdhaocoated.txt");

        ifstream f5("pbhaocoateddata.txt");
        ofstream f6("dsvar.txt");

        //read particle size distribution from file into code

        while(!f4.getline(string[0], STRLEN, FIRSTDELIMITER).eof())
        {
          f4.getline(string[1], STRLEN, SECONDDELIMITER);
          rad[nn]=atof(string[0]);
```

```
   num[nn]=atof(string[1]);
   nn=nn+1;
 }

while(!f5.getline(string1[0], STRLEN, FIRSTDELIMITER).eof())
{
f5.getline(string1[1], STRLEN, SECONDDELIMITER);
t[nnn]=atof(string1[0]);
data[nnn]=atof(string1[1]);
 nnn=nnn+1;
 }

//check particle size distribution correct from file output

  for (k=0; k<nn; k++)
{
f3<<rad[k]<<"\t"<<num[k]<<endl;
}

//get particle external surface concentration

Ct=Cs*Kd;

//obtain total concentration

 for (ii=1; ii<=10; ii++)
{

 //defne diffusivity

D=Ds/(1+E/(p*Ki));

sum1=0.0;
sum2=0.0;
persum=0.0;

for (j=0; j<nnn; j++)
{
summ[j]=0.0;

for (k=0; k<nn; k++)
{
sum=0.0;
for (i=1; i<=n; i++)
```

```
        a=1/pow(i,2)*exp(-D*pow(i,2)*pow(pi,2)*t[j]*86400/(pow(rad[k],2)*pow(10.0, -
        8)));

          sum=sum+a;
          }

        mass[k]=4*pi*pow(rad[k],3)*pow(10, -12)/3*(1-6/pow(pi,2)*sum)*num[k]*Ct*p;

          summ[j]=summ[j]+mass[k];
          }

          summ[j]=summ[j]+Ct;
          diff=fabs(data[j]-summ[j]);
          percent=(diff/summ[j])*100.0;
          diff2=pow(diff,2);
          sum1=sum1+diff;
          sum2=sum2+diff2;
          persum=percent+persum;
          f2<<t[j]<<", "<<summ[j]<<", "<<data[j]<<endl;
          }

          var=(sum2-(pow(sum1,2)/nnn))/(nnn-1);
          sd=pow(var, 0.5);
          aveer=persum/nnn;

          f6<<Ds<<", "<<var<<", "<<aveer<<endl;
          cout<<Ds<<", "<<var<<", "<<aveer<<",sd"<<sd<<endl;
          Ds=Ds+pow(10, -18);
          }
}
```

Code for Orthogonal Collocation

```
#include<math.h>
#include "matrix.h"

#ifndef _NO_NAMESPACE
using namespace std;
using namespace math;
#define STD std
#else
#define STD
#endif

#ifndef _NO_TEMPLATE
typedef matrix<double> Matrix;
#else
typedef matrix Matrix;
#endif

void main ()
{
        int n=0, nn, i;
        long double B=100, x[6], u[6], cb, a=1, deltat=0.001, eu, eu1, avgu=0;
        Matrix M(6, 6), M1(6, 6), e(6, 6), f(6, 6), uiun(6, 6), un(6, 6), y(6, 6), du(6, 6),

        ai(6,6), w(2,2), w1(2,2), w2(2,2), w3(2,2);


        for (i=0; i<=5; i++)
        {
        n=n+1;
        x[i]=n/6.0;

        }

        for (i=0; i<=5; i++)
        {
        u[i]=0.0;
        }
        cout<<endl;
        for (i=0; i<=4; i++)
        {
        for(int j=0; j<=5; j++)
        {
        M(i,j)=pow(x[i], (j+1)*2)-1;
        }
```

```
}

for(int j=0; j<=5; j++)
{
M(5,j)=2.0*(j+1);
}

cout << "\nMatrix:\nM = \n" << M << endl;
M1 = !M;
cout << "\nMatrix inversion:\nInv M1 = \n" << M1 << endl;
for(j=0; j<=5; j++)
{
f(0,j)=2.0*(j+1)/(2.0*(j+1)+3);
}
for (i=1; i<=5; i++)
{
for(j=0; j<=5; j++)
{
f(i,j)=0;
}
}
cout << "\nMatrix:\nf = \n" << f << endl;
e=-f*M1;
cout << "\nMatrix:\ne = \n" << e << endl;
eu=0;
for(j=0; j<=4; j++)
{
eu1=e(0,j)*(u[j]-u[5]);
eu=eu1+eu;
}
cout<<"eu="<<eu<<endl;
for (i=0; i<=5; i++)
{
for(j=0; j<=5; j++)
{
un(i,j)=2*(j+1)*(2*(j+1)+1)*pow(x[i],2*(j+1)-2);
}
}
cout << "\nMatrix:\nun = \n" << un << endl;
cb=1.0;
cout<<"cb="<<cb<<endl;
cout << "\nStart looping \n" << endl;
for (nn=1; nn<=100 ; nn=nn+1)
{
for(j=0; j<=4; j++)
{
```

```
        uiun(j,0)=u[j]-u[5];
        }
        uiun(5,0)=B*(cb-u[5]);
        for (i=1; i<=5; i++)
        {
        for(j=0; j<=5; j++)
        {
        uiun(j,i)=0;
        }
        }

        cout << "\nMatrix:\nuiun = \n" << uiun << endl;
        ai=M1*uiun;
        cout << "\nMatrix:\nai = \n" << ai << endl;
        du=un*M1*uiun;
        cout << "\nMatrix:\ndu = \n" << du << endl;
        for(j=0; j<=5; j++)
        {
        u[j]=u[j]+deltat*du(j, 0);
        cout<<"u["<<j<<"]="<<u[j]<<",";
        }
        cout<<endl;

        for(j=0; j<=4; j++)
        {
        eu1=e(0,j)*(u[j]-u[5]);
        eu=eu1+eu;
        }

        cout<<"eu"<<eu<<endl;
        cb=1-(u[5]+eu+e(0, 5)*B*(1-u[5]))/(a+e(0,5)*B);
        cout<<"cb="<<cb<<endl;
        avgu=a*(1-cb);
        cout<<"avgu="<<avgu<<endl;
        cout<<endl;
        }
}
```

Code for Finite Difference

```
#include <iostream.h>
#include <fstream.h>
#include <math.h>
void main ()
{
        double u[1110], u0[1110], pi=3.14159, deltaT=0.00001, deltaX=0.01, T=0.001,
        sum, cb, c, a=1, B=100;
        int j, k, nh, kk;
        ofstream f2("new3.txt");
        nh=1/deltaX;
        for (int i=0; i<=nh; i++)
        {
        u0[i]=0;
        }
        c=0.0;
        cb=1-c/a;
        u0[nh+1]=2.0*deltaX*B*(cb-u0[nh])+u0[nh-1];

        for (int n=1; n<=(T/deltaT); n++)
        {
        sum=0.0;
        for (j=1; j<=nh; j++)
        {
      u[j]=u0[j]+deltaT*((u0[j+1]-u0[j-1])/(j*deltaX*deltaX)+(u0[j+1]-2*u0[j]+u0[j-

      1])/(deltaX*deltaX));

        sum=sum+u[j];
        }
        c=sum/nh;
        cb=1-c/a;
        u[0]=u[2];
        u[nh+1]=2*deltaX*B*(cb-u[nh])+u0[nh-1];
        for (k=0; k<=nh+1; k++)
        {
        u0[k]=u[k];
        }
        }
        for (j=0; j<=nh+1; j++)
        {
        cout<<"u["<<j<<"],"<<u[j]<<",";
        f2<<"u["<<j<<"],"<<u[j]<<endl;
        }
}
```

APPENDIX H

SORPTION EXPERIMENTAL DATA

Pb Adsorption Edges at 25°C

HAO

	IS 0.06		IS 0.6
pH	% Pb Sorbed	pH	% Pb Sorbed
4.5	88.308	4.5	85.174
5.0	90.846	5.0	88.806
5.5	93.134	5.5	93.284
6.0	94.279	6.0	93.93
6.0	95.955	6.0	95.025
6.5	98.149	6.5	96.318

HFO

	IS 0.028		IS 0.1
pH	% Pb Sorbed	pH	% Pb Sorbed
3.5	54.298	3.5	47.879
4.0	82.675	4.0	79.393
4.0	82.433	4.2	87.115
4.2	87.259	4.4	93.823
4.4	92.52	4.6	96.578
4.6	96.583	4.6	96.689
4.8	98.441	4.8	98.239
5.0	99.073	5.0	99.32
5.5	99.596	5.5	99.484
6.0	99.804	6.0	99.834

HMO

	IS 0.015		IS 0.15
pH	% Pb Sorbed	pH	% Pb Sorbed
1.0	72.394	1.0	27.606
1.5	86.438	1.0	30.985
2.0	97.376	1.5	57.239
2.5	99.533	2.0	77.992
3.0	99.939	2.5	98.687
3.0	99.922	3.0	99.756
3.5	99.997	3.5	99.995
4.0	99.996	4.0	99.985
4.5	99.998	4.5	99.995
5.0	99.997	5.0	99.998

Montmorillonite

	IS 0.01		IS 0.0025
pH	% Pb Sorbed	pH	% Pb Sorbed
4.0	69.957	4.0	44.258
4.5	78.704	4.5	62.895
5.0	82.083	5.0	71.430
5.5	91.337	5.5	92.422
6.0	97.901	6.0	90.768
6.5	98.926	6.5	86.102
6.5	99.348	6.5	89.132
6.8	99.361	7.0	96.175
7.0	99.542	7.5	94.043
7.5	99.674	6.8	87.969

HAO-coated montmorillonite

	IS 0.06		IS 0.6
pH	% Pb Sorbed	pH	% Pb Sorbed
4.0	43.705	4.0	37.042
4.5	47.932	4.5	45.405
5.0	54.819	5.0	50.593
5.5	62.835	5.5	51.353
6.0	67.308	6.0	54.081
6.5	75.447	6.5	58.207

Pb Adsorption Isotherm at 25°C

HAO [Pb] (M)	pH 6 Mole Pb Sorbed/g HAO	HFO [Pb] (M)	pH 6 Mole Pb Sorbed/g HFO
1.72E-05	1.26E-04	1.05E-08	3.99E-06
9.31E-06	1.01E-04	4.44E-09	6.00E-06
5.60E-06	6.88E-05	5.79E-09	7.99E-06
2.70E-06	3.46E-05	8.59E-09	9.99E-06
1.28E-06	1.74E-05	1.02E-08	2.00E-05
4.23E-07	1.52E-05	1.75E-08	3.00E-05
3.29E-07	1.13E-05	6.18E-08	4.99E-05
2.44E-07	7.51E-06	5.69E-08	4.99E-05
5.07E-08	3.90E-06	1.84E-07	7.98E-05
1.73E-06	1.65E-05	1.78E-07	9.98E-05
		3.41E-09	8.00E-06
		1.19E-08	9.99E-06
		1.32E-08	2.00E-05
		1.29E-08	3.00E-05
		9.99E-08	4.99E-05
		7.87E-08	4.99E-05
		8.45E-08	7.99E-05
		1.42E-07	9.99E-05

HMO [Pb] (M)	pH 5 Mole Pb Sorbed/g HMO	Clay [Pb] (M)	pH 6 Mole Pb Sorbed/g Clay
4.06E-07	0.0025936	5.80E-09	2.42E-05
6.54E-07	0.004346	1.40E-08	1.46E-04
8.21E-06	0.11679	1.83E-08	1.82E-04
1.16E-05	0.17591	1.76E-08	1.82E-04
1.42E-05	0.23579	5.83E-08	3.42E-04
1.53E-05	0.23471	7.67E-08	4.23E-04
1.99E-05	0.29263	9.34E-08	5.07E-04
2.43E-05	0.35068		
2.80E-05	0.40951		
4.16E-05	0.45845		

Coatings [Pb] (M)	pH 6 Mole Pb Sorbed/g Coatings
2.98E-06	0.0011673
2.35E-06	8.49E-04
1.47E-06	5.88E-04
8.04E-07	2.78E-04
4.97E-07	1.17E-04
3.85E-07	9.65E-05
2.38E-07	8.43E-05
2.19E-07	4.21E-05

Pb CBC Studies

HAO Time (d)	Mole Pb Sorbed/g HAO	Coatings Time (d)	Mole Pb Sorbed/g Coatings	Clay Time (d)	Mole Pb Sorbed/g Clay
0.000	0.000E+00	0.000	0.000E+00	0.000	0.000E+00
0.002	1.200E-03	0.002	1.550E-03	0.010	3.990E-04
0.004	1.210E-03	0.004	1.590E-03	0.021	4.040E-04
0.007	1.230E-03	0.007	1.610E-03	0.031	4.060E-04
0.014	1.240E-03	0.014	1.620E-03	0.042	4.020E-04
0.021	1.250E-03	0.021	1.620E-03	0.063	4.010E-04
0.028	1.250E-03	0.028	1.660E-03	0.090	4.010E-04
0.035	1.260E-03	0.035	1.690E-03	0.104	4.040E-04
0.042	1.270E-03	0.042	1.700E-03	0.125	4.050E-04
0.083	1.270E-03	0.083	1.710E-03	0.146	4.030E-04
0.125	1.290E-03	0.167	1.690E-03	0.167	4.050E-04
0.167	1.290E-03	0.500	1.740E-03	0.208	4.030E-04
0.583	1.290E-03	1.000	1.760E-03	0.250	4.100E-04
1.000	1.310E-03	1.500	1.760E-03	0.292	4.030E-04
1.500	1.300E-03	2.000	1.770E-03	0.333	4.020E-04
2.000	1.300E-03	2.417	1.740E-03	0.375	4.100E-04
2.500	1.300E-03	3.042	1.770E-03	0.417	4.100E-04
3.000	1.300E-03	3.375	1.740E-03	0.458	4.070E-04
3.500	1.310E-03	4.000	1.760E-03	0.500	4.090E-04
4.000	1.330E-03	4.500	1.790E-03	1.000	4.090E-04
5.000	1.460E-03	5.000	1.760E-03	1.167	4.120E-04
14.167	1.490E-03	5.500	1.760E-03	1.271	4.080E-04
15.080	1.570E-03	6.500	1.780E-03	1.375	4.070E-04
17.380	1.610E-03	7.500	1.790E-03	2.019	4.090E-04
18.040	1.640E-03	8.625	1.780E-03	2.167	4.070E-04
19.080	1.720E-03	9.625	1.790E-03	2.375	4.100E-04
20.330	1.780E-03	10.604	1.830E-03	3.156	4.120E-04
21.167	1.830E-03	19.729	1.810E-03	3.333	4.090E-04
24.125	1.850E-03	20.625	1.830E-03	4.375	4.080E-04
26.167	1.840E-03	22.917	1.830E-03	5.167	4.100E-04
28.167	1.860E-03	23.583	1.860E-03	6.229	4.170E-04
31.208	1.900E-03	24.625	1.840E-03	7.250	4.220E-04
33.250	1.930E-03	25.875	1.870E-03	8.250	4.220E-04
35.083	1.920E-03	26.708	1.920E-03	10.208	4.250E-04
41.167	1.920E-03	29.667	1.910E-03	12.278	4.270E-04
43.208	1.950E-03	31.708	1.910E-03	13.958	4.220E-04
45.167	1.950E-03	33.708	1.880E-03	19.938	4.250E-04
47.125	1.990E-03	36.750	1.920E-03	22.208	4.220E-04
52.167	2.020E-03	38.875	1.900E-03	25.063	4.210E-04
		40.708	1.940E-03	30.000	4.460E-04
		46.792	1.960E-03	32.111	4.340E-04

	48.833	1.960E-03	36.167	4.480E-04
	50.792	1.930E-03		
	52.750	1.950E-03		
	57.792	1.970E-03		

HFO Time (d)	Mole Pb Sorbed/g HFO	HMO Time (d)	Mole Pb Sorbed/g HMO
0.000	0.000E+00	0.000	0.000E+00
0.010	7.824E-04	0.007	2.624E-03
0.021	7.926E-04	0.014	2.625E-03
0.031	8.067E-04	0.017	2.630E-03
0.042	8.181E-04	0.023	2.625E-03
0.083	8.260E-04	0.028	2.634E-03
0.125	8.323E-04	0.035	2.635E-03
0.167	8.465E-04	0.042	2.641E-03
0.208	8.385E-04	0.063	2.651E-03
0.257	8.536E-04	0.083	2.667E-03
0.292	8.626E-04	0.104	2.669E-03
0.344	8.770E-04	0.125	2.660E-03
0.375	8.853E-04	0.146	2.651E-03
0.427	8.946E-04	0.167	2.653E-03
0.458	8.911E-04	0.208	2.649E-03
0.802	9.080E-04	0.250	2.668E-03
1.000	9.161E-04	0.292	2.681E-03
1.188	9.145E-04	0.333	2.659E-03
1.333	9.213E-04	0.375	2.678E-03
1.875	9.321E-04	0.417	2.668E-03
2.125	9.509E-04	0.458	2.654E-03
2.344	9.621E-04	0.500	2.687E-03
2.885	9.693E-04	0.604	2.708E-03
3.052	9.758E-04	1.125	2.695E-03
3.268	9.757E-04	1.250	2.709E-03
3.396	9.831E-04	1.375	2.698E-03
3.896	9.774E-04	1.563	2.728E-03
4.122	9.794E-04	1.750	2.713E-03
4.344	9.822E-04	2.125	2.753E-03
4.962	9.900E-04	2.250	2.767E-03
5.333	9.925E-04	2.382	2.765E-03
6.031	9.997E-04	2.503	2.753E-03
6.066	1.033E-03	2.646	2.783E-03
6.146	1.033E-03	3.125	2.787E-03
6.302	1.032E-03	3.271	2.785E-03
8.896	1.029E-03	3.986	2.785E-03
9.271	1.039E-03	4.188	2.797E-03
9.896	1.033E-03	4.583	2.803E-03

10.260	1.042E-03	5.292	2.834E-03
11.083	1.046E-03	5.542	2.836E-03
12.049	1.051E-03	8.146	2.817E-03
13.000	1.048E-03	9.132	2.852E-03
14.045	1.055E-03	9.604	2.851E-03
15.066	1.069E-03	10.354	2.829E-03
16.000	1.083E-03	11.292	2.844E-03
17.167	1.088E-03	12.274	2.873E-03
18.097	1.086E-03	13.292	2.859E-03
19.090	1.094E-03	14.313	2.851E-03
20.000	1.095E-03	15.375	2.844E-03
20.976	1.099E-03	16.375	2.850E-03
22.219	1.091E-03	17.333	2.857E-03
23.156	1.104E-03	18.333	2.854E-03
24.188	1.100E-03	19.236	2.868E-03
24.983	1.096E-03	20.216	2.880E-03
26.224	1.099E-03	21.458	2.874E-03
27.063	1.101E-03	22.403	2.852E-03
28.042	1.108E-03	23.472	2.911E-03
29.938	1.096E-03	24.333	2.879E-03
33.302	1.119E-03	25.397	2.863E-03
37.229	1.113E-03	26.299	2.890E-03
42.054	1.113E-03	27.431	2.879E-03
48.979	1.117E-03	28.403	2.897E-03
53.250	1.108E-03	33.583	2.884E-03
62.333	1.104E-03	38.521	2.890E-03
73.075	1.111E-03	43.625	2.908E-03
106.879	1.103E-03	54.319	2.883E-03
123.067	1.108E-03	72.590	2.901E-03
134.846	1.143E-03	86.382	2.877E-03
148.021	1.153E-03	107.257	2.908E-03
		120.372	2.908E-03

APPENDIX I

GROUNDWATER FLOW SIMULATION STEPS WITH GMS

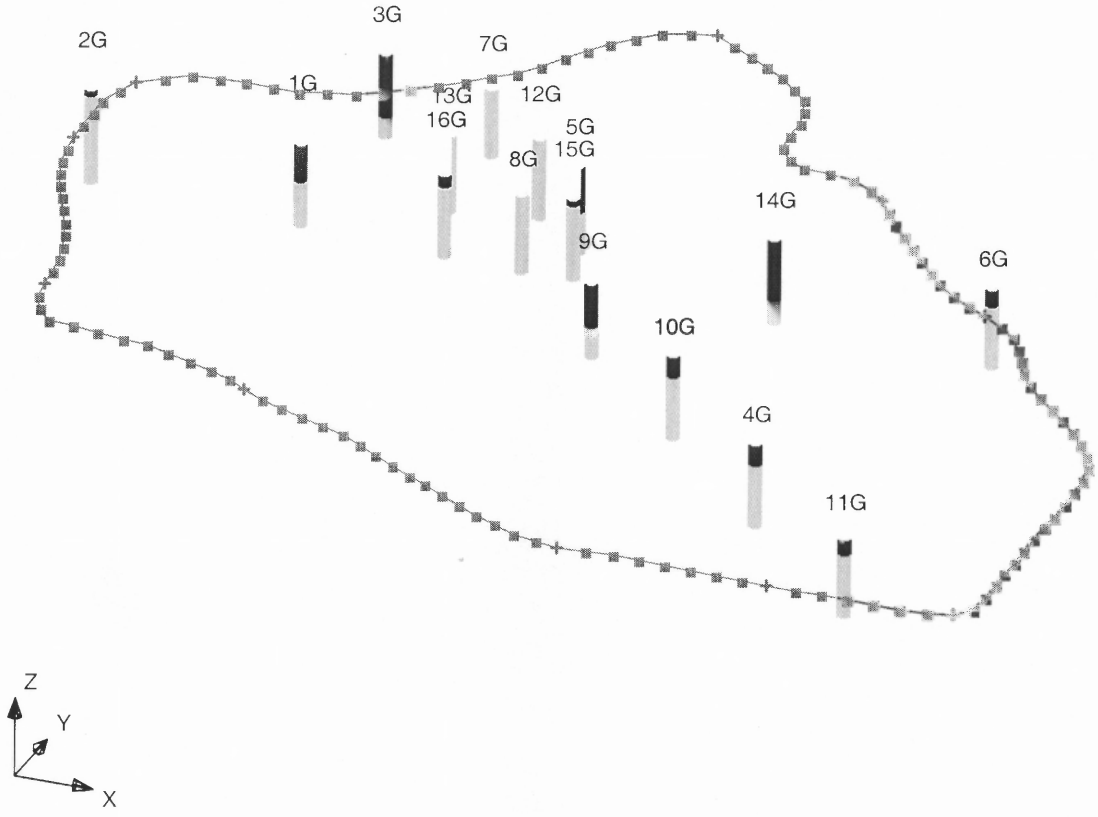

Figure I-1 Borehole model of the Hanford Site

Table I-1 Borehole Elevation Data (adapted from Vermeul *et al.* (2003)) (Unit: m)

Borehole Number	Hanford Formation	Ringold Formation	Basalt Formation
1G	190	100	25
2G	190	125	110
3G	150	100	-20
4G	130	100	60
5G	160	110	20
6G	125	95	60
7G	175	115	-20
8G	135	90	-60
9G	140	85	0
10G	130	100	60
11G	135	90	60
12G	160	100	-60
13G	140	90	-60
14G	150	100	-15
15G	170	100	85
16G	180	100	75

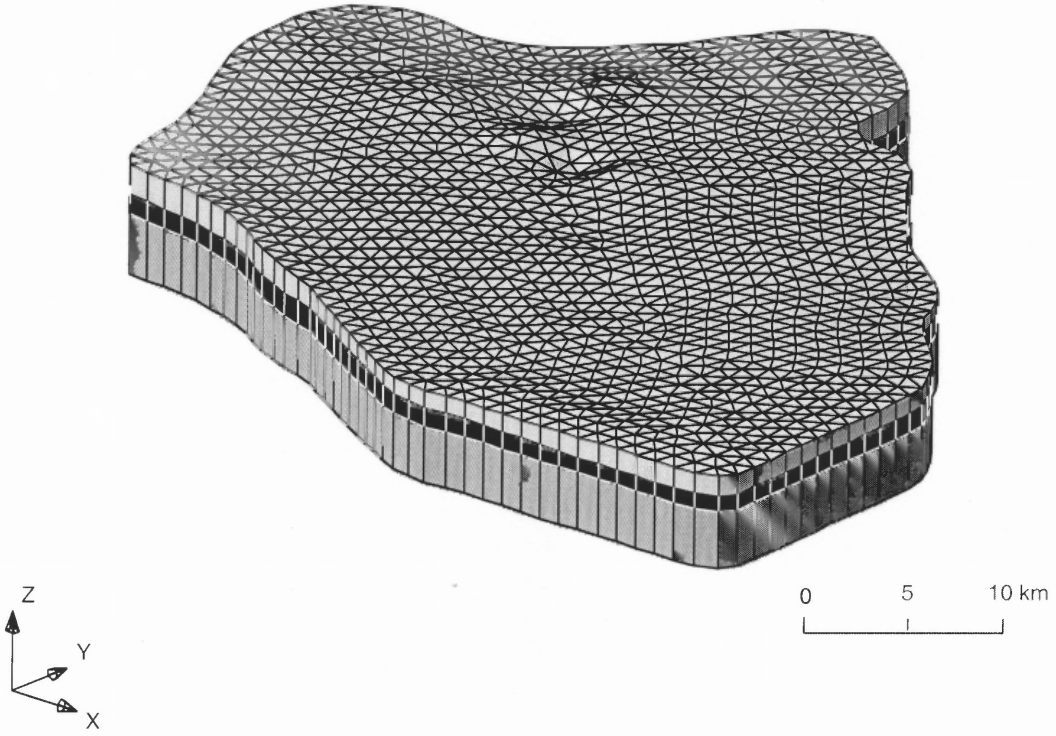

Figure I-2 Aquifer model of the Hanford Site (light grey: the Hanford Formation, black: the Ringold Formation, and dark grey: the Basalt Formation), where the Ringold Formation is the primary aquifer.

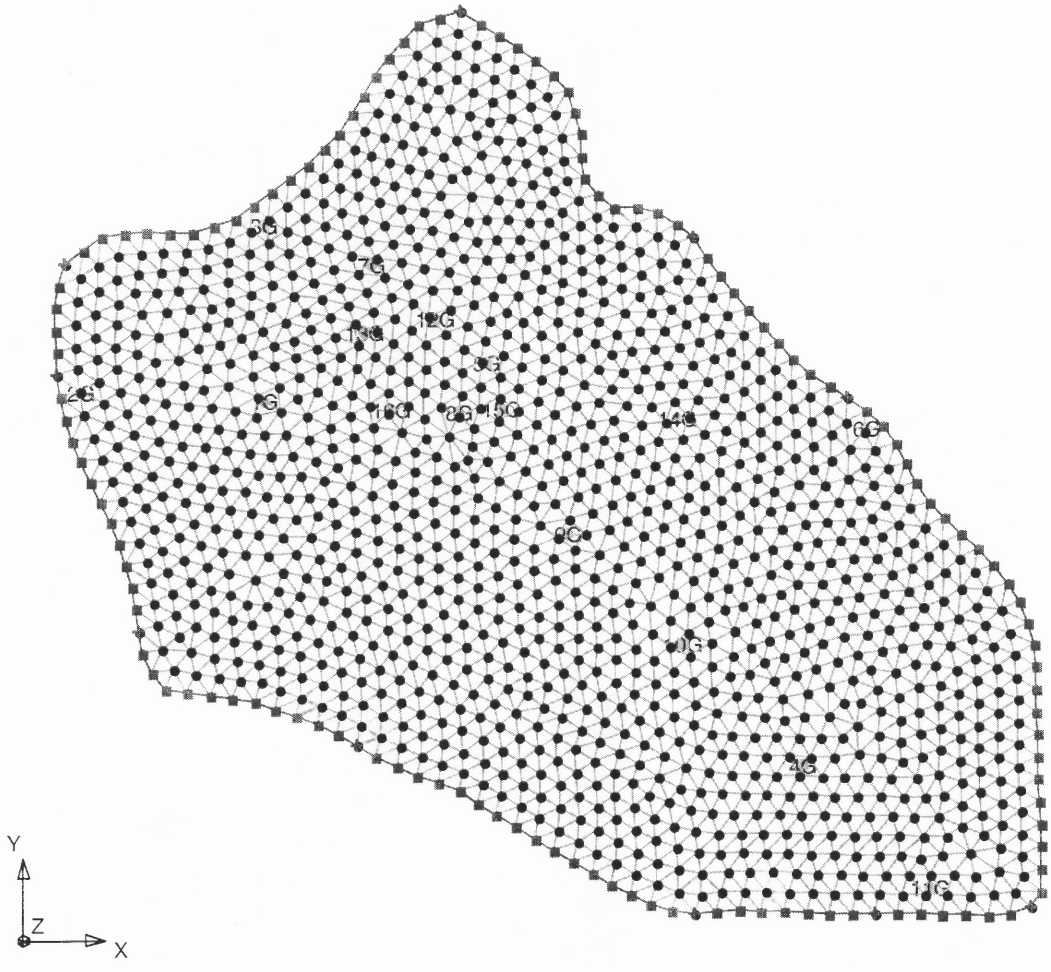

Figure I-3 TINs of the Hanford Site

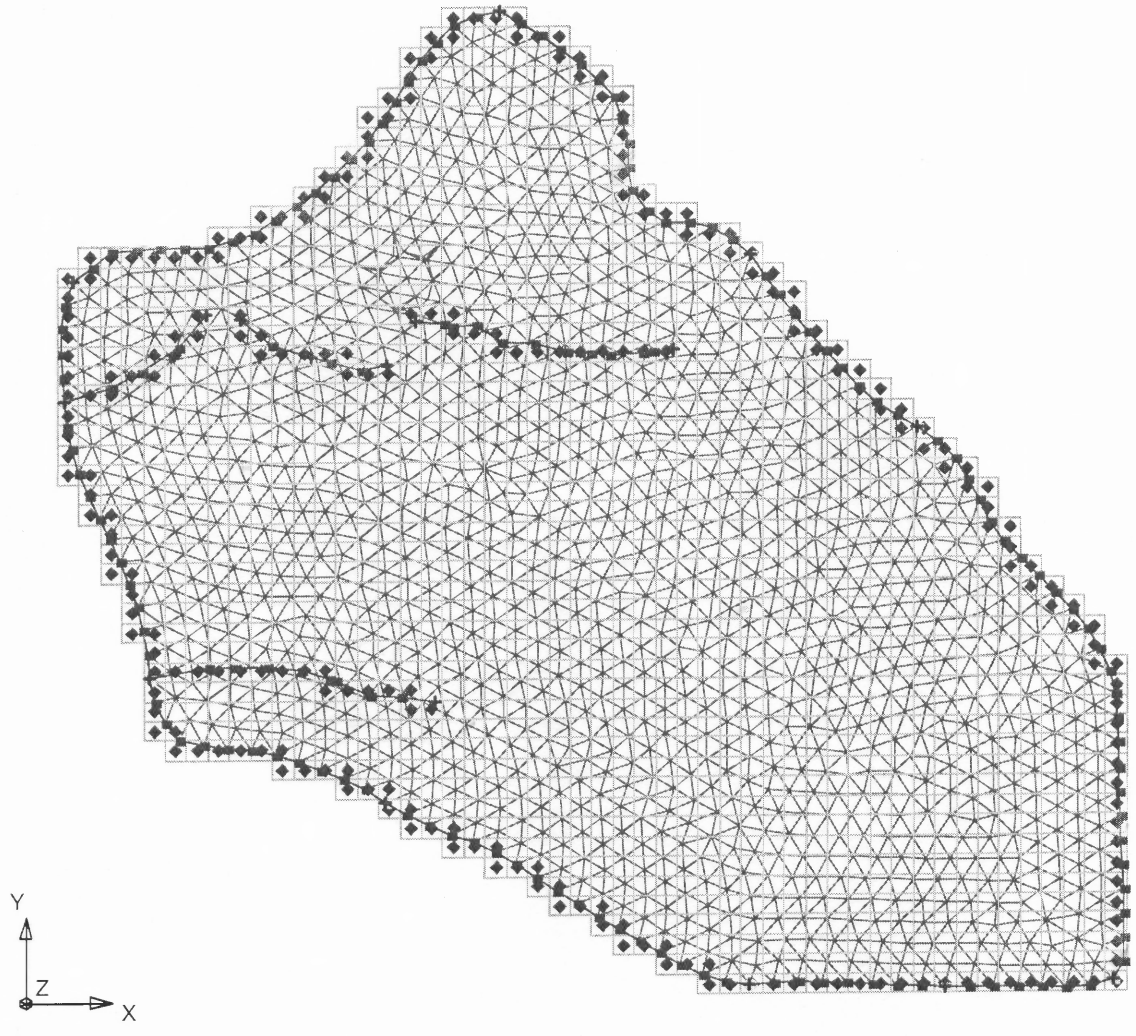

Figure I-4 Grid model of the Hanford Site

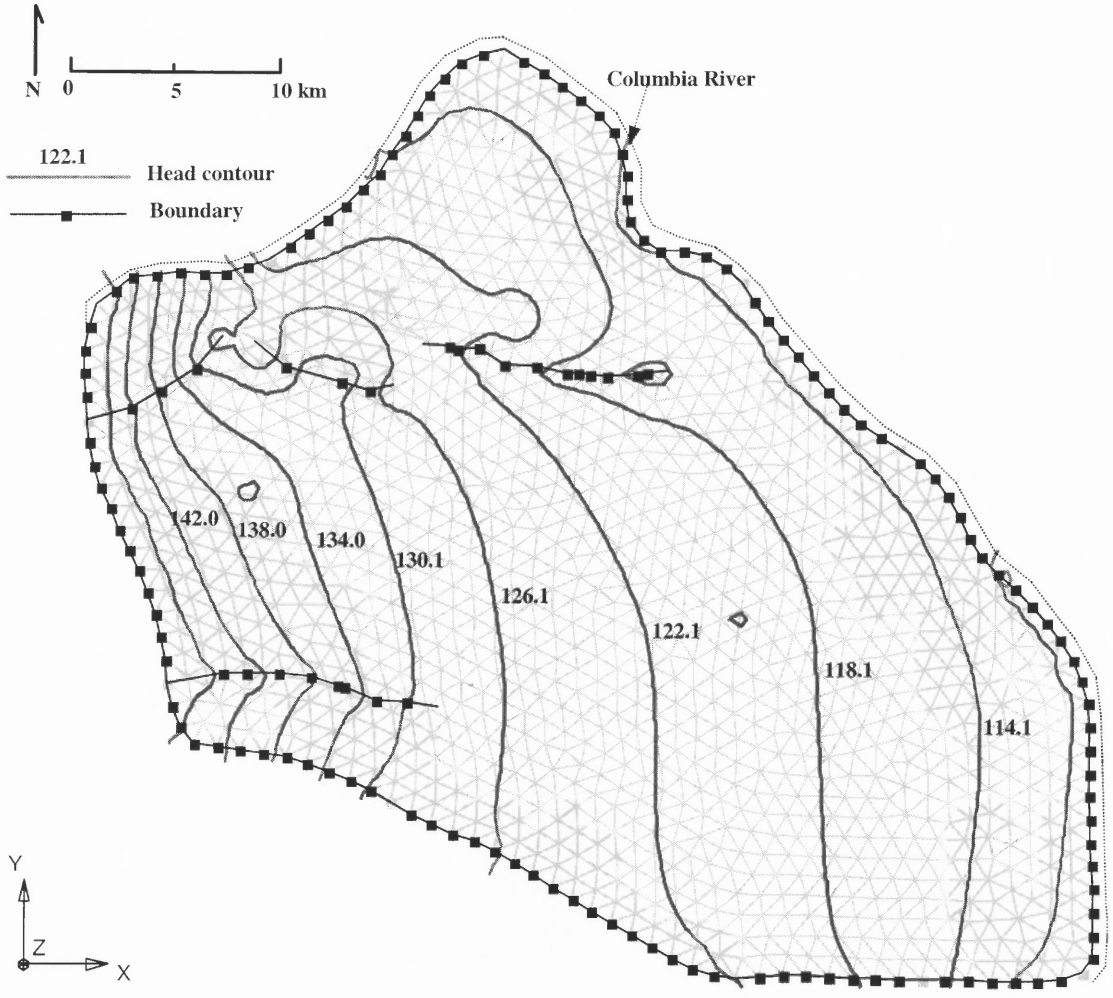

Figure I-5 Groundwater head profile of the Hanford Site (Unit: m)

REFERENCES

Abbott, M.B., 1966. An Introduction to the Method of Characteristics. American Elsevier, New York.

Absallom, J.P., Young, S.D., Crout, N.M.J., Nisbet, A.F., Woodman, R.F.M., Smolders, E., Gillett, A.G., 1999. Predicting soil to plant transfer of radiocesium using soil characteristics. Environ. Sci. Technol. 33, 1218-1223.

Agency for Toxic Substances and Disease Registry (ATSDR), 1990. U.S. Public Health Service , Toxicologic profile for uranium.

Aharoni, C., Sparks, D.L., 1991. Kinetics of soil chemical reactions - a theoretical treatment, rates of soil chemical processes, Soil Science Society of America Special Publication no. 27, Madison, WI.

Allison, J.D., Brown, D.S., Novo-Gradac, K.J., 1991. MINTEQA2/PRODEFA2, a geochemical assessment model for environmental systems: version 3.0 user's manual.

Altin, O., Ozbelge, H.O., Dogu, T., 1998. Use of general purpose adsorption isotherms for heavy metal-clay mineral interactions. J. Colloid Interface Sci. 198, 130-140.

Anderson, P.R., Benjamin, M.M., 1990. Surface and bulk characteristics of binary oxide suspensions. Enviorn. Sci. Technol. 24 (5), 692-698.

Anderson, M.P., Hunt, R.J., Krohelski, J.T., Hung, K., 2002. Using high hydraulic conductivity nodes to simulate seepage lakes. Ground Water 40 (2), 117-122.

Army Environmental Policy Institute (AEPI), 1995. Health and environmental consequences of depleted uranium use in the U.S. Army. Technical Report.

Avena, M.J., De Pauli, C.P., 1998. Proton adsorption and electrokinetics of an Argentinean montmorillonite. J. Colloid Interface Sci. 202, 195.

Axe, L., Anderson, P.R., 1995. Sr diffusion and reaction within Fe oxides: evaluation of the rate-limiting mechanism for sorption. J. Colloid Interface Sci. 175 (1), 157-65.

Axe, L., Anderson, P.R., 1997. Experimental and theoretical diffusivities of Cd and Sr in hydrous ferric oxide. J. Colloid Interface Sci. 185 (2), 436-448.

Axe, L., Anderson, P.R., 1998. Intraparticle diffusion of metal contaminants in amorphous oxide minerals. In: Jenne, E.A. (Ed.), Adsorption of Metals by Geomedia. Academic Press, San Diego, CA, pp. 193-208.

Axe, L., Bunker, G., Anderson, P.R., Tyson, T.A., 1998. An XAFS analysis of strontium at the hydrous ferric oxide surface. J. Colloid Interface Sci. 199, 44-52.

Axe, L., Trivedi, P., 2002. Intraparticle surface diffusion of metal contaminants and their attenuation in microporous amorphous Al, Fe, and Mn oxides. J. Colloid Interface Sci. 247, 259-265.

Axe, L., Tyson, T.A., Trivedi, P., Morrison, T., 2000. Local structural analysis of strontium sorption to hydrous manganese oxide J. Colloid Interface Sci. 224, 408-416.

Baca, R.G., Arnett, R.C., King, I.P., 1981. Numerical modeling of flow and transport in a fractured-porous rock system, Oper. Rep. RHO-BWI-SA-113, Rockwell Hanford Nucl. Facil., Hanford, WA.

Bacci, E., Calamari, D., Gaggi, C., Vighi, M., 1990. Bioconcentration of organic chemical vapors in plant leaves: experimental measurements and correlation. Environ. Sci. Technol. 24, 885-889.

Baes, C.F., Mesmer, R.E., 1986. The Hydrolysis of Cations. John Wiley and Sons, NY.

Ball, J.W., Nordstrom, D.K., 1991. WATEQ4F—User's manual with revised thermodynamic data base and test cases for calculating speciation of major, trace and redox elements in natural waters: U.S. Geological Survey Open-File Report.

Barnett, M.O., Jardine, P.M., Brooks, S.C., 2002. U(VI) adsorption to heterogeneous subsurface media: application of a surface complexation model. Environ. Sci. Technol. 36, 937-942.

Barrow, N.J., Gerth, J., Brummer, G.W., 1989. Reaction kinetics of adsorption and desorption of nickel, zinc, and cadmium on goethite. II. Modeling extent and rate of reaction. J. Soil Sci. 40, 437-450.

Barry, D.A., Miller, C.T., Culligan, P.J., Bajracharya, K., 1997. Analysis of split operator methods for nonlinear and multispecies groundwater chemical transport models. Mathematics and Computers in Simulation 43, 331-341.

Bassett, R.L., Melchior, D.C., 1990. Chemical modeling of aqueous systems. An overview. In Chemical Modeling of Aqueous Systems II., Vol. ACS Symposium Series No. 416, 1-14. American Chemical Society.

Baverman, C., Strömbert, B., Moreno, L., Neretnieks, I., 1999. CHEMFRONTS: a coupled geochemical and transport simulation tool. J. Contam. Hydrol. 36, 333-351.

Baeyens, B., Bradbury, M.H., 1997. A mechanistic description of Ni and Zn sorption on Na-montmorillonite, Part I: Titration and sorption measurements. J.Contam. Hydrol. 27, 199-222.

Benjamin, M.M., 2001. Water Chemistry. McGraw-Hill, Inc., New York.

Benjamin, M.M., Leckie, J.O., 1981. Multiple-site adsorption of Cd, Cu, Zn, and Pb on amorphous iron oxyhydroxide. J. Colloid Interface Sci. 79, 209-221.

Bertell, R., 1999. Gulf War veterans and depleted uranium. In: Depleted Uranium: A Post-war Disaster for Environment and Health. http://www.antenna.nl/wise/uranium/dhap99f.html

Bethke, C.M., 1996. Geochemical Reaction Modeling: Concepts and Applications. Oxford University Press, Inc., New York.

Bethke, C., 1997. Modeling transport in reacting geochemical systems. C. R. Acad. Sci. 324, 513-528. Bird, R.B., Stewart, W.E., Lightfoot, E.N., 2002. Transport Phenomena. John Wiley & Sons, New York.

Bleise, A., Danesi, P.R., Burkart, W., 2003. Properties, use and health effects of depleted uranium (DU): a general overview. J. Environ. Radioact. 64 (2-3), 93-112.

Blume, H.P., Schwertmann, U., 1969. Genetic evaluation of profile distribution of aluminium, iron and manganese oxides. Soil Sci. Soc. Am. Proc. 33, 438.

Bowen, R., 1986. Groundwater. Elsevier Applied Science Publishers, New York.

Brewer, P.G., 1975. Minor elements in seawater. In: Riley, J.P., Skirrow, G. (Eds.), Chemical Oceanography. Academic Press, London, 1, 415.

Briggs, G.G., Bromilow, R.H., Evans, A.A., Williams, M., 1983. Relationships between lipophilicity and the distribution of non-ionised chemicals in barley shoots following uptake by the roots. Pestc. Sci. 14, 492-500.

Brown, J.G., Bassett, R.L., Glynn, P.D., 2000. Reactive transport of metal contaminants in alluvium-model comparison and column simulation. Applied Geochemistry 15, 35-49.

Bruno, J., De Pablo, J., Duro, L., Figuerola, E., 1995. Experimental study and modeling of the U(VI)-Fe(OH)3 surface precipitation/coprecipitation equilibria. Geochim. Cosmochim. Acta 59 (20), 4113-4123.

Butler, J.N., Cogley, D.R., 1998. Ionic Equilibrium: Solubility and pH Calculations. John Wiley & Sons, Inc., New York.

BYU (Brigham Young University), 2002. The Department of Defense Groundwater Modeling System, GMS v4.0 Tutorials. Brigham Young University-Environmental Modeling Research Laboratory.

Carbonell, G., Ramos, C., Pablos, M.V. Ortiz, J.A., Tarazona J.V., 2000. A system dynamic model for the assessment of different exposure routes in aquatic ecosystems, The Science of The Total Environment 247 (2-3), 107-118.

Carbone, J.P., Havens, P.L., Warren-Hicks, W., 2002. Validation of pesticide root zone model 3.12: employing uncertainty analysis. Environ. Toxicol. Chem. 21 (8), 1573-1590.

Celis, R., Cox, L., Hermosin, M.C., Cornejo, J., 1997. Sorption of thiazafluron by iron- and humic acid-coated montmorillonite. J. Environ. Qual., 26, 472-479.

Chang, F-R.C., Sposito, G., 1996. The electrical double layer of a disk-shaped clay mineral particle: Effects of electrolyte properties and surface charge density. J. Colloid Interface Sci. 178, 555-564.

Cheng, J.J., 1998. RESRAD-ECORISK: A Computer Code for Ecological Risk Assessment Beta Version 1.01, Argonne National Laboratory Environmental Assessment Division, Control No. 1452 Argonne, IL.

Cheng, H.P., Yeh, G.T., 1998. Development and demonstrative application of a 3-D numerical model of subsurface flow, heat transfer, and reactive chemical transport: 3DHYDROGEOCHEM. J. Contam. Hydrol. 34, 47-83.

Chilakapati, A., Yabusaki, S., Szecsody, J., MacEvoy, W., 2000. Groundwater flow, multicomponent transport and biogeochemistry: development and application of a coupled process model. J. Contam. Hydrol. 43, 303-325.

Christl, I., Kretzschmar, R., 1999. Competitive sorption of copper and lead at the oxide-water interface, implications for surface site density. Geochim. Cosmochim. Acta 63 (19/20), 2929-2938.

Chu, X., Basagaoglu, H., Marino, M.A., Volker, R.E., 2000. Aldicarb transport in subsurface environment: comparison of models. J Environ. Eng. 126 (2), 121-129.

Clement, T.P., 2003. RT3D (version 2.5): a modular computer code for simulating reactive multispecies transport in 3-dimensional groundwater systems. Report PNNL-11720 under contract DE-AC06-76RLO 1830, updated document. Pacific Northwest National laboratory, Richland, WA.

Clement, T.P., Jones, N.L., 2000. RT3D Tutorials for GMS 3.1 user (Draft Version).

Clement, T. P., Johnson, C.D., Sun, Y., Klecka, G.M., Bartlett, C., 2000. Natural attenuation of chlorinated ethane compounds: model development and field-scale application at the Dover site. J. Contam. Hydrol. 42, 113-140.

Cockerham, L.G., Shane, B.S., 1994. Basic Environmental Toxicology. CRC Press, Inc., Boca Raton, Florida.

Cole, C.R., Thorne, P.D., Bergeron, M.P., Wurstner, S.K., Murray, C.J., Rogers, P.M., 2001. Uncertainty Analysis Framework-Hanford Site-Wide Groundwater Flow and Transport Model, PNNL-13641, Pacific Northwest National Laboratory, Richland, Washington.

Coughlin, B.R., Stone, A.T., 1995. Nonreversible adsorption of divalent metal ions (Mn^{II}, Co^{II}, Ni^{II}, Cu^{II}, and Pb^{II}) onto goethite. Effects of acidification, Fe^{II} addition, and picolinic acid addition. Environ. Sci. Technol. 29 (9), 2445-2455.

Crank, J., 1975. The Mathematics of Diffusion. Oxford University Press Inc., New York.

Crawford, M.B., 1996. PHREEQEV: the incorporation of a version of model V for organic complexation in aqueous solutions into the speciation code PHREEQE. Computers & Geoscience 22 (2), 109-116.

Cross, J., Haworth, A., Neretnieks, I., 1991. Modeling of redox front and uranium movement in a uranium mine at Poços de Caldas. Radiochim. Acta 52/53, 445-451.

Cullen, A.C., Frey, H.C., 1999. Probabilistic Techniques in Exposure Assessment: A Handbook for Dealing with Variability and Uncertainty in Models and Inputs. Plenum Press, New York.

Davis, P.A., Olague, N.E., Goodrich, M.T., 1991. Approaches for the validation for models used for performance assessment of high-level nuclear waste repositories. SAND90-0575/NUREG CR5537, Sandia National Laboratories, Albuquerque, NM.

Decisioneering, 2002. Crystal Ball2000: Risk Analysis: an Overview. http://www.decisioneering.com/risk-analysis-start.html

Dong, D., Nelson, Y.M., Lion, L.W., Shuler, M.L., Ghiorse, W.C., 2000. Adsorption of Pb and Cd onto metal oxides and organic material in natural surface coatings as determined by selective extractions: new evidence for the importance of Mn and Fe oxides. Wat. Res. 34 (2), 427-436.

Dong, D., Hua, X., Li, Y., Zhang, J., Yan, D., 2003. Cd adsorption properties of components in different freshwater surface coatings: the important role of ferromanganese oxides. Environ. Sci. Technol. 37, 4106-4112.

Donnelly, C.A., Tenbus, F.J., 1998. Temporal and Vertical Variation of Hydraulic Head in Aquifers in the Edgewood Area, Aberdeen Proving Ground, Maryland. Water Resources Investigations Report 98-4047.

Draw, E.B., Lehmann, F., Ackerer, P., 2001. One dimensional simulation of solute transfer in saturated-unsaturated porous media using the discontinuous finite element method. J. Contam. Hydrol. 51, 197-213.

Duffy, S., Schaffner, D.W., 2002. Monte Carlo simulation of the risk of contamination of apples with Escherichia coli O157:H7. Int. J. Food Microbiol. 78, 245-255.

Duvall, S.E., Barron, M.G., 2000. A screening level probabilistic risk assessment of mercury in Florida everglades food webs. Ecotoxicol. Environ. Saf. 47 (3), 298-305.

D.A. Dzombak, F.M.M. Morel, 1986. Sorption of cadmium on hydrous ferric oxide at high sorbate/sorbent ratios: equilibrium, kinetics and modeling. J. Colloid Interface Sci. 112, 588-598.

Dzombak, D.A., Morel, F.M.M., 1990. Surface Complexation Modeling Hydrous Ferric Oxide. John Wiley & Sons, New York.

Ebinger, M.H., 2002. Personal communication.

Ebinger, M.H., Kennedy, P.L., Myers, O.B., Clements, W., Bestgen, H.T., Beckman, R.J., 1996. Long-term fate of depleted uranium at Aberdeen and Yuma Proving Grounds, Phase II: Human health and ecological risk assessments. Los Alamos National Laboratory Report LA-13156-MS.

Edwards, M., Benjamin, M.M., 1989. Adsorptive filtration using coated sand: A new approach for treatment of metal-bearing wastes. J. Water Pollution Control Fedn. 61, 1523-1533.

Efroymson, R.A., Will, M.E., Suter II, G.W., Wooten, A.C., 1997. Toxicological benchmarks for screening contaminants of potential concern for effects on terrestrial plants: 1997 revision. Reporting Code EW 20, Lockheed Martin Energy Systems, INC.

Engesgaard, P., Kipp, K.L., 1992. A geochemical transport model for redox-controlled movement of mineral fronts in groundwater flow systems: a case of nitrate removal by oxidation of pyrite. Water Resour. Res. 28 (10), 2829-2844.

Engle, R., Normand M., Horowitz, J., Peleg, M., 2001. A model of microbial contamination of a water reservoir. Bull. Math. Biol. 63, 1005-1023.

Entech Engineers, Inc., 1988. Geohydrologic Study of the Yuma Proving Ground with Particular Reference to the Open Burning/Open Detonation Facility. Yuma: U.S. Army Yuma Proving Ground.

Environmental Modeling Systems (EMS), 2002. http://www.ems-i.com/gms.htm.

Environmental Modeling Systems and Waterloo Hydrogeological, 2002. Personal communication.

Environmental Simulations, Inc. (ESI)., 2002. http://www.esinternational.com.

Environmental Simulations, Inc. (ESI)., 2001. Groundwater Vistas Introductory Tutorial.

Fadali, O.A., 2003. Effect of gas strirring on external mass transfer, intraparticle diffusion and energy consumption during adsorption. Adsorption Science and Technology 21, 935-950.

Farago, E.M. 1994. Plants and the Chemical Elements: Biochemistry, Uptake, Tolerance and Toxicity. VCH Publishers, New York.

Fendorf, S.E. Sparks, D.L., 1994. Mechanisms of chromium (III) sorption on silica: 2. Effect of reaction conditions. Environ. Sci. Technol. 26, 79-85.

Finley, B.L., Scott, P.K., Mayhall, D.A., 1994. Development of a standard soil-to-skin adherence probability density function for use in Monte Carlo analyses of dermal exposure. Risk Anal. 14 (4), 555-569.

Fogler, H.S., 1992. Elements of Chemical Reaction Engineering. Prentice Hall, NJ.

Ford, R.G., Scheinost, A.C., Scheckel, K. G., Sparks, D.L., 1999. The link between clay mineral weathering and the stabilization of nickel surface precipitates. Environ. Sci. Technol. 33 (18), 3140-3144.

Freeze, R.A., Cherry, J.A., 1979. Groundwater. Prentice-Hall, Englewood Cliffs, New Jersey.

Frey, H.C., Burnaster, D.E., 1999. Methods for characterizing variability and uncertainty: comparison of bootstrap simulation and likelihood-based approaches. Risk Anal. 19 (1), 109-129.

Frey, H.C, Rhodes, S.D., 1998. Characterization and simulation of uncertainty frequency distributions: Effects of distribution choice, variability, uncertainty, and parameter dependence. Hum. Ecol. Risk Assess. 4 (2), 423-468.

Frind, E. O., Trudeau, P.J., 1980. Finite-element analysis of salt transport (SALTRP), User's Manual Gt-034, Geotech. Div., Stone and Webster Eng., Inc., Boston, MA.

Froment, G.F., Bischoff, K.B., 1990. Chemical Reactor Analysis and Design. Wiley, New York.

Fulco, C.E., Liverman, C.T., Sox, H.C., 2000. Gulf War and Health, Volume 1: Depleted Uranium, Pyridostigmine Bromide, Sarin, Vaccines. National Academy Press, Washington, D.C.

Fuller, C.C., Davis, J.A., Waychunas, G.A., 1993. Surface chemistry of ferrihydrite: Part 2. Kinetics of arsenate adsorption and coprecipitation. Geochim. Cosmochim. Acta 57 (10): 2271-2282.

Gadde, R.R., Laitinen, H.A., 1974. Studies of heavy metal adsorption by hydrous iron and manganese oxides. Anal. Chem. 46, 2022-2026.

Gallo, Y.L., Bildstein, O., Brosse, E., 1998. Coupled reaction-flow modeling of diagenetic changes in reservoir permeability, porosity and mineral compositions. J. Hydrol. 209, 366-388.

Ganguly, C., Matsumoto, M.R., Rabideau, A.J., Van Benschoten, J.E., 1998. Metal ion leaching from contaminated soils: model calibration and application. J. Environ. Eng. 124 (12), 1150-1158.

Ganns, P.F.M., 1998. The role of modeling in geochemical engineering - a (re)view. Journal of Geochemical Exploration 62, 41-55.

Ganor, J., Mogollon, J.L., Lasaga, A.C., 1999. Kinetics of gibbsite dissolution under low ionic strength conditions. Geochim. Cosmochim. Acta 63, 1635-1651.

Garrels, R.M., Thompson, M.E., 1962. A chemical model for sea water at 25°C and one atmosphere total pressure. American Journal of Science 260, 57-66.

Gavaskar, A., Gupta, N., Sass, B., 1997. Design guidance for application of permeable barriers to remediate dissolved chlorinated sovlents. (Appendix C: Supporting information for geochemical modeling). http://www.usace.army.mil/inet/usace-docs/design-guides/dg1110-345-117/cover.pdf

GeoTrans, 1982. FTRANS-A two-dimensional code for simulating fluid flow and transport of radioactive nuclides in fractured rock for repository performance assessment. Rep. ONWI/E512-02900/CD-17, Battelle Mem. Inst., Columbus, OH.

Gemeay, A.H., El-Sherbiny, A.S., Zaki, A.B., 2002. Adsorption and kinetic studies of the intercalation of some organic compounds onto Na^+-montmorillonite. J. Colloid Interface Sci. 245, 116-125.

Gerard, F., Clément, A., Fritz, B., 1998. Numerical validation of a Eulerian hydrochemical code using a 1D multisolute mass transport system involving heterogeneous kinetically controlled reactions. J. Contam. Hydrol. 30, 201-216.

Greenland, S., 2001. Sensitivity analysis, Monte Carlo risk analysis, and Bayesian uncertainty assessment. Risk Anal. 21 (4), 579-583.

Green-Pederson, H., Pind, N., 2000. Preparation, characterization, and sorption properties for Ni(II) of iron oxyhydroxide-montmorillonite. Colloids and Surfaces A: Physicochem. Eng. Aspects 168, 133-145.

Grove, D.B., 1977. The use of Galerkin finite element methods to solve mass transport equations, U.S. Geological Survey. Water Resour. Invest. 77, 49, 55.

Gupta, S.K., Kincaid, C.T., Meyer, C.A., 1982. A multidimensional finite element code for the analysis of coupled fluid, energy, and solute transport (CFEST), Rep. PNL-4260, Pac. Northwest Lab., Richland, WA.

Guiguer, N., Franz, T., 2002. Demonstration instructions for Visual MODFLOW. Waterloo Hydrological Software, Inc.

Gustafsson, J.P., 2001. Visual MINTEQA version 2.01. Royal Institute of Techmology, Sweden. http://www.lwr.kth.se/english/OurSoftware/vminteq/index.htm.

Harbaugh, A.W., Banta, E.R., Hill, M.C., McDonald, M.G., 2000. MODFLOW-2000, the U.S. Geological Survey modular ground-water model -- User guide to modularization concepts and the Ground-Water Flow Process: U.S. Geological Survey Open-File Report 00-92.

Harbaugh, A.W., McDonald, M.G., 1996. User's documentation for MODFLOW-96, an update to the U.S. Geological Survey modular finite-difference ground-water flow model: U.S. Geological Survey Open-File Report 96-485.

Hartman, M.J., Morasch, L.F., Webber, W.D., 2002. Hanford Site Groundwater Monitoring for Fiscal Year 2001, PNNL-13788. Pacific Northwest National Laboratory, Richland, Washington.

Hartman, M.J., Morasch, L.F., Webber, W.D., 2003. Summary of Hanford Site Groundwater Monitoring for Fiscal Year 2002, PNNL-14187-SUM. Pacific Northwest National Laboratory, Richland, Washington.

Hartman, M.J., Morasch, L.F., Webber, W.D., 2003. Hanford Site Groundwater Monitoring for Fiscal Year 2002, PNNL-14187. Pacific Northwest National Laboratory, Richland, Washington.

Hartman, M.J., Morasch, L.F., Webber, W.D., 2004. Hanford Site Groundwater Monitoring for Fiscal Year 2003, PNNL-14548. Pacific Northwest National Laboratory, Richland, Washington.

Hartmann, H.M., Monette, F.A., Avci, H.I., 2000. Overview of toxicity data and risk assessment methods for evaluating the chemical effects of depleted uranium compounds. Hum. Ecol. Risk Assess. 6 (5), 851-874.

Harvie, C.E., Møller, N., Weare, J.H., 1984. The prediction of mineral solubilities in natural waters: the Na-K-Mg-Ca-H-Cl-SO4-OH-HCO3-CO3-CO2-H2O system to high ionic strengths at 25°C. Geochim. Cosmochim. Acta 48, 723-751.

Hattis, D., Russ, A., Goble, R., Banati, P., Chu, M., 2001. Human interindividual variability in susceptibility to airborne particles. Risk Anal. 21 (4), 585-599.

Helmy, A.K., Ferreiro, E.A., De Bussetti, S.G., 1994. Cation exchange capacity and condition of zero charge of hydroxy-Al montmorillonite. Clays and Clay Mineral, 43, 444-450

Herbert, B., 2001. Application of geochemical speciation models for groundwater chemistry modeling and evaluation of remediation technologies. http://lava.tamu.edu/courses/geol641/notes/pdfdocs/SpeciationModelingReview.pdf

Hertwich, E,G., McKone, T.E., Pease, W.S., 1999. Parameter uncertainty and variability in evaluative fate and exposure models. Risk Anal. 19 (6), 1193-1204.

Hiemstra, T., De Wit, J.C.M., Van Riemsdijk, W.H., 1989. Multisite proton adsorption modeling at the solid/solution interface of (hydr)oxides: A new approach. II. Application to various important (hydr)oxides. J. Colloid Interface Sci. 133, 105-117.

Hill, M.C., 1992. A computer program (MODFLOWP) for estimating parameters of a transient, three-dimensional, ground-water flow model using nonlinear regression: U.S. Geological Survey Open-File Report 91-484.

Hill, M.C., 1998. Methods and guidelines for effective model calibration: U.S. Geological Survey Water-Resources Investigations Report 98-4005.

Hill, M.C., Banta, E.R., Harbaugh, A.W., Anderman, E.R., 2000. MODFLOW-2000, the U.S. Geological Survey modular ground-water model -- User guide to the Observation, Sensitivity, and Parameter-Estimation Processes and three post-processing programs: U.S. Geological Survey Open-File Report 00-184.

Holmen, B.A. Gschwend, P.M., 1997. Estimating sorption rates of hydrophobic organic compounds in iron oxide- and aluminosilicate clay-coated aquifer sands. Environ. Sci. Technol. 31, 105-113.

Hope, B.K., 1995. A review of models for estimating terrestrial ecological receptor exposure to chemical contaminants. Chemosphere 30 (12), 267-2287.

Hope, B.K., 1999. Assessment of risk to terrestrial receptors using uncertainty analysis-a case study. Hum.Ecol.Risk Assess. 5(1), 5-170.

Hope, B.K., 2000. Generating probabilistic spatially-explicit individual and population exposure estimates for ecological risk asssessment. Risk Anal. 20 (5), 573-589.

Hubbert, M.K., 1940. The theory of groundwater motion. Journal of Geology 48 (8), 785-944.

Hunter, K.S., Wang, Y., Cappellen, P.V., 1998. Kinetic modeling of microbially-driven redox chemistry of subsurface environments: coupling transport microbial metabolism and geochemistry. J. Hydro. 209, 53-80.

HydroGeoLogic, 1999. Diffuse-layer sorption reactions for use in MINTEQA2 for HWIR metals and metalloids. U.S. EPA (Environmental Protection Agency), National Exposure Research Laboratory, Ecosystems Research Division.

HydroGeoLogic, Allison Geoscience Consultants, 1999. MINTEQA2/PRODEFA2, a geochemical systems: user manual supplement for version 4.0. U.S. EPA (Environmental Protection Agency), National Exposure Research Laboratory, Ecosystems Research Division.

Islam, J., Singhal, N., 2002. A one-dimensional reactive multi-component landfill leachate transport model. Environmental Modeling & Software 17, 531-543.

Jackman, A.P., Kennedy, V.C., Bhatia, N., 2001. Interparticle migration of metal cations in stream sediments as a factor in toxics transport. J. Hazard. Mater. B82, 27-41.

Jackson, R.E., Inch, K.J., 1989. The in-situ adsorption of strontium-90 in a sand aquifer at the Chalk River Nuclear Laboratories. J. Contam. Hydrol. 4(1), 27-50, 1989.

Jager, T., den Hollander, H.A., van der Poel, P., Rikken, M.G.J., Vermeire, T., 2001. Probabilistic environmental risk assessment for Dibutylphthalate (DBP). Hum. Ecol. Risk Assess. 7 (6), 1681-1697.

Jain, C.K., Ram, D., 1997. Adsorption of lead and zinc on bed sediments of the river Kali. Water Res. 31, 154-162.

Jenne, E.A., 1968. In: Gould, R F. (Ed.), Trace Inorganics in Water. Americal Chemical Society, Washington, D.C. pp. 337-387.

Jenne, E.A. (Ed.), 1998. Adsorption of Metals by Geomedia. Academic Press, San Diego, CA.

Jenne, E.A., 1998. Adsorption of metals by geomedia: data analysis, modeling, controlling factors, and related issues. In: Jenne, E. A. (Ed.), Adsorption of Metals by Geomedia. Academic Press, San Diego, CA. pp. 2-74.

Jenne, E.A., Zachara, J.M., 1987. Factors influencing the sorption of metals. In: Dickson, K.L., Maki, A.W., Brungs, W., (Eds.), Fata and Eeffects of Sediment-bound Chemicals. Proceedings of the Sixth Pellston Workshop. Pergamon Press, New York. pp. 83-98.

Johnson, C., 2002. Personal communication.

Jorgensen, S.E., Nielsen, S.N., Jorgensen, L.A., 1991. Handbook of Ecological Parameters and Ecotoxicology. Elsevier Publishing, New York.

Karger, J., Ruthven, D.M., 1992. Diffusion in Zeolites and Other Microporous Solids. Wiley-Interscience, New York.

Karthikeyan, K.G., Elliott, H.A., Chorover, J., 1999. Role of surface precipitation in copper sorption by the hydrous oxides of iron and aluminum. J. Colloid Interface Sci. 209, 72-78.

Kenaga, E.E., Goring, C.A.I., 1980. Relationship between water solubility, soil sorption, octanol-water partitioning, and concentration of chemicals in biota. Aquat. Toxicol. ASTM STP 707, American Society for Testing and Materials, 78-115.

Ketterer, M.E., Wetzel, W.C., Layman, R.R., Matisoff, G., Bonniwell, E.C., 2000. Isotopic studies of sources of uranium in sediments of the Ashtabula River, Ohio, U.S.A. Environ. Sci. Technol. 34, 966-972.

Kharaka, Y.K., Gunter, W.D., Aggarwal, P.K., 1988. SOLMINEQUATION88: A computer program for geochemical modeling of water-rock interactions. U.S. Geological Survey, Water Resources Investigation, 88-4227.

Kincaid, C.T., Morrey, J.R., Rogers, J.E., 1984. Geohydrochemical models of solute migration, vol. 1: Process description and computer code selection, EA-3417, Electric Power Research Institute, Palo Alto, CA.

Kincaid, C.T., Morrey, J.R., 1984. Geohydrochemical models of solute migration, vol. 2: Preliminary evaluation of selected computer codes, EA-3417, Electric Power Research Institute, Palo Alto, CA.

Kipp, K.L., Jr., 1987. HST3D: A computer code for simulation of heat and solute transport in three dimensional groundwater systems, U.S. Geol. Surv. Water Resour. Invest., 86-4095.

Knocke, W.R., Hamon, J.R., Thompson, C.P., 1988. Soluble manganese removal on oxide-coated filter media. J. AWWA December 65-70.

Ko, D.C.K., Porter, J.F., Mckay, G., 2003. Fixed bed studies for the sorption of metal ion onto peat. Trans. IchemE. Part B 81, 73-86.

Koeppenkastrop, D., De Carlo, E., 1993. Uptake of rare earth elements from solution by metal oxides. Environ. Sci. Technol. 27, 1796-1802.

Konikow, L.K., Bredehoeft, J.D., 1978. Computer model of two-dimensional solute transport and dispersion in groundwater, in Techniques of Water-Resources Investigations of the United States Geological Survey, Book 7, chap. C2, USGS, Reston, VA.

Konikow, L.F., Bredehoeft, J.D., 1992. Gound-water models cannot be validated. Advances in Water Resources 15 (1), 75-83.

Konikow, L.F., Goode, D.J., Hornberger, G.Z., 1996. A three-dimensional method-of-characteristics solute-transport model (MOC3D): U.S. Geological Survey Water-Resources Investigations Report 96-4267, 87.

Konikow, L.F., Harbaugh, A.W., 2002. Personal communication.

Kraepiel, A.M.L., Keller, K., Morel, F.M.M., 1999. A model for metal adsorption on montmorillonite. J. Colloid Interface Sci. 210, 43-54.

Ku, H.H., 1966. Notes on the use of propagation of error formulas. J. Res. Natl. Bur. Standards-C. Eng. Instrum. 70, 263-273.

Kubiak, T.J, Best, D.A., 1991. Wildlife Risks Associated with Passage of Contaminant Anadromous Fish at Federal Energy Regulatory Commission Licensed Dams in Michigan. U.S. Fish and Wildlife Service, Contaminated Program, Division of Ecological Services. East Lansing, MI.

Kunze, G.W., Dixon, J.B., 1986. Pretreatment for mineralogical analysis. In: Kulte, A. (Ed.), Methods of Soil Analysis: Part 1: Physical and Mineralogical Methods. Chapter 5. American Society of Agronomy/Soil Science Society of America, Madison, WI, pp. 91.

Lahkim, M.B., Garcia, L.A., Nuckols, J.R., 1999. Stochistic modeling of exposure and risk in a contaminated hetergeneous aquifer. 2: application of Latin Hypercube sampling. Environ. Eng. Sci. 16 (5), 329-343.

Lai, C.H., Bodvarsson, G.S., Witherspoon, P.A., 1986. Second-order upwind differencing method for nonisothermal chemical transport in porous media, Numerical Heat Transfer 9, 453-471.

Lai, C.H., Lo, S.L., Chiang, H.L., 2000. Adsorption/desorption properties of copper ions on the surface of iron-coated sand using BET ns EDAX analysis. Chemosphere 41, 1249-1255.

Langmuir, D., 1997. Aqueous Environmental Geochemistry. Prentice Hall, NJ.

Lasserre, F., Razack, M., Banton, O., 1999. A GIS-linked model for the assessment of nitrate contamination in groundwater. J. Hydrol. 224 (3-4), 81-90.

Lee, J.V.D., Windt, L.D., 2001. Present state and future directions of modeling of geochemistry in hydrogeological systems. J. Contam. Hydrol. 47, 265-282.

Levy, R., Tamura, T., 1973. Calcium-magnesium exchange in aluminum hydroxide-coated montmorillonite. Israel J. Chem. 11 (2-3), 285-292.

Liao, C.M., Ling, M.P., Chen, J.S., 2003. Appraising zinc bioaccumulation in Abalone Haliotis Diversicolor Supertexta and alga Gracilaria Tenuistipitata var. Liui by probabilistic analysis. Aquaculture 217, 285-299.

Linville, C.D., Hobbs, B.E., Venkatesh, B.N., 2001. Estimation of error and bias in baysian Monte Carlo decision analysis using the bootstrap. Risk Anal. 21 (1), 63-74.

Lion, L.W., Altmann, R.S., Leckie, J.O., 1982. Trace metal adsorption characteristics of estuarine particulate matter: evaluation of contributions of Fe/Mn oxide and organic surface coatings. Environ. Sci. Technol. 1982, 16, 660-666.

Liu, C., Narashimhan, T., 1989. Redox-controlled multiple-species reactive chemical transport. 2 verification and application. Water Resour. Res. 25 (5), 883-910.

Lohman, K., Pai, P., Seigneur, C., Mitchell, D., Heim, K., Wandland, K., Levin, L., 2000. A probabilistic analysis of regional mercury impacts on wildlife. Hum. Ecol. Risk Assess. 6 (1), 103-130.

Longsine, D.E., Bonano, E.J., Harlan, C.P., 1987. User's manual for the NEFTRAN computer code. Rep. NUREG/CR-4766 and SAND86-2405, Sandia Natl. Lab., Albuquerque, NM.

Lopez-Pila, J.M., Szewzyk, R., 2000. Estimating the infection risk in recreational waters from the faecal indicator concentration and from the ratio between pathogens and indicators. Water Res. 34 (17), 4195-4200.

Lothenbach, B., Furrer, G., Schulin, B., 1997. Immobilisation of heavy metals by polynuclear aluminum and montmorillonite compounds. Environ. Sci. Technol. 31, 1452-1462.

Lu, H., Axe, L., Tyson, T.A., 2003. Development and application of a computer simulation tool for ecological risk assessment. Environmental Modeling & Assessment 8, 311-322.

Lu, G., Clement, T.P., Zheng, C., Wiedemeier, T.H., 1999. Natural attenuation of BTEX compounds: model development and field-scale application. Ground Water 37 (5), 707-717.

Lydersen, E., Salbu, B., Poleo, A.B.S., Muniz, I.P., 1991. Formation and dissolution kinetics of Al(OH)3(s) in synthetic freshwater solutions. Water Resour. Res. 27, 351-357.

Lyman, W.J., Reehl, W.F., Rosenblatt, D.H., 1990. Handbook of Chemical Property Estimation Methods, Environmental Behavior of Organic Compounds. American Chemical Society, Washington, D.C.

MacIntosh, D.L., Suter II, G.W., Hoffman, O., 1994. Uses of probabilistic exposure Models in ecological risk assessments of contaminated sites. Risk Anal. 14 (4), 405-419.

McDonald, M.G., Harbaugh, A.W., 1984. MODFLOW: A Modular Three-Dimensional Finite-Difference Groundwater Flow Model. U.S. Geological Survey OFR 83-875, 1984.

Mangold, D.C., Tsang, C.F., 1991. A summary of subsurface hydrological and hydrochemical model. Review of Geophysics 29 (1), 51-79.

Manju, G.N., Krishnan, K.A., Vinod, V.P., Anirudhan, T.S., 2002. An investigation into the sorption of heavy metals from wastewaters by polyacrylamide-grafted iron(III) oxide. J. Hazard. Mater. B91, 221-238.

Marlon-Lambert, J., 1978. Computer program for ground water flow and solute transport analysis, Rep. N25090, Golder Association, Vancouver, B. C.

Marmier, N., Delisee, A., Fromage, F., 1999. Surface complexation modeling of Yb(III) and Cs(I) sorption on silica. J. Colloid Interface Sci. 212, 228-233.

Martin, C.O., Fischer, R.A., 2000. Regional strategies for managing threatened, endangered, and sensitive species on DOD sites, U.S. ongoing project by waterways Experimental Station, Vicksburg, MS.

Mattson, E.D., Bowman, R.S., Lindgren, E.R., 2002. Electrokinetic ion transport through unsaturated soil: 2. Application to a heterogeneous field site. J. Contam. Hydrol. 54 (1-2), 121-140.

Maughan, J.T., 1993. Ecological Assessment of Hazardous Waste Sites. Van Nostrand Reinhold, New York, NY.

May, H.M., Kinniburgh, D.G., Helmke, P.A., Jackson, M.L., 1986. Aqueous dissolution, solubilities and thermodynamic stabilities of common aluminosilicate clay minerals: Kaolinite and smectites. Geochim. Cosmochim. Acta. 50, 1667-1677.

McDiarmid, M.A., Keogh, J.P., Hooper, F.J., McPhaul, K., Squibb, K., Kane, R., DiPino, R., Kabat, M., Kaup, B., Anderson, L., Hoover, D., Brown, L., Hamilton, M., Jacobson-Kram, D., Burrows, B., Walsh, M., 2000. Health effects of depleted uranium on exposed Gulf War veterans. Environ. Res. 82 (2), 168-180.

McKone, T.E., 1993. The precision of QSAR methods for estimating transfer factors in exposure assessment. SAR and QSAR in Environ. Res. 1, 41-51.

Mckone, T.E., 1994. Uncertainty and variability in human exposures to soil contaminants though home-grown food: a Monte Carlo assessment. Risk Anal. 14 (14), 449-463.

McClain, D.E., Benson, K.A., Dalton, T.K., 2001. Biological effects of embedded depleted uranium (DU): summary of Armed Forces Radiobiology Research Institute research. The Science of the Total Environment 274: 115-118.

McPhail, M., Page, A.L., Bingham, F.T., 1972. Adsorption interactions of monosilicic and boric acid on hydrous oxides of iron and aluminum. Soil Sci. Soc. Am. J. 36, 510.

Manceau, A., Charlet, L., Boisset, M.C., Didier, B., Spadini, L., 1992. Sorption and speciation of heavy metals on hydrous Fe and Mn oxides. From microscopic to macroscopic. Applied Clay Science 7, 201-223.

Meeussen, J.C.L., 2003. ORCHESTRA: an object-oriented framework for implementing chemical equilibrium models. Environ. Sci. Technol. 37 (6), 1175-1182.

Mehl, S.W., Hill, M.C., 2001. MODFLOW-2000, the U.S. Geological Survey modular ground-water model -- user guide to the Link-AMG (LMG) package for solving matrix equations using an algebraic multigrid solver: U.S. Geological Survey Open-File Report 01-177, 33.

Merkle, P.B., Knocke, W.R., Gallagher, D.L., Little, J.C., 1997. Dynamic model for soluble Mn^{2+} removal by oxide-coated filter media. J. Environ. Eng. 123, 650.

Middleburg, J.J., Comans, R.N.J., 1991. Sorption of cadmium on hydroxyapatite. Chemical Geology 90, 45-53.

MIDEQ (Department of Environmental Qaulity, State of Michigan), 2001. Groundwater Modeling Theory. Groundwater Modeling Program, Hydrologic Studies Unit, Department of Environmental Quality, MI.

Misak, N.Z., Ghoneimy, H.F., Morcos, T.N., 1996. Adsorption of $Co^{2+}$and Zn^{2+} ions on hydrous Fe(III), Sn(IV), and Fe(III)/Sn(IV) oxides: II. Thermal behavior of loaded oxides, isotopic exchange equilibria, and percentage adsorption–pH curves. J. Colloid Interface Sci. 184 (1), 31-43.

Moore, D.R.J., Sample, B.E., Suter, G.W., Parkhurst, B.R., Teed, R.S., 1999. A probabilistic risk assessment of the effects of methylmercury and PCBs on mink and kingfishers along East Fork Poplar Creek, Oak Ridge, Tennessee, USA. Environ. Toxicol. Chem. 18 (12), 2941-2953.

Morgan, M.G., Henrion, M., 1998. Uncertainty: a Guide to Dealing with Uncertainty in Quantitative Risk and Policy Analysis. Cambridge University Press, Cambridge, UK

Morrey, J.R., 1988. FASTCHEM package, vol.4, User's guide to the ECHEM equilibrium geochemistry code, Rep. EA-5870-CCM, Electric Power Research Institute, Palo Alto, CA.

Morrey, J.R., Shannon, D.W., 1981. Operator's manual for EQUILIB- A computer code for predicting mineral formation in geothermal brines, vol. 1 and 2, final report, project RP653-1 Electric Power Research Institute, Palo Alto, CA.

Morrey, J.R., Kincaid, C.T., Hostetler, C.T., 1986. Geohydrochemical models of solute migration, vol. 3: Evaluation of selected computer codes, EA-3417, Electric Power Research Institute, Palo Alto, CA.

Morrissey, F.A., Grismer, M.E., 1999. Kinetics of volatile organic compound sorption/desorption on clay minerals. J. Contam. Hydrol. 36, 291-312.

Moschandreas, D.J., Karuchit, S., 2002. Scenario-model-parameter: a new method of cumulative risk uncertainty analysis. Environ. Int. 28, 247-261.

Naidja, A., Huang, P.M., Bollag, J.-M., 1997. Activity of tyrosinase immobilized on the hydroxyaluminum-montmorillonite complexes. Journal of Molecular Catalysis A: Chemical 115, 305-316.

Naito, W., Miyamoto, K., Nakanishi, J., Masunaga, S., Bartell, S. M., 2002. Application of an ecosystem model for aquatic ecological risk assessment of chemicals for a Japanese lake. Water Res. 36, 1-14.

National Council on Radiation Protection and Measurements, 1996. A Guide for Uncertainty Analysis in Dose and Risk Assessments Related to Environmental Contamination: NCRP Commentary No.14. National Council on Radiation Protection and Measurements, Bethesda, MD.

National Council on Radiation Protection and Measurements, 1999. Recommended Screening Limits for Contaminated Surface Soil and Review of Factors Relevant to Site-Specific Studies. Recommendations of the National Council on Radiation Protection and Measurements. NCRP Report No.29, Bethesda, MD.

Nayak, T.K., Kundu, S., 2001. Calculating and describing uncertainty in risk assessment: the Bayesian approach. Hum. Ecol. Risk Assess. 7 (2), 307-328.

Noorishad, J., 1989. Simulation of fractionation of C-13 during nonequilibrium reactive solute transport in geologic systems: formulation and example calculation. Water Resour. Res. 25 (4), 754-756.

Nordstrom, D.K., Plummer, L.N., Langmuir, D., 1990. Revised chemical equilibrium data for major water-mineral reactions and their limitations, in Bassett, R.L. and Melchior, D. Eds., Chemical Modeling in Aqueous Systems II: Washington D.C., American Chemical Society Symposium Series 416, Chapter 31, 398–413.

O'Day, P.A., Brown, G.E., Parks, G.A., 1994. X-Ray absorption spectroscopy of cobalt(II) multinuclear surface complexes and surface precipitates on kaolinite. J. Colloid Interface Sci. 165, 269.

OLI Systems, Inc., 1999. OLI Software Manual. OLI Systems, Inc., Morris Plains, NJ.

Oreskes, N., Shrader-Frechette, K., Belitz, K., 1994. Verification, validation, and confirmation of numerical models in the earth sciences. Science 263 (4): 641-646.

Osiensky, J. L., Williams, R.E., 1996. A two-dimensional MODFLOW numerical approximation of mise-a-la-masse electrical flow through porous media. Ground Water 34 (4), 727-733.

Ott, W.R., 1990. A physical explanation of the lognormality of pollutant concentrations. J.Air Waste Manage. Assoc. 40, 1378-1383.

Owen, B.A., 1990. Literature-derived absorption coefficient for 39 chemicals via oral and inhalation routes of exposure. Regulatory Toxicol. Pharmacol. 11, 237–252.

Oxenberg, T.P., 1997. The use of catchboxes to minimize the impact to the environment from testing depleted uranium penetrators. Master Thesis. Georgia Institute of Technology.

Pace, M.N., Mayers, M.A., Jardine, P.M., Zachara, J.M., Bjornstad, B.N., 2003.Quantifying the effects of small-scale heterogeneities on flow and transport in undisturbed cores from the Hanford Formation. Vadose Zone Journal 2, 664-676.

Pacific Northwest National Laboratory (PNNL), 1998. Screening Assessment and Requirements for a Comprehensive Assessment, Columbia River Comprehensive Impact Assessment, DOE/RL-96-16 Draft, U.S. Department of Energy. http://www.hanford.gov/crcia/crcia.htm.

Palisade Corporation, 2002. @Risk: About risk analysis. http://www.palisade.com/html/risk/facts.html.

Papelis, C, Roberts, P.V., Leckie, J.O., 1995. Modeling the rate of cadmium and selenite adsorption on micro- and mesoporous transition aluminas. Environ. Sci. Technol. 29 (4), 1099-1108.

Papini, M.P., Bianchi, A., Majone, M., Beccari, M., 2002. Equilibrium modeling of lead adsorption onto a "red soil" as a function of the liquid-phase composition. *Ind. Eng. Chem. Res.* 41 (8), 1946-1954.

Parkhurst, D.L., Appelo, C.A., 1999. User's guide to PHREEQC (version2)-a computer program for speciation, batch-reaction, one-dimensional transport, and inverse geochemical calculations. Water - Resources Investigations Report 99-4259.

Parkhurst, D.L., Thorstenson, D.C., Plummer, L.N., 1980. PHREEQE--A computer program for geochemical calculations: U.S. Geological Survey Water-Resources Investigations Report (Revised and reprinted August, 1990).

Pickens, J.F., Grisak, G.E., 1979. Finite element analysis of liquid flow, heat transport and solute transport in a groundwater flow system: Governing equations and model formation, Report TR-81. At. Energy of Can., Ltd., Ottawa, Ont.

Pitzer, K.S., 1979. Theory: ion interaction approach, in Pytkowicz, R.M. (Ed.), Activity Coefficients in Electrolyte Solutions. CRC Press, Boca Raton, FL, pp. 157-208.

Poeter, E.P., Hill, M.C., 1998. Documentation of UCODE, a computer code for universal inverse modeling. U. S. Geological Survey, Water-Resources Investigations Report 98-4080.

Polder, M.D., Hulzeebos, E.M., Jager, D.T., 1998. Bioconcentration of gaseous organic chemicals in plant leaves: comparison of experimental data with model predictions. Environ. Toxicol. Chem. 17 (5), 952-968.

Pollock, D.W., 1994. User's guide for MODPATH/MODPATH-PLOT, Version 3: a particle tracking post-processing package for MODFLOW, the U.S. Geological

Survey finite difference groundwater flow model: U.S. Geological Survey Open-File Report 94-464.

Post, V. E.A., 2001. User's guide to PHREEQC for Windows. http://www.geo.vu.nl/users/posv/phreeqc.html

Price, K.R., 1991. The analysis of soil and vegetation samples collected from the Yuma Proving Ground. Pacific Northwest Laboratory Report TD 2761.

Pruess, K., 1991. TOUGH2: a general numerical simulator for multiphase fluid and heat flow, Technical Report LBL-29400, Lawrence Berkeley Laboratory, CA.

Rai, S.N., Krewski, D., 1998. Uncertainty and variability analysis in multiplicative risk models. Risk Anal. 18 (1), 37-45

Rai, S.N., Bartlett, S., Krewski, D., Paterson, J., 2002. The use of probabilistic risk assessment in establishing drinking water quality objectives. Hum. Ecol. Risk Assess. 8 (3), 493-509.

Reeves, M., Ward, D.S., Davis, P.A., 1986. Theory and implementation for SWIFT II, Release 4.84, Rep. NUREG/CR-3328 and SAND83-1159, Sandia Natl. Lab., Albuquerque, NM.

Regan, H.M., Sample, B.E., Ferson, S., 2002. Comparison of deterministic and probabilistic calculation of ecological soil screening levels. Environ. Toxicol. Chem. 21 (4): 882-890.

Rhee, S.W., Reible, D.D., Constant, W.D., 1993. Stochastic modeling of flow and transport in deep-well injection disposal systems. J. Hazard. Mater. 34 (3), 313-333.

Riley, W.J., McKone, T.E., Lai, A.C.K., Nazaroff, W.W., 2002. Indoor particulate matter of outdoor origin: importance of size-dependent removal mechanisms. Environ. Sci. Technol. 36, 200-207.

Roberts, D.R., Scheidegger, A.M., Sparks, D.L., 1999. Kinetics of mixed Ni-Al precipitate formation on a soil clay fraction. Environ. Sci. Technol. 33, 3749-3754.

Ross, M.S., 1994. Toxic Metals in Soil–Plant Systems. John Wiley & Sons, New York.

Rostker, B., 1998. Depleted Uranium in the Gulf. Environmental Exposure Report, U.S. Department of Defense.

Rubin, J., 1983. Transport of reacting solutes in porous media: relation between mathematical nature of problem and chemical nature of reactions. Water Resour. Res. 19 (5), 1231-1252.

Runchal, A.K., 1985. PORFLOW: A general purpose model for fluid flow, heat transfer and mass transport in anisotropic, inhomogeneous, equivalent porous media, Tech. Note TN-011, Anal. and Comput. Res., Inc., Los Angeles, CA.

Runchal, A.K., Treger, J., Segal, G., 1979. Program EP21 (GWTHERM): Two-dimensional fluid flow, heat, and mass transport in porous media. Tech. Note TN-LA-34, Adv. Technol. Group, Dames and Moore, Los Angeles, CA.

Runkel, R.L., Bencala, K.E., Broshears, R.E., 1996. Reactive solute transport in streams: 1. Development of an equilibrium-based model. Water Resour. Res. 32 (2), 409-418.

Runkel, R.L., McKnight, D.M., Bencala, K.E., 1996. Reactive solute transport in streams: 2. Simulation of a pH modification experiment. Water Resour. Res. 32 (2), 419-430.

Rybicka, E.H., Calmano, W., Breeger, A., 1995. Heavy metals sorption/desorption on competing clay minerals; an experimental study. Applied Clay Science 9, 369-381.

Salmon, S.U.J., 1999. Overview of models for biogeochemical modeling of acid mine drainage. http://www.ce.kth.se/aom/AVAT/pdf-report/model-overview.pdf

Sample, B.E., Arenal, C.A., 1999. Allometric model for interspecies extrapolation of wildlife toxicity data. Bull. Environ. Contam. Toxicol. 62, 653-663.

Sample, B.E., Opresko, D.M., Suter II, G.W., 1996. Toxicological benchmarks for wildlife: 1996 revision. Reporting Code EW 20, Lockheed Martin Energy Systems, INC.

Sample, B.E., Suter II, G.W., Efroymson, R.A., 1998. A Guide to the ORNL Ecotoxicological Screening Benchmarks Background, Development, and Application. Oak Ridge National Laboratory under contract to U.S. Department of Energy, Oak Ridge, TN.

Samsoe-Petersen, L., Larsen, E.H., Larsen, P.B., Bruun, P., 2002. Uptake of trace elements and PAHs by fruit and vegetables from contaminanted soils. Environ. Sci. Technol. 36, 3057-3063.

Sanga, R.N., Bartell, S.M., Ponce, R.A., Boischio, A.A.P., Joiris, C.R., Pierce, C.H., Faustman, E.M., 2001. Effects of uncertainty on exposure estimates to

methylmercury: a Monte Carlo analysis of exposure biomakers versus dietary recall estimation. Risk Anal. 21 (5), 859-868.

Schecher, W.D., McAvoy, D.C., 1998. MINEQL$^+$: A chemical equilibrium modeling system, version 4.0 for Windows, user manual, 1st ed. Environmental Research Software, Hallowell, ME.

Schecher, W.D., McAvoy, D.C., 2001. MINEQL$^+$: version 4.5. Environmental Research Software, Hallowell, Maine. http://www.mineql.com/mineql.html.

Scheckel, K.G., Scheinost, A.C., Ford, R.G., Sparks, D.L., 2000. Stability of layered Ni hydroxide surface precipitates-a dissolution kinetics study. Geochim. Cosmochim. Acta 64 (16), 2727-2735.

Scheidegger A.M., Strawn, D.G., Lamble, G.M., 1998. The kinetics of mixed Ni-Al hydroxide formation on clay and aluminum oxide minerals: A time-resolved XAFS study. Geochim Cosmochim. Acta 62 (13), 2233-2245.

Scheinost, A.C., Abend, S., Pandya, K.I., Sparks, D.L., 2001. Kinetic control on Cu and Pb sorption by ferrihydrite. Environ. Sci. Technol. 35 (6), 1090-1096.

Schlegel, M.L., Manceau, A., Chateigner, D., Charlet, L., 1999. Sorption of metal ions on clay minerals. I. Polarized EXAFS evidence for the adsoption of Co on the edges of hectorite particles. J. Colloid Interface Sci. 215, 140-158.

Schumacher, M., Meneses, M., Xifro, A., Domingo, J.L., 2001. The use of Monte Carlo simulation techniques for risk assessment: study of a municipal waste incinerator. Chemosphere 43, 787-799.

Schwartz, S., Berding, V., Matthies, M., 2000. Aquatic fate assessment of the polycyclic musk fragrance HHCB scenario and variability analysis in accordance with the EU risk assessment guidelines. Chemosphere 41, 671-679.

Sen, T.K., Mahajan, S.P., Khilar, K.C., 2002. Adsorption of Cu and Ni on iron oxide and kaolin and its importance on Ni transport in porous media. Colloids and Surface A: Physicochem. Eng. Aspects 211, 91-102.

Sharpe, S. Mackay, D., 2000. A framework for evaluating bioaccumulation in food webs, Environ. Sci. Technol. 34, 2373–2379.

Shuman, L.M., 1977. Adsorption of Zn by Fe and Al hydrous oxides as influenced by aging and pH. Soil Sci. Soc. Am. J. 41, 703.

Smith, R.L., 1994. Use of Monte Carlo simulation for human exposure assessment at a superfund site. Risk Anal. 14 (4), 433-439.

Solomon, K.R., Sibley, P., 2002. New concept in ecological risk assessment: where do we go from here? Mar. Pollut. Bull. 44, 279-285.

Sparks, D.L., 1995. Environmental Soil Chemistry. Academic Press, San Diego, CA.

Sportisse, B., Bencteux, G., Plion, P., 2000. Method of lines versus operator splitting for reaction-diffusion systems with fast chemistry. Environmental Modeling & Software, 15, 673-679.

Sposito, G., 1986. Distinguishing adsorption from surface precipitation. Geochemical Processes at Mineral Surfaces, ACS (American Chemical Society) Symposium Series, 323, 216-228.

Sposito, G., 1989. The Chemistry of Soils. Oxford University Press, New York.

Sposito, G., Coves, J., 1989. SOILCHEM: A computer program for the calculation of chemical speciation in soils, report, Kearny Found., Univ. of Calif., Riverside and Berkeley.

Sposito, G., Mattigod, S.V., 1980. GEOCHEM: A computer program for the calculation of chemical equilibria in soil solutions and other natural water systems, report, Kearny Found., Univ. of Calif., Riverside and Berkeley.

Stefanova, R.Y.J., 2001. Removal of metal ions from water solutions by iron/cobalt oxide coated keramzite. J. Environ. Sci. Health Part A: Toxic-Hazard. Subst. Environ. Eng. 36, 1287-1301.

Stow, C.A., Qian, S., 1998. A size-based probabilistic assessment of PCB exposure from Lake Michigan fish consumption. Environ. Sci. Technol, 32, 2325-2330.

Strawn, D.G., Schidegger, A.M., Sparks, D.L., 1998. Kinetics and mechanisms of Pb(II) sorption and desorption at the aluminum oxide-water interface. Environ. Sci. Technol. 32 (17), 2596-2601.

Strawn, D.G., Sparks, D.L., 1999. The use of XAFS to distinguish between inner and outer-sphere lead adsorption complexes on montmorillonite. J. Colloid Sci. 216, 257.

Strenge, D.L., Peterson, S.R., 1989. Chemical Database for the Multimedia Environmental Pollutant Assessment System (MEPAS): Version 1. PNL-7145, prepared by Pacific Northwest Laboratory under contract to U.S. Department of Energy, Office of Environmental Audit, Washington, D.C.

Stumm, W., Morgan, J.J., 1996. Aquatic Chemistry, Chemical Equilibria and Rates in Natural Waters. John Wiley & Son, New York.

Swallow, C.K., Hume, D.N., Morel, F.M.M., 1980. Sorption of copper and lead by hydrous ferric oxide. Environ. Sci. Technol. 14 (11), 1326-1331.

Swartout, J., Rice, G., 2000. Uncertainty analysis of the estimated ingestion rates used to derive the methylmercury reference dose. Drug Chem. Toxicol. 23 (1), 293-306.

Sydelko, P.J., Hlohowskyj, I., Majerus, K., Christiansen, J., Dolph, J., 2001. An object-oriented framework for dynamic ecosystem modeling: application for integrated risk assessment. The Science of the Total Environment 274: 271-281.

Tannenbaum, L.V., Johnson, M.S., Bazar, M., 2003. Application of the hazard quotient method in remedial decision: a comparison of human and ecological risk assessment. Hum Ecol Risk Assess. 9 (1): 387-401.

Tebes-Stevens, C., Valocchi, A.J., VanBriesen, J.M., Rittmann, B.E., 1998. Multicomponent transport with coupled geochemical and microbiological reactions: model description and example simulations. J. Hydrol. 209, 8-26.

Tellinghusen, J., 2000. A Monte Carlo study of precision, bias, inconsistency, and non-Gaussian distributions in nonlinear least squares. J. Phys. Chem. 104, 2834-2844.

The Scientific Software Group, 2002. http://www.scisoftware.com.

Thiez, P.L., Lemonnier, P., 1990. An in-situ combustion reservoir simulator with a new representation of chemical reactions. SPE Reservoir Eng. 9, 285-292.

Thomann, R.V., Connollly, J.P., Parkerton, T.F., 1992. An equilibrium model of organic chemical accumulation in aquatic food webs with sediment interaction. Environ. Sci. Technol. 11, 615-629.

Thompson, H.A., Parks, G.A., Brown, G.E., Jr., 1999. Dynamic interactions of dissolution, surface adsorption, and precipitation in an aging cobalt (II)-clay-water system. Geochim. Cosmochim. Acta 63 (11/12), 1767-1779.

Thompson, M.K., Graham, J.D., 1996. Going beyond the single number: using probabilistic risk assessment to improve risk management. Hum. Ecol Risk Assess. 2 (4), 1008-1034.

Todd, D.K., 1980. Groundwater Hydrology. Wiley, New York.

Tonkin, J.W., Balistrieri, L.S., Murray, J.W., 2002. Modeling metal removal onto natural particles formed during mixing of acid rock drainage with ambient surface water. Environ. Sci. Technol. 36, 484-492.

Traas, T.P., Luttik, R., Jongbloed, R.H., 1996. A probabilistic model for deriving soil quality criteria based on secondary poisoning of top Predators: I. model description and uncertainty analysis. Ecotoxicol. Environ. Saf. 34, 264-278.

Tracy, F., 2002. SEEP2D software. The U.S. Army Engineer Waterways Experiment Station (WES).

Travis, C.C., Arms, A.D., 1988. Bioconcentration of organics in beef, milk, and vegetation. Environ. Sci. Technol, 22 (3), 271-274.

Trivedi, P., Axe, L., 1999. A comparison of strontium sorption to hydrous aluminum, iron, and manganese oxides. J. Colloid Interface Sci. 218 (2). 554-563.

Trivedi, P., Axe, L., 2000. Modeling Cd and Zn sorption to hydrous metal oxides. Environ. Sci. Technol. 34 (11), 2215-2223.

Trivedi, P., Axe, L., 2001. Predicting divalent metal sorption to hydrous Al, Fe, and Mn Oxides. Environ. Sci. Technol. 35 (9), 1779-1784.

Trivedi, P., Axe, L., Tyson, T.A., 2001. XAS studies of Ni and Zn sorbed to hydrous manganese oxide. Environ. Sci. Technol. 35, 4515-4521.

Trivedi, P., Dyer, J.A., Sparks, D.L., 2003. Lead sorption onto ferrihydrite. 1. A macroscopic and spectroscopic assessment. Environ. Sci. Technol. 37 (5), 908-914.

Turekian, K.K., 1977. In: National Research Council (Ed.), Estuaries Geophysics and the Environment. National Academy of Sciences Press, Washington, DC, 1977, pp. 121.

U.S. Environmental Protection Agency, 1989. Risk Assessment Guidance for Superfund (RAGS): Volume I Human Health Evaluation Manual (Part A), Office of Emergency and Remedial Response, Washington, D.C.

U.S. Environmental Protection Agency, 1991. Exposure Point Concentrations In Groundwater, Region III, Technical Guidance Manual. Office of Superfund, Hazardous Waste Management Division, Philadelphia, PA.

U.S. Environmental Protection Agency, 1992a. Framework for Ecological Risk Assessment. EPA/630/R-92/001. Risk Assessment Forum, Washington, D.C.

U.S. Environmental Protection Agency, 1992b. Dermal Exposure Assessment: Principles and Applications. EPA/600/8-91/011B. Office of Health and Environmental Assessment, U.S. Environmental Protection Agency, Washington, D. C.

U.S. Environmental Protection Agency, 1992c. Preparation of Soil Sampling Protocols: Sampling Techniques and Strategies. EPA/600/R-92/128.Office of Research and Development, Washington, D.C.

U.S. Environmental Protection Agency, 1993a. Wildlife Exposure Handbook. Office of Research and Development, Vol. I of II, Washington, D.C.

U.S. Environmental Protection Agency, 1993b. Addendum: Methodology for Assessing Health Risks Associated with Indirect Exposure to Combustor Emissions, Working Group Recommendations, Office of Solid Waste and Office of Research and Development, Washington, D.C.

U. S. Environmental Protection Agency, 1994. Health Effects Assessment Summary Tables. Annual FY-1994. Prepared by the Office of Health and Environmental Assessment, Environmental Criteria and Assessment Office, Cincinnati, OH, for the Office of Emergency and Remedial Response, Washington, D.C.

U.S. Environmental Protection Agency, 1996. Safe Drinking Water Act Amendments. Washington, D.C.

U.S. Environmental Protection Agency, 1997a. Exposure Factors Handbook, Volume I. General Factors, Office of Research and Development, Washington, D.C.

U.S. Environmental Protection Agency, 1997b. Guiding Principles for Monte Carlo Analysis. Office of Research and Development, Washington D.C.

U.S. Environmental Protection Agency, 1997c. The Lognormal Distribution in Environmental Applications: Technology Support Center Issue, Office of Research and Development, Office of Solid Waste and Emergency Response, Washington D.C.

U.S. Environmental Protection Agency, 1998. Guidelines for Ecological Risk Assessment, EPA/630/R-95/002F, U.S. Environmental Protection Agency, Washington, D. C.

U.S. Environmental Protection Agency, 2001. Supplemental Guidance for Developing Soil Screening Levels for Superfund Sites, Office of Emergency and Remedial Response, Washington, D.C.

U.S. Environmental Protection Agency, 2003. ECOTOX Database, http://www.epa.gov/ecotox/ecotox_home.htm.

U.S. Geological Survey, 2002. Summary of MODFLOW-2000.

Van Benschoten, J.E., Reed, R.E., Matsumoto, M.R., McGarvey, P.J., 1994 Effects of iron oxides on soil washing a metal contaminated sandy soil. Water Environ. Res. 66, 168-174.

Vardoulakis, S., Fisher, B.E.A., Gonzalez-Flesca, N., Pericleous, K., 2002. Model sensitivity and uncertainty analysis using roadside air quality measurements. Atmospheric Environment 36, 2121-2134.

Vaughn, W.R., 1998. Hitchhiker's Guide to Visual Basic and SQL Server. Microsoft Press. Redmond, WA.

Veith,G.D., Macek, K.J., Petrocelli, S.R., Carroll, J., 1980. An evaluation of using partition coefficients and water solubility to estimate bio-concentration factors for organic chemicals in fish. aquatic toxicology. ASTM STP 707, American Society for Testing and Materials, 116-129.

Verhaar, H.J.M., De Jongh, J., Hermens, J.L.M., 1999. Modeling the bioconcentration of organic compounds by fish: a novel approach. Environ. Sci. Technol. 33, 4069-4072.

Vermeire, T., Jager, T., Janssen, G., Bos, P., Pieters, M., 2001. A probabilistic human health risk assessment for environmental exposure to Dibutylphthalate. Hum. Ecol. Risk Assess. 7 (6), 1663–1679.

Vermeul, V.R., Scheibe, T.D., Bergeron, M.P., Thome, P.D. Cole, C.R., Waichler, S.R., Murray, C.J., Xie, Y., Nichols, W.E., 2003. Transient Inverse Calibration of the Site-Wide Groundwater Flow Model (ACM-2): FY 2003 Progress Report, PNNL-14398, Pacific Northwest National Laboratory, Richland, WA.

Waddill, D.W., Widdowson, M.A., 1997. SEAM3D: A numerical model for three-dimensional solute transport and sequential electron acceptor-based bioremediation in groundwater: Virginia Polytechnic Institute and State University Final Technical Report, prepared for the U.S. Army Corps of Engineers, 336-344.

Walter, A., Frind, E., Blowes, D., Ptacek, C.J., Molson, J.W., (1994a). Modeling of multicomponent reactive transport in groundwater: 1. Model development and evaluation. Water Resour. Res. 30 (11), 3137-3148.

Walter, A., Frind, E., and Blowes, D., Ptacek, C.J., Molson, J.W., (1994b). Modeling of multicomponent reactive transport in groundwater: 2.Metal mobility in aquifers impacted by acidic mine tailings discharge. Water Resour. Res. 30 (11), 3149-3158.

Wang, M., Zheng, C., 1997. Optimal remediation policy selection under general conditions. Ground Water 35 (5), 757-764.

Warner, J.W., 1981. Finite element two dimensional transport model of groundwater restoration for in-situ solution mining of uranium, Ph.D. thesis, Colo. State Univ., Fort Collins.

Warren-Hicks, W.J., Moore, D.R.J., 1998. Uncertainty Analysis in Ecological Risk Assessment. SETAC Press, FL.

Warren-Hicks, W., Carbone, J.P., Havens, P.L., 2002. Using Monte Carlo techniques to judge model prediction accuracy: validation of the pesticide root zone model 3.12. Environ. Toxicol. Chem. 21 (8), 1570-1577.

Waterloo Hydrogeologic, Inc., 1999. WinPEST user manual, Waterloo Hydrogeologic, Inc.

Water Numerical Computing, Inc., 2000. PEST, model-independent parameter estimation, Water Numerical Computing, Inc.

Waterloo Hydrogeologic, Inc., 2002. Visual MODFLOW Software, Waterloo Hydrogeologic, Inc.

Waychunas, G.A., Fuller, C.C., Davis, J.A., 2002. Surface complexation and precipitate geometry for aqueous Zn(II) sorption on ferrihydrite I: X-ray absorption extended fine structure spectroscopy analysis. Geochim. Cosmochim. Acta 66 (7), 1119-1137.

Weber, W.J. Jr., McGinley, P.M., Katz, L.E., 1991. Sorption phenomena in subsurface systems: concepts, models and effects on contaminant fate and transport. Water Res. 25 (5), 499-528.

Weiss, E.J., 1999. Preliminary ecological risk assessment to assess the implications of replacing chromium plating with tantalum coatings, Master Thesis, New Jersey Institute of Technology, NJ.

Weng, L., Temminghoff, E.J.M., Van Riemsdijk, W.H., 2001. Contribution of individual sorbents to the control of heavy metal activity in a sandy soil. Envrion. Sci. Technol. 35, 4436-4443.

Wenning, R.J., 2002. Uncertainty and data needs in risk assessment of three commercial polybrominated diphenyl ethers: probabilistic exposure analysis and comparison with European commission results. Chemosphere 46, 779-796.

West, R.W., Kodell, R.L., 1999. A comparison of methods of benchmark-dose estimation for continuous response data. Risk Anal. 19 (3), 453-459.

Westall, J.C., Zachary, J.L., Morel, F.M.M., 1976. MINEQL, A computer program for the calculation of chemical equilibrium composition of aqueous system. Tech.

Note 18, Dep. Civil Eng., Massachusetts Institute of Technology, Cambridge, MA.

Wiwatanadate, P., Claycamp, H.H., 2000. Exact propagation of uncertainty in multiplicative models. Hum. Ecol. Risk Assess. 6 (2), 355-368.

Wolery, T.J., 1978. Some chemical aspects of hydrothermal processes at mid-orean ridge-a theoretical study: Ph.D thesis, Northwestern University, Evanston, IL.

Wolery, T.J., 1992. EQ3/6, a software package for geochemical modeling of aqueous systems: package overview and installation guide (version 7.0). Lawrence Livermore National Laboratory.

Wong, H.S., Yeh, W., 2002. Uncertainty analysis in contaminated aquifer management. Journal of Water Resources Planning and Management 128 (1), 33-45.

Xu, T., Pruess, K., Brimhall, G., 1999. An improved equilibrium-kinetics speciation algorithm for redox reactions in variably saturated subsurface flow systems. Computer Geoscience 25, 655-666.

Yabusaki, S., Steefel, C., Wood, B., 1998. Multidimensional, multicomponent, subsurface, reactive transport in nonuniform velocity fields: code verification using an advective reactive streamtube approach. J. Contam. Hydrol. 30, 299-331.

Yanenko, N.N., 1971. The Method of Fractional Steps. Springer, New York.

Yang, C.T., 1973. Incipient motion and sediment transport. J. Hydr. Div., 99 (HY10), 1679-1704.

Yao, C., Tien, C., 1992. Approximations of uptake rate of spherical adsorbent pellets and their applications to batch adsorption calculations. Chem. Engng. Sci. 48 (1), 187-198.

Yeh, G., Salvage, K.M., 1997. HYDROGEOCHEM 2.0: A coupled model of hydrologic transport and mixed geochemical kinetic/equilibrium reactions in saturated-unsaturated media.

Yeh. G., Sharp-Hansen, S., Lester, B., 1992. 3DFEMWATER/3DLEWASTE: numerical codes for delineating wellhead protection areas in agricultural regions based on the assimilative capacity criterion. Office of Research and Development, U.S. Environmental Protection Agency, Athens, GA. EPA/600/R-92/223 278.

Yeh, G.T., Tripathi, V.S., 1989. A critical evaluation recent developments in hydrogeochemical transport models of reactive multi-chemical components. Water Resour. Res. 25 (1), 93-108.

Yeh, G., Tripathi, V., 1991. A model for simulating transport of reactive multispecies components: model development and demonstration. Water Resour. Res. 27 (12), 3075-3094.

Yegnan, A., Williamson, D.G., Graettinger, A.J., 2002. Uncertainty analysis in air dispersion modeling. Environmental Modeling & Software 17, 639-649.

York, J.P., Filby, S., Person, M., Wright, H., Gutowski, W.J., 2000. A holocene hydrologic model of the Crow Wing Watershed, Minnesota. Journal of Geochemical Exploration 69-70, 419-422.

Zheng, C., 1990. MT3D, a modular three-dimensional transport model for simulation of advection, dispersion and chemical reactions of contaminants in groundwater systems, Report to the U.S. EPA (Environmental Protection Agency), 170.

Zheng, C., Wang, P., 1999. MT3DMS, a modular three-dimensional multi-species transport model for simulation of advection, dispersion and chemical reactions of contaminants in groundwater systems; documentation and user's guide, U.S. Army Engineer Research and Development Center Contract Report SERDP-99-1, Vicksburg, MS, 202.

Zheng, C., Bennett, G., 2002. Applied Contaminant Transport Modeling. John Wiley and Sons, Inc., New York.

Zhuang, J., Yu, G., 2002. Effects of surface coatings on electrochemical properties and contaminant sorption of clay minerals. Chemosphere 49, 619-628.